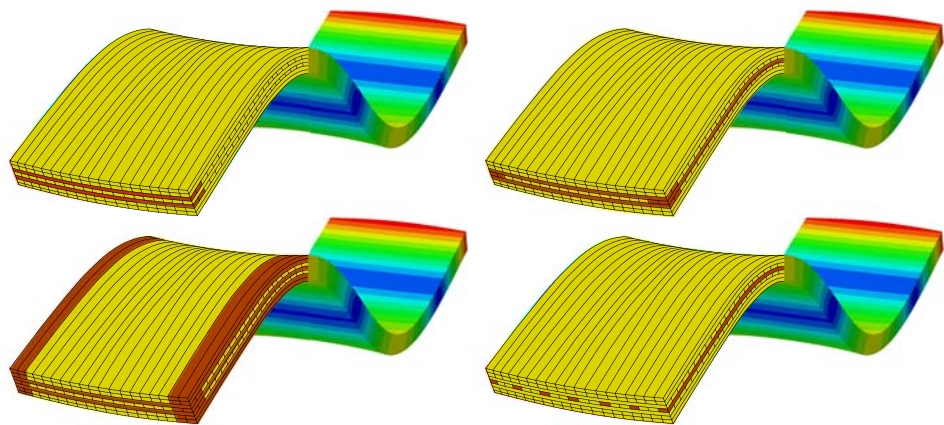




LUND
UNIVERSITY



UTILIZATION OF DIFFERENT WOOD MATERIALS IN CROSS-LAMINATED TIMBER ELEMENTS

A Study of Different Configurations

THALEB ABDALLAH and ERIK JEPSON

Structural
Mechanics

Master's Dissertation

DEPARTMENT OF CONSTRUCTION SCIENCES
DIVISION OF STRUCTURAL MECHANICS
ISRN LUTVDG/TVSM--24/5271--SE (1-160) | ISSN 0281-6679
MASTER'S DISSERTATION

UTILIZATION OF DIFFERENT WOOD MATERIALS IN CROSS-LAMINATED TIMBER ELEMENTS

A Study of Different Configurations

THALEB ABDALLAH and ERIK JEPSON

Supervisor: **PETER PERSSON**, Associate Professor, Division of Structural Mechanics, LTH.
Assistant Supervisor: **ANNIE BOHMAN**, MSc, Division of Structural Mechanics, LTH.
Examiner: **HENRIK DANIELSSON**, Associate Professor, Division of Structural Mechanics, LTH.

Copyright © 2024 Division of Structural Mechanics,
Faculty of Engineering LTH, Lund University, Sweden.
Printed by V-husets tryckeri LTH, Lund, Sweden, June 2024 (*Pl*).

For information, address:
Division of Structural Mechanics,
Faculty of Engineering LTH, Lund University, Box 118, SE-221 00 Lund, Sweden.
Homepage: www.byggmek.lth.se

Abstract

Cross-laminated timber (CLT) is an engineered wood product constructed by combining multiple layers of wood lamellae with adhesives. In the serviceability state, structural timber elements, that are light-weight, are more susceptible to complications regarding the vibration level, than heavier structural elements such as concrete. Contemporary standard practice in the building industry, is to use CLT-plates constructed of the wood species spruce. In Europe, and especially in Sweden, the hardwood species birch is quite common. Previous research indicates that incorporating hardwood in CLT-plates has a great potential of improving the vibration performance of the plate. An engineered product of spruce, namely, densified spruce, can also be used to improve the vibrational performance. The aim of this dissertation is to determine if the performance of CLT-plates can be further improved by incorporating birch, densified spruce or varying strength grades of spruce. The implementation of these wood materials is in terms of constructing various configurations of the CLT-plate, with specific lamellae arrangements of said wood materials.

At first, a numerical model was created, modelling the layers in a CLT-plate. This model was used to match the mechanical properties of the named wood materials, to an experiment conducted on CLT-plates of the wood materials analysed in this dissertation. In that capacity, the well-known optimization scheme of Newton-Raphson was used to determine appropriate material parameters. Multiple calibration setups were tested and evaluated based on their normalized relative frequency differences (NRFDs) for the first five modes.

A case study, following a systematic approach, was conducted implementing birch, densified spruce and varying spruce strength class, in CLT-plates made of spruce strength class C24. A unit load was imposed on one of the plate corners, with a measure point in the opposite corner, used to determine the acceleration response of the plate. For a more nuanced case study, two differently sized CLT-plates were considered.

The case study revealed that implementing the considered wood materials in favourable arrangements in a CLT-plate can significantly reduce the vibration level, without requiring much of the original spruce to be replaced. It was also revealed that greater reduction of the vibration level is obtained when combining spruce and the different wood materials, compared to simply replacing the entire CLT-plate with said materials.

Acknowledgements

This dissertation is the final step of our journey at the Faculty of Engineering at Lund University, conducted at the Division of Structural Mechanics. A few people have been influential in shaping the outcome of this dissertation, due to their support and assistance during the entire work, towards whom we would like to express our sincerest gratitude.

We would like to thank our main supervisor, Dr. Peter Persson, our assistant supervisor M.Sc. Annie Bohman and our examiner Dr. Henrik Danielsson, for the continuous support during this entire master's dissertation, helping us overcome any obstacle, and in shaping the results with their never-ending assistance. We would also like to thank M.Sc. Johannes Jonasson for providing the Python script used to calibrate the material parameters of the wood materials. Special thanks are extended to Mr. Bo Zadig for his skilled assistance in producing the printed version of this dissertation.

We are also grateful to Sweco Helsingborg for offering us a place in their office, to write our dissertation. Thanks are also due to Södra AB for inviting us to the CLT-plate factory, as well as giving many insightful thoughts on this dissertation. We would also like to extend our gratitude to Swedish Wood for granting us permission to use their beautiful illustrations.

Finally, we would like to express our appreciation towards our friends and families, for their support during this work, but also throughout our lives.

Lund, 2024

Contents

Abstract	I
Acknowledgements	III
Table of Contents	VIII
1 Introduction	1
1.1 Background	1
1.2 Main Objective	1
1.2.1 Subgoals	2
1.2.2 Research question	2
1.3 Method	3
1.4 Limitations	3
2 Cross-laminated Timber	5
2.1 Wood as a Construction Material	5
2.1.1 Wood Structure	5
2.1.2 Differences in Wood	8
2.1.3 Densified Wood	9
2.2 Cross-laminated Timber	10
2.2.1 Manufacturing CLT	11
2.2.2 Rolling shear	11
3 Mechanical Properties of Timber	13
3.1 Literature Review	13
3.2 Gathering of Material Properties	15
4 Fundamental Theory of Structural Dynamics	17
4.1 Motion of a Structural Dynamic System	17
4.2 Structural Dynamic Model	17
4.2.1 Stiffness	17
4.2.2 Damping	18
4.2.3 Mass	18
4.2.4 One-Dimensional Motion	19
4.3 Equation of Motion	19
4.3.1 SDOF System	20
4.3.2 MDOF System	20
4.4 Damping Matrix	20
4.5 Structural Vibration	21
4.6 Modal Analysis	21

4.6.1	Calculation of Eigenmodes and Natural Frequencies	22
4.6.2	Modal Dynamics	22
4.6.3	Modal Truncation	23
5	Elementary Multidimensional Search	25
5.1	Resumé of Multivariable Differential Calculus	25
5.1.1	The Multidimensional space \mathbf{R}^n	25
5.1.2	Smoothness	25
5.1.3	Hessian matrix	26
5.1.4	Quadratic functions	26
5.1.5	Taylor’s Formula	26
5.1.6	Optimization	27
5.2	Newton-Raphson’s Method	27
5.2.1	Principle of Newton-Raphson’s Method	27
5.2.2	Multidimensional Newton-Raphson Scheme	28
5.3	Numerical Treatment	28
5.3.1	Newmark’s Method	28
5.3.2	Central Difference Formula	29
6	Finite Element Models	31
6.1	Establishing the FE-models	31
6.2	Material model	31
6.3	Element Mesh	32
6.4	Boundary Conditions	32
6.5	Mesh Convergence Study	33
7	Methods of Evaluation	35
7.1	FE-model Validation	35
7.1.1	Sensitivity Analysis	35
7.1.2	Calibrations of Material Parameters	35
7.2	Evaluating metrics	36
7.2.1	Root Mean Square	36
7.2.2	Frequency Response Functions	37
7.2.3	Third-octave Band Filter	37
8	Model Calibration	39
8.1	Experiment	39
8.2	Outline of Validation Approach	41
8.3	FE-model	43
8.4	Model Calibration	44
8.4.1	Sensitivity Analysis	45
8.4.2	Initiation of Newton–Raphson’s Method	49
8.4.3	Calibration of Material Parameters	49
8.4.4	Final Parameters	53
9	Case Study – Introduction	57
9.1	Models of the Case Study	57
9.1.1	Dimensions of the Models	58

9.1.2	Material Properties	58
9.1.3	Load Configuration	59
9.2	Setup of L-sized CLT-panel	59
9.2.1	Frequency Step Convergence	60
9.2.2	Mesh Convergence	61
9.2.3	Truncated Modal Analysis – Convergence Study	65
9.3	Setup of S-sized CLT-panel	67
9.4	Outline of the Configuration Study	69
9.4.1	Distribution of Lamellae – Thickness Direction	70
9.4.2	Distribution of Lamellae – Longitudinal Direction	70
9.4.3	Distribution of Lamellae – Transversal Direction	70
9.4.4	Distribution of Lamellae – Combined Directions	70
9.5	Outline of the Results	71
10	Case Study – Birch	73
10.1	L-sized CLT-plate	73
10.1.1	Distribution of Lamellae – Thickness Direction	73
10.1.2	Distribution of Lamellae – Longitudinal Direction	77
10.1.3	Distribution of Lamellae – Transversal Direction	81
10.1.4	Distribution of Lamellae – Combined Directions	84
10.1.5	Conclusion – L-sized CLT-plate	90
10.2	S-sized CLT-plate	92
10.2.1	Distribution of Lamellae – Thickness Direction	92
10.2.2	Distribution of Lamellae – Longitudinal Direction	94
10.2.3	Distribution of Lamellae – Transversal Direction	98
10.2.4	Distribution of Lamellae – Combined Directions	101
10.2.5	Conclusion – S-sized CLT-plate	105
11	Case Study – Densified Spruce	107
11.1	L-sized CLT-plate	107
11.1.1	Distribution of Lamellae – Thickness Direction	107
11.1.2	Distribution of Lamellae – Longitudinal Direction	111
11.1.3	Distribution of Lamellae – Transversal Direction	115
11.1.4	Distribution of Lamellae – Combined Directions	123
11.1.5	Conclusion – L-sized CLT-plate	128
11.2	S-sized CLT-plate	129
11.2.1	Distribution of Lamellae – Thickness Direction	130
11.2.2	Distribution of Lamellae – Longitudinal Direction	133
11.2.3	Distribution of Lamellae – Transversal Direction	136
11.2.4	Distribution of Lamellae – Combined Direction	139
11.2.5	Conclusion – S-sized CLT-plate	143
12	Case Study – Spruce Strength Classes	145
12.1	L-sized CLT-plate	145
12.1.1	Conclusion – L-Sized CLT-plate	150
12.2	S-sized CLT-plate	151
12.2.1	Conclusion – S-sized CLT-plate	151
13	Discussion	153

13.1 Mechanical Properties of Wood	153
13.2 Reference Experiment	153
13.3 FE-model	154
13.4 Loading Case and Measure Point	154
13.5 Model Validity	154
13.6 Variation of Wood Material	155
13.7 Results	156
14 Concluding Remarks	159
14.1 Key Results	159
14.2 Main Conclusions	159
14.3 Future Work	160
Bibliography	163

1 Introduction

This chapter is designed to give insight into the dissertation. The main objective is described with the subgoals necessary to achieve it. This is followed by a description of the methods used as well as the limitations considered.

1.1 Background

In Europe, and particularly Sweden, there exists an abundance of timber which can increase sustainability if utilized properly by today's society. One option for making use of the timber is as cross-laminated timber panels in housing and industrial building projects. While the increased adaptation of CLT in structural engineering presents a sustainable solution for urban development, CLT is dynamically sensitive and is thus susceptible to complications regarding comfort.

Traditionally, softwood has been used in timber construction, due to higher availability and economic reasons [1]. However, other wood types, such as hardwoods, can also be used. Hardwood has different properties than softwood and previous studies have shown promising results when hardwood is incorporated into the CLT, with respect to the dynamical response [2]. A proposed solution to mitigate the dynamical challenges is to introduce hardwood lamellae in CLT-panels. Different systematic configurations can be investigated, in order to obtain the most optimal design.

The forest coverage in Europe, which represents 44% of the total land area, experiences an annual, continuous expansion [1]. The European forest is divided into separate regions containing different divisions of the various wood species available. In Sweden, the most common wood species are spruce and pine. The remaining forest is made up of birch and other deciduous species. The share between different forest species can be viewed in Figure 1.1. 1

1.2 Main Objective

The main objective of this dissertation is to investigate the feasibility of replacing lamellae in CLT-panels of spruce, with birch, densified spruce and timber of various strength classes, with regards to structural dynamical response pertaining to human comfort in the built environment. This entails determining the optimum configurations by investigating different arrangements and patterns in which the spruce lamellae are replaced. The hardwood of interest is primarily birch, although densified and different quality spruce is also of interest.

Two different sizes of CLT-panels will be modeled and investigated with varying length

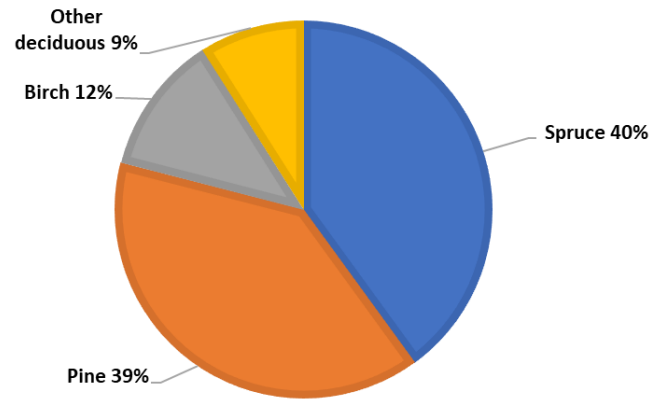


Figure 1.1: Different forest species in the Swedish forest [1].

and height, although constant width. The most detailed analysis and investigations will be conducted with the larger CLT-panel. The analysis of the smaller panel will be based upon the former analysis.

1.2.1 Subgoals

In order to achieve the main objective, the following subgoals are defined:

- Develop suitable computational models and perform calibrations against a laboratory experiment, to confirm aptness of computer model.
- Determine the influence of different qualities of wood by considering several different arrangements in CLT-panels.
- Perform frequency response studies and modal analyses.
- Investigate structural dynamic response at corresponding configurations and identify optimum configurations.
- Evaluate the human comfort level of these optimums.

1.2.2 Research question

The research questions to be answered are:

- How is the acceleration response of CLT-panels affected with different arrangements of lamellas, made from birch, densified spruce, and varying strength grades of spruce?
- What configurations have the greatest reduction of the acceleration response, with respect to the used loading and boundary conditions?

1.3 Method

In order to answer the research questions and thereby fulfill the main objective, the commercial software Abaqus was used for finite element analyses. Furthermore, an experiment was utilized in order to validate the computational models. Various CLT configurations were constructed in a systematic manner and steady-state analyses were performed. These different CLT-panels were simulated by defining different material parameters for lamellae in specific arrangements. Furthermore, frequency-sweep analyses were performed in order to establish several relevant frequency response functions.

1.4 Limitations

- The different types of wood materials that were utilized, apart from the softwood spruce, are birch and densified spruce
- The wood material behaviour is constrained to be linear elastic
- The wood material is assumed to be exposed to indoors climate
- The analyses are restricted to structural dynamic properties of CLT-panels
- The analyses will be conducted in the frequency range of 0-562 Hz

2 Cross-laminated Timber

This chapter presents wood as a construction material, described from a construction materials science point of view. The material properties of wood and its functions are presented to give a basic understanding of wood as a construction material. Furthermore, cross-laminated timber is presented, how it is manufactured as well as a dimensional instability phenomenon called rolling shear.

2.1 Wood as a Construction Material

This section presents how wood is structured, the variability in the material and the main principles of densified wood.

2.1.1 Wood Structure

Wood is an orthotropic material with different material properties in three principal directions, namely longitudinal, tangential and radial [1]. The longitudinal direction is parallel to the fibres of the wood. The tangential direction is perpendicular to the longitudinal direction and runs tangentially to the annual growth rings of wood. The radial direction of wood is perpendicular to the longitudinal direction and normal to the annual growth rings. The principal directions are presented in Figure 2.1.

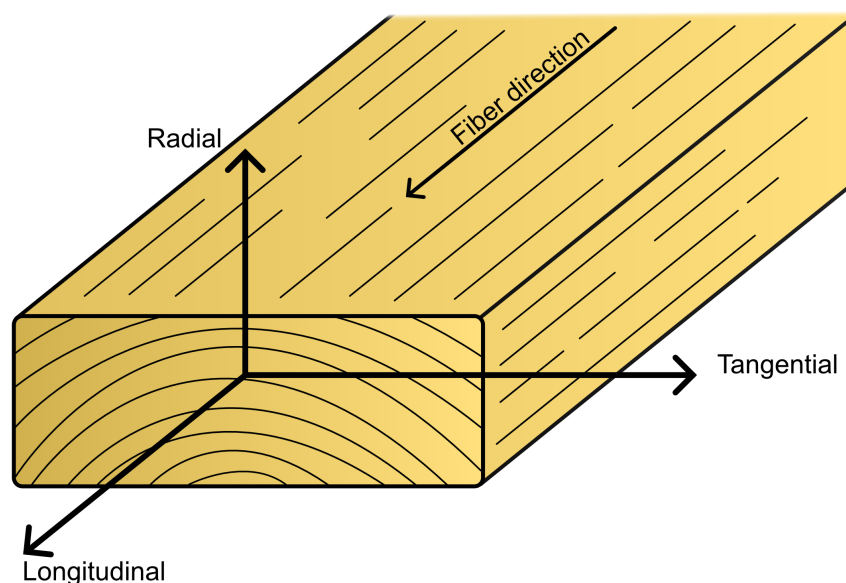


Figure 2.1: Principal directions of wood.

The peak strength and stiffness of wood is obtained when load is applied parallel to the longitudinal direction [1]. The capacity of timber is reduced significantly when loading is done in the tangential or radial direction. This variation in strength is caused by how trees have been naturally optimized to carry its own weight in conjunction to resisting lateral wind loads, essentially acting as a vertical cantilever. Trees have local growth stresses which reduce the risk of the tree crushing during elevated stress levels when in its' natural environment. When wood is considered as a construction material, local defects have a negative impact on performance.

The properties of wood can be studied at varying levels of detail, the main ones being macro- and microscopic as well as on a chemical level [1]. A basic introduction to these different levels will be presented, however the reader is referred to literature in materials science for further readings. Wood can be divided into conifers and deciduous, also referred to as softwood and hardwood, respectively. The softwood typically used in CLT-plates is spruce, while the hardwood to be utilized in this dissertation is birch.

Chemical Composition of Wood

Wood is a composite material made up of carbon, hydrogen and oxygen in the form of lignin, cellulose and hemicellulose [1]. Lignin acts as a glue facilitating the structural integrity arising from the cellulose. For Nordic softwood, the average tree has approximately 40% cellulose, 30% hemicellulose and 30% lignin.

Microstructure of Wood

The microstructure level of wood denotes to the microscopic level of structural study [1]. The cellulose in the wood is encased by hemicellulose and lignin, which combined create strands. These form tube shaped cell walls. The cell walls are oriented in the longitudinal direction, constituting multiple layers, which is believed to induce higher strength in this direction. Again, the reader is referred to literature in materials science for further readings [1]. The structure of wood cell walls can be seen in Figure 2.2

Macrostructure of Wood

Macrostructure denotes the level of structural study that can be performed ocularly [1]. The trees are clad in bark, with the essential purpose of protecting the medium that is transporting nutrients to the tree crown, as well as protecting the interior wood. The bark and the interior wood are separated by a layer, the cambium, that maintains continuous cell division resulting in the growth of the tree as a whole, including the bark. The actual wood of the tree can be separated into two different kinds, heartwood and sapwood [3]. Heartwood is created when the central parts of the tree stop the transportation of water, which usually occurs when the tree reaches about 30 years of age. Even though the moisture content is lower in the heartwood, there are no

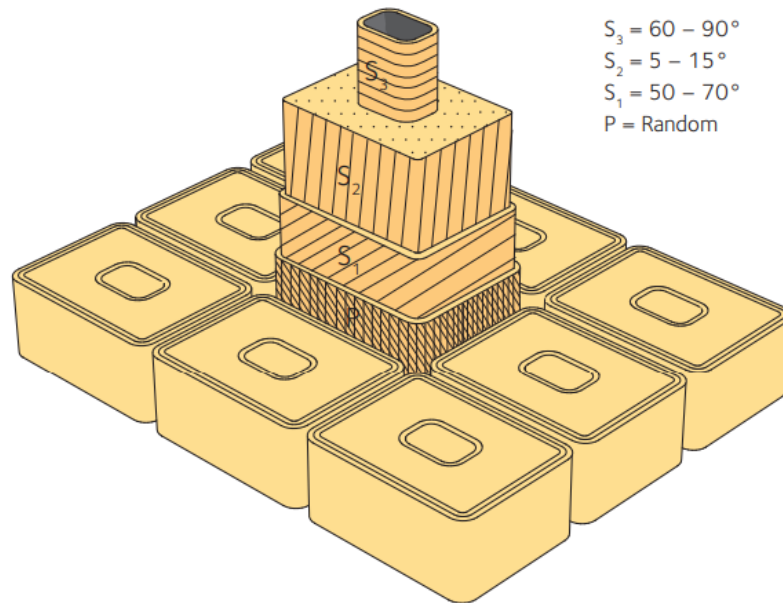


Figure 2.2: Composition of wood cell walls [1].

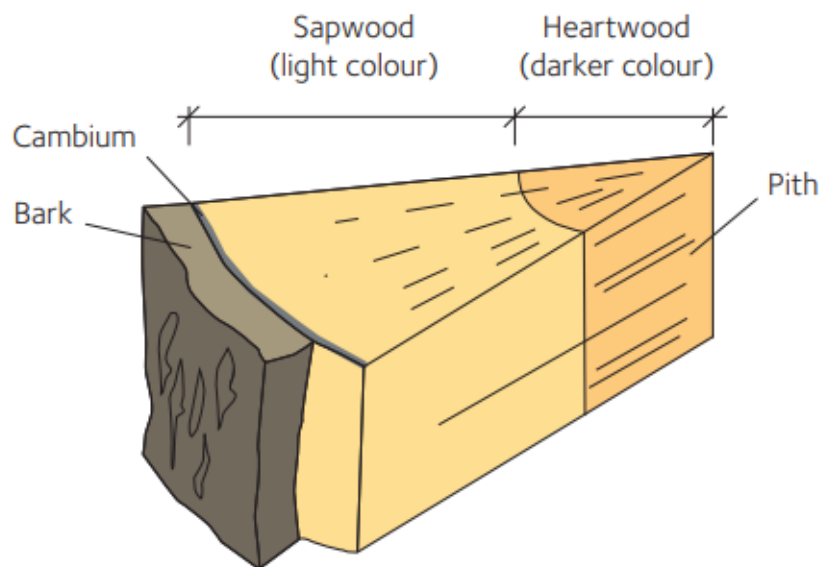


Figure 2.3: Different parts of wood [1].

differences in terms of strength between respective parts. The pith is the center of the tree. The different sections of wood can be seen in Figure 2.3.

Softwood versus Hardwood

As previously mentioned, hardwoods are deciduous, meaning that they shed their leaves annually [3]. Softwoods, on the other hand, are conifers, meaning that they keep their foliage for longer periods. Consequently, softwoods typically have lower densities than hardwoods. Due to the rapid growth, lower economical cost as well as being easier to process, softwood is the dominant type of wood used in contemporary

structural engineering.

2.1.2 Differences in Wood

Wood is an organic material, naturally produced in uncontrollable and variable environments, as opposed to concrete or steel [3]. As such, wood materials inherit significant variability in quality and properties. While different species of wood have different properties, further variations can also be found within the same wood species. This can be attributed to the growth conditions as well as the several types of local imperfections that are formed during the growth period.

Clear Wood and Timber

Two distinctions can be made between wood specimens, regarding imperfections [1]. Smaller specimens with no imperfections are usually called clear woods, where all the fibres are aligned uniformly, and the material properties are determined by the type of wood being used. In contrast, larger timber specimens usually include defects such as knots, juvenile wood, spiral grain angle and reaction wood. While the properties of the wood dictate the strength of the timber, these imperfections can have significant effect on the strength.

Imperfections in Wood

Photosynthesis occurs in leaves and needles, hence these are necessary for trees to survive[1]. Leaves grow on branches in order to maximize the covered surface area. However, these branches create knots in the wood which distorts the wood fibres. During loading, these local distortions cause unwanted stress concentrations.

Strength Grading

In order to utilize wood as a construction material, knowledge of the material strength is essential. Since wood shows significant variability, a mandatory standardized strength grading is employed. A simple way to describe the strength value of timber is that the values reflect the value on an element level, and not material level [1].

Following the manufacturing process of wood to timber, grading based upon the bending strength is initialized, following standards set by SS-EN 338:2016 [4]. The elastic modulus parallel to the grain, as well as the density is determined for the timber. These parameters are then correlated to a standardized strength grade. Based on this grading, the remaining elastic and shear moduli, respectively, are estimated. Both visual and machine strength grading methods are used for grading timber. The 5-percentile rule is used for characteristic strength of the timber. That is, following a statistical Gauss distribution of the experimentally measured strengths, only those pertaining to the 5-percentile are benchmarked.

Moisture Content

The moisture content in wood is a critical factor, since wood is an absorptive and a living material [1]. Both volume and moisture capacity can vary in a timber sample based upon the relative humidity in the surrounding climate. An increasing moisture content in the wood has negative impact on strength and stiffness. In order to account for the interplay between the moisture content and the strength of timber, a standardized set of service classes is defined, whereby the ambient temperature and relative humidity are used as benchmarks in accordance with SS-EN 1995-1-1. An acceptable moisture content for experimental testing of timber is usually about 12% [4]. This moisture content is equivalent to service class 1 according to SS EN 1995-1-1 [5]. Service class 1 is well suited to describe indoor ambient conditions, which are highly relevant for this dissertation.

2.1.3 Densified Wood

In the early 1900s, the concept of wood densification was proposed in the United States [6]. Wood densification is essentially a compression process of wood, by which the density thereof increases. The principle is that wood fibres can be mechanically compressed and bundled into each other, reducing the bulk volume while the mass stays constant, and thereby an increased density is obtained. Furthermore, the densification improves the surface conditions of the wood, primarily hardness [7]. Hardness is a material property that directly relates to the resistance of indentation and abrasion, which is a sought-after property found in high-quality wood products. Thus, low-quality wood products can be processed into wood products that may compete with high-quality wood products. However, the densification process of wood, which results in improved mechanical properties, was first intended for high-stress applications [6].

There are two distinctive types of densification processes, namely, bulk and surface densification, respectively. Bulk densification refers to the densification process that affects the whole bulk of the wood product, whereas the surface densification process is tailored to only densify the surface portion of the wood product [6]. The densified wood used in the experimental lab performed in [8], and by extension the densified wood of interest in this dissertation, is bulk densified.

Bulk Densification

There are several different procedures to accomplish the desired bulk densification. The fundamental idea is to plasticize the wood specimen to soften it, enabling adequate compression. The plasticization is usually achieved by thermal treatment, and the subsequent compression by way of mechanical presses. The degree of compression is quantified by a compression ratio (CR) defined as a relative difference,

$$CR = \frac{t_i - t_f}{t_i} \quad (2.1)$$

where t_i and t_f are the initial and final thicknesses, respectively. The densified wood of interest, that which is used in [8], has an initial thickness of 48 mm and a final thickness of 21 mm, yielding the compression ratio $CR = \frac{48-21}{48} \approx 56\%$.

2.2 Cross-laminated Timber

Cross-laminated timber (CLT) consists of wooden lamellae grouped together in layers, with each layer orientated orthogonal to the surrounding layers, see Figure 2.4. The total number of layers is typically odd, no less than three in total. It is common to alter material orientation in each layer, although in some cases it can be beneficial to have the two layers closest to the surface in the same direction.

It is estimated that the varying orientations diminish, to some degree, the influence of woods innate anisotropy [9]. The orientation of the outer layers is set to coincide with the load bearing direction of the CLT-panel. In comparison with moisture related movements of regular timber, CLT-panels expand and contract less. CLT-panels are commonly designed for a moisture content of 12%, and with excessive deviation of moisture content, the panel can take on an unwanted curved shape.

The use of cross-laminated timber has increased significantly in recent decades. CLT-panels are commonly prefabricated in a factory, before being transported to the clients [9]. It is possible to construct CLT-panels spanning as long as 30 m, and with a width of up to 4.8 m meters and with a thickness of up to 0.5 m. With respect to the current building regulations, as well as to the ease of transportation, the most common sizes range 12–16 m in length, 1.2–3 m in width and 80–300 mm in thickness. The corresponding number of layers range between 3 and 9. The most common species of wood used in CLT-plates are pine and spruce.

All lamellae used in a CLT-panel must be of the same dimensions, however they may be of different strength qualities [9]. Individual lamellae are commonly 80–200 mm wide, 20–45 mm thick with a thickness to width ratio of 1:4. Wood of different strength classes can be used in a CLT-panel. The wood of the highest quality is used in the load bearing direction as well as in the surface layers and the wood of lower quality can be used for lamellae oriented in the transverse direction, resulting in different types of wood used in the panel.

Cross-laminated timber has many uses, the most common one being as a structural element [9]. It is often used for wall or floor structures in office buildings, schools, multi-storey buildings or houses. CLT is more environmentally friendly than other popular construction materials such as concrete and steel. Furthermore, CLT can obtain a long service life if adequately protected from fire and moisture. This in conjunction with the fact that CLT can be recycled in new building projects or as a fuel source, further improves CLT from a life-cycle perspective.

Large CLT-panels are commonly used as floors and walls in structures, in contrast to systems using pillars and beams to achieve desired levels of strength and stability [9]. Due to the ability to make cross-sections substantial, significant strength and stability

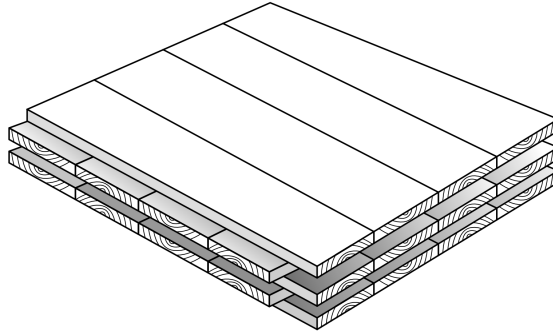


Figure 2.4: Cross-laminated timber element, 5 layers.

can be attributed to the panels. CLT-panels are especially used as diaphragms to stabilize large timber buildings. Since the CLT-panels are manufactured in controlled environments, the degree of prefabrication is very high. Moreover, the CLT-plates can be easily transported due to their low self-weight. Additionally, CLT-panels as exterior walls facilitate readily installed thermal isolation, directly on the plates interior surface, minimizing the amount of thermal bridges.

2.2.1 Manufacturing CLT

CLT-panels are manufactured by gluing together lamellae of either coniferous or deciduous wood [9]. The CLT-panels have to comply with the adopted construction regulations and codes, specifically to the standard SS-EN 16351, as well as the properties declared by each manufacturer in their European Technical Assessment.

The process of manufacturing CLT-panels is generally independent of region or country [9]. Wood is sawn into timber planks, which are then finger jointed together to obtain large spanning lamellae. The lamellae are planed on their flat side, whereby glue is applied and mechanical pressure is exerted compressing the lamellae, creating the sheets. The compression can be generated using either vacuum or hydraulic pressure. When the gluing is finished, a CNC (Computer Numerical Control) machine is used to apply the finishing touches. An overview of the production steps used to create CLT-panels is presented in Figure 2.5.

It is most common to only apply glue at the top and bottom of the lamellae, although it is possible to glue the edges of the laminates as well [9]. Edge-gluing of the timber allows stresses to be distributed horizontally between individual lamellae, although it can cause dimensional stability problems [10]. The dimensional stability problems are caused by the removal of stress relief zones between lamellae. Additionally, if edge-gluing is used during construction of a panel, planing of the edges would be necessary, causing increased manufacturing costs.

2.2.2 Rolling shear

While the tensile strength of the surface layers often is a vital part of CLT design, the rolling shear strength of the panel can also be crucial when loading is applied in

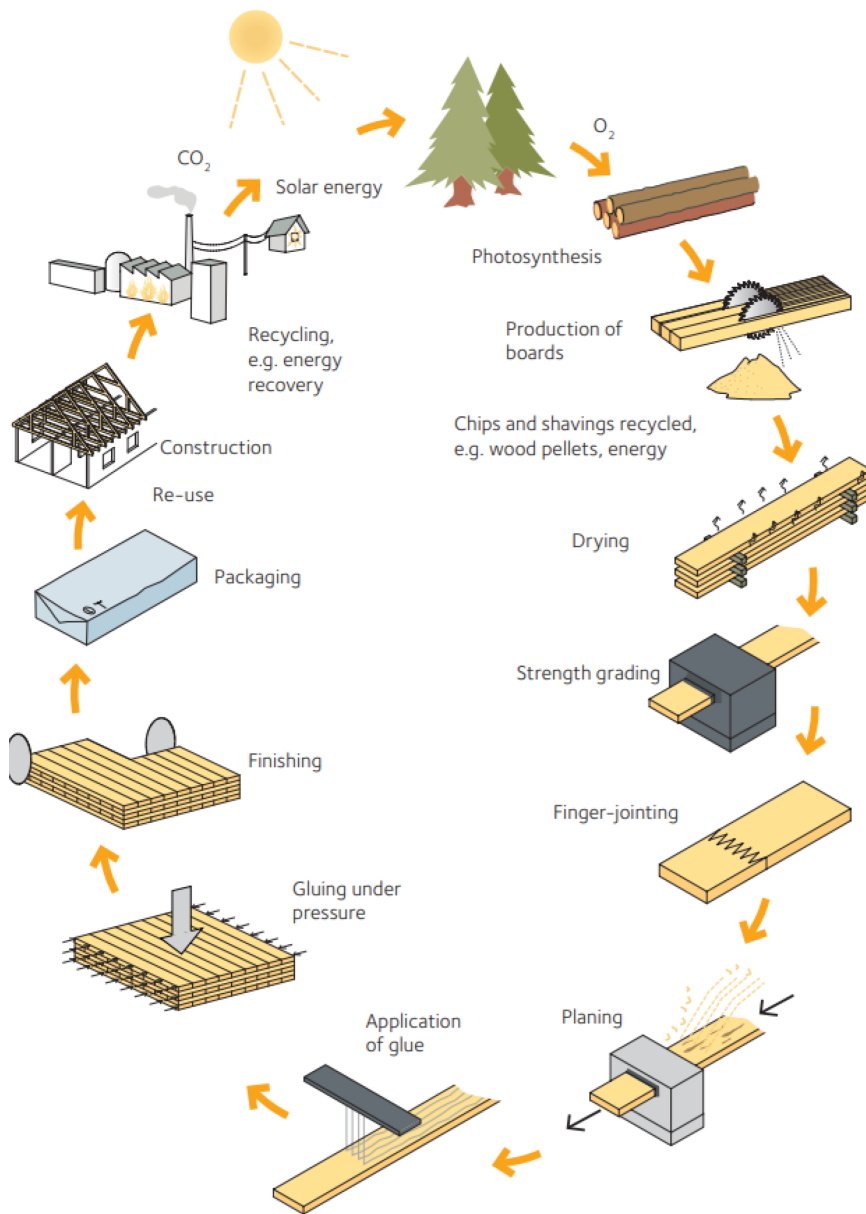


Figure 2.5: Manufacturing cycle of CLT [11] (translated to English).

the transverse direction [9]. Rolling shear failure occurs when the fibres deform under significant shear stress causing deformation as well as a reduction in shear capacity.

3 Mechanical Properties of Timber

This chapter presents a literary study reviewing wood properties from different sources. The different testing methods, specimens and concluding parameters are presented if available.

The species of wood covered are spruce and birch. Due to the difficulties determining wood properties, sources outside of Europe have been included in the literary review.

There is no standardized method to obtain properties of wood, resulting in discrepancies when comparing properties obtained from different testing methods.

Previous investigations showed that Poisson's ratio had negligible influence on the natural frequencies of CLT-panels [12]. Thus, Poisson's ratio has been excluded from the literature review as well as the parameter study conducted in this dissertation.

The wood in a tree trunk grows in a circular geometry, although the timber cuts are usually rectangular. This implies some difficulty in assigning the transversal principal directions. This has implications regarding the modelling of the CLT-plates. An approximation that sets identical material parameters in the tangential and radial direction will be adopted in this dissertation.

3.1 Literature Review

In [13], a literature review of mechanical properties of various wood species is presented, using 20 different papers. In the aforementioned article, each source was given a unique ID-number. The ID of each source is provided here to facilitate the reader with the means of finding the original source. The different works reviewed are not all written in English, preventing use of the original sources.

The authors of [13] emphasize the challenge in determining mechanical properties of wood. Numerous different methods are used to obtain the properties, resulting in characteristics that are incomparable between tests. Two correlations noted by the authors are higher elastic modulus and density for hardwood when compared to softwood.

In [14], rolling shear properties of 6 wood species was investigated. The species of wood tested were Norway spruce, pine, European beech, European ash, poplar and European birch. It was found that the ratio between width and thickness of a laminate as well as the sawing pattern had significant influence on the rolling shear properties. The test setup used was similar to the method described in EN 408, designed to determine the longitudinal shear properties, see Figure 3.1 [15]. The average aspect ratio between width and thickness was 4 and the average sawing pattern, center of the board to the

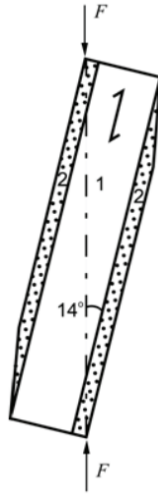


Figure 3.1: Test method according to SS-EN 408 [15].

pith, was 60 mm. These values were varied to determine how they contribute to the rolling shear strength of a timber board. All test specimens were conditioned at 20°C and a relative humidity of 65%. In total 342 tests were conducted. It was found that Norway spruce had a rolling shear modulus of 100 MPa and that the rest of the species has higher modulus. The resulting rolling shear properties were determined by taking the mean value obtained from the testing, and the method used was determined to be an effective method of determining rolling shear properties of the base material used for CLT.

In [16], experiments were conducted on both timber lamellae and cross-laminated timber panels of birch sourced from Russia. The timber sample utilized in the experiments underwent cutting and kiln-drying processes to achieve a moisture content of 12%. A visual grading according to DIN 4074-5 was conducted, to sort out lamellae not fulfilling the grading class LS13. Additionally, the material was stress graded according to the material's dynamic modulus of elasticity, using GoldenEye 706 from MiCROTEC. Initially, tensile tests according to EN 408 were carried out to gather information about the raw material [15]. The mean longitudinal modulus of elasticity was measured at 16 000 MPa. A total of 20 CLT panels of 5 layers were tested in bending according to EN 16351:2013, to determine the bending stiffness as well as the rolling shear strength. To determine the compressive strength perpendicular to grain, 20 test specimen were tested according to ÖNORM EN 408:2010 [15]. Most of the resulting mechanical properties were determined based upon the previously mentioned tests, the rest were based upon formal relationships.

In [17], the mechanical properties of various species of wood found in Scandinavia are presented. How the aforementioned properties are derived is not presented in the test.

In [18], the mechanical properties of numerous species of wood are presented. The specimen used for the tests were clear wood and did not exhibit any imperfections. Further insight into how the tests were conducted is not presented in the paper. The mechanical properties are given as a ratio towards the longitudinal modulus of elasticity, in 3.2 E_L is estimated based upon the other sources.

Mechanical Properties of Densified Wood

Various studies have been conducted investigating the mechanical properties of wood densification, both in terms of bulk and surface densification, respectively. Surface densification have been extensively researched in [19], [6], [20] and [7]. For the purposes of this dissertation, the work presented in [21] is highly relevant, portraying a relationship between the enhancement of the mechanical properties of densified wood and the pertaining compression ratio. It should be noted, though, that the densification process has a significant influence on the outcome of the wood mechanical properties [21]. Hence, the compression ratio in and of itself is not deemed as a sufficiently reliable measure of the wood densification. Especially when considering the wood used in the lab experiment [8].

Instead, the effect of densification on the longitudinal Young's modulus is approximated to be proportional to the increase in density. Thus, the compression ratio is supplied with the density ratio of the densified specimen to the standard spruce specimen. Thereupon, the mechanical properties thereto are determined and compared with the results in [21]. With the densified wood density being 787 kg/m^3 , and standard spruce density being 428 kg/m^3 , the change factor becomes $787/428 = 1.84$. Accordingly, the elastic moduli of the densified wood can be approximated as those of the standard spruce, scaled with the factor 1.84.

3.2 Gathering of Material Properties

Table 8.9 presents the mechanical properties of spruce according to SS-EN 338, with the exclusion of the rolling shear modulus, G_{RT} [4]. G_{RT} is derived using the average ratio of the longitudinal shear moduli and the rolling shear modulus obtained from [22].

Table 3.1: Mechanical properties of spruce according to SS-EN 338, excluding G_{RT} . Moduli are displayed in MPa and mass density in kg/m^3 .

Wood class	E_L	E_T	E_R	G_{LT}	G_{LR}	G_{RT}	ρ
C14	7 000	230	230	440	440	31	350
C16	8 000	270	270	500	500	35	370
C18	9 000	300	300	560	560	40	380
C20	9 500	320	320	590	590	42	350
C22	10 000	330	330	630	630	45	410
C24	11 000	370	370	690	690	49	420
C27	11 500	380	380	720	720	51	430
C30	12 000	400	400	750	750	53	460
C35	13 000	430	430	810	810	57	470
C40	14 000	470	470	880	880	62	480
C45	15 000	500	500	940	940	67	490
C50	16 000	530	530	1 000	1 000	71	520

Table 3.2 presents the mechanical properties of birch according to the various sources explained previously in this chapter. For source [18], each material parameter was given as a ratio to E_L , although no value was given for the longitudinal modulus of elasticity.

Table 3.2: Mechanical properties of birch according to multiple sources (ID:s given in the first column). Moduli are displayed in MPa and mass density in kg/m³.

Source ID	E_L	E_T	E_R	G_{LT}	G_{LR}	G_{RT}
[13] ID: 6	14 500 - 16 500					
[13] ID: 19	15 250	640	1 260			
[13] ID: 17		620	1 110			
[14]						180
[16]	15 000	650	650	850	850	175
[17]	13 000 - 15 000					
[18]	(15 000)	750	1 170	1 020	1 110	255

4 Fundamental Theory of Structural Dynamics

In this chapter, the underlying theory that governs the analyses and simulations presented in this dissertation is outlined on a fundamental level. The aim is to only present the quintessential theory of linear-elastic structural dynamics. For an exhaustive exposition on this subject, the reader is referred to [23].

4.1 Motion of a Structural Dynamic System

A *dynamic system* exhibits motion, contrary to a static system. Dynamic systems can be categorized based on the nature of the motion. The motion of an object could be classified as one-, two- or three-dimensional. Furthermore, a dynamical system can be assigned *degrees of freedom*, which characterize the number of principal movements the objects of interest can take on. In structural dynamics, these principal movements are predominantly translations and rotations. By employing a Cartesian coordinate system, the principle movements can be defined with respect to the principal axes.

4.2 Structural Dynamic Model

In order to incorporate the structural essence in a dynamical system, use of an expedient model thereof is in place.

4.2.1 Stiffness

Structures constitutes several elements joined together, with a degree of *compliance* thereto. This compliance, or inversely, the *stiffness* of the considered structure must be taken into account. The consideration is both in terms of the inherent stiffness of the structural element, as well as the stiffness in the junctions connecting said elements. In order to capture the influence of the stiffness, Hooke's law is appropriately employed, denoting the time-dependent displacement as $u(t)$ and the stiffness as k ,

$$F_s = ku(t) \tag{4.1}$$

whereby the stiffness can be physically modelled as a *spring* as shown below.

When the spring is acted upon by an external force, either in compression or in tension, then by Newton's third law, a force will be generated. Namely, the spring force. According to Eq. (4.1), and for a constant displacement u , a large spring stiffness results in a large spring force.

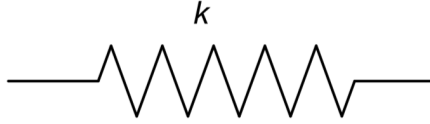


Figure 4.1: Spring element.

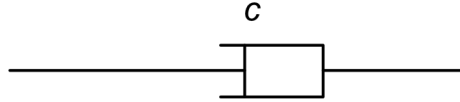


Figure 4.2: Dashpot element.

4.2.2 Damping

Motion is attributed with *damping*. Damping occurs naturally in conjunction with vibratory motion and dissipates the kinetic energy of the object in motion [23]. The damping effect is usually ascribed to internal friction of the structural element as well as the interaction between structural elements. Although other phenomena are also in play, such as heat evolution from repeated elastic straining of the material [23]. However, the respective damping phenomena are difficult to accurately model mathematically, whereby the collective damping effect is idealised as *viscous*.

In the study of continuum mechanics, damping in general is ordinarily interpreted as a counteracting force. More specifically, viscous damping is defined in a constitutive manner as being proportional to the velocity of the mass in motion. The constant of proportionality is called the *damping constant*, denoted as c . Using Newton's dot notation, the velocity is denoted as $\dot{u}(t)$ and the viscous damping force is written as

$$F_c = c\dot{u}(t) \quad (4.2)$$

Thus, the damping can be physically modelled as a *dashpot*, cf. Figure 4.2. A dashpot is essentially a cylindrical tube equipped with a piston. The tube is filled with a viscous fluid, characterized by its damping constant c . According to the constitutive model (4.2), the damping force generated by the viscous fluid will be large for large velocities, and marginal for marginal velocities.

4.2.3 Mass

An apparent consideration, regarding the mass of the structure, should be made. The mass distribution in a structural element follows the density distribution, which is usually uniform. However, at times, modelling mass as spatially uniformly distributed can be arduous. Therefore, the mass of a structural element is appropriately *lumped* and approximated as a point-mass, which is a common practice in the study of Newtonian mechanics. This approximation facilitates a straight-forward application of Newton's second law, i.e., forces are generated by acceleration of discrete masses. Again, by adopting Newton's dot notation, the acceleration is denoted as $\ddot{u}(t)$ and thus

$$\sum F = m\ddot{u}(t) \quad (4.3)$$

4.2.4 One-Dimensional Motion

The simplest case of motion is one-dimensional, with a *single degree of freedom (SDOF)*, namely translation along a principal axis. The forcing action is in the general case time-dependent. Thus, the simplest model is derived from the simplest case, assembling the elementary constituents discussed above, as showcased below. This model readily encompasses the mass, stiffness and damping of the system. Along with the model, is the free-body diagram incorporating the stiffness force and the damping force.

This model lends itself to be appropriately applied to simple dynamical systems, due to its simplicity. The model can be tuned to reflect the system at hand. For example, the dashpot or the forcing action can be disregarded, if required. Furthermore, this model is easily extensible to model multiple structural bodies in motion. This is done by concatenating multiple SDOF systems, thus forming a system of *multi degree of freedom (MDOF)*. The movement is still restrained to a single dimension, that is, a uniaxial MDOF system. An example of a generalized form of this particular system is showcased in the figure below.

The one-dimensional case is naturally extended to two- and three-dimensions. This extension is achieved by considering SDOF models along several principal axes. As such, modeling multi-dimensional movement implies usage of MDOF systems.

4.3 Equation of Motion

The differential equation that governs motion is the so-called *equation of motion*. This differential equation encapsulates the movement of a solid body, in terms of displace-

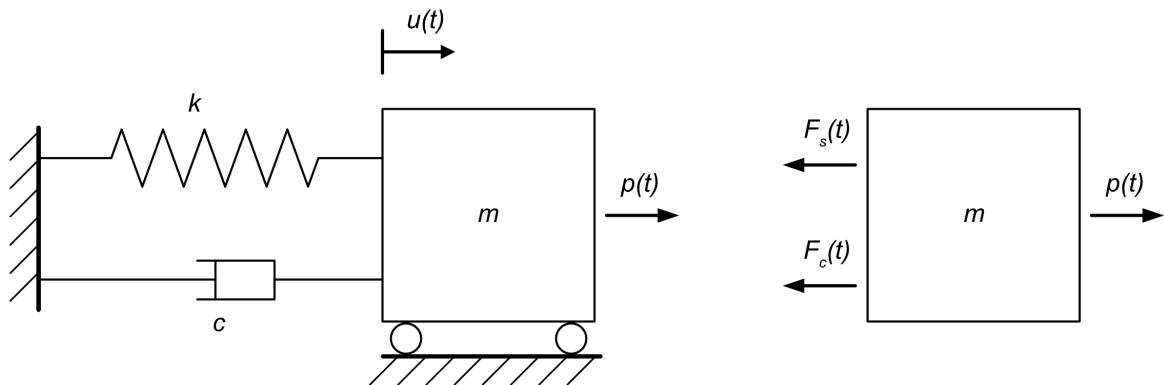


Figure 4.3: a) SDOF model. b) Free-body diagram.

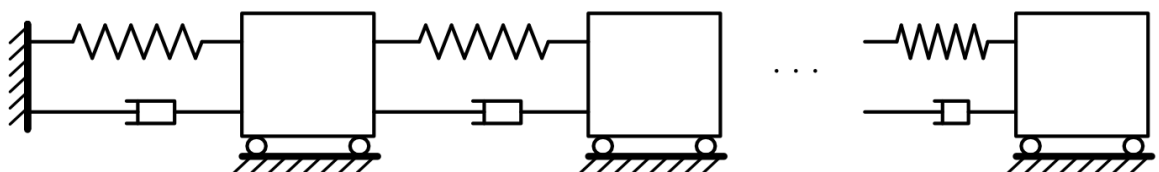


Figure 4.4: Schematic uniaxial MDOF model of n degrees of freedom.

ment, velocity and acceleration. The equation of motion is obtained by applying *Newton's third law*, followed by Eq. (4.3) to a dynamic system.

4.3.1 SDOF System

By considering Figure 4.3, the free-body diagram is obtained by Newton's third law. Application of Eq. (4.3) yields

$$p(t) - F_s(t) - F_c(t) = m\ddot{u}(t)$$

whereby insertion of (4.1) and (4.2) yields

$$m\ddot{u} + c\dot{u} + ku = p(t) \quad (4.4)$$

where the notation $u = u(t)$ has been adopted to avoid redundancy. Eq. (4.4) is thus the SDOF equation of motion. The *natural angular frequency* is then defined as $\omega_n = \sqrt{\frac{k}{m}}$, and the *damping factor* is defined as $\zeta = \frac{c}{2m\omega_n}$.

4.3.2 MDOF System

The equation of motion for the more general MDOF model is obtained by repeating the previous steps for each degree of freedom, generating a *system of differential equations*. By adopting matrix notation, the system of differential equations is succinctly written as

$$\mathbf{m}\ddot{\mathbf{u}} + \mathbf{c}\dot{\mathbf{u}} + \mathbf{k}\mathbf{u} = \mathbf{p}(t) \quad (4.5)$$

where \mathbf{m} is the lumped mass matrix, \mathbf{c} is the damping matrix, \mathbf{k} is the stiffness matrix and $\mathbf{p}(t)$ is the force column matrix.

4.4 Damping Matrix

The damping matrix \mathbf{c} in Eq. (4.5) can be constructed in several different manners. The straight-forward method is to assemble the damping matrix, akin to the stiffness matrix, consisting of the individual damping coefficients corresponding to the respective dashpots. Although, this approach assumes well-defined damping stiffnesses, which is not readily available, as mentioned in Section 4.2.2.

An alternative damping model is the *modal damping*, where each individual eigenmode is damped to a specific degree by applying the damping ratio. This model is suitable for cases where the damping ratio is known for specific eigenmodes, as will be explained in Section 4.6.

Influence of Damping

The influence of damping on the natural angular frequency of an SDOF system is observed by the following equation

$$\omega_D = \omega_n \sqrt{1 - \zeta_n^2} \quad (4.6)$$

where ω_D denotes the dynamic natural eigenfrequency, and ζ_n denotes the damping ratio of the natural eigenfrequency ω_n . It is duly noted that for damping ratios $\zeta_n < 20\%$, the eigenfrequencies remain rather unfazed.

4.5 Structural Vibration

Structures are excited into motion by application of external forces. These forces may be arbitrary *spatio-temporally*. That is, they may vary across the volume of the structure, as well as in the time domain. The nature of the structural motion can be described as *perturbations* or *vibrations* about the *static equilibrium state*.

When a structure is released from a state of equilibrium, then the structure will remain in motion, according to *Newton's first law*. This case is referred to as *free vibration* and is obtained by setting $p(t) = 0$ in the equation of motion (4.4) and $\mathbf{p}(t) = \mathbf{0}$ in Eq. (4.5), respectively. Although, energy losses may occur, diminishing the vibrations, which is taken into account by the imposed damping in Eq. (4.3).

Ultimately, different scenarios are created by considering different sets of excitation forces and damping constants. The simplest vibration motion is obtained by considering an undamped system exhibiting free vibration. This is simulated by neglecting the damping and force, in the equation of motion. That is, setting $c = 0$ and $p(t) = 0$ in Eq. (4.4), yielding the linear homogeneous differential equation

$$m\ddot{u} + ku = 0 \quad (4.7)$$

As motion is initiated, the mass is in rest, hence the starting velocity and acceleration, respectively, are null. Thus, the following initial values are appropriate,

$$\begin{cases} u_0 = u(0) = 0 \\ \dot{u}_0 = \dot{u}(0) = 0 \end{cases} \quad (4.8)$$

4.6 Modal Analysis

Structural dynamical modeling of large systems entails many degrees of freedom, hence generating large MDOF models. This translates directly to large systems of differential

equations, whereby solving these systems can be time-consuming. Thus, instead of describing the structural dynamical system with the equation of motion, usage of the *modal properties* thereof is made. That is, the structural dynamical system is described by its eigenmodes and their natural frequencies and damping. This procedure makes up a *modal analysis*.

Using modal analysis instead of directly solving the equation of motion can be an efficient alternative, especially when dealing with multiple degrees of freedom. The idea is to transform the equation of motion, from a differential equation, to a system of algebraic equations, which would then be a linear combination of all the occurring eigenmodes in the chosen frequency spectrum.

4.6.1 Calculation of Eigenmodes and Natural Frequencies

Modal analysis is initiated by determination of the eigenmodes along with the corresponding natural frequencies. By Eq. (4.6), the damping can be neglected, provided low damping ratios. Hence, the free vibration system, with multiple degrees of freedom, becomes

$$\mathbf{m}\ddot{\mathbf{u}} + \mathbf{k}\mathbf{u} = \mathbf{0} \quad (4.9)$$

The displacement vector \mathbf{u} has the dimension of length, while also being time-dependent. The displacement is then defined in terms of the mode shapes. The mode shapes are described by dimensionless vectors, φ_n . However, the displacement is time-dependent, and thus a time-dependent quantity is introduced, namely, *modal coordinates* vector denoted $\mathbf{q}_n(t)$. The modal coordinates are constructed in such a way that the displacement vector can be described as a linear combination of the respective eigenmodes,

$$\mathbf{u} = \boldsymbol{\varphi}\mathbf{q}(t) = \sum_{n=1}^N \varphi_n q_n(t) \quad (4.10)$$

By substituting Eq. (4.10) into Eq. (4.9), the following matrix eigenvalues problem can be derived according to [23],

$$(\mathbf{k} - \omega_n^2 \mathbf{m}) \varphi_n = \mathbf{0} \quad (4.11)$$

Thus, solving this matrix eigenvalue problem yields the eigenvalues $\omega_n^2 = \frac{k}{m}$, from which the eigenfrequencies are obtained. Thereby, the corresponding eigenmodes can be obtained as eigenvectors.

4.6.2 Modal Dynamics

With the eigenmodes and eigenfrequencies at hand, from above, the solution of the equation of motion (4.5) can be readily obtained. By employing the modal expansion

(4.10), as well as pre-multiplying by Φ^T , Eq. (4.5) becomes

$$\mathbf{M}\ddot{\mathbf{q}} + \mathbf{C}\dot{\mathbf{q}} + \mathbf{K}\mathbf{q} = \mathbf{P}(t) \quad (4.12)$$

where

$$\begin{cases} \mathbf{M} = \Phi^T \mathbf{m} \Phi \\ \mathbf{C} = \Phi^T \mathbf{c} \Phi \\ \mathbf{K} = \Phi^T \mathbf{k} \Phi \\ \mathbf{P}(t) = \Phi^T \mathbf{p}(t) \end{cases} \quad (4.13)$$

The damping matrix is governed by the employed damping model. The *modal damping* model is appropriately employed, defined as the diagonal damping matrix $\text{diag}(2\zeta_n\omega_n M_n)$, where ζ_n is the *modal damping ratio*. Insertion of this into Eq. (4.12) yields an uncoupled system of equation, which is expressed component-wise as

$$M_n \ddot{q}_n + 2M_n \omega_n \zeta_n \dot{q}_n + \omega_n^2 M_n q_n = P_n(t) \quad (4.14)$$

where $n \in [1, N]$ is the number of the respective eigenmodes in the frequency spectrum of interest. In conclusion, a system of uncoupled equations was obtained, characterized by the linearity property and hence the ability to fundamentally express the displacement by using the principle of superposition.

4.6.3 Modal Truncation

Alluding to the superposition principle mentioned before, it is possible to approximate the modal expansion (4.10), by truncating the number of eigenmodes to be included. This can be mathematically formulated as

$$\mathbf{u} = \sum_{n=0}^J \varphi_n q_n \quad (4.15)$$

where $J < N$ denotes the number of eigenmodes to be considered, while N denotes the number of all possible eigenmodes in the dynamical system of interest.

Thus, the size of the system of equations can be reduced drastically, which implies computational efficiency. Note, however, that the truncation may exclude crucial eigenmodes, which may significantly impair the accuracy of the modal analysis. This fact gives rise to the importance of a convergence study, regarding the number of eigenmodes to be included in the truncated modal analysis.

5 Elementary Multidimensional Search

In this chapter, the mathematical theory of the Newton-Raphson method is outlined. The employed method is an extension of the one-dimensional case, which allows for simultaneous optimization of several parameters. Some prerequisites for understanding this method are key concepts from multivariable differential calculus. Furthermore, the numerical treatment of these concepts is also briefly explained. Thus, the subject that concerns optimization in several variables, *multidimensional search*, is conceived, on an elementary level.

5.1 Resumé of Multivariable Differential Calculus

An overview of the essential notions of multivariable differential calculus is provided, in order to facilitate understanding of the Newton-Raphson method.

5.1.1 The Multidimensional space \mathbf{R}^n

An extension of a variable in single-variable calculus is the notion of an *n-tuple* denoted $\mathbf{x} = (x_1, x_2, \dots, x_n)$, with $x_i \in \mathbf{R}$. This is also simply called a *tuple*, where it is understood that that it is of the size n . All such possible tuples make up the real-valued space denoted as \mathbf{R}^n . A tuple is interchangeably called a *point*, in the usual manner. Furthermore, a tuple is conveniently viewed as a *vector*, specifically a *column matrix*,

$$\mathbf{x} = \begin{bmatrix} x_1 \\ x_2 \\ \vdots \\ x_n \end{bmatrix}$$

The arithmetic operations in the space \mathbf{R}^n are performed in the usual manner.

5.1.2 Smoothness

Functions can be classified by the differentiability property. In order to quantify this property, the notion of *smoothness* is introduced. A smooth function is defined as a continuous function with continuous derivatives. In particular, a function can be differentiated several times, inducing a certain *degree of smoothness*. In general terms,

a multivariable function $f : \mathbf{R}^n \rightarrow \mathbf{R}$ that is k -times differentiable, with all partial derivatives being continuous, is said to be of class \mathcal{C}^k . This is denoted as $f \in \mathcal{C}^k(\mathbf{R}^n)$, or more loosely as $f \in \mathcal{C}^k$. Even more loosely, the former notation can be summarized as, a function f being \mathcal{C}^k .

5.1.3 Hessian matrix

Let $f : \mathbf{R}^n \rightarrow \mathbf{R}$ be a twice differentiable function. The Hessian matrix is a generalization of the gradient, a quadratic matrix containing all second-order partial derivatives of the function f computed at a tuple \mathbf{x} . The notation adopted here is

$$\mathbf{H}(\mathbf{x}) = [f_{x_i x_j}(\mathbf{x})] = \begin{bmatrix} f_{x_1 x_1}(\mathbf{x}) & f_{x_1 x_2}(\mathbf{x}) & \cdots & f_{x_1 x_n}(\mathbf{x}) \\ f_{x_2 x_1}(\mathbf{x}) & f_{x_2 x_2}(\mathbf{x}) & \cdots & f_{x_2 x_n}(\mathbf{x}) \\ \vdots & \vdots & \ddots & \vdots \\ f_{x_n x_1}(\mathbf{x}) & f_{x_n x_2}(\mathbf{x}) & \cdots & f_{x_n x_n}(\mathbf{x}) \end{bmatrix}$$

By requiring that $f \in \mathcal{C}^2$, i.e., that all second-order partial derivatives are continuous, the mixed second partial derivatives become symmetric and thus follows the symmetry of the Hessian matrix.

5.1.4 Quadratic functions

In general, a *quadratic function* is defined as a real-valued function on \mathbf{R}^n of the form

$$q(\mathbf{x}) = \frac{1}{2} \mathbf{x}^T \mathbf{A} \mathbf{x} + \mathbf{b}^T \mathbf{x} + \text{const.}$$

where \mathbf{A} is an $n \times n$ and \mathbf{b} an $n \times 1$ arbitrary matrix, respectively. A quadratic function describes a *manifold* in the space \mathbf{R}^n . Restricting the space to \mathbf{R}^3 , the manifold described degenerates to a surface in three dimensions. Note that the constant only translates the manifold, or surface, and can therefore be ignored. Moreover, a second order term is called a *quadratic form*, denoted as $\mathbf{x}^T \mathbf{A} \mathbf{x}$, up to a scaling factor.

In order to facilitate lucid explanations further on, a definition regarding quadratic forms is in place. Assume first that the quadratic matrix \mathbf{A} is symmetric. If $\mathbf{x}^T \mathbf{A} \mathbf{x} > 0$ for all $\mathbf{x} \neq \mathbf{0}$, then the quadratic matrix is designated as *positive definite*. If the inequality sign is reversed, the designation becomes *negative definite*.

5.1.5 Taylor's Formula

Taylor's formula describes the *Taylor expansion* about a point $\mathbf{a} \in \mathbf{R}^n$. The Taylor expansion in the one-dimensional case approximates a function locally by fitting a *tangent polynomial*, the Taylor polynomial, to the function in the desired neighbourhood.

The Taylor polynomial enfolds the function of interest in larger neighbourhoods, with higher order of the former. In the multivariable case, the Taylor expansion generalizes the concept of tangent polynomials to higher dimensions. A Taylor expansion performed in the two-dimensional space generates a *tangent surface*. As before, the extent of enfolding is governed by the order of the Taylor expansion. In matrix notation, Taylor's formula, of the second order, is formulated for the space \mathbf{R}^n as

$$f(\mathbf{x}) = f(\mathbf{a}) + \nabla f(\mathbf{a})^T (\mathbf{x} - \mathbf{a}) + \frac{1}{2} (\mathbf{x} - \mathbf{a})^T \mathbf{H}(\mathbf{a}) (\mathbf{x} - \mathbf{a}) + \mathcal{O}(\|\mathbf{x} - \mathbf{a}\|^3)$$

where $\mathcal{O}(t)$, with the property that $\lim_{t \rightarrow 0} \frac{\mathcal{O}(t)}{t} = 0$, is used to denote the error term.

5.1.6 Optimization

Usually, optimization problems can be characterized as finding a point that is either a *minimum* or a *maximum*, collectively called *extremum*. A function $f : \mathbf{R}^n \rightarrow \mathbf{R}$ to be optimized is called the *objective function*. The objective function is usually subjected to some specified conditions, *constraints*. Any point $\bar{\mathbf{x}} \in \mathbf{R}^n$ that satisfy $\nabla f(\bar{\mathbf{x}}) = \mathbf{0}$ is called a *stationary point*. Any stationary point that satisfies the constraints is called a *feasible solution*.

There exist certain procedures in order to quantify if a certain point of interest is a minimum or maximum. In single-variable calculus, the derivative test is employed. This test consists of tabulating the signs, positive or negative, of the first and second derivatives of the function of interest, in a neighbourhood of the point of interest. Based on these signs, a conclusion is drawn about whether the certain point of interest is a minimum or maximum. This concept is generalized in multivariable calculus, whereby the Hessian matrix, containing all second-order derivatives, is of central importance.

In particular, if the Hessian matrix computed at a certain point of interest is positive definite, then that point of interest is a minimum. In the same light, negative definiteness would imply a maximum. These conditions assume that the Hessian matrix is symmetric, which is the case if the objective function is \mathcal{C}^2 .

5.2 Newton-Raphson's Method

The Newton-Raphson scheme is outlined here for the generalized multivariable case.

5.2.1 Principle of Newton-Raphson's Method

The principle behind Newton-Raphson's method is to generate a sequence $\{\mathbf{x}_k\}_1^\infty$ of points that converge to a stationary point $\bar{\mathbf{x}}$. The fundamental idea is to apply Taylor's formula and locally approximate the function of interest, in a neighbourhood to the actual stationary point $\bar{\mathbf{x}}$. This approximation is then set to be the objective function,

facilitating facile search for a stationary point. Thus, a stationary point is sought, such that the approximation coincides with the actual stationary point, up to some specified degree of error. Thereby, a feasible solution is found.

5.2.2 Multidimensional Newton-Raphson Scheme

Consider a function $f \in \mathcal{C}^2(\mathbf{R}^n)$. By Taylor's formula, the function f can be approximated locally to a point \mathbf{x}_k , by a quadratic function

$$f_{app}(\mathbf{x}) = f(\mathbf{x}_k) + \nabla f(\mathbf{x}_k)^T (\mathbf{x} - \mathbf{x}_k) + \frac{1}{2} (\mathbf{x} - \mathbf{x}_k)^T \mathbf{H}(\mathbf{x}_k) (\mathbf{x} - \mathbf{x}_k)$$

where the Hessian matrix \mathbf{H} of the function f is computed at \mathbf{x}_k . Whenever this matrix is positive or negative definite, a stationary point exists in which the equation of stationarity $\nabla f_{app}(\mathbf{x}) = \mathbf{0}$ is fulfilled. Hence,

$$\begin{aligned} \nabla f_{app}(\mathbf{x}) = \mathbf{0} &\iff \nabla f(\mathbf{x}_k) + \mathbf{H}(\mathbf{x}_k) (\mathbf{x} - \mathbf{x}_k) = \mathbf{0} \\ &\iff \mathbf{x} = \mathbf{x}_k - \mathbf{H}(\mathbf{x}_k)^{-1} \nabla f(\mathbf{x}_k). \end{aligned}$$

By defining the root of the equation of stationarity as

$$\mathbf{x}_{k+1} = \mathbf{x}_k - \mathbf{H}(\mathbf{x}_k)^{-1} \nabla f(\mathbf{x}_k),$$

a recursion formula is obtained. An initial guess, \mathbf{x}_1 , that is close enough to the true stationary point, is required in order to construct the convergent sequence $\{\mathbf{x}_k\}_1^\infty$. Observe that the Hessian matrix, computed at \mathbf{x}_k , is also required to be *invertible*. This requirement is fulfilled whenever the Hessian matrix is either positive or negative definite. Otherwise, Newton-Raphson's method will not work.

5.3 Numerical Treatment

In this section, the analytical methods are tailored for numerical treatment. This is topical, if only numerical values are available, which calls for expedient derivative formulations. An encompassing numerical scheme is the well-known *Newmark's method*, which forms the basis for the numerical derivative formula, the well-known *central difference formula*.

5.3.1 Newmark's Method

Newmark's method is a procedure, specifically developed to solve the system of second-order ordinary differential equations [24]. Thus, this method is suitable to solve the system of differential equations that arises from structural dynamical systems. The idea is to turn the system of differential equations, to be solved, into a system of algebraic equations.

Structural dynamic systems are time-dependent, whereby the time-domain is partitioned into time increments. Thus, the velocity and displacement can be determined for each time increment, hence being a time-stepping method. Consider the MDOF equation of motion in matrix form,

$$\mathbf{M}\ddot{\mathbf{u}} + \mathbf{C}\dot{\mathbf{u}} + \mathbf{K}\mathbf{u} = \mathbf{f}(t) \quad (5.1)$$

along with the boundary conditions

$$\begin{cases} \mathbf{u}_0 = \mathbf{u}(0) \\ \dot{\mathbf{u}}_0 = \dot{\mathbf{u}}(0) \end{cases} \quad (5.2)$$

By Newmark's method, the velocity and displacement are obtained as

$$\begin{cases} \dot{\mathbf{u}}_{n+1} = \dot{\mathbf{u}}_n + (1 - \gamma) \Delta t \ddot{\mathbf{u}}_n + \gamma \Delta t \ddot{\mathbf{u}}_{n+1} \\ \mathbf{u}_{n+1} = \mathbf{u}_n + \Delta t \dot{\mathbf{u}}_n + (\Delta t)^2 \left(\frac{1}{2} - \beta\right) \ddot{\mathbf{u}}_n + (\Delta t)^2 \beta \ddot{\mathbf{u}}_{n+1} \end{cases} \quad (5.3)$$

where Δt is the time-increment, and the parameters β, γ dictates the variation of the acceleration within a time-increment. The choice of these parameters determines the *numerical stability*, as well as accuracy of Newmark's method. The former refers to the property that numerical errors do not grow and propagate uncontrollably, otherwise rendering the solution useless.

5.3.2 Central Difference Formula

The central difference formula is an appropriate numerical formulation of the derivative. It is derived from Newmark's method, by setting the parameters to $\beta = 0$ and $\gamma = \frac{1}{2}$, yielding

$$\begin{cases} \dot{\mathbf{u}}_n = (\mathbf{u}_{n+1} - \mathbf{u}_{n-1}) / (2\Delta t) \\ \ddot{\mathbf{u}}_n = (\mathbf{u}_{n+1} - 2\mathbf{u}_n + \mathbf{u}_{n-1}) / (\Delta t)^2 \end{cases} \quad (5.4)$$

These formulations can be interpreted as a numerical definition of the first and second derivative, which are employed in the numerical algorithm of the Newton-Raphson's method.

6 Finite Element Models

In this chapter, a description of how the FE-models were established using the commercial software Abaqus, supplied with a general description of the procedure thereto. These FE-models were used in the subsequent analyses, comprising simple frequency sweeps, as well as more intricate steady-state analyses. Additionally, the procedure of mesh convergence analyses is treated.

6.1 Establishing the FE-models

The FE-models considered are all created in a similar fashion, by first defining a single solid part, extruded to the desired thickness of the CLT-plate. Then, the CLT layers are defined by partitioning the single solid part into the sought amount of layers. Such a model was used in the calibration of the material parameters, cf. Figure 6.1.

Additionally, material orientations are defined in order to account for the different in-plane orthogonal orientation between the respective layers, cf. Figure 2.1. Finally, the layers are partitioned into individual lamellae, cf. Figure 6.2, which is the model used to conduct the case study, providing full interaction between the individual layers, as well as the lamellae therein.

6.2 Material model

The material model for timber materials is suitably chosen as orthotropic. In reality, each individual lamella has a unique set of material parameters. This stems from the fact that timber exhibits considerable variability with respect to measurable material parameters, noted in Chapter 3. Furthermore, the lamellae have their own unique material orientation, predominantly due to the manufacturing process, where different

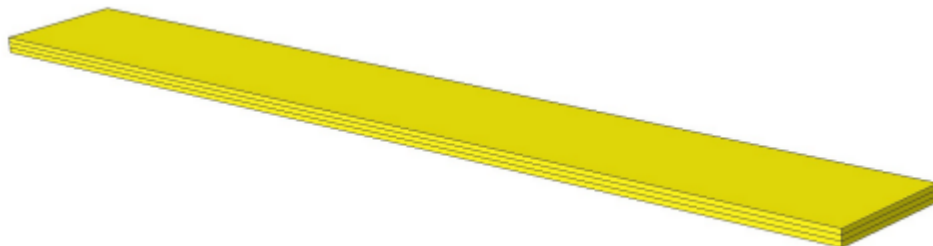


Figure 6.1: Layer partitioned FE-model of the CLT-plate, used for the calibrations.

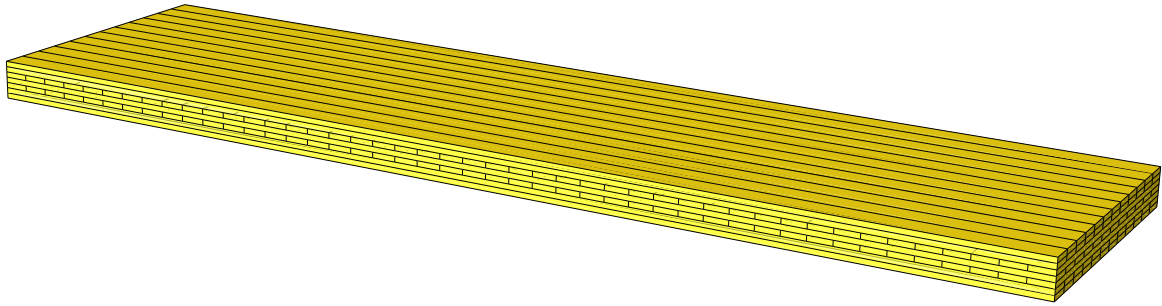


Figure 6.2: Fully partitioned FE-model of the CLT-plate, used for conducting the case study.

lamellae are sawn from different parts of tree trunks.

However, as an approximation, these discrepancies are considered to be smoothed out in the complete model of the CLT-plate. Specifically, each considered layer in the CLT-plate will be assigned appropriate material orientation. As stated in Chapter 3, the material properties in the radial and tangential were direction modelled as equal.

6.3 Element Mesh

The element type used for the mesh is a modified version of the solid elements, the so-called continuum solid shell elements. This type of element behaves in a similar manner to a conventional shell element, although it is still a solid volume element. Using the continuum solid shell element is especially convenient since it has reduced amount of degrees of freedom, in contrast to the conventional shell element. Hence, the computational cost is decreased which facilitates efficient execution of parameter studies.

6.4 Boundary Conditions

The boundary conditions dictate the behaviour of the structure, and is supposed to simulate the actual structural set-up. The laboratory experiment, as will be explained in Chapter 8.1, has been based on the CLT-plate suspended by rubber bands, that do not constrain the CLT-plate in any direction with respect to vibrational movement. This is modelled with free-free boundary condition.

Free-Free Boundary Condition

The free-free boundary condition is a fundamental concept in structural dynamics and finite element analysis, representing a scenario where a structure is unconstrained at both ends. In this configuration, the structure is allowed to move and deform freely without any external restrictions or support. This condition is particularly relevant in vibration analysis and modal analysis, where it enables the determination of the natural frequencies and mode shapes of a structure.

Imposing the free-free boundary condition facilitates the study of the intrinsic dynamic behavior of a system, unaffected by external influences such as fixed supports or constraints. Although, this boundary condition is not realistic as structures are almost always constrained to some degree. Furthermore, CLT-plates are usually used as floor panels, interacting with other structural elements, that would have an effect on the dynamical behaviour. However, in the context of this dissertation, modeling and analysing the dynamical behaviour of the various CLT-configurations, the free-free boundary condition was deemed adequate and used for all performed analyses.

6.5 Mesh Convergence Study

A convergence study of the element mesh is duly performed in order to obtain a computationally sound FE-model. Too fine of a mesh in the FE-model certainly yields accurate results, however at a heavy cost of computational resources. Conversely, too coarse of a mesh would certainly come at a lower computational cost, however with a loss of accuracy in the results. Thereby, a balance is sought between the accuracy of the FE-model and the computational cost. This is achieved by studying the behavior of the FE-results with respect to the mesh size.

7 Methods of Evaluation

7.1 FE-model Validation

In this section, an encompassing validation approach will be adopted, whereby the validation of the FE-models against experimental results is described. This entails validating correct FE-models, amounting to a comparison between the results obtained from the FE-model with the results obtained from the experimental testing. The comparison is made with respect to suitable metrics.

However, due to the variability of timber material properties, calibrations of the material parameters are in order. The calibrations are to be performed against experimental results presented in Section 8.1. The calibrations are preceded by a sensitivity analysis determining the material parameters to be calibrated.

7.1.1 Sensitivity Analysis

A sensitivity analysis entails the investigation of the interplay between the material parameters and the modal behaviour of the CLT-plate. This is performed in order to identify the material parameters that dominates the modal behaviour, whereby the total number of material parameters to be calibrated is reduced.

The metric used in the sensitivity analysis is the *Normalized Relative Frequency Difference* (NRFD), defined as

$$\text{NRFD} = \frac{f_{n,i,\text{FE}} - f_{n,i,\text{Exp}}}{f_{n,i,\text{Exp}}} \quad (7.1)$$

where $f_{n,i,\text{FE}}$ and $f_{n,i,\text{Exp}}$ are defined as the natural frequencies corresponding to the i :th eigenmode of the FE-model and the experimental model, respectively. This metric facilitates concise and easily manageable comparisons between experimental models and FE-models.

7.1.2 Calibrations of Material Parameters

Due to the variability of timber, the material parameters thereto are not well defined. Instead, they span a range of values following a statistical spread.

Thus, a calibration of material parameters is in order. In essence, the calibration to be performed constitutes mathematical optimization of the material parameters, where an initial guess of material parameters is done on the basis of existing literat-

ure. Thereafter, an optimization algorithm is employed, specifically the well-known Newton-Raphson method.

The optimization criterions commonly used in the literature are NTFD and the *Modal Assurance Criterion* (MAC). The MAC can be used to compare two mode shapes and attain a statistical indication of their conformity. As a statistical indicator, the MAC is relatively insensitive to small discrepancies in the mode shapes, while being more sensitive to large discrepancies thereby. The MAC can be defined as the square of the inner product of the mode shapes to be compared, normalized with their respective norms,

$$\text{MAC} = \left(\frac{|\Phi_{\text{FE},i} \cdot \Phi_{\text{Exp},j}|}{\|\Phi_{\text{FE},i}\| \|\Phi_{\text{Exp},j}\|} \right)^2 \quad (7.2)$$

where Φ denotes a mode shape in vector form, and the indices i, j denotes the respective mode shapes pertaining to the two models of interest, namely the FE-model and the experimental model. Therefore, the MAC takes on values between 0 and 1, where values close to unity implies consistent mode shapes whereas values close to zero implies non-consistent mode shapes. In particular, the term CrossMAC is used when referring to the MAC value of eigenmodes in different sets. In this case, the FE-model constitutes one set while the experimental model constitutes another set. In contrast, the term AutoMAC refers to the MAC value of eigenmodes of the same set.

7.2 Evaluating metrics

In this section, methods used to assess and evaluate the results are presented.

7.2.1 Root Mean Square

A frequency analysis contains numerous values that are displayed with their corresponding frequency in a plotted diagram. In some cases, it might be beneficial to simplify the response to a single value. The simplest form is to take the mean value of a set of values. The root mean square is another, which can be described as the square root of the mean of the squares of a set of values. The equation is displayed in equation (7.4).

$$x_{\text{mean}} = \frac{1}{n} \sum_{i=1}^n x_i \quad (7.3)$$

$$x_{\text{RMS}} = \sqrt{\frac{1}{n} \sum_{i=1}^n x_i^2} \quad (7.4)$$

7.2.2 Frequency Response Functions

Frequency response functions (FRFs) are an essential tool in analysing the dynamic behavior of systems across a range of frequencies [25]. FRFs allow analysis in the frequency domain instead of the time domain and consist of an input and output signal.

In this master's dissertation, a force is to be applied to CLT-panels and the response is to be measured as acceleration. The relation between these two signals is called accelerance, as seen in Eq. 7.5, with \mathbf{A} being accelerance, \mathbf{a} acceleration and \mathbf{F} the force.

$$\mathbf{A}(\omega) = \mathbf{a}(\omega)/\mathbf{F}(\omega) \quad (7.5)$$

If the force applied is a unit force, the acceleration measured is equal to the accelerance.

7.2.3 Third-octave Band Filter

Upon conducting a frequency analysis studying the signal response over a frequency range, simplifications can be made to the curve. Third-octave band filter is one of said simplifications, where standardized center frequencies are used to divide the frequency axis into multiple band filters. Table 7.1 presents the band numbers 1 to 30 for the third octave band filter.

Table 7.1: Third-octave band filter, frequencies in Hz [25].

Band number	1	2	3	4	5	6	7	8	9	10
Center frequency, f_c	1.25	1.6	2	2.5	3.15	4	5	6.3	8	10
Lower band filter, f_l	1.12	1.41	1.78	2.24	2.82	3.55	4.47	5.62	7.08	8.91
Upper band filter, f_u	1.41	1.78	2.24	2.82	3.55	4.47	5.62	7.08	8.91	11.2
	11	12	13	14	15	16	17	18	19	20
Center frequency, f_c	12.5	16	20	25	31.5	40	50	63	80	100
Lower band filter, f_l	11.2	14.1	17.8	22.4	28.2	35.5	44.7	56.2	70.8	89.1
Upper band filter, f_u	14.1	17.8	22.4	28.2	35.5	44.7	56.2	70.8	89.1	112
	21	22	23	24	25	26	27	28	29	30
Center frequency, f_c	125	160	200	250	315	400	500	630	800	1000
Lower band filter, f_l	112	141	178	224	282	355	447	562	708	891
Upper band filter, f_u	141	178	224	282	355	447	562	708	891	1120

8 Model Calibration

In this chapter the mechanical properties of each material are analysed by a sensitivity analysis, followed by calibration of the material parameters with the most influence on the dynamic behaviour of the CLT-panels. Furthermore, a validation approach will be outlined. In this context, a validation entails the assurance of the veracity of the employed model.

8.1 Experiment

In the following chapter, an experiment performed by Fredrik Ljunggren at LTU is to be presented in brief terms, for more in-depth reading the reader is referred to [8]. The results of the experiment are to be used as reference when calibrating the material parameters used in this dissertation.

The aforementioned experiment was conducted in order to determine the mechanical properties of spruce (C24), densified spruce (C24) and birch. The measurements were taken during his thesis "Innovative solutions to improved sound insulation of CLT floors"

The experiment set-up is displayed in Figure 8.1, with the shorter sides of the CLT-panel suspended with elastic straps to simulate free-free conditions. The panel was excited by a randomized noise signal fed into an electromagnetic shaker. The initial force and the resulting acceleration were measured with an impedance head.

The panels in the experiment had a width of 0.5 m and length of either 2.4 m or 4 m, see Figure 8.2. The response was measured by accelerometers, a total of 21 and 27 accelerometers were used, respectively. All CLT-panels had a thickness of 60 mm. All panels were constructed with three layers, the outer layers oriented in the longitudinal direction and the middle layer rotated 90 degrees.

The experiment resulted in the natural frequencies being determined for the first five eigenmodes. The mode shapes of the first five eigenmodes can be seen in Figure 8.3.



Figure 8.1: Setup used in experiment [8].

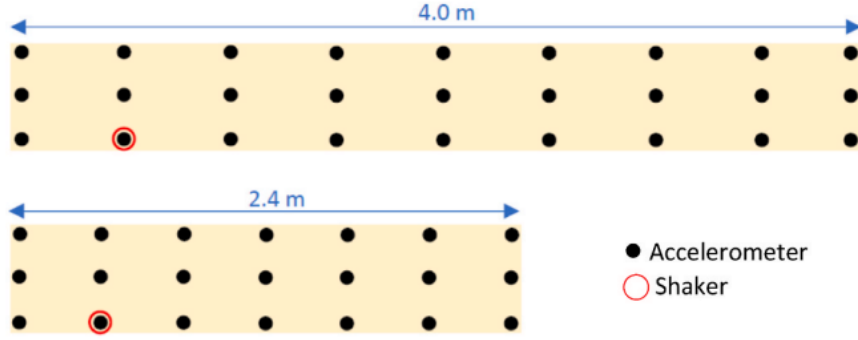


Figure 8.2: Position of measure points used in experiment [8].

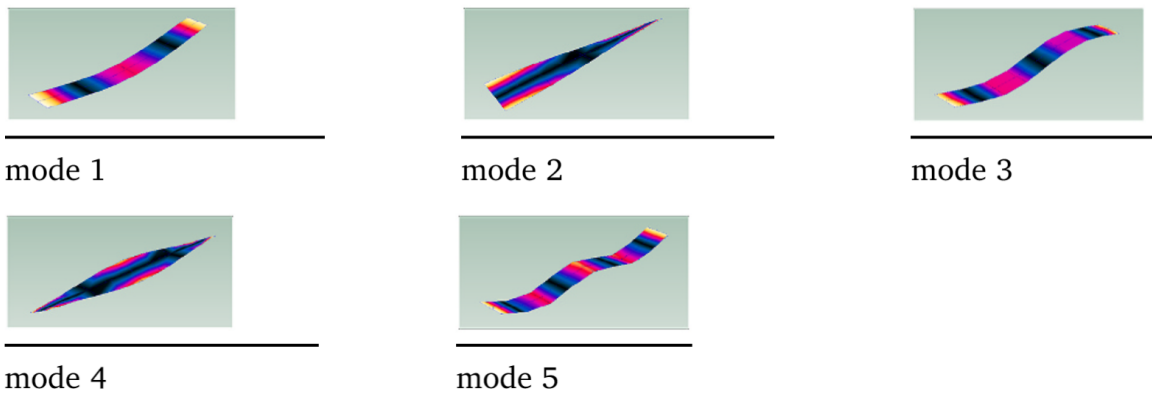


Figure 8.3: Mode shapes obtained by experiment [8].

Table 8.1: Mean natural frequency f_i [Hz], damping ratio ζ [%] and mean density ρ [kg/m³] for spruce, birch and densified spruce.

Material	f_1	f_2	f_3	f_4	f_5	ζ	ρ
Spruce, 4 m	19.7	32.4	52.1	67	98.7	0.69	428
Birch, 4 m	18.1	33.2	49.8	69.3	94.5	0.74	606
Densified spruce, 2.4 m	43.4	68.9	111	138	202.5	1.19	787

A total of 16 CLT-panels were constructed in spruce with the length 4 meters and thickness 60 mm. Four panels with the same dimensions were constructed in birch. CLT-panels of densified spruce were constructed with the length 2.4 meters.

The natural frequencies and damping ratios were determined for the first five modes. In Table 8.1, the mean values for each mode can be viewed for all materials. For spruce, all 16 panels were used. For birch, panel “Birch #4” was excluded due to showing significant deviation from the rest, and thus considered as an outlier. For densified spruce, both tests were used in calculating the mean values. The last columns contain the mean damping ratio for all modes as well as the mean density for each material.

8.2 Outline of Validation Approach

The encompassing validation approach is performed in according to [26]. This approach is necessitated by the importance of accurate mathematical and physical modeling, requiring a high degree of reliability. A summary is given below in a step-wise manner.

Step 1. Specification of the model use, purpose and decisions to be made

The model is developed for a specific application, pertaining to the physical system of interest and the reigning conditions thereof. Therefore, achieving a computational model that is consistent with the physical model, requires well-defined purposes regarding the use of the model. These purposes have been laid out in Chapter 1. That is, analysing and evaluating the structural dynamical behaviour of the CLT-panels.

Step 2. Specification of validation experiments

Validation experiments are due to generate sufficient data to be compared against the model. Emphasis is on using experiments that are in line with the purpose of the computational model, and consistent with the physical model. The validation experiments are presented in Chapter 2.1. Therein, frequency-sweeps have been performed, yielding a set of natural frequencies and damping ratios corresponding to first five mode shapes.

Step 3. Specification of the conceptual model

The conceptual model consists of the descriptions of the physical processes, governing the behaviour of the system therein, supplied with the adopted set of assumptions. The foregoing has been covered in Chapters 1 and 6, however, a summary is given below:

- The wood material behaviour was assumed to be completely linear-elastic.
- The wood material model was assumed to be orthotropic.
- The CLT-panel was approximated to be homogeneous, disregarding the individual lamellae material variability.

Step 4. Specification of the mathematical model

The mathematical model acts as a prelude for the computational model. Furthermore, the mathematical model needs to encapsulate the physical system of interest, taking

into account the conceptual model in a suitable manner. Thus, the mathematical model employed was the system of MDOF equation of motion. That is, a system of second-order linear ordinary differential equations, modeling structural dynamical behaviour, as is described in Chapter 4. Thereby, the equations of motion act as a general setting, in which the adopted assumptions are catered to.

Step 5. Specification of the computational model

The computational model equates to a numerical computational framework, specifically tailored for the implementation of the mathematical model of interest. As the latter constitutes a system of differential equations, the finite element method was suitable deployed as the computational model. The finite element method is introduced in [27] and the finite element model is presented in Chapter 6.

Step 6. Specification of the physical system response measures of interest

The response measures of the physical system are physical quantities of interest that are to be measured. Usually, the acceleration response is to be measured, however, due to the nature of the reference lab experiment, the eigenmodes of the CLT-panels and their corresponding natural frequencies were set as the response measures.

Step 7. Specification of the validation metrics

Validation metrics are mathematical formulations that serve the purpose of comparing the experimental results against the model results. The metrics deployed in this case pertain to the respective response measures. Regarding the mode shapes, the MAC is used as a validation metric, while NRFD is used for the natural frequencies, as explained in Chapter 7.

Step 8. Specification of the domain of comparison

The domain of comparison entails the spectrum of interest with respect to the response measures. That is, for the eigenmodes, the domain was chosen in accordance with the reference lab experiment to the first five eigenmodes. However, the frequency range was determined by the need to capture the relevant vibro-acoustic phenomena. The frequency range of interest was determined to be 0-562 Hz. The details thereof are presented in Chapter 9.

Step 9. Specification of the calibration experiments

Calibration experiments differ from validation experiments in the sense that the former is in order to identify the relevant parameters to be used in the model. Thereby,

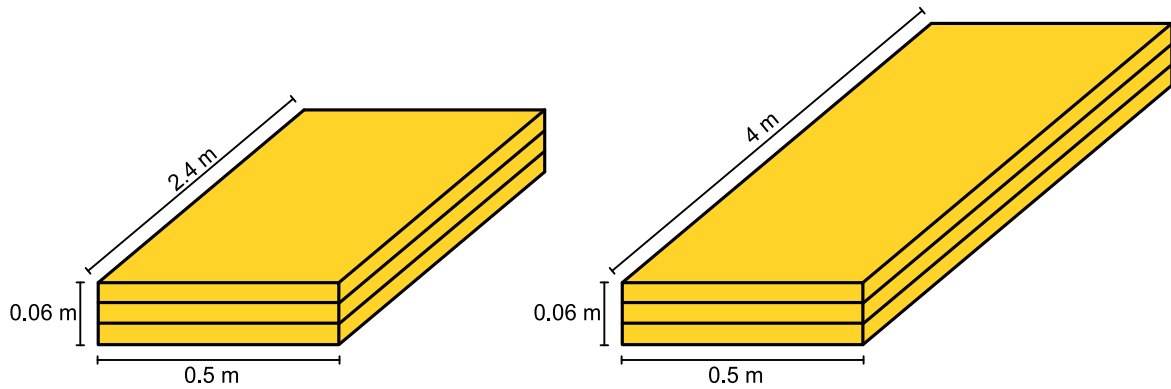


Figure 8.4: The different sized models, layered.

the relevant parameters in the model are calibrated to the parameters used in the validation experiment. Hence, a model is obtained that is in line with the physical system. The calibration experiments consist of sensitivity analyses, identifying relevant material parameters, as is to be explained further on in this chapter. Thereafter, an optimization algorithm is utilized, calibrating the initial set of model parameters towards the true set of parameters in the validation experiment. This is explained in Chapter 5 .

Step 10. Specification of the adequacy criterions

The adequacy criterions are requirements imposed on the validation metrics, in order to determine the level of fidelity of the model. It is desired to obtain a model that is as accurate as possible. However, this comes at a heavy computational cost and thus computational time, a detriment to the efficiency of the model. Therefore, a balance is sought between the accuracy and the efficiency of the model. This is explained in Chapter 6.

8.3 FE-model

In order to calibrate the mechanical properties of the materials, FE-models in Abaqus were created. The dimensions used were identical to those presented in Chapter 8.1. Two different CLT-panels were created, with the width 0.5 m, thickness 0.06 m and the lengths 2.4 m and 4 m, respectively. Both panels were created with three layers, the middle one rotated orthogonal to the two outer layers, which were oriented in the longitudinal direction.

The model used in Abaqus was the so-called layered model, where the CLT-plate have been partitioned into layers, cf. Figure 6.1. Notably, it was not necessary to divide each layer into lamellae in the computer model, which follows from the homogeneity of the CLT-plate used in the experiment.

As explained in Chapter 6, a mesh convergence study is necessary in order to achieve

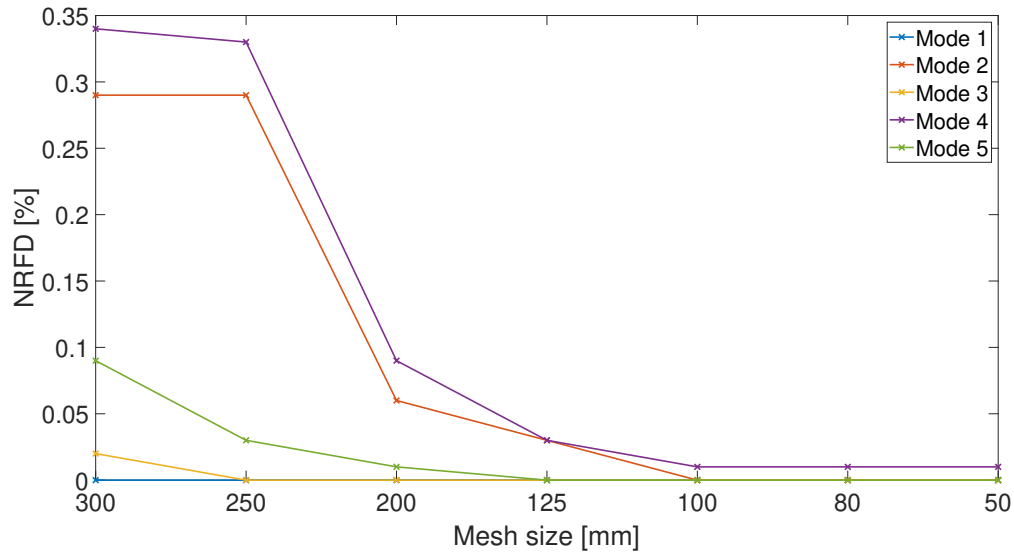


Figure 8.5: Mesh convergence for CLT-panel with length 4 m.

an efficient and accurate FE-model. For the larger plate, the natural frequency for the first five eigenmodes were determined for eight different meshes. The smallest mesh was 36 mm used as a reference value when noting the deviation for each mesh size larger. The other mesh sizes can be seen in Figure 8.5, with the corresponding NRFD-values to each eigenmode.

In Figure 8.5, the variation at an element size of 200 mm is deemed sufficiently small and used for the following sensitivity analysis and material parameter calibration. The larger panel is to be used for both spruce and birch.

In similar fashion as the 4 m long CLT-panel, a mesh convergence study was performed on the CLT-panel with a length of 2.4 m. Only six different mesh sizes were used in the study, with 30 mm as the smallest. The results are presented in the same manner as for the larger CLT-panel, in Figure 8.6.

In Figure 8.6, the variation at an element size of 100 mm is deemed accurate and will be used in further studies. The smaller CLT-panel is to be used for densified spruce, and the element type used for both panels are Solid 3D elements.

8.4 Model Calibration

This section covers the calibration of the material parameters used in the finite element model, for all three materials, divided into three steps. Firstly, a sensitivity analysis is performed on each individual material parameter, followed by the determination of initial values for the Newton optimisation. Finally, Newton optimisation is performed on the necessary material parameters.

The Python script used for performing the Newton optimisation was provided by Johannes Jonasson, based upon his work conducted in [2] and [28].

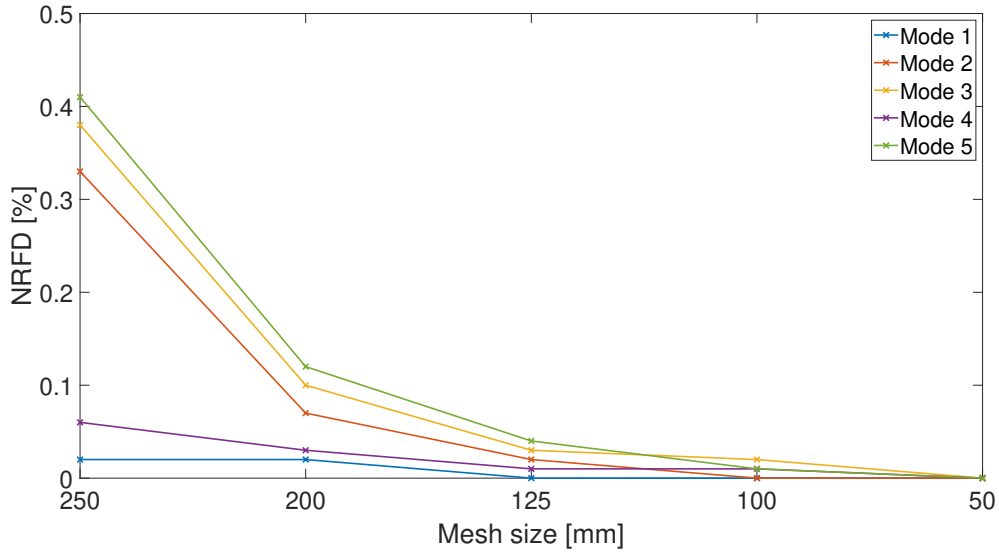


Figure 8.6: Mesh convergence for CLT-panel with length 2.4 m.

8.4.1 Sensitivity Analysis

In order to determine the influence of each material parameter on the modal order and natural frequencies, each parameter was varied individually in the sensitivity analysis. The range used for each material was based upon plausible estimations. The effect on modal order was noted and NTFD-values were calculated to determine the influence of each parameter. The upper and lower limits can be seen in Tables 8.2–8.4. Four values were studied for each parameter, two lower and two higher than the reference value.

For spruce, the range was based upon the parameters found in Table 8.9. With C16 being the lower limit, C40 the upper limit and C24 being the reference value. The ranges used in analysis is presented in Table 8.2.

For birch, the range was based upon a guess that material parameters may vary as much as 25%. Therefore, the upper and lower limits were offset 25% from the reference value, which was determined based upon the findings in Table 3.2. The ranges used in the analysis are presented in Table 8.3.

The set of material parameters of densified spruce are presented in Table 8.4, and is simply a scaled set of the spruce material parameters given in Table 8.2, as was explained in Section 3.1.

Table 8.2: Limits and reference values used for sensitivity analysis on spruce, with moduli in MPa and density in kg/m^3 .

	E_L	E_T	E_R	ν_{LT}	ν_{LR}	ν_{RT}	G_{LT}	G_{LR}	G_{RT}	ρ
Upper limit	14 000	470	470	0.42	0.38	0.34	880	880	62	428
Lower limit	8 000	270	270	0.42	0.38	0.34	500	500	35	428
Ref. value	11 000	370	370	0.42	0.38	0.34	690	690	49	428

Table 8.3: Limits and reference values used for sensitivity analysis for birch, with moduli in MPa and density in kg/m³.

	E_L	E_T	E_R	ν_{LT}	ν_{LR}	ν_{RT}	G_{LT}	G_{LR}	G_{RT}	ρ
Upper limit	18 672	1 156	1 156	0.45	0.43	0.43	1 197	1 197	254	606
Lower limit	11 203	694	694	0.45	0.43	0.43	718	718	153	606
Ref. value	14 938	925	925	0.45	0.43	0.43	958	958	203	606

Table 8.4: Limits and reference values used for sensitivity analysis for densified spruce, with moduli in MPa and density in kg/m³.

	E_L	E_T	E_R	ν_{LT}	ν_{LR}	ν_{RT}	G_{LT}	G_{LR}	G_{RT}	ρ
Upper limit	25 743	864	864	0.42	0.38	0.34	1 618	1 618	114	787
Lower limit	14 710	496	496	0.42	0.38	0.34	919	919	65	787
Ref. value	20 227	680	680	0.42	0.38	0.34	1 269	1 269	90	787

The average densities were known from the reference experiment, presented in Table 8.1 and, as mentioned in Chapter 3, Poisson's ratio has negligible influence on the natural frequencies. Therefore, the aforementioned parameters were not included in the sensitivity analysis.

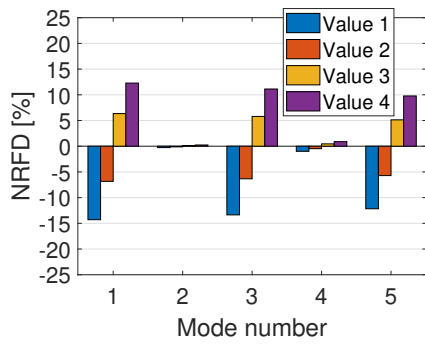
When studying the results of the sensitivity analysis, some variations of parameter values resulted in a change in the modal order for the first five modes. In the results presented in Figures 8.7–8.9, the order was rearranged when necessary, resulting in modes one, three and five being the first three bending modes and modes 2 and 4 being the first two torsional modes. This order similar to the one presented in Figure 8.3. Only the parameters indicating significant influence on the natural frequencies are included in the results.

In Figure 8.7, the resulting NTFD-values from the parameter study are shown for spruce. The parameters that showed significant influence on the natural frequencies were E_L , G_{LT} and G_{RT} . E_L had large influence on the bending modes and insignificant influence on the torsional modes. As an opposite of the longitudinal modulus of elasticity, G_{LT} had insignificant influence on the bending modes and large influence on the torsional modes. The rolling shear modulus, G_{RT} , has less influence per mode, although some notable influence on each eigenmode.

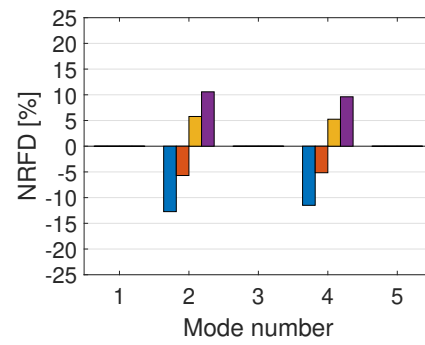
In Figure 8.8, the NTFD-values are shown for birch. In similar fashion as spruce, the parameters of notable influence on the natural frequencies were E_L , G_{LT} and G_{RT} . The longitudinal modulus of elasticity had significant influence on the bending modes and negligible on the torsional modes. G_{LT} showed negligible influence on the bending modes and significant influence on the torsional modes. The rolling shear modulus, G_{RT} , showed minor influence on all of the five first modes.

In Figure 8.9, the NTFD-values are shown for densified spruce. In a similar fashion to both spruce and birch, E_L , G_{LT} and G_{RT} were the parameters with notable influence on the natural frequencies. E_L had significant influence on the bending modes and negligible influence on the torsional modes. G_{LT} showed negligible influence on the

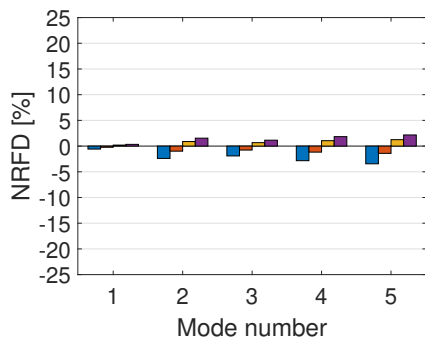
mending modes and significant influence on the torsional modes. The rolling shear modulus, G_{RT} , showed notable influence on all of the five first modes.



(a) E_L

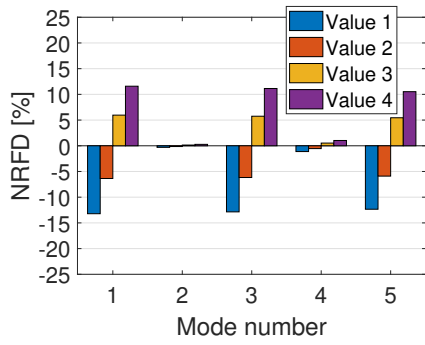


(b) G_{LT}

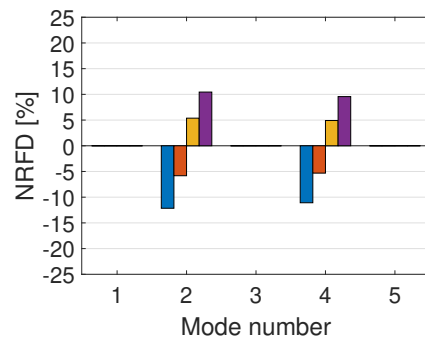


(c) G_{TR}

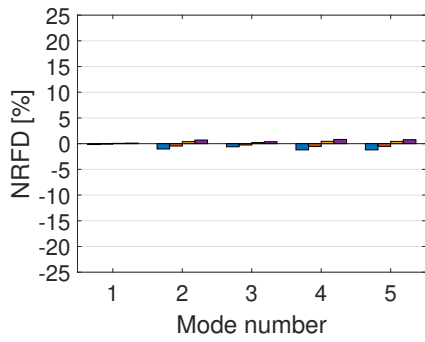
Figure 8.7: Results from the sensitivity analysis performed on spruce.



(a) E_L

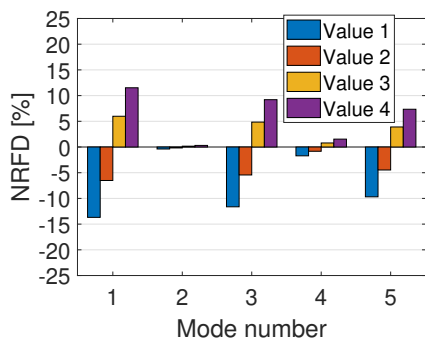


(b) G_{LT}

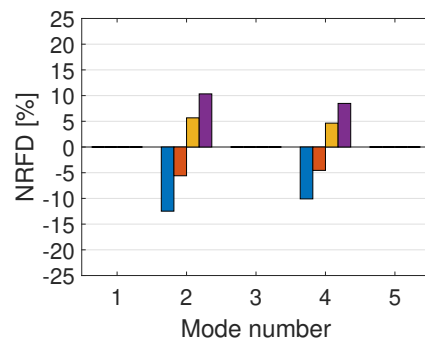


(c) G_{TR}

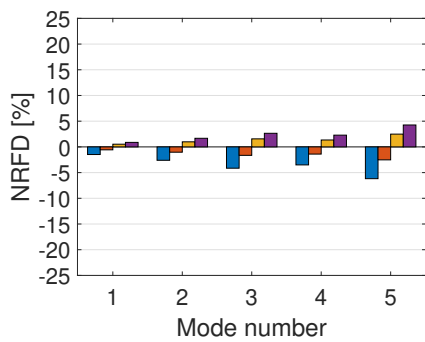
Figure 8.8: Sensitivity analysis for birch.



(a) E_L



(b) G_{LT}



(c) G_{TR}

Figure 8.9: Sensitivity analysis for densified spruce.

8.4.2 Initiation of Newton–Raphson’s Method

The Newton–Raphson’s method is initiated by determining an adequate initial guess of the material parameters. The quality of the initial guess used in Newton–Raphson’s method is crucial for a successful convergence. In order to avoid strenuous methods to determine an appropriate initial guess, literature was used as a reference for the initial guesses for each material, according to Chapter 3.

For spruce, the initial guess was set as the reference value used in Table 8.2, which is the strength class C24 in SS-EN 388:2016 [4]. This guess was used for all calibrations.

For birch, the initial guess was set to the reference value in Table 8.3.

For densified spruce, the initial guess was set according to the reference value in Table 8.4 for calibration 1 and 2. For calibration 3, the initial guess of all elastic moduli was set according to the reference value for spruce in Table 8.2, since the consequences of the densification of the spruce were unclear.

8.4.3 Calibration of Material Parameters

Different calibration tests were performed for each material, and each test is explained individually in the following subsections.

The method used for calibrating the material parameters was Newton–Raphson’s method, as briefly explained in Chapter 5. The Newton–Raphson’s method is an iterative method and, in each iteration, the mode shapes simulated in Abaqus were matched to the modes shapes obtained from the experiment, presented in Chapter 8.1. This was achieved by utilizing CrossMACs, Eq. (7.2), as explained in Section 7.1.2. The lower limit allowed for the CrossMACs was 0.85 during all iterations. Due to limited access to the experiment presented in Chapter 8.1, the mode shapes used as reference for the experiments were obtained from Abaqus prior to the calibration runs. The way the calibration is performed requires two parameters to be calibrated simultaneously, whereby Newton–Raphson’s method proves to be advantageous.

The results of the performed calibrations will be compared to the natural frequencies obtained from the experiment, presented in Table 8.1.

Calibration of Spruce

A total of five calibration tests were performed for spruce. The parameters included in the calibration runs were the ones with the most influence on the natural frequencies, according to Chapter 8.4.1. All five calibration tests had C24 as the initial guess, as mentioned in Chapter 8.4.2.

Calibration 1 was run in two steps, first E_L and G_{RT} were calibrated, followed by G_{LT} and G_{RT} . All five eigenmodes were included in the function.

Calibration 2 was only run in one step, with E_L and G_{LT} being calibrated due to their high influence on the natural frequencies.

Calibration 3 was run in two steps, with E_L and G_{RT} run first due to their high influence on the first three bending modes followed by G_{LT} and G_{RT} due to their high influence on the torsional modes. In the first step, only bending modes were included, modes 1, 3 and 5, and in the second step, only torsional modes were included, modes 2 and 4.

Calibration 4 was run in in two steps, in the same manner as calibration 3 with the steps in reverse order.

Calibration 5 was run in three steps, in step one E_L and G_{LT} were calibrated, followed by G_{LT} and G_{RT} and finally E_L and G_{RT} were adjusted. All five modes were used in the objective function for all runs.

More runs using three steps were performed, although calibration 5 had the lowest mean of averaged NRFD-values and is thus the only one presented.

In Table 8.5, the initial guesses for all the calibrations are presented together with the resulting parameters after the calibrations. The inputs and the results for each round of calibration are highlighted in bold text. The last row in the table shows the results from calibration 5, rounded to two significant numbers.

In Figure 8.10, the results from the calibrations can be seen as NRFD-values averaged over the modes, compared to the natural frequencies obtained from the experiment. Calibration 5 is a combination of Calibrations 1 and 2 and achieved the lowest average deviation from the reference values. Subsequently, the results from Calibrations 3 and 4 were averaged, due to the variation of G_{RT} between roughly 40 and 80 MPa. This variation depended on the order in which the parameters were calibrated, which is the only difference between the two calibrations. The results of Calibration 5 were reduced to two significant figures, as presented in Table 8.5.

Calibration 5 showed significant lower NRFD values than the other calibration, with an average of 0.6%. The material parameters are deemed as reasonable since both E_L and G_{RT} increased above the initial guess of C24. The value of G_{LT} decreased with the calibration, which follows the trend with all other calibrations as well. When the results of the calibration were rounded to 2 significant numbers, the average NRFD increased to 0.7%. When rounding the parameters, the shear moduli G_{LR} and G_{LT} , were set to the same value, as mentioned in Chapter 6.

Both Calibration 3 and 4 utilized fitting parameters solely to modes they had high influence on. This method resulted in the biggest average deviation according to NRFD and is deemed an ineffective method of calibrating material parameters.

Calibration of Birch

Based upon the sensitivity analysis presented in Figure 8.8, the parameters with the most influence on the natural frequencies are E_L and G_{LT} , with G_{RT} showing some minimal influence as well. Multiple calibrations were tested, although only the presented calibration was able to run without one of the parameters increasing towards infinity or becoming negative. The initial guess is based upon the literature review presented previously, as mentioned in Section 8.4.2.

Calibration 1 was run in three steps, in step one E_L and G_{LT} were calibrated, followed by G_{LT} and G_{RT} and finally E_L and G_{RT} were adjusted. All five modes were used in the objective function for all runs. This calibration is identical to Calibration 5 for spruce.

In Table 8.6, the initial guesses as well as the calibrated parameter values are presented. The calibrated parameters of each round are highlighted in bold. The last row in the table shows the results from round 2, rounded to two significant figures.

Table 8.5: Calibration of spruce material parameters.

	E_L	E_T	E_R	G_{LT}	G_{LR}	G_{RT}	ρ
Calibration 1, round 1, initial guess	11 000	370	370	690	690	49	428
Calibration 1, round 1, results	12 800	370	370	690	690	36.3	428
Calibration 1, round 2, initial guess	12 800	370	370	690	690	36.3	428
Calibration 1, round 2, final results	12 800	370	370	617	690	45.3	428
Calibration 2, round 1, initial guess	11 000	370	370	690	690	49	428
Calibration 2, round 1, final results	12 303	370	370	610	690	49	428
Calibration 3, round 1, initial guess	11 000	370	370	690	690	49	428
Calibration 3, round 1, results	11 745	370	370	690	690	78	428
Calibration 3, round 2, initial guess	11 745	370	370	690	690	78	428
Calibration 3, round 2, final results	11 745	370	370	639	690	39	428
Calibration 4, round 1, initial guess	11 000	370	370	690	690	49	428
Calibration 4, round 1, results	11 000	370	370	631	690	43	428
Calibration 4, round 2, initial	11 000	370	370	631	690	43	428
Calibration 4, round 2, final results	11 746	370	370	631	690	77	428
Calibration 5, round 1, initial guess	11 000	370	370	690	690	49	428
Calibration 5, round 1, results	12 303	370	370	610	690	49	428
Calibration 5, round 2, initial guess	12 303	370	370	610	690	49	428
Calibration 5, round 2, results	12 303	370	370	597	690	56	428
Calibration 5, round 3, initial guess	12 303	370	370	597	690	56	428
Calibration 5, round 3, final results	11 976	370	370	597	690	62	428
Calibration 5, results rounded	12 000	370	370	600	600	62	428

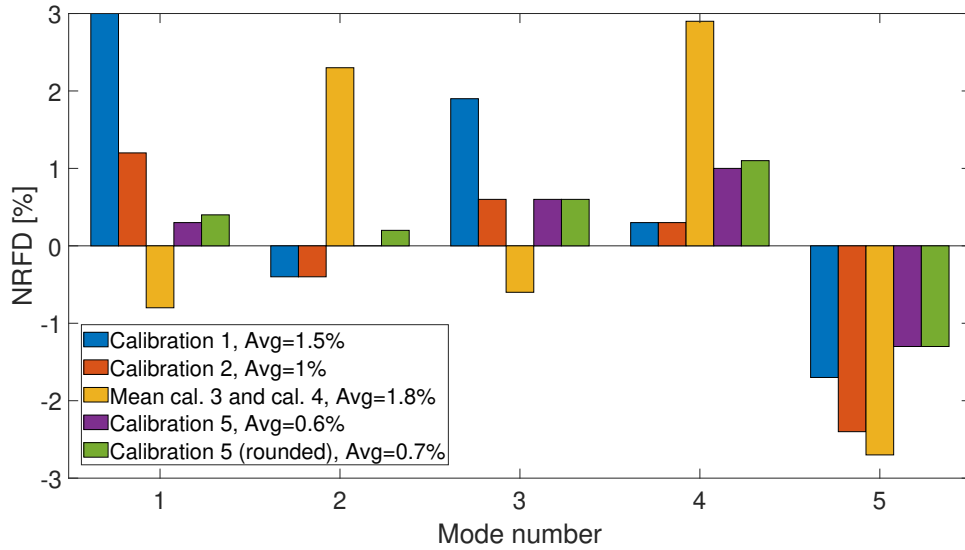


Figure 8.10: Calibration of spruce, averaged NRFD-values.

Table 8.6: Calibration of birch material properties.

	E_L	E_T	E_R	G_{LT}	G_{LR}	G_{RT}	ρ
Calibration 1, round 1, initial guess	14 938	925	925	958	958	203	606
Calibration 1, round 1, results	14 505	925	925	825	958	203	606
Calibration 1, round 2, initial guess	14 505	925	925	825	958	203	606
Calibration 1, round 2, results	14 505	925	925	843	958	158	606
Calibration 1, round 3, initial guess	14 505	925	925	843	958	158	606
Calibration 1, round 3, final results	14 790	925	925	843	958	141	606
Calibration 1, results rounded	15 000	930	930	840	840	160	606

In Figure 8.11, the results of the performed calibrations are presented as NRFD-value for all modes. Due to being limited to only one calibration, round 2 and round 3 of said calibration are presented. Due to the average of round 2 being lower, the properties of round 2 were rounded to two significant figures. The resulting average deviation from the reference values, 0.8%, is sufficiently low.

Calibration of Densified Spruce

The sensitivity analysis presented in Figure 8.9 shows that E_L and G_{LT} have significant influence on the natural frequencies, but also that G_{LT} has some effect. The initial guess for all calibrations was based upon an estimation of how densification would affect the mechanical properties of spruce. Due to uncertainty, the initial guess for Calibration 3 includes unchanged elastic moduli according to C24 for spruce, as seen in Table 8.9.

Calibration 1 was run in three steps, in step one E_L and G_{LT} were calibrated, followed by G_{LT} and G_{RT} and at last E_L and G_{RT} were calibrated. All 5 modes were used for

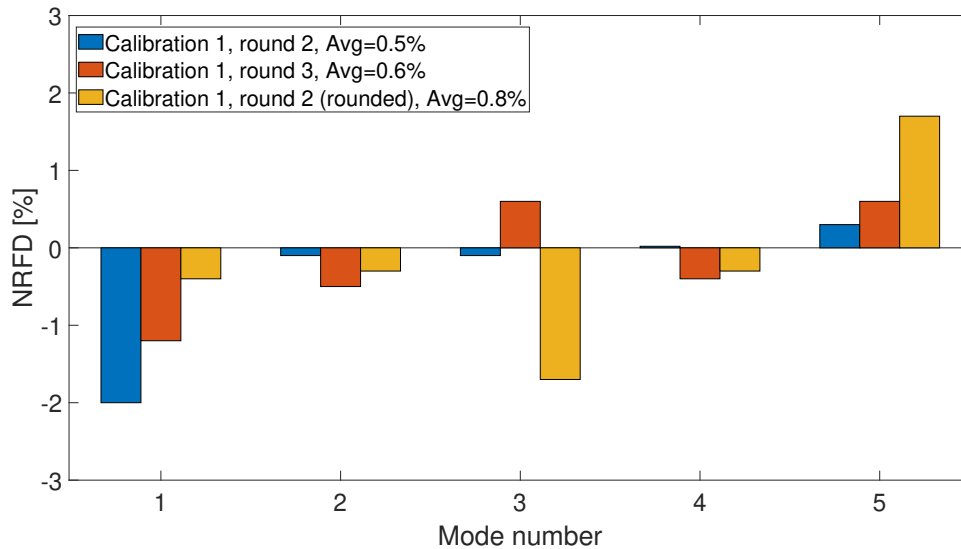


Figure 8.11: Calibration of birch, averaged NTFD-values.

all steps.

Calibration 2 was run in 3 steps, similar to calibration 1 except the parameters calibrated in round 2 and 3 had changed order.

Calibration 3 was run in one step, with the first step being identical to the previous two calibrations. The initial guess for E_L was different, using the mechanical properties of C24.

It should be noted that different combinations of the parameters were tested, but only calibrations varying E_L and G_{LT} in the first step were able to find equilibrium.

In Table 8.7, both the initial guesses and the calibrated parameters are presented. The calibrated parameters of each round are highlighted in bold. Both Calibrations 1 and 2 resulted in similar results. Calibration 3, with a different initial guess, finished with similar values as round 1 in the other calibrations, indicating Independence of initial guess. The final row in table shows the average values of Calibrations 1 and 2, rounded down to two significant figures.

In Figure 8.12, the results of the calibrations are presented as NTFD-values to each eigenmode. The parameter combinations in Calibrations 1 and 2 were very similar and the results were also similar, with an average deviation of 1% and 1.1%, respectively. The rounded parameters showed a similar average accuracy, with an average NTFD-value of 1.0%

8.4.4 Final Parameters

The resulting material parameters for each type of wood are gathered in Table 8.8. Using the results rounded to two significant figures from Tables 8.5–8.7.

Table 8.7: Calibration of densified spruce material parameters.

	E_L	E_T	E_R	G_{LT}	G_{LR}	G_{RT}	ρ
Calibration 1, round 1, initial guess	20 227	680	680	1 268	1 268	90	787
Calibration 1, round 1, results	14 570	680	680	1 992	1 268	90	787
Calibration 1, round 2, initial guess	14 570	680	680	1 992	1 268	90	787
Calibration 1, round 2, results	14 570	680	680	1 951	1 268	97	787
Calibration 1, round 3, initial guess	14 570	680	680	1 951	1 268	97	787
Calibration 1, round 3, final results	14 217	680	680	1 951	1 268	102	787
Calibration 2, round 1, initial guess	20 227	680	680	1 268	1 268	90	787
Calibration 2, round 1, results	14 570	680	680	1 992	1 268	90	787
Calibration 2, round 2, initial guess	14 570	680	680	1 992	1 268	90	787
Calibration 2, round 2, results	14 356	680	680	1 992	1 268	97	787
Calibration 2, round 3, initial guess	14 356	680	680	1 992	1 268	97	787
Calibration 2, round 3, final results	14 356	680	680	1 927	1 268	102	787
Calibration 3, round 1, initial guess	11 000	370	370	1 268	1 268	90	428
Calibration 3, round 1, results	14 604	370	370	1 993	690	90	428
Average of Calibrations 1 and 2, results rounded	14 000	680	680	1 900	1 900	100	787

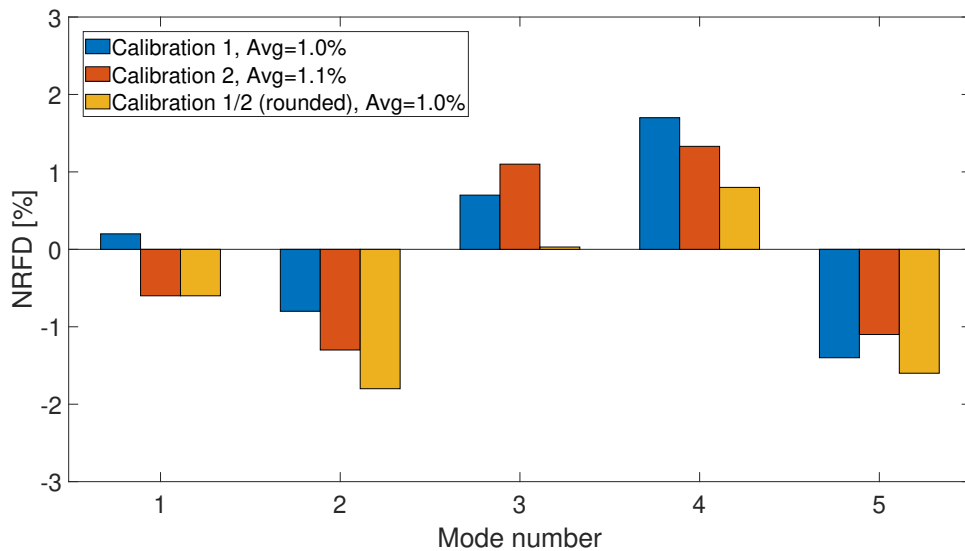


Figure 8.12: Calibration of densified spruce, averaged NRFD-values.

Table 8.8: Summary mechanical material properties, with moduli in MPa and density in kg/m³.

	E_L	E_T	E_R	ν_{LT}	ν_{LR}	ν_{RT}	G_{LT}	G_{LR}	G_{RT}	ρ
Spruce	12 000	370	370	0.42	0.38	0.34	600	600	62	428
Birch	15 000	930	930	0.45	0.43	0.43	840	840	160	606
Dens. spruce	14 000	680	680	0.42	0.38	0.34	1 900	1 900	100	787

Table 8.9: Mechanical properties of spruce according to SS-EN 338, excluding G_{RT} .
Moduli is displayed in MPa and mass density is denoted in kg/m^3 .

Strength grade	E_L	E_T	E_R	G_{LT}	G_{LR}	G_{RT}	ρ
C24	11 000	370	370	690	690	49	420
C50	16 000	530	530	1 000	1 000	71	520

9 Case Study – Introduction

This chapter introduces the core principle of this dissertation, namely, the FE-analysis of different CLT configurations. The FE-analysis is initiated by performing convergence studies, both in terms of the frequency domain as well as the mesh size domain. Note that the case study uses solid shell elements, in contrast to the calibration of the material properties, which utilized solid elements.

9.1 Models of the Case Study

Two differently sized CLT models are to be evaluated. For convenience, the CLT-panels are named in order of size. That is, S-sized panel and L-sized panel, short for small and large, as shown in Figure 9.1.

The reason for two different-sized models is two-fold. Firstly, it is to affirm whether or not the behaviour and potential patterns of the configurations are size-dependent. This includes if the potential optimums perform as expected on a differently sized CLT-panel. Secondly, it is to obtain comparable results, as well as facilitate comparisons to future work in this subject.

The analysis of the L-sized CLT-panel is more extensive than that of the S-sized CLT-panel, since the larger CLT-panel offers more detailed information, to avoid redundancy and limit the extent of the results. The chosen S-sized CLT-panel is deemed representative to common sizes produced in Sweden. The current Eurocode provisions restrict the span of CLT-panels due to the susceptibility to vibrational phenomena.

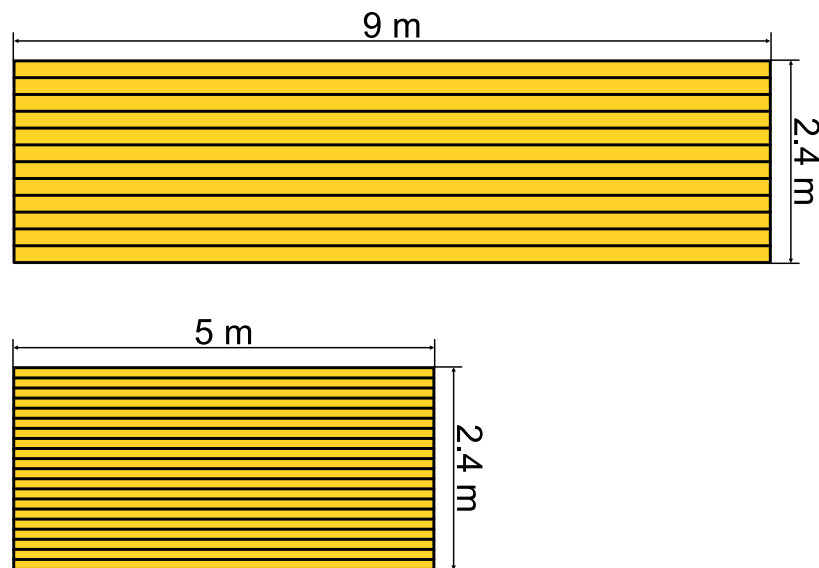


Figure 9.1: The small and the large CLT-panels, viewed from above

Hence, the L-sized CLT-panel was chosen to be extensively investigated and assessed in terms of potential performance parity with the S-sized standard spruce CLT-panel.

9.1.1 Dimensions of the Models

The large CLT-panel is built up by 7 layers of lamellae, starting with two longitudinal layers on either side of the panel, followed by one transverse and one longitudinal in the center, as can be seen in Figure 9.2. The large CLT-panel is constructed of 45 lamellae along the longitudinal direction, each with a width of 200 mm and a thickness of 45 mm

The small CLT-panel consists of 5 layers or lamellae, starting with one longitudinal layer on either surface of the panel, and alternating direction with each layer, as seen in Figure 9.2. The small CLT-panel is constructed of 41 lamellae in the longitudinal direction, the one on the edge on either side with a width of 160 mm and the remaining 39 lamellae with a width of 120 mm.

In the transverse direction, the large CLT-panel is 2.4 m wide, and each layer consists of 12 lamellae, as can be seen in Figure 9.3. Each lamella is 200 mm wide and 45 mm thick. In the same direction, the small CLT-panel is also 2.4 m wide, although each layer consists of 20 lamellae, where each lamella is 120 mm wide and 30 mm thick.

9.1.2 Material Properties

Based on previous calibrations of material parameters, performed in Chapter 8, a summary of the resulting mechanical properties are presented in Table 8.8, and were used

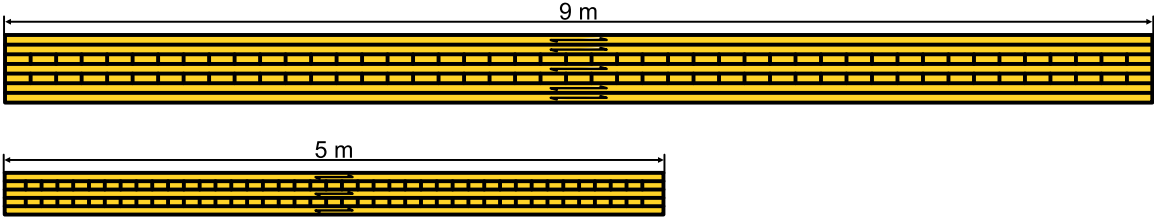


Figure 9.2: View of longitudinal direction of the CLT-plates. Large CLT-panel (top) and small CLT-panel (bottom).

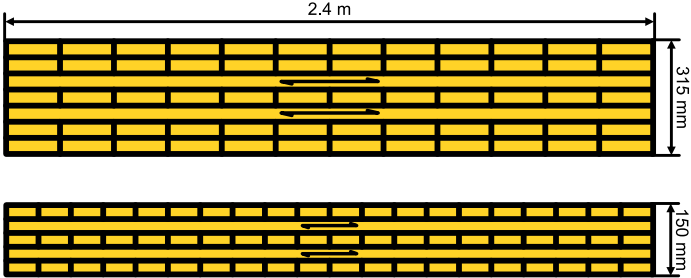


Figure 9.3: View of transversal direction of the CLT-plates. Large CLT-panel (top) and small CLT-panel (bottom).

in subsequent analyses. The average damping ratio for each material was presented in Table 8.1, and for the following analyses a damping ratio of 0.7% was adopted.

9.1.3 Load Configuration

The boundary conditions, load placement and measure point were independent of which CLT-panel was modelled. As mentioned in Chapter 6, free-free boundary conditions were used for the models. The unit load was applied in one corner of the CLT-panel and the measuring point was situated in the opposite corner, visualized for the large CLT-panel in Figure 9.4. The frequency range of interest that was investigated was 0-562 Hz.

9.2 Setup of L-sized CLT-panel

In Chapter 8, a FE-model was developed and used to perform several sensitivity analyses, followed by calibrations of material parameters. In this section, a new FE-model has been considered, modelling the different configurations to come, using a different type of element. Thus, a convergence study is required in order to assure the accuracy of the results to be obtained. This convergence study is divided into two studies. The first regards the convergence of the frequency step, while the second concerns the convergence of the element mesh. Both types of convergence studies are in terms of direct steady-state analyses.

An important aspect to consider is the interdependence of these two convergence studies. A certain frequency step may be convergent, however only corresponding to a preset element size. Changing the FE-element to a smaller size may reveal that the

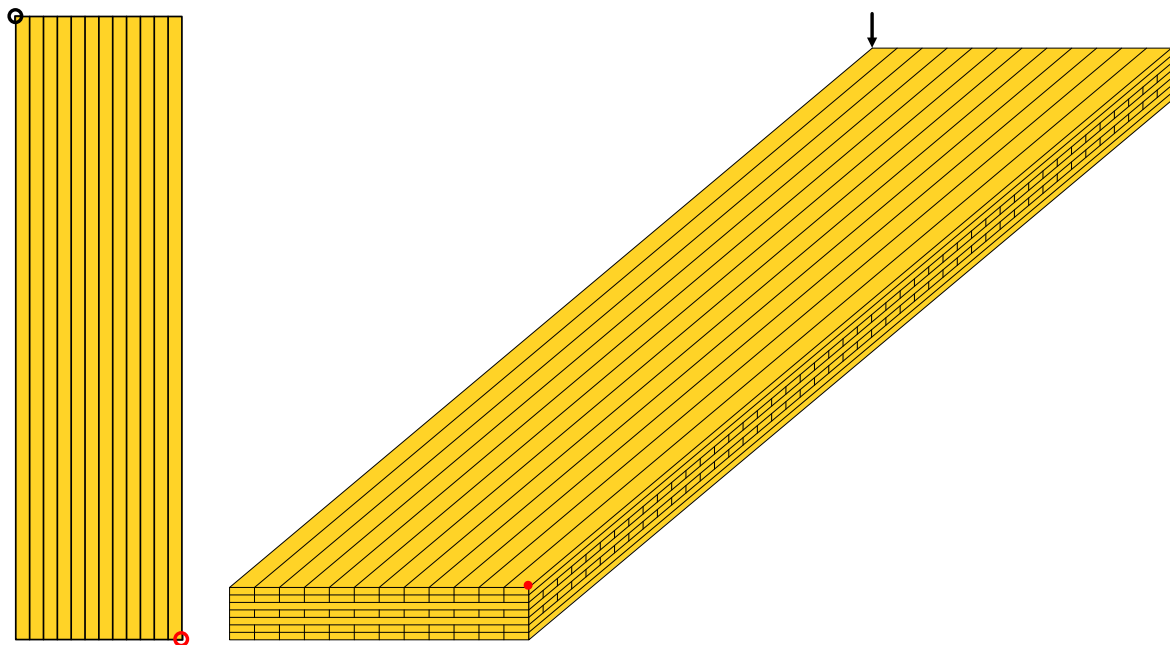


Figure 9.4: Test configuration of FE-model.

previously chosen frequency step is not converging. Thus, an initial element size has to be chosen. In this case, the element size was set to 50 mm.

9.2.1 Frequency Step Convergence

The size of the frequency step governs the accuracy of the results, as well as the amount of frequency increments to be performed in the FE-analysis. This convergence study is analogous to the element mesh convergence study. A smaller frequency step, while yielding more accurate results, implies larger amounts of increments, which directly translates to an extensive usage of computing resources and time-consuming analyses. Hence, a balance is sought between the accuracy of the results and the computational costs of the performed analyses.

The variation of frequency step during steady-state analysis, over the complete frequency range, is shown in Figure 9.5 below. The response corresponding to the respective frequency step, seem to overlap. However, a zoom-in around the frequency range of 76-90 Hz shows the discrepancies of the responses in some of the response peaks, as is depicted in Figure 9.6. In order to obtain further confirmation about the convergence, the relative error of the responses can be calculated. The reference case is chosen as the smallest frequency step, yielding the most accurate results, i.e. 0.1 Hz.

For a more readable depiction, the figure is presented with a cut-off at 20% error on the y-axis and is shown in Figure 9.7. Note carefully that the large peaks are generated due to a slight shift in the response curves along the x-axis, thus giving a spurious image of the actual error. This fact is explained in detail later on in this chapter. Furthermore, the RMS value of the relative error with frequency increment 0.5 Hz was 3.4%, while the RMS value of relative error with frequency increment 0.3 Hz was 1.4%.

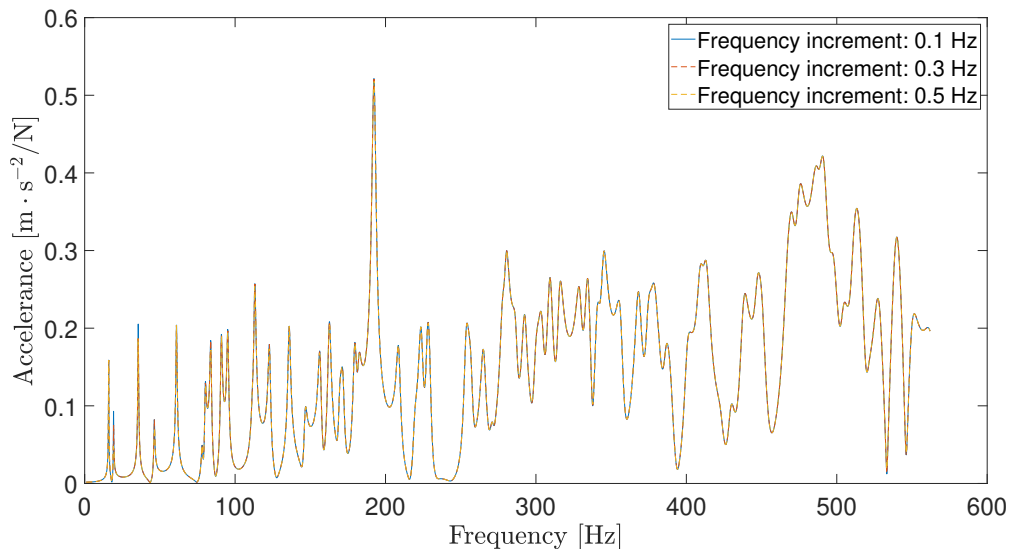


Figure 9.5: Response of steady-state analysis with various frequency increments.

Therefore, the frequency step is chosen to be 0.3 Hz, as this conserves the accuracy while not causing too computationally heavy analyses.

9.2.2 Mesh Convergence

Keeping the frequency step constant at 0.3 Hz, steady-state analyses have been performed with varying element mesh sizes, see Figure 9.8. Just like the frequency step study, the response curves from the mesh size study do not exhibit observable discrepancies in the lower frequency range. Thus, a zoom-in is depicted in Figure 9.9, in the frequency range of 76-96 Hz. However, the response curves exhibit observable dis-

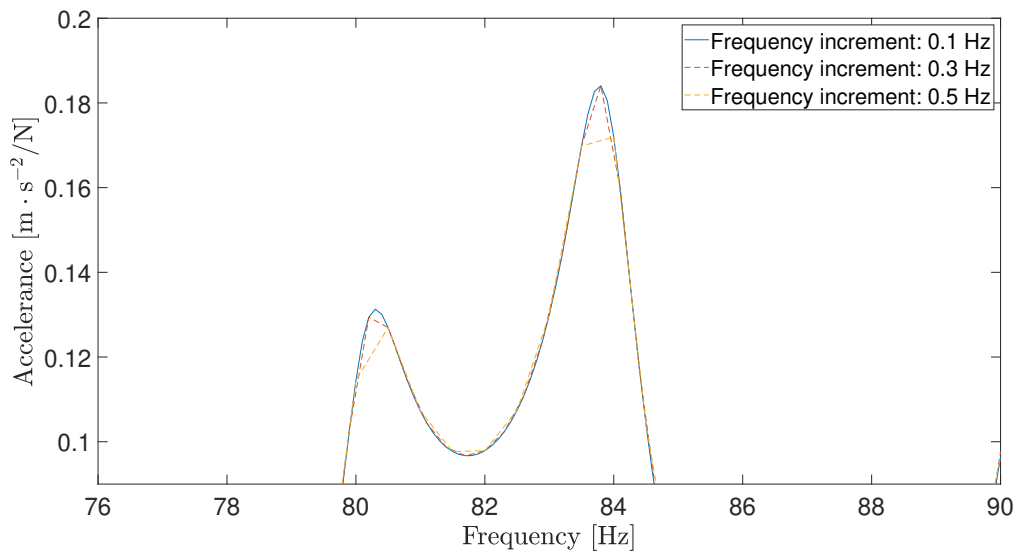


Figure 9.6: Response of steady-state analysis with various frequency increment, frequency range 76-90 Hz.

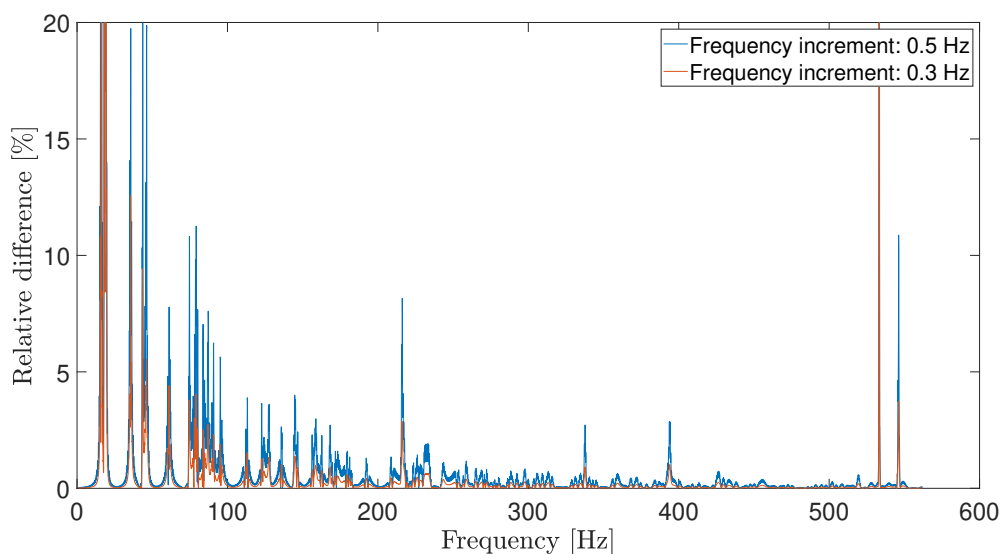


Figure 9.7: Relative error of different frequency increments using 0.1 Hz as a reference, with an upper limit of 20%.

crepancies in the higher frequency range, especially in the frequency range of 400-562 Hz, as shown in Figure 9.10. While different element sizes were analysed for the mesh convergence, each layer was set to one element in the thickness direction.

To further complement these plots, the relative error of the different responses has been calculated, presented in Figure 9.11 using the smallest mesh size of 40 mm as a reference. Just like before, the large peaks are due to the slight shift in the response curves, causing the relative error to tend to large values. Thus, a cut-off is made at 200% error, Figure 9.12, providing a better depiction.

The RMS of the relative error with mesh size 67 mm was 53.8%, while the RMS of the relative error with mesh size 50 mm was 17.7%. The latter is not an exceedingly

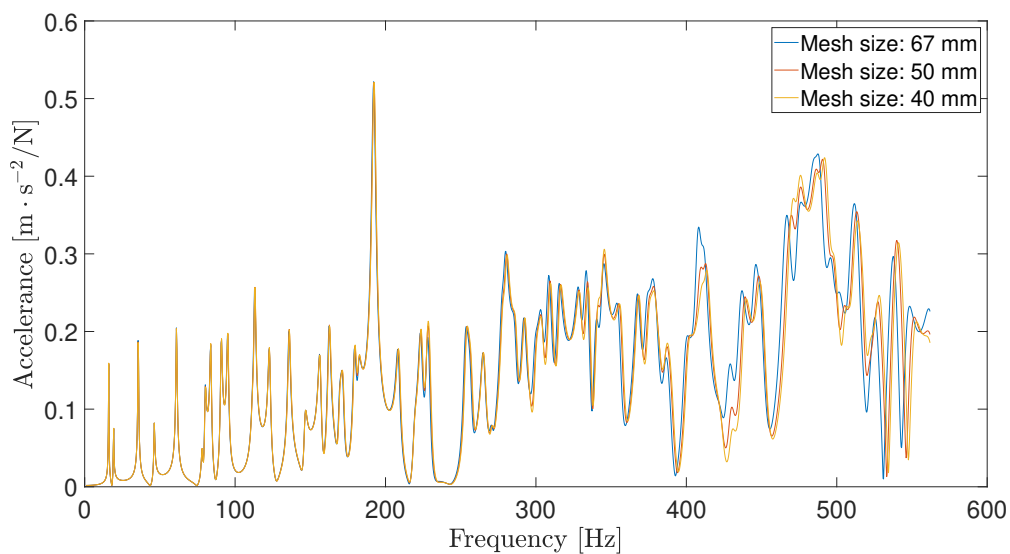


Figure 9.8: Response from steady-state analysis with various mesh sizes.

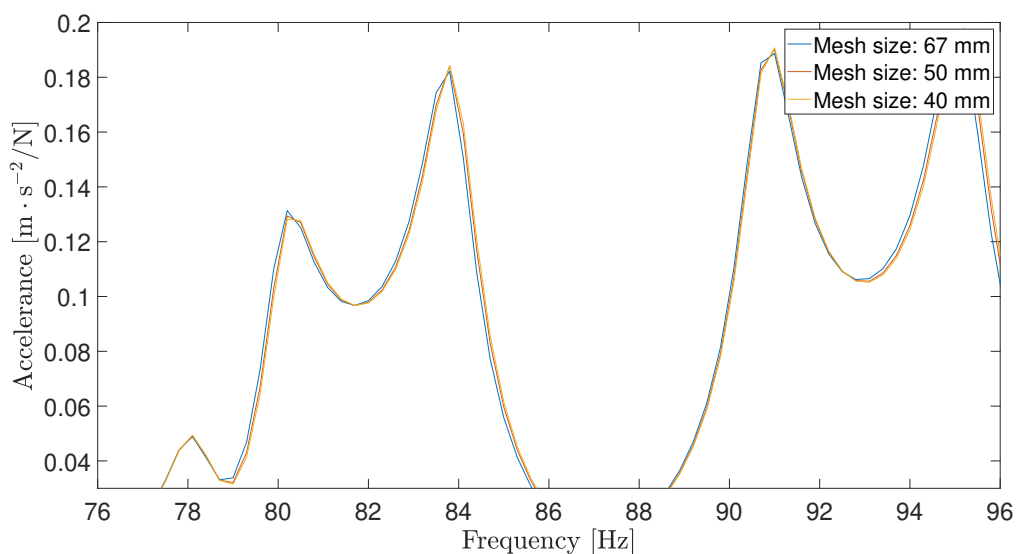


Figure 9.9: Response from steady-state analysis with different mesh sizes, frequency range 76-96 Hz.

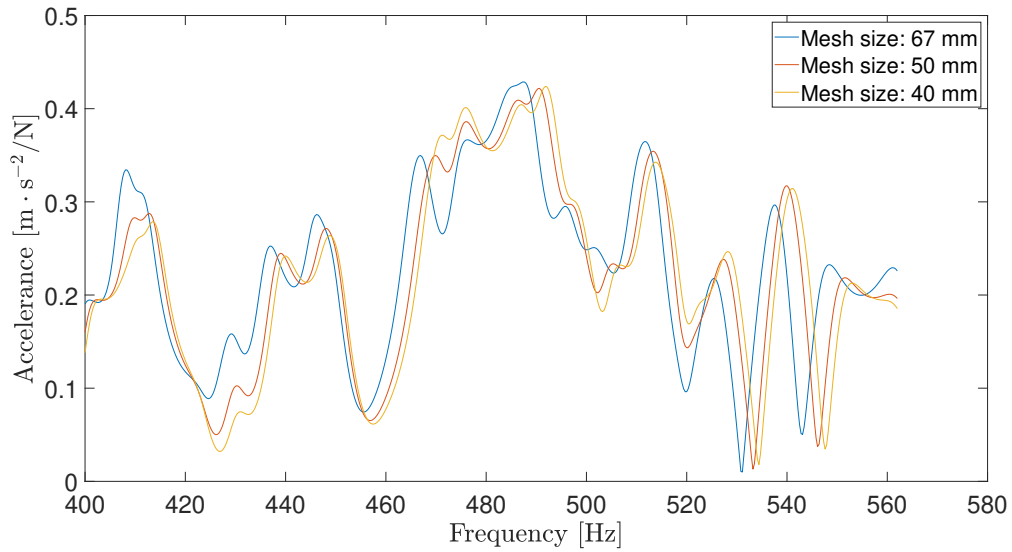


Figure 9.10: Response from steady-state analysis with different mesh sizes, frequency range 400-562 Hz.

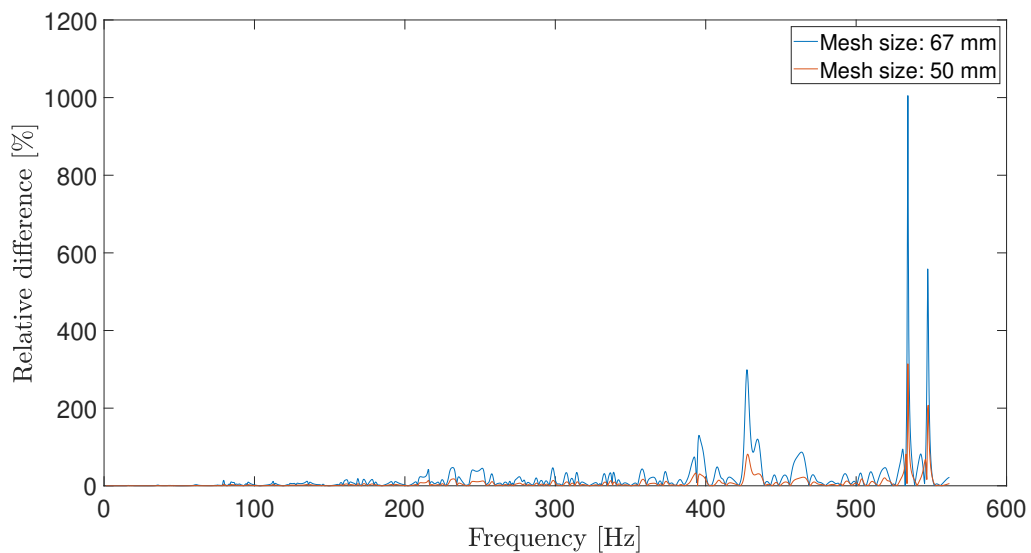


Figure 9.11: Relative error of different mesh sizes using size 40 mm as a reference.

large value, especially when considering the spurious error peaks.

Therefore, based on these RMS values, as well as the previous response curves, the element mesh size was chosen as 50 mm.

Remark

To further emphasize the effect of the slight shift in the response curves, a zoom-in of Figure 9.10 about the peak about 540 Hz is depicted in Figure 9.13. The relative error of the response corresponding to the element size 67 mm is approximately calculated as 50%. This is a direct consequence of considering the relative error of the responses

at corresponding frequency points. However, calculating the relative error of the peak values, instead of the former, yields approximately 5%.

Hence, very large peaks in the relative error plots should not be taken at face value. Although, calculating the relative error of the corresponding peaks would be cumbersome. Therefore, a collective evaluation considering the response plots, relative error plots thereto, and the RMS values, was made for the choice of mesh size 50 mm.

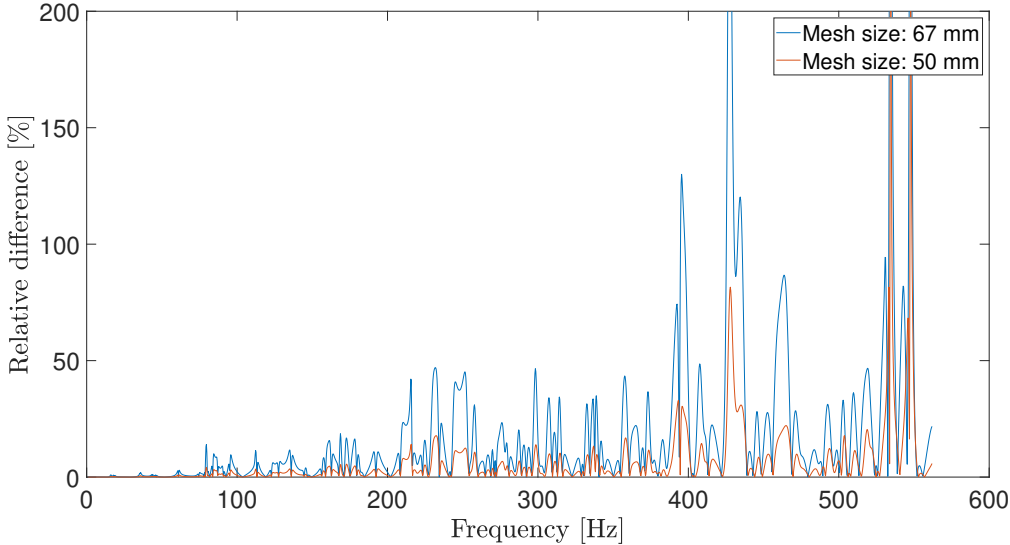


Figure 9.12: Relative error of different mesh sizes using size 40 mm as a reference, with an upper limit of 200% error.

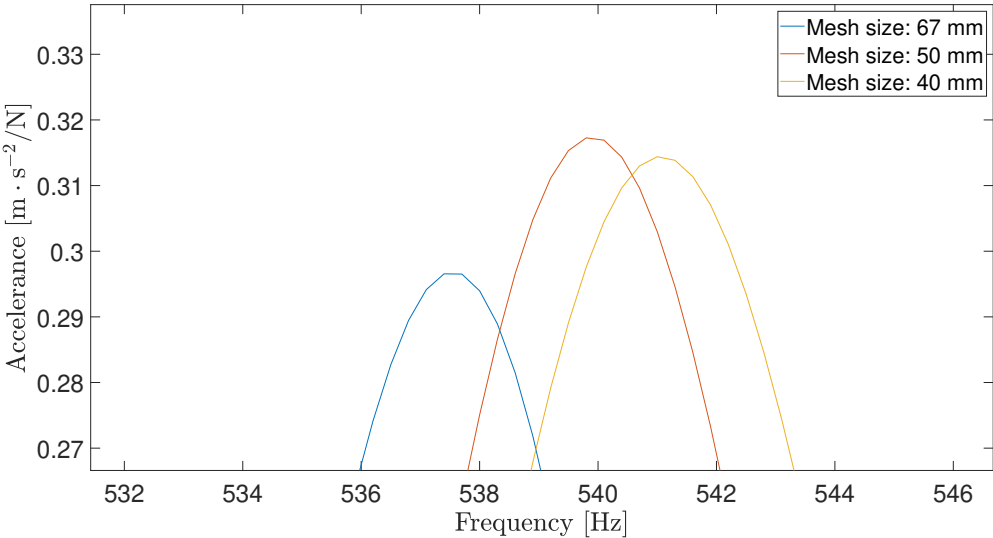


Figure 9.13: Zoom-in of the peak at 540 Hz.

9.2.3 Truncated Modal Analysis – Convergence Study

The direct steady-state analysis can be further refined, in terms of cost-efficiency, by utilizing truncated modal analysis, as explained in Chapter 4. The truncated mode-based steady-state analysis has to converge to the direct steady-state analysis, in order for it to be adequately used.

The upper frequency range used in the truncated modal analysis have been set to be two times the upper frequency range in the direct analysis. In this case, the upper frequency limit becomes $2 \cdot 562 = 1124$ Hz. The reason for this is that the truncated model up to 562 Hz may be too crude, hence the need to include a larger frequency interval.

A convergence study is required in order to establish a sufficient amount of eigenmodes to be included in the reduced model. The principle is similar to the previous convergence studies. By truncating the amount of eigenmodes, the amount of degrees of freedom is drastically reduced, implying the same for the number of differential equations to be solved. Hence, the reduced modal-based steady-state analysis becomes more time-efficient than the full modal-based analysis. However, reducing the amount of eigenmodes leads to less accurate results, and thus a balance is sought between the accuracy and the time-efficiency thereof.

Additionally, there is a need to quantify the reduction in a manner that is invariant with respect to the specifics of the FE-model, such as the geometry. Such a measure of the reduction can be defined by calculating the ratio of the highest eigenfrequency in the reduced set of eigenmodes, to the imposed upper frequency limit used for direct steady-state analyses. The cut-off frequency can then be chosen approximately equal to the highest eigenfrequency in the truncated set of eigenmodes,

$$\kappa_{red} = \frac{f_{cut}}{f_{lim}}; f_{cut} \sim f_{n,max}. \quad (9.1)$$

Thereby, a factor is obtained that can be multiplied by the specific upper frequency limit at hand, yielding the cut-off frequency. Although, a more straightforward measure is simply the number of eigenmodes included. However, the disadvantage of this is that different CLT-panel geometries cause different modal behaviour, and thus different amounts of eigenmodes, whereby the said amount will not be representative. Therefore, a frequency-based measure is advantageous.

Several truncated mode-based steady-state analyses have been performed, with different sized truncations. These are compared with the direct steady-state analysis in Figure 9.14. The deviations of the responses can be observed in the upper frequency range. A zoom-in of Figure 9.14, elucidating said deviations, is provided in Figure 9.15.

To further complement these plots, the relative errors have been calculated of the responses, Figure 9.16, using the direct steady-state response as the reference. Again, a zoom-in is also provided in Figure 9.17.

Moreover, the RMS of these error plots have been calculated, presented in Table 9.1, as well their relative difference to the direct steady-state case.

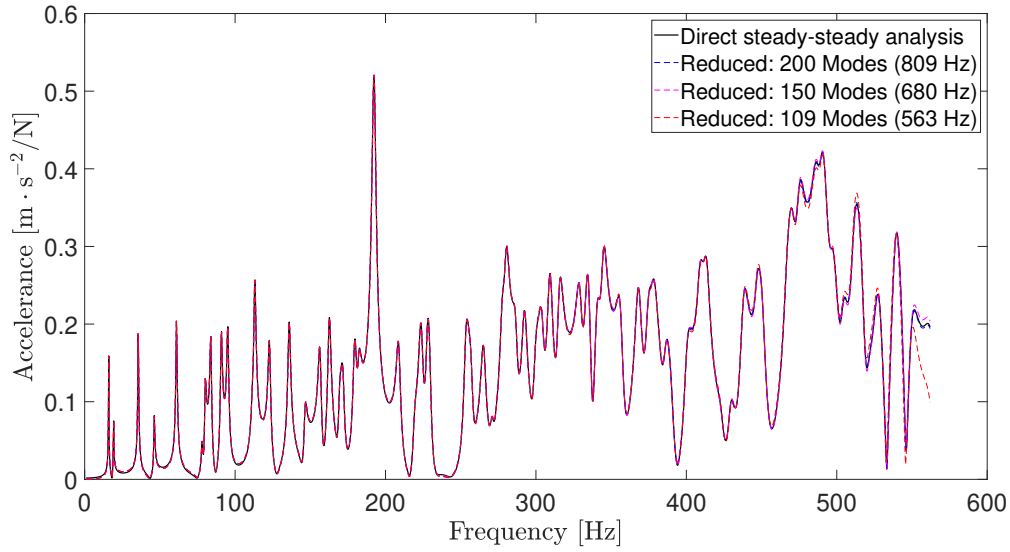


Figure 9.14: Response from truncated modal analysis, with different number of eigenmodes

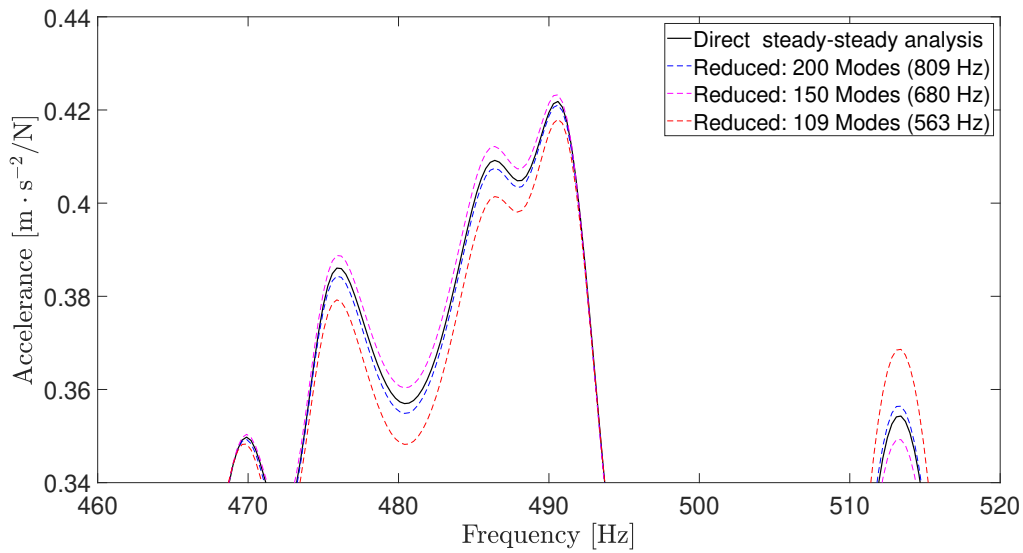


Figure 9.15: Response from truncated modal analysis, with different number of eigenmodes, frequency range 460-520 Hz

Table 9.1: RMS values of the truncated model responses.

No. modes (f_{cut})	RMS [m ² /s]	Relative difference [%]
Direct steady-state	0.1780	
200 Modes (809 Hz)	0.1780	-0.007
150 Modes (680 Hz)	0.1781	0.066
109 Modes (563 Hz)	0.1773	-0.387

Based on the responses in Figure 9.14, the relative error plot in Figure 9.16, and the

RMS values given in Table 9.1, a choice was made to truncate the modal analysis to 200 eigenmodes. This corresponds to a cut-off frequency of 809, and by Eq. 9.1, $\kappa_{red} = 809/562 \approx 1.44$.

9.3 Setup of S-sized CLT-panel

In a similar fashion to the convergence studies conducted in Chapter 9.2, regarding the L-sized CLT-panel, it was necessary to perform similar analyses for the S-sized CLT-panel. Due to the limited time available during this master's dissertation, a simplified

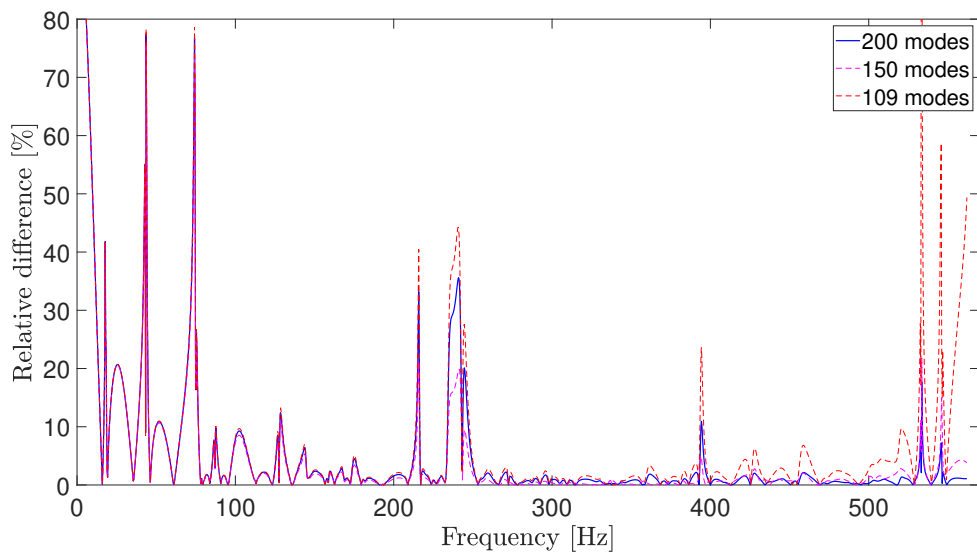


Figure 9.16: Relative error of different truncated model sizes using direct steady state analysis as a reference

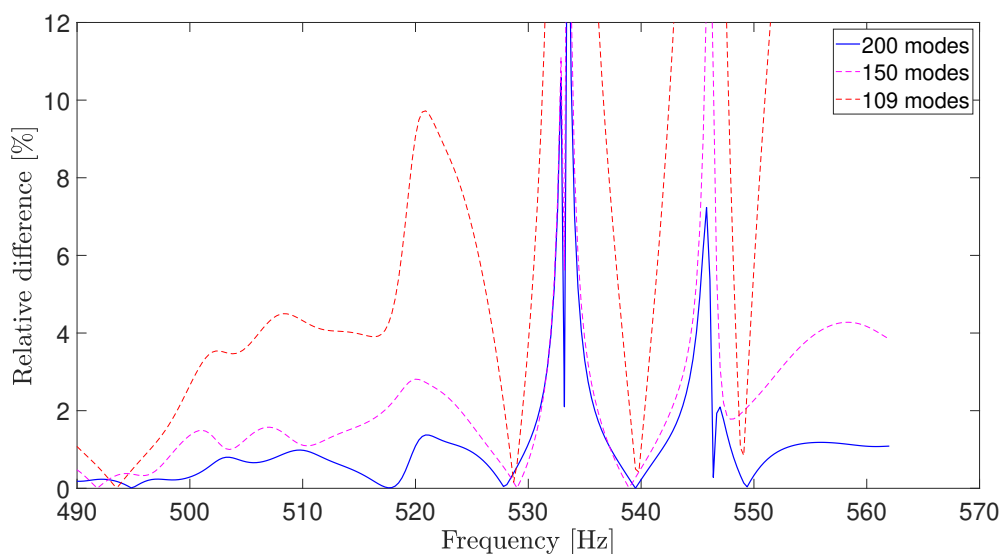


Figure 9.17: Relative error of different truncated model sizes using direct steady state analysis as a reference. Frequency range limited to 490-562 Hz

approach was utilized for the S-sized CLT-panel, in an effort to save time.

For the large CLT-panel, a frequency increment of 0.3 Hz was deemed sufficient. The same frequency increment was estimated to be satisfactory for the small CLT-panel, due to the many similarities in the analyses and models, such as the same frequency range and boundary conditions.

The length of the smaller CLT-panel is almost half of the large CLT-panel, requiring a mesh convergence analysis to be performed. However, a simplified approach and simpler analysis was performed. The model derived for the large CLT-panel in Chapter 9.2 contained 70 952 nodes and 60 480 elements. A hypothesis is assumed that if the model of the smaller CLT-panel contains the same amount of nodes and elements, the model will be sufficient. A mesh size of 30 mm on the entire model, except for the outer lamellae, with a mesh of 40 mm, resulted in 80 190 nodes and 65 600 elements. The different mesh sizes were necessary for the elements to either be square or rectangular. This mesh size was compared to a finer mesh, in order to determine if the elements were sufficiently small. The finer mesh had elements of 24 mm, except for the outer lamellae, which were 32 mm. The resulting steady-state analyses are presented in Figure 9.18.

The RMS-value for each mesh size was calculated and the values were similar with 61.43 for the bigger mesh and 61.1 for the smaller mesh. This, combined with the previous figures highlighting little deviation between the two mesh sizes, resulted in mesh size 30 mm being adopted for the S-sized CLT-panel.

Due to the extent of conducting steady-state analyses, a truncation was necessary for the small CLT-panel. The upper range of the frequency span investigated was 562 Hz, for the large CLT-panel a ratio of 1.44 and 200 modes was deemed sufficient to represent the steady-state results. The same ratio was assumed to be sufficient for the smaller CLT-panel, resulting in 217 modes, for comparison.

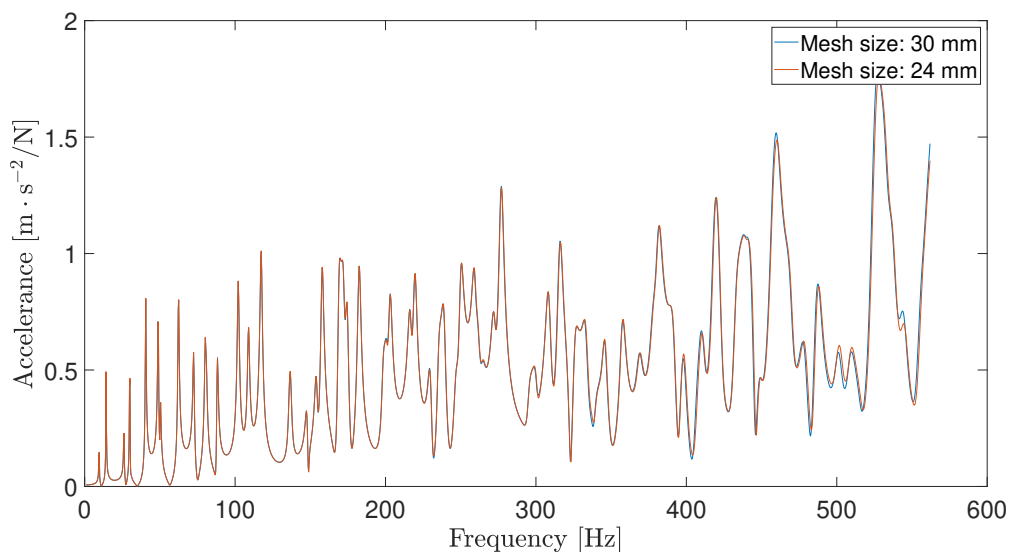


Figure 9.18: Response from steady-state analysis with different mesh sizes.

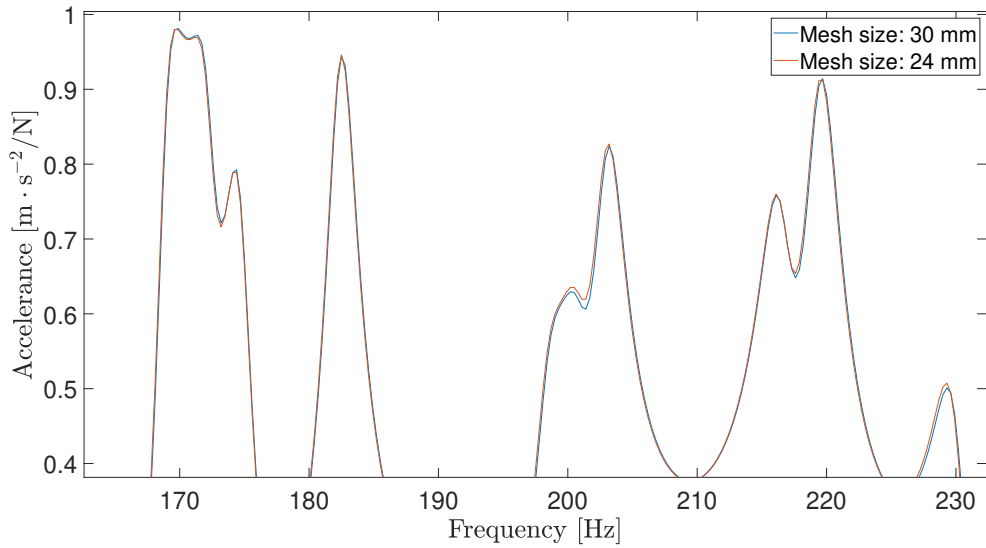


Figure 9.19: Response from steady-state analysis with different mesh sizes, frequency range 164-232 Hz.

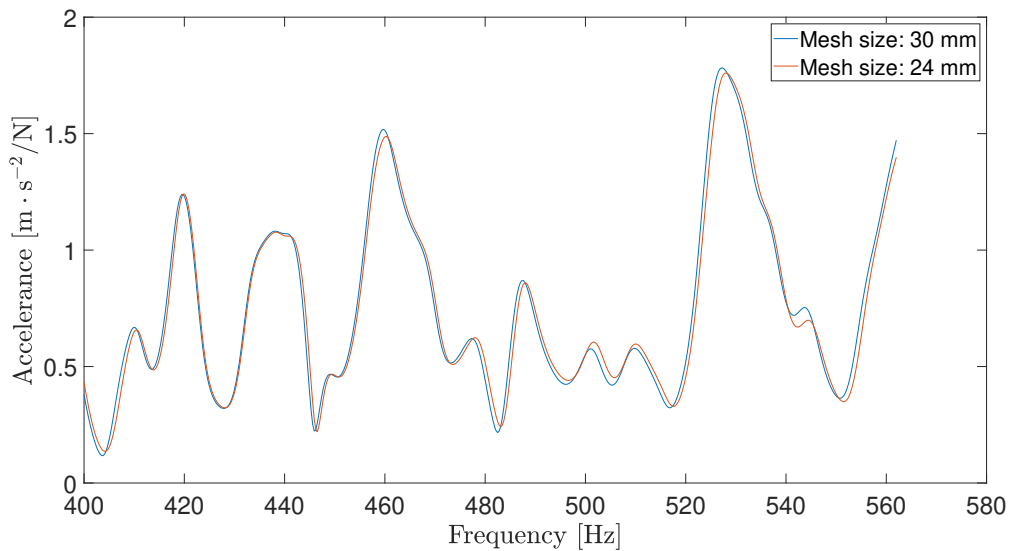


Figure 9.20: Response from steady-state analysis with different mesh sizes, frequency range 400-562 Hz.

9.4 Outline of the Configuration Study

The configuration study entails the study of various CLT configurations and comparing them against the reference case of the homogeneous spruce CLT-panel. As mentioned before, all the mechanical properties used are collected in Table 8.8. The configuration study is initiated by investigating how the distribution of exchanged lamellae influences the steady-state response. This would potentially reveal a pattern or indication of how the lamellae should be exchanged. This is done in the three principal directions, namely, the thickness, longitudinal and transversal directions, respectively. Finally, a combination of the distributions along these three principal directions are studied.

9.4.1 Distribution of Lamellae – Thickness Direction

The configuration study started by considering the layers of the CLT-panel. These configurations were based on the number of layers exchanged in concert with the desire to keep the CLT-panel cross-section as symmetric as possible. Some configurations mixed longitudinal layers and transversal layers. The former refers to layers containing longitudinal lamellae, while the latter refers to layers containing transversal lamellae. The influence of the exchanged lamella distribution was of interest, both in the longitudinal direction as well as in the transversal direction.

9.4.2 Distribution of Lamellae – Longitudinal Direction

The investigation along the longitudinal direction was performed by an initial consideration of a fully exchanged single transversal layer. Thereafter, the amount of lamellae was sequentially reduced from the centre of the longitudinal direction, towards the edges. Likewise, the same was executed starting from the edges and sequentially reducing the amount of exchanged lamellae, towards the centre of the longitudinal direction. Furthermore, some systematic distributions along the longitudinal direction were performed, considering different spacings between the exchanged lamellae.

9.4.3 Distribution of Lamellae – Transversal Direction

The investigation along the transversal direction, i.e., in the cross-sectional plane, was conducted by an initial consideration of a fully exchanged longitudinal layer. Note that this layer coincided with the middle layer of the CLT-panel. In a similar fashion as before, the amount of lamellae was sequentially reduced from the edges of the cross-section towards the centre thereof. Likewise, the same was executed starting from the centre of the cross-section, and sequentially reducing the amount of exchanged lamellae towards the edges of the cross-section. Additionally, some systematic distributions along the cross-section were performed, considering different spacing between the exchanged lamellae.

9.4.4 Distribution of Lamellae – Combined Directions

Finally, the investigation of the influence of the exchanged lamellae distribution, along multiple principal directions, was performed. This was carried out by combining the outcomes from the previous observations, with the objective of finding unambiguous lamellae schemes.

9.5 Outline of the Results

The results following this introductory chapter will be presented in three separate chapters, each pertaining to the different wood materials of interest. That is, the configurations containing birch will be presented in Chapter 10, while those containing densified wood will be presented in Chapter 11. Likewise, the configurations containing the respective Eurocode structural timber strength classes are presented in Chapter 12. The results are subdivided by the two different sized CLT-panels, namely the S-sized and L-sized panels, respectively. The results will be in terms of figures showing the various considered configurations, supplied with tables containing the evaluation metric adopted, namely, the RMS of the responses. Additionally, the volumetric amount of exchanged material will also be provided, to further indicate what configurations are more efficient material-wise.

A simple flowchart depicts the structure of the forthcoming chapters in Figure 9.21. Note the independence of these chapters. Subsequent discussions are then in order, summarizing the results of the respective chapters. Thereafter follows a discussion that encompasses the complete configuration study.

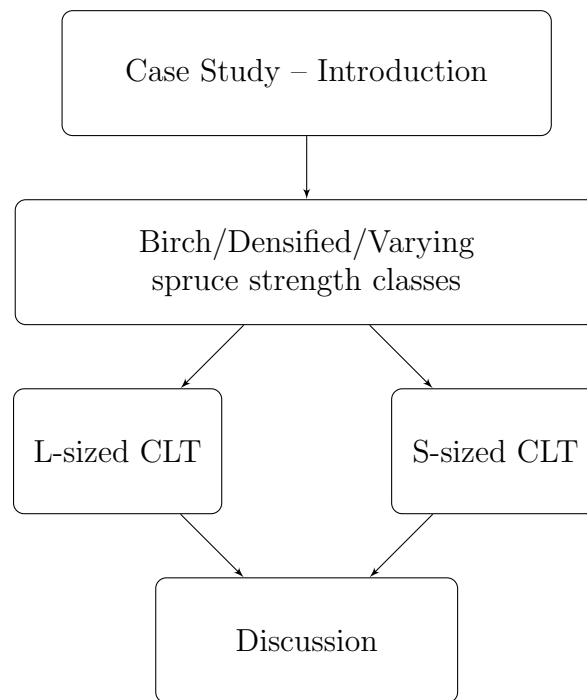


Figure 9.21: Flowchart of the presentation of the results.

10 Case Study – Birch

This chapter presents the results from the reduced modal-based steady-state analyses of different CLT-plate configurations with birch. The frequency range is up to 562 Hz.

The results of the analyses will be presented as 3rd-octave RMS plots, for select configurations. The data is presented in said plots with the RMS-value of acceleration calculated for each 3rd-octave band. The amount of birch used in each configuration tested will be presented as a percentage of the total amount of timber in the CLT-plate.

10.1 L-sized CLT-plate

This section presents the results concerning the L-sized CLT-plate. As mentioned in Section 9.4, the presentation is subdivided according to the three principle axes. Throughout this section, the reference case has been the homogeneous L-sized CLT-plate, made out of spruce with calibrated parameters.

10.1.1 Distribution of Lamellae – Thickness Direction

The layer configurations, pertaining to the thickness direction of the L-sized CLT-plate, are presented in Figure 10.1. Additionally, the relative difference of acceleration RMS-values, along with the volumetric rates of the exchanged material, are presented in Table 10.1. The 3rd-octave band plots can be seen in Figure 10.2, for select configurations.

Table 10.1: Layer configurations, relative difference of RMS-values and volumetric rates of birch.

ID	RMS diff. [%]	Vol. rate [%]	ID	RMS diff. [%]	Vol. rate [%]
ID1	−4	14	ID13	−23	29
ID2	0	14	ID14	−21	29
ID3	−13	14	ID15	−26	43
ID4	−15	14	ID16	−19	43
ID5	−11	14	ID17	−20	43
ID6	−2	14	ID18	−14	43
ID7	−4	14	ID19	−12	43
ID8	−3	29	ID20	−29	57
ID9	2	29	ID21	−17	57
ID10	−22	29	ID22	−33	71
ID11	−2	29	ID23	−30	71
ID12	−3	29	ID24	−46	100

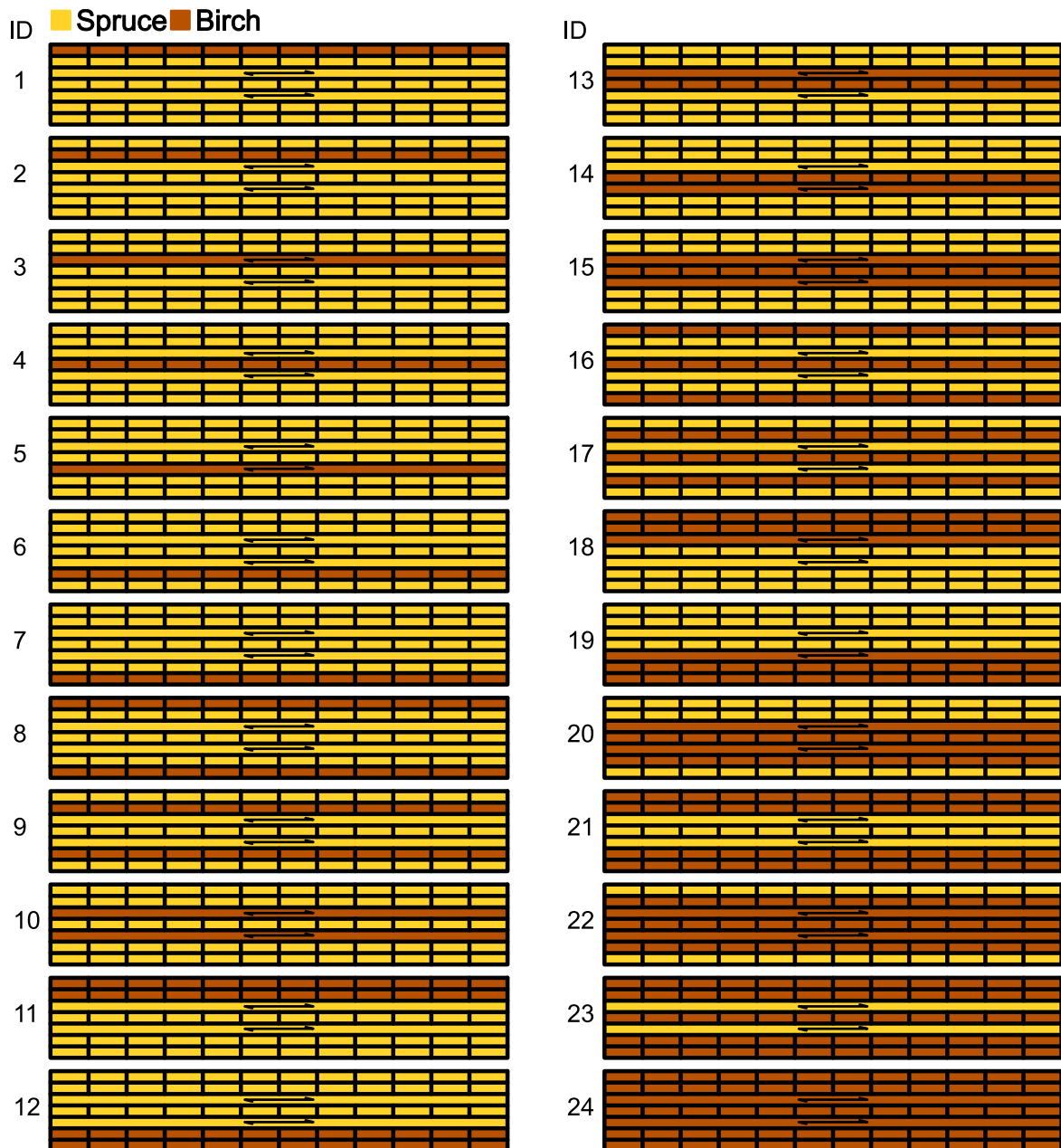


Figure 10.1: Layer configurations, spruce and birch.

In Figure 10.2, improvement is found for a majority of the 3rd-octave bands for IDs 3, 4, 13, 15 and 20. Improvement across all octave bands is found for ID22 and ID24.

Single-layer Configurations

The single-layer configurations, ID1 through ID7, exhibited pronounced reduction of the acceleration RMS-values, when the birch was concentrated to the central layer. That is, ID3, ID4 and ID5, with an average reduction of 13%. Meanwhile, the configurations with birch concentrated to the external layer displayed insignificant reduction, thus hinting at a favourable birch placement close to the central layer. Due to the geometric similarity between ID3 and ID5, configuration ID5 was deemed redundant and

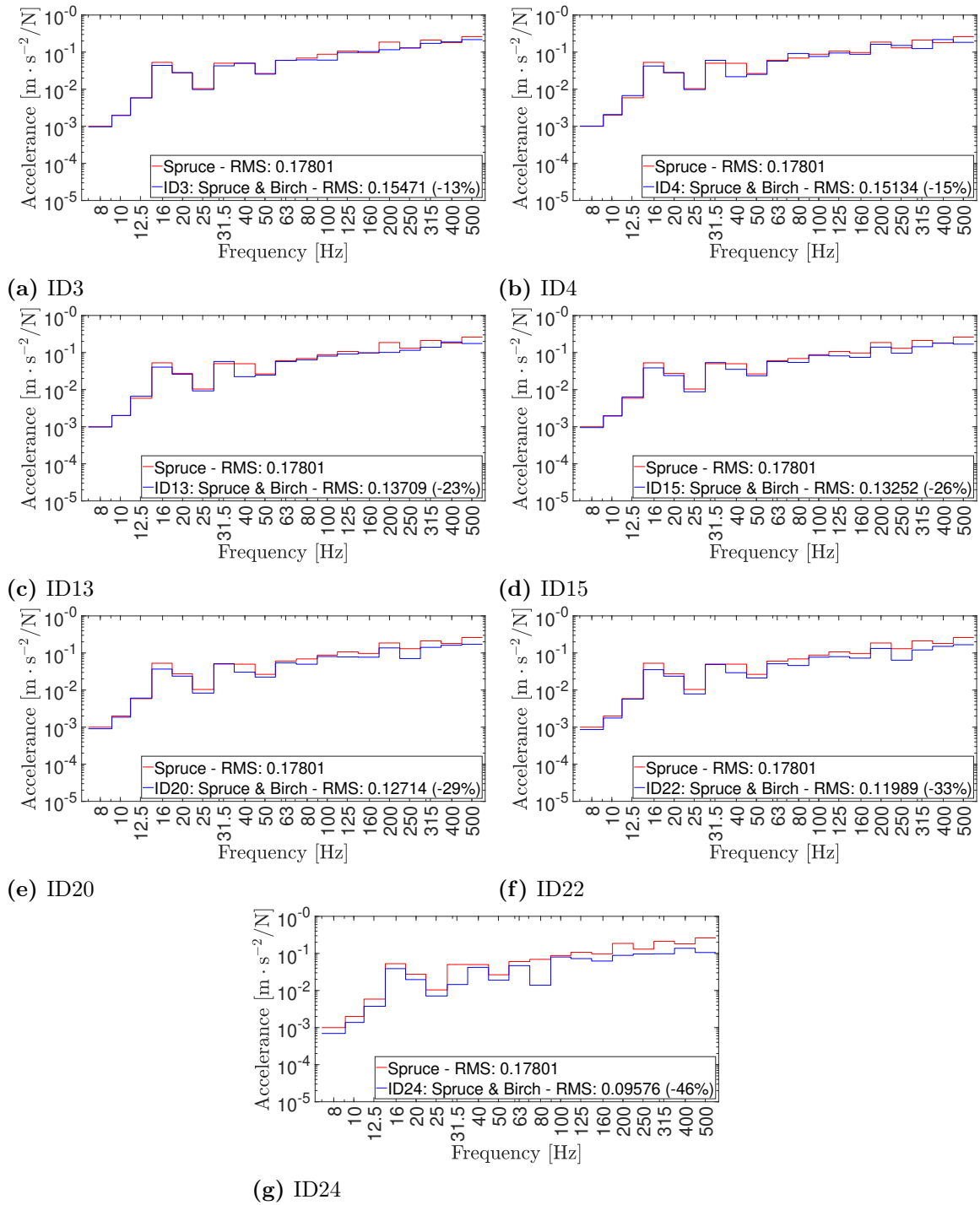


Figure 10.2: Accelerance plots, 3rd-octave band filters with RMS-values. Birch configurations ID3, ID4, ID13, ID15, ID20, ID22 and ID24.

only ID3 as well as ID4 were further investigated. This was in terms of replacing specific lamellae in the respective layer. Configuration ID3 regards transversal lamellae along the longitudinal direction and is presented in Section 10.1.2, while configuration ID4 regards longitudinal lamellae along the transversal direction and is presented in Section 10.1.3.

Multilayer Configurations

With regards to the multilayer configurations, different implications are observed with respect to the number of layers involved. The number of layers involved varied between 2-5. Additionally, a homogeneous CLT-plate of birch was analysed for more lucid comparisons.

The 2-layer configurations, ID8 through ID14, displayed significant reduction of the accelerance RMS-values, when the birch is concentrated to the central layers. Namely, ID10, ID13 and ID14, displayed a reduction of the RMS-values of roughly 20%, while the remaining 2-layer configurations displayed insubstantial reduction thereof. This hints at a favourable birch placement close to the central layer. Due to the geometric similarity between ID13 and ID14, ID14 was deemed redundant and only ID10 as well as ID13 were further investigated. This was in terms of replacing specific lamellae in the respective layers. Configuration ID10 regards transversal lamellae and is presented in Section 10.1.2, while configuration ID13 regards a combination of transversal and longitudinal lamellae and is presented in Section 10.1.4.

The 3-layer configurations, ID15 through ID19, displayed substantial reduction of the accelerance RMS-values, respectively. Significantly so when the central layer was involved, as in ID15, ID16 and ID17, with an average reduction of the RMS-values of roughly 22%. This hints at the importance of involving the central layer in future configurations. Although, this is not entirely necessary as pronounced reduction of the RMS-values could be achieved without involving the central layer, as evidenced by ID18 and ID19.

The 4-layer configurations, ID20 and ID21, displayed pronounced reduction of the accelerance RMS-values, respectively. Notably, ID20 with more birch concentrated to the central layers, outperforms ID21 with more birch concentrated to the external layers, approximately by a factor of 2 in terms of the RMS-value reduction. This indicates a favourable birch placement centred about the central layer. However, as a limited number of 4-layer configurations have been conducted, an unequivocal conclusion cannot be drawn about that including the central layer is the most optimal approach.

The 5-layer configurations, ID22 and ID23, exhibited great reduction of the accelerance RMS-values, respectively. Although the central layer has been involved in both configurations, a clear indication regarding the birch placement cannot be discerned, as 71% of the CLT-plate consists of birch. The only statement that can be made is that these configurations perform well.

Conclusion – Thickness Direction

By the conducted layer configurations, pertaining to the thickness direction of the CLT-plate, it was observed that a predominantly favourable placement of the birch would be close to the central layer. Even though some configurations involved external layers, by involving the central layer, these configurations could perform well. Furthermore, multilayer configurations profit of greater reduction when the birch layers are stacked

to the central layer. Thus, it is overall desirable to concentrate birch to the centre of the thickness direction of the CLT-plate.

Moreover, some configurations were deemed of interest for further studies regarding the distribution of lamellae, namely configurations ID3, ID4, ID10 and ID13, cf. Figure 10.1.

In terms of performance of the studied configurations, with respect to the reduction in accelerance RMS-values, the homogeneous birch CLT-plate, ID24, outperforms the rest with an RMS-value reduction of 46%. Although, the remaining configurations utilize less birch, as seen in the volumetric rates, cf. Table 10.1. Furthermore, the latter configurations can perform at an adequate level, e.g., ID10 with an RMS-value reduction of 22% while only making up roughly one-third birch material of the CLT-plate. Altogether, it would be of benefit to investigate configurations which minimizes the birch material used, while maximizing the accelerance RMS-value reduction as much as possible. With this in mind, the following sections set out to further investigate this idea.

10.1.2 Distribution of Lamellae – Longitudinal Direction

The investigation of the lamellae distribution along the longitudinal direction have been performed with a single layer. The choice of this layer coincides with configuration ID3, alluding to the promising results thereto, as explained in Section 10.1.1.

Figure 10.3 shows the tested sub-configurations for ID3, namely, ID3-1 through ID3-16. The respective relative difference of accelerance RMS-values are collected in Table 10.2, along with the volumetric rate of exchanged birch. The study conducted here is as explained in Section 9.4. The 3rd-octave band plots can be seen in Figure 10.4, for select configurations.

Distribution Towards the Edges

Starting from ID3, with a whole layer exchanged to birch, the birch lamellae are reduced in the centre of the longitudinal direction, with greater reduction incrementing towards the edges. These sub-configurations, ID3-1 through ID3-5, exhibited pronounced reduction of the accelerance RMS-values. More specifically, sub-configuration ID3-5 with birch lamellae exclusively in the CLT-plate edges, performs on par with configuration ID3. However, ID3-3 and ID3-4 exhibited insignificant reduction thereof. This hints to using less birch close to the centre, while maintaining birch lamellae close to the edges.

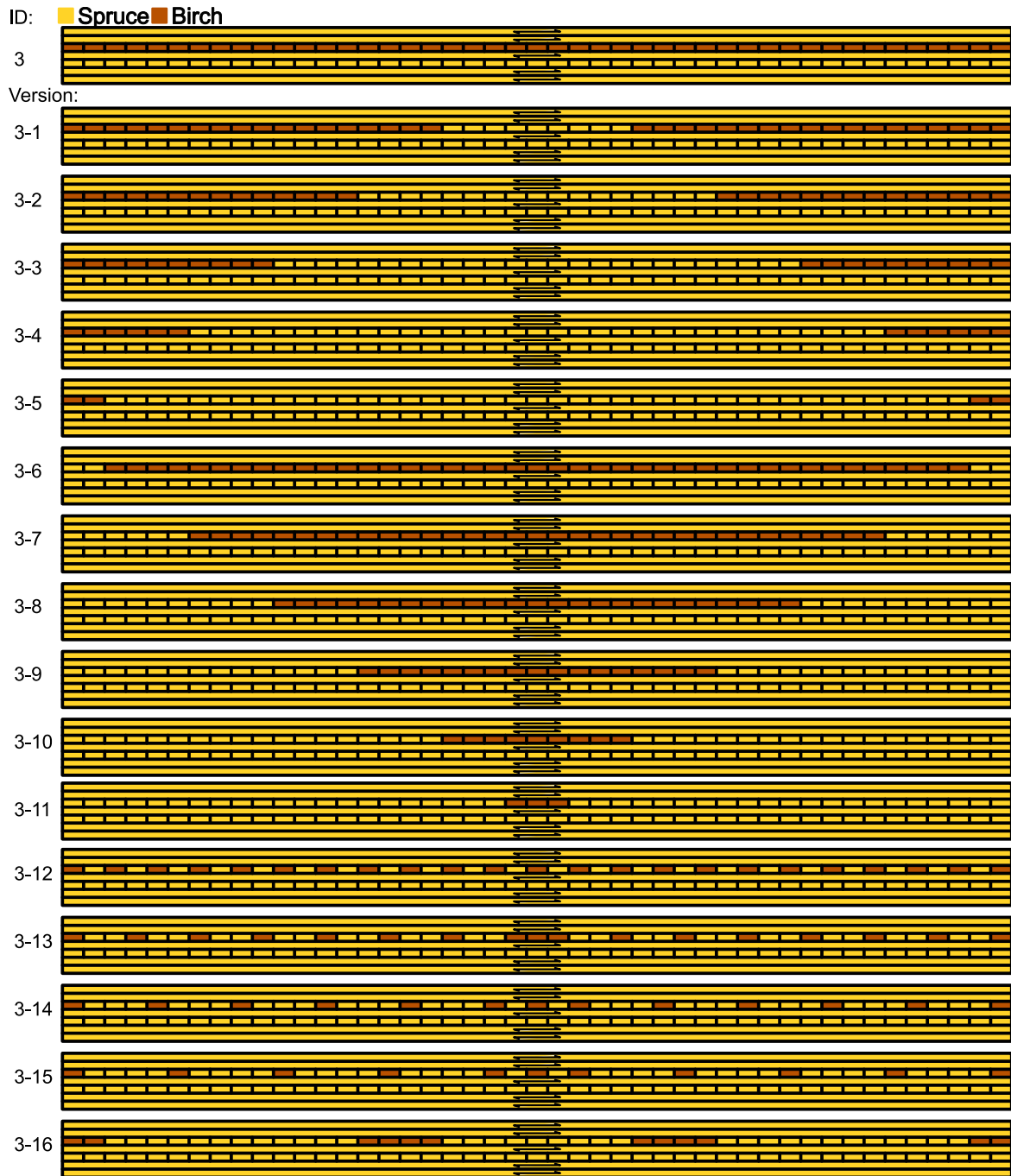


Figure 10.3: Birch sub-configurations of ID3.

Distribution Towards the Centre

Conversely to above, birch lamellae are excluded incrementally from the edges, towards the centre. These sub-configurations, ID3-6 through ID3-11, displayed unfavourable increase of the acceleration RMS-values. This indicates that birch lamellae should preferably be placed towards the edges, and less so towards the centre.

In Figure 10.4, improvement is found for a majority of the 3rd-octave bands for ID3-1, ID3-2 and ID3-5. For ID3-9, a worsening of vibration levels is found across most 3rd-octave bands.

Table 10.2: Birch sub-configurations of ID3, relative difference of RMS-values and volumetric rates of birch.

ID	RMS diff. [%]	Vol. rate [%]	ID	RMS diff. [%]	Vol. rate [%]
ID3	-13	14	ID3-9	10	5
ID3-1	-16	11	ID3-10	8	3
ID3-2	-10	9	ID3-11	0	1
ID3-3	-4	6	ID3-12	6	7
ID3-4	-5	4	ID3-13	-1	5
ID3-5	-13	1	ID3-14	-6	4
ID3-6	0	13	ID3-15	-4	3
ID3-7	-2	10	ID3-16	-10	4
ID3-8	8	8			

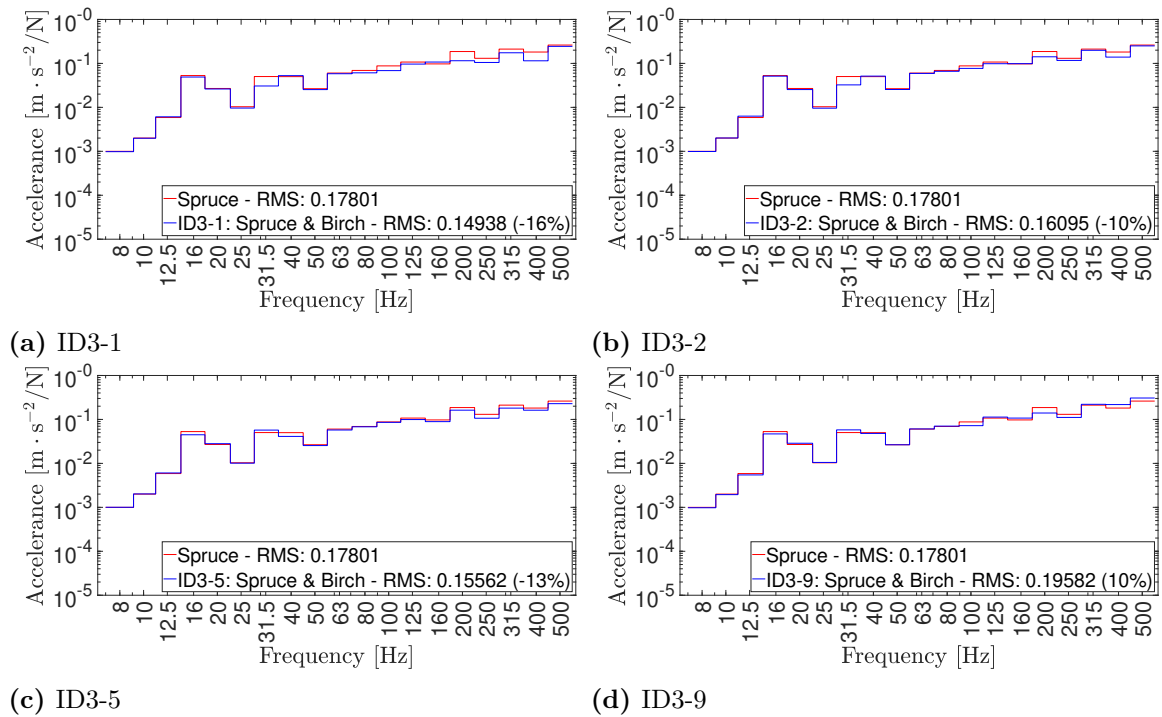


Figure 10.4: Accelerance plots, 3rd-octave band filters with RMS-values. Birch sub-configurations of ID3.

Systematic Distributions

Some distributions, with systematic spacing between the birch lamellae, have been performed. These sub-configurations, ID3-12 through ID3-16, displayed marginal reduction of the accelerance RMS-values, overall. More specifically, sub-configuration ID3-12 slightly increased the RMS-value, while ID3-16 reduced the RMS-value with 10%.

2-layer Configurations

In order to further study the distribution along the longitudinal direction, some 2-layer sub-configurations, corresponding to the most promising single-layer sub-configurations ID3-1, ID3-5, ID3-14 and ID3-16, have been analysed. These 2-layer sub-configurations, ID10-1 through ID10-4, are presented in Figure 10.3, along with the relative difference of acceleration RMS-values in Table 10.3.

In Figure 10.6, improvement is found for a majority of the 3rd-octave bands for both sub-configurations.

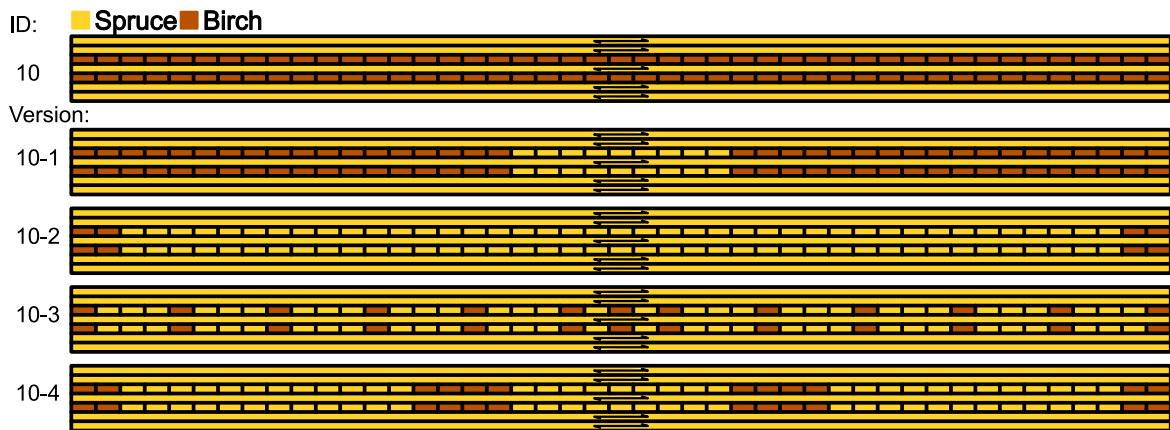
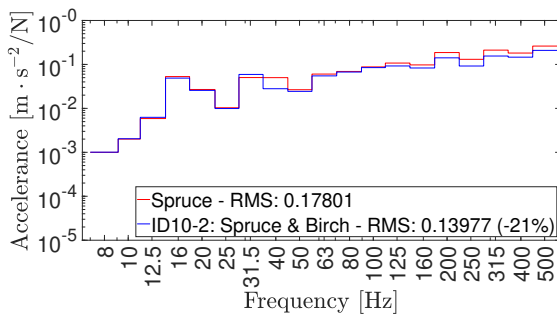


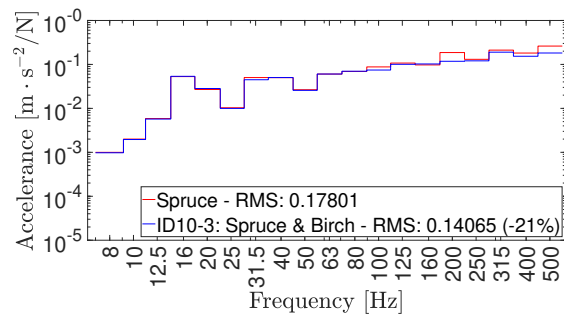
Figure 10.5: Birch sub-configurations of ID10.

Table 10.3: Birch, sub-configurations of ID10, relative difference of RMS-values and volumetric rates of birch.

ID	RMS diff. [%]	Vol. rate [%]
ID10	-22	29
ID10-1	-22	23
ID10-2	-22	3
ID10-3	-21	8
ID10-4	-22	8



(a) ID10-2



(b) ID10-3

Figure 10.6: Accelerance plots, 3rd-octave band filters with RMS-values. Birch sub-configurations of ID10.

These respective sub-configurations exhibited substantial reduction in the accelerance RMS-values, on average about 20%. This is roughly double the reduction, on average, compared to the reduction obtained from the promising single-layer sub-configurations. However, the sub-configurations perform equally well as the layer configuration.

Conclusion – Longitudinal Direction

By the conducted transversal lamellae configurations, pertaining to the longitudinal direction of the CLT-plate, it was observed that a favourable placement of the birch would be towards the edges. However, the extent of birch towards the edges cannot be well defined, since sub-configurations ID3-1, ID3-2 and ID3-5 perform roughly on the same level, while ID3-3 and ID-3-4 are deemed insignificant, although, the former two sub-configurations utilize more birch towards the centre contrary to the latter sub-configurations. Yet, the overall theme of keeping birch towards the edges remains relevant.

It is interesting, though, that sub-configuration ID3-5 with only four birch lamellae, performs on par with configuration ID3 with the whole layer in birch. Therefore, this specific arrangement of placing lamellae exclusively in the edges, will be further analysed in later stages.

Furthermore, the systematic sub-configurations, ID3-12 through ID3-16, with different periodic spacings of the birch lamellae, displayed differing responses. Hence, based on these limited number of configurations, the periodicity is deemed inconclusive. Although, the pronounced reduction of the RMS-values may be attributed to the fact that the lamellae are generally more concentrated towards the edges than the centre, as per the previous observation.

Additionally, increasing the number of layers involved seem to increase the reduction of the RMS-values. However, these sub-configurations, ID10-1 through ID10-4, perform equally as well as the layer configuration ID10. Thus, it is not possible to discern between the effect of having two layers of birch, and the effect of placing birch towards the edges. Hence, an unequivocal statement cannot be made about the placement of birch lamellas towards the edges, in this specific regard. Although, it can be concluded that these sub-configurations, ID10-1 through ID10-4, performs adequately by involving two layers, in a symmetric fashion. Moreover, these sub-configurations reduce the amount of birch by a substantial rate, in contrast to the full layer configuration ID10, while keeping the same performance.

10.1.3 Distribution of Lamellae – Transversal Direction

The investigation of the lamellae distribution along the transversal direction have been performed with a single layer, namely, the central layer, keeping the cross-section symmetric. This was done in order to capture the influence of birch along the transversal direction, without sway from non-symmetrical material distribution.

Figure 10.7 shows the tested sub-configurations of ID4, namely, ID4-1 through ID4-15. The respective relative difference of acceleration RMS-values are collected in Table 10.4, along with the volumetric rate of exchanged birch. The study conducted here is analogous to the study of the longitudinal direction. The 3rd-octave band plots can be seen in Figure 10.8, for select configurations.

In Figure 10.8, improvement is found for a majority of the 3rd-octave bands for ID4-7, ID4-9 and ID4-15. For ID4-1, improvement is found in a minority of the 3rd-octave bands.

Distribution Towards the Centre

Starting from ID4, with a whole layer exchanged with birch, the birch lamellae are reduced in the edges of the transversal direction, with greater reduction increment-

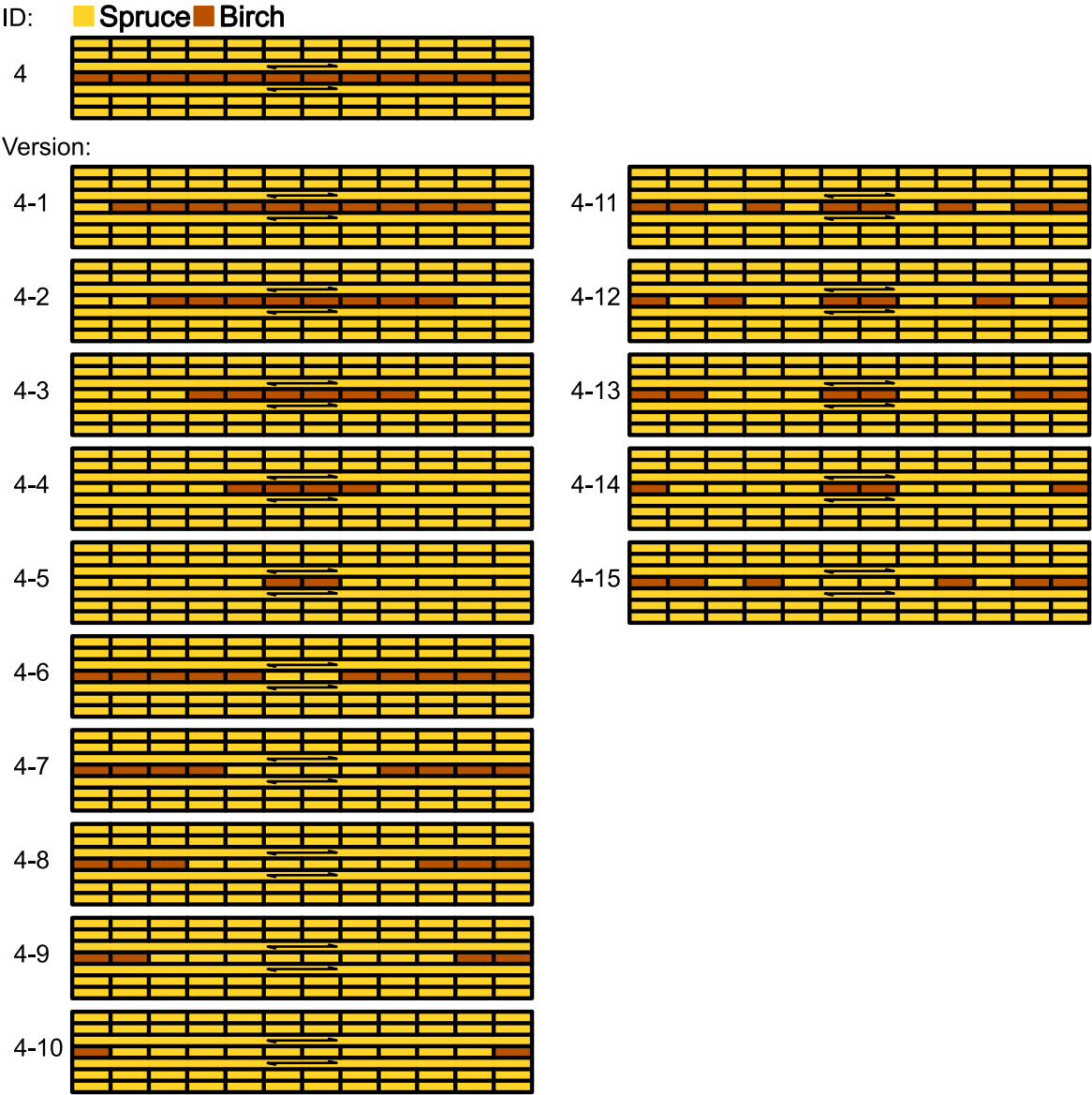


Figure 10.7: Birch sub-configurations of ID4.

ing towards the centre. These sub-configurations, ID4-1 through ID4-5, increased the accelerance RMS-values moderately. This hints at a preferable placement of birch lamellae towards the edges, as opposed to towards the centre of the transversal direction.

Table 10.4: Birch sub-configurations of ID4, relative difference of RMS-values and volumetric rates of birch.

ID	RMS diff. [%]	Vol. rate [%]	ID	RMS diff. [%]	Vol. rate [%]
ID4	-15	14			
ID4-1	10	12	ID4-11	-10	10
ID4-2	11	10	ID4-12	-2	7
ID4-3	7	7	ID4-13	-5	7
ID4-4	3	5	ID4-14	-3	5
ID4-5	7	2	ID4-15	-12	7
ID4-6	-9	12			
ID4-7	-11	10			
ID4-8	-7	7			
ID4-9	-12	5			
ID4-10	-11	2			

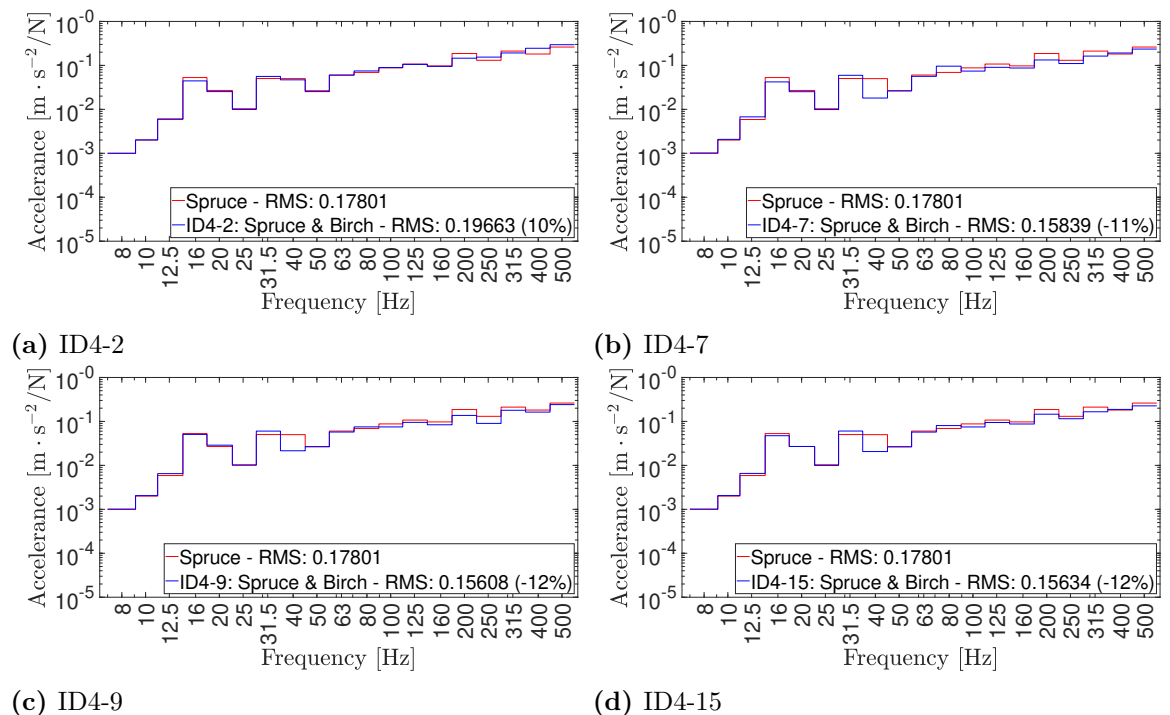


Figure 10.8: Accelerance plots, 3rd-octave band filters with RMS-values. Birch sub-configurations of ID4.

Distribution Towards the Edges

Conversely to above, birch lamellae are excluded incrementally from the centre, towards the edges. These sub-configurations, ID4-6 through ID4-10, reduced the accelerance RMS-values moderately, an average of 10%. This indicates that less birch should be used in centre, while maintaining birch lamellae to the edges.

Systematic Distribution

Some distributions, with systematic arrangement of the birch lamellae, have been performed. These sub-configurations, ID4-11 through ID4-15, displayed various degrees of reduction of the accelerance RMS-values. Sub-configurations ID4-11 and ID4-15 had an average reduction 11%, while the remaining sub-configurations had an insignificant RMS-value reduction. The commonality of the latter sub-configurations is that the central birch lamellae are included, even though the outer birch lamellae are also included.

Conclusion – Transversal Direction

By the conducted longitudinal lamellae configurations, pertaining to the transversal direction of the CLT-plate, it was observed that a favourable placement of the birch would be towards the edges, while keeping the central parts unexchanged with birch. The latter is further evidenced by the behaviour of the systematic sub-configurations, ID4-11 through ID4-15. These showcased that the central lamellae should not be exchanged with birch, as the response changed insignificantly with ID4-12, ID4-13 and ID4-14. However, ID4-11 and ID4-15 are almost identical, differing only in that the latter does not include the central lamellae of birch, while still performing equally well. By comparing ID4-11 with ID4-12, the latter performs worse than the former, by only removing one birch lamellae from each edge. This hints at the importance of keeping the edge lamellae of birch. Hence, the theme of keeping the birch concentrated towards the edges, away from the central part, remain profound. It is also interesting that ID4-15 performs on par with ID4, while having 50% less birch usage.

10.1.4 Distribution of Lamellae – Combined Directions

Based on the previous distributions and conclusions thereof, a combination is made of these former observations. The theme maintained here is that of keeping birch concentrated towards the edges in the transversal and longitudinal direction, respectively, as well as towards the centre of the thickness direction. Multilayer configurations, cf. Figure 10.1, are altered in order to combine transversal and longitudinal lamellae. The choice of these sub-configurations was based on the feasibility to apply the previous recorded conclusions. These sub-configurations are categorised into the number of layers involved.

2-layer Sub-configurations

The chosen configuration to be further studied coincides with the previously promising configuration ID13. The following sub-configurations, ID13-1 through ID13-4, have been constructed and are presented in Figure 10.9, and their respective relative difference of acceleration RMS-values in Table 10.5. All sub-configurations exhibited significant reduction of the RMS-values, averaging about 24%. However, this is on par with the 2-layered configuration ID13. The 3rd-octave band plots can be seen in Figure 10.10, for select configurations.

In Figure 10.10, improvement is found for a majority of the 3rd-octave bands for ID13-3 and ID13-4.

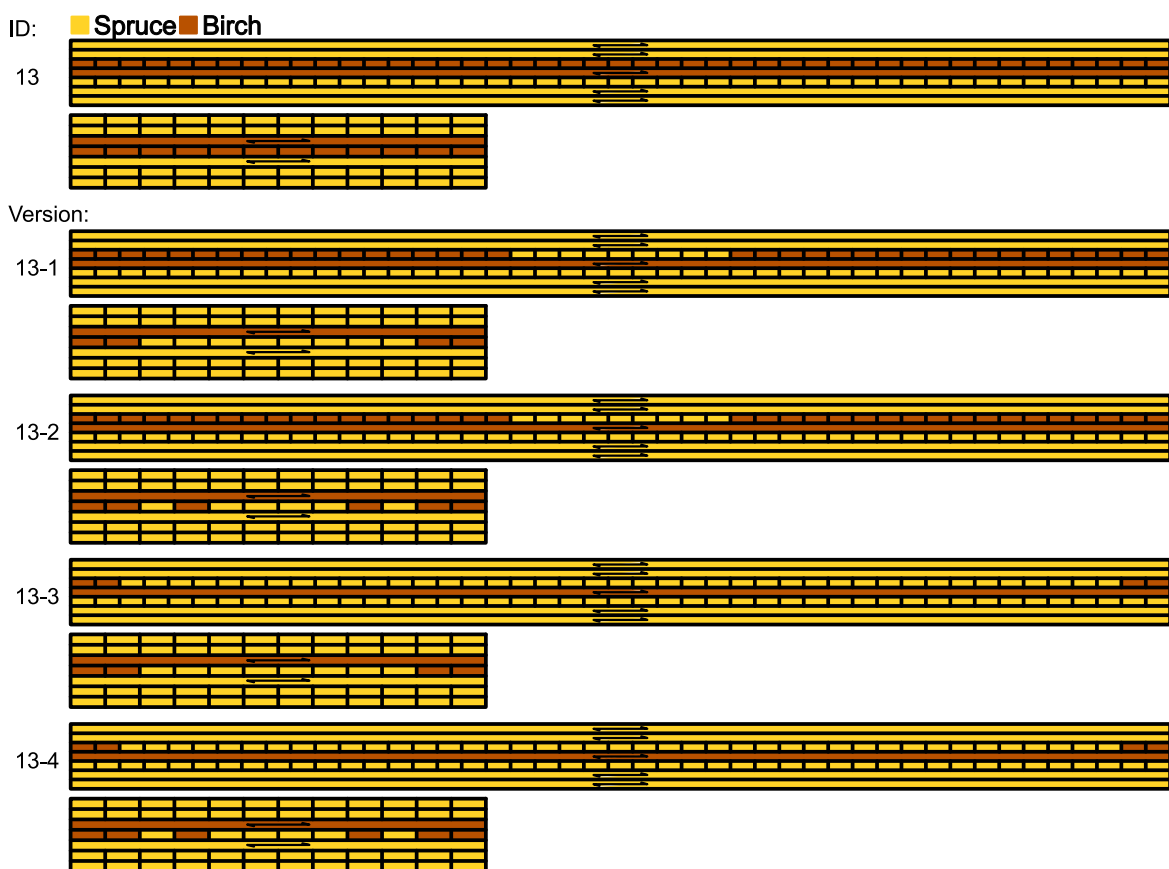


Figure 10.9: Birch sub-configurations of ID13.

Table 10.5: Birch sub-configurations of ID13, relative difference of RMS-values and volumetric rates of birch.

ID	RMS diff. [%]	Vol. rate [%]
ID13	-23	29
ID13-1	-21	16
ID13-2	-19	19
ID13-3	-28	6
ID13-4	-27	8

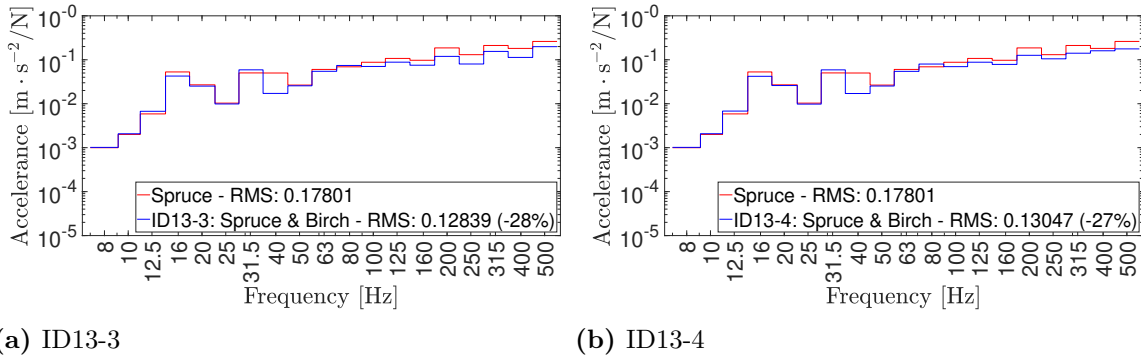


Figure 10.10: Accelerance plots, 3rd-octave band filters with RMS-values. Birch sub-configurations of ID13.

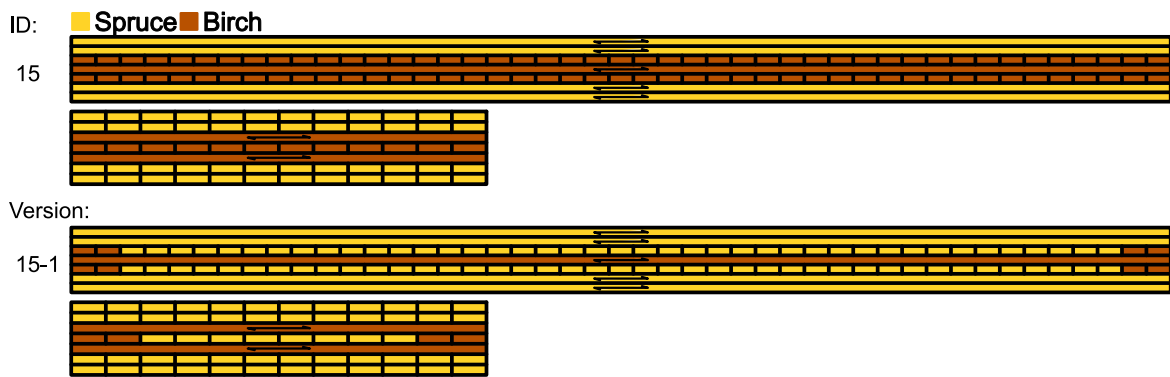


Figure 10.11: Birch sub-configurations of ID15.

Table 10.6: Birch sub-configurations of ID15, relative difference of RMS-values and volumetric rates of birch.

ID	RMS diff. [%]	Vol. rate [%]
ID15	-26	43
ID15-1	-38	7

3-layer Sub-configuration

Configuration ID15 have been sub-configured into ID15-1, keeping only the external birch lamellae in the transversal and longitudinal direction, respectively, while maintaining the distribution about the central layer in the thickness direction, cf. Figure 10.11. The reduction of RMS-value, cf. Table 10.6, was 38%. The 3rd-octave band plots can be seen in Figure 10.12, for select configurations.

In Figure 10.12, improvement is found for a majority of the 3rd-octave bands for ID15-1.

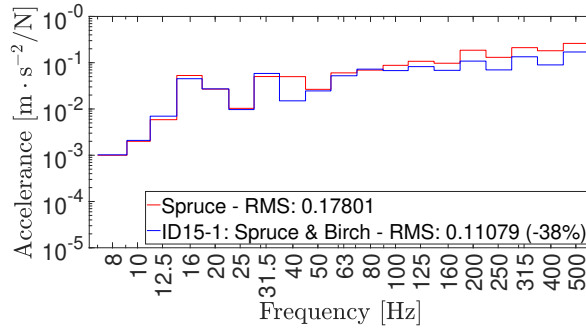


Figure 10.12: Accelerance plot, 3rd-octave band filters with RMS-values. Birch sub-configuration ID15-1.

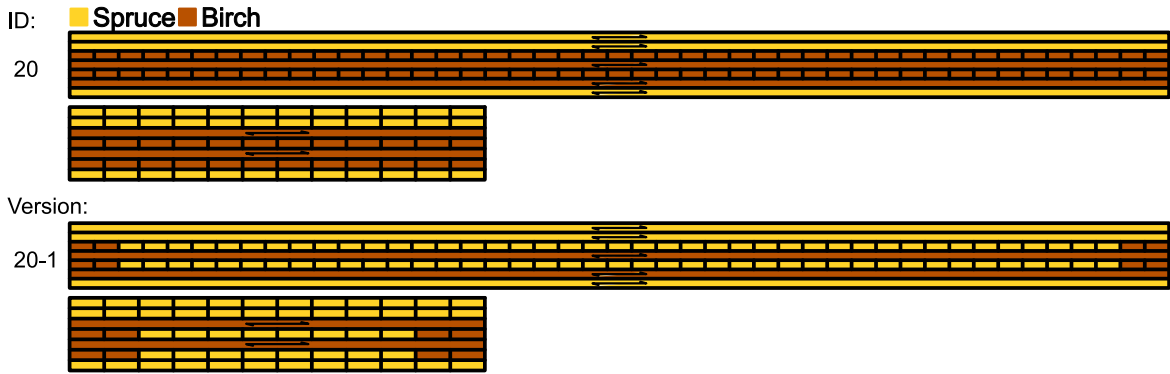


Figure 10.13: Birch sub-configurations of ID20.

Table 10.7: Birch sub-configurations of ID20, relative difference of RMS-values and volumetric rates of birch.

ID	RMS diff. [%]	Vol. rate [%]
ID20	-29	57
ID20-1	-44	12

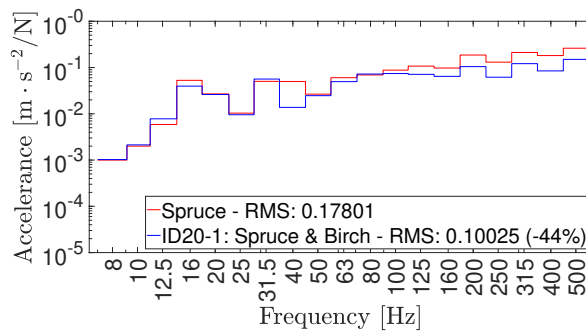


Figure 10.14: Accelerance plot, 3rd-octave band filters with RMS-values. Birch sub-configuration ID20-1.

4-layer Configuration

Configuration ID20 have been sub-configured into ID20-1, keeping only the external birch lamellae in the transversal and longitudinal direction, respectively, involving the central layer in the thickness direction, cf. Figure 10.13. The reduction of RMS-value,

cf. Table 10.7, was 44%. The 3rd-octave band plots can be seen in Figure 10.14, for select configurations.

In Figure 10.14, improvement is found for a majority of the 3rd-octave bands for ID20-1.

5-layer Configuration

Configuration ID22 have been sub-configured into ID22-1, keeping only the external birch lamellae in the transversal and longitudinal direction, respectively, while maintaining the distribution about the central layer, cf. Figure 10.15. The reduction of RMS-value, cf. Table 10.8, was 56%. The 3rd-octave band plots can be seen in Figure 10.16, for select configurations.

In Figure 10.12, improvement is found for a majority of the 3rd-octave bands for ID15-1.

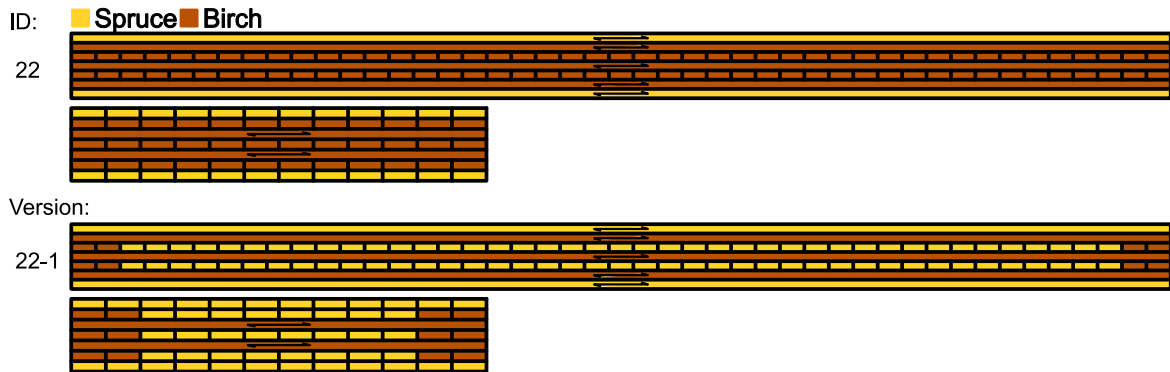


Figure 10.15: Birch sub-configurations of ID22.

Table 10.8: Birch sub-configurations of ID22, relative difference of RMS-values and volumetric rates of birch.

ID	RMS diff. [%]	Vol. rate [%]
ID22	-33	71
ID22-1	-49	17

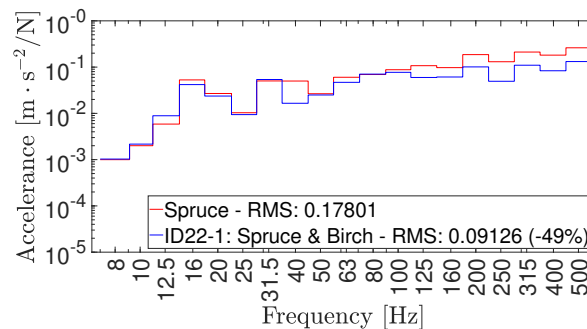


Figure 10.16: Accelerance plot, 3rd-octave band filters with RMS-values. Birch sub-configuration ID22-1.

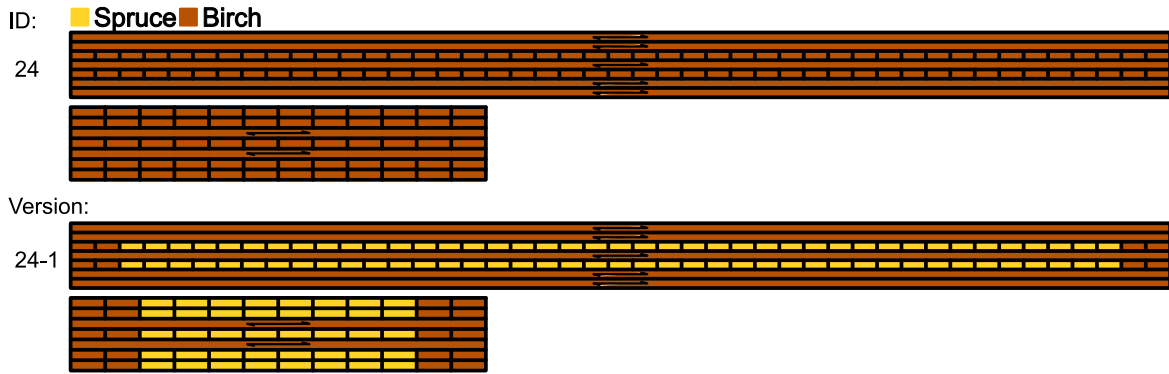


Figure 10.17: Birch sub-configurations of ID24.

Table 10.9: Birch sub-configurations of ID24, relative difference of RMS-values and volumetric rates of birch.

ID	RMS diff. [%]	Vol. rate [%]
ID24	-46	100
ID24-1	-56	26

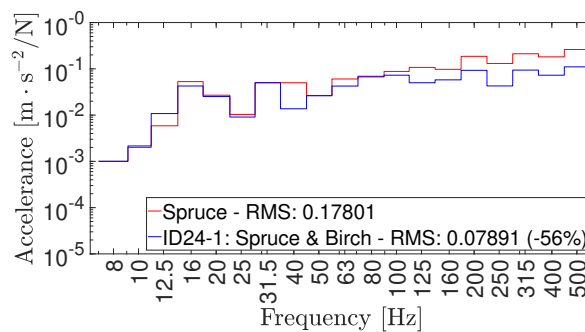


Figure 10.18: Accelerance plot, 3rd-octave band filters with RMS-values. Birch sub-configuration ID24-1.

7-layer Configuration

Configuration ID24, which is the homogeneous CLT-plate of birch, have been sub-configured into ID24-1. This sub-configuration keeps only the external birch lamellae in the transversal and longitudinal direction, respectively, while maintaining the distribution about the central layer, cf. Figure 10.17. The reduction of RMS-value, cf. Table 10.9, was 38%. The 3rd-octave band plots can be seen in Figure 10.18, for select configurations.

In Figure 10.18, improvement is found for a majority of the 3rd-octave bands for ID24-1.

Conclusion – Combined Directions

The sub-configurations with combined transversal and longitudinal lamellae, respectively, have performed exceptionally, proving that the observed birch scheme is highly

relevant. That is, placing birch lamellae in the perimeter of the CLT-plate, stacked about the central layer. Great reductions in RMS-values were obtained by applying this scheme, by upmost of roughly 60% percent as seen for ID24-1. Furthermore, this scheme alludes perfectly to the concept of keeping the birch usage relatively limited, while maintaining heightened performance with regards to the acceleration response.

Additionally, the insignificant discrepancy between the performance of the respective sub-configurations have been noted. Although, these sub-configurations are quite similar, mainly differing in the inclusion of birch lamellae close to the centre in transversal and longitudinal direction, respectively. This may indicate that it suffices to adhere to the birch scheme partially, e.g., only having birch lamellae in the longitudinal perimeter, while allowing central birch lamellae in the transversal direction. However, from a material efficiency standpoint, fully adhering to the birch scheme would be preferable, due to the minimized usage of birch lamellae.

10.1.5 Conclusion – L-sized CLT-plate

This section ties together the previous observations, concluding them in a concise manner. Throughout the performed case study of the L-sized CLT-plate, the birch placement was predominantly favourable when collected along the perimeter of the CLT-plate, stacked about the central layer. This birch scheme proved to ameliorate the acceleration response, by heavily reducing said response. Even though periodic birch schemes have been studied, none hinted at a consistent behaviour and is hence deemed inconclusive, with respect to the limited amount of such periodic schemes performed.

Furthermore, it was possible to achieve birch schemes that reduced the accelerance RMS-values significantly, without exchanging large amounts of the original spruce. This is advantageous from a material efficiency point of view, proving that there is a profit of investigating the lamellae distribution in CLT-plates, and not blindly incorporating stiffer and heavier material in abundance. The notable sub-configurations are collected in Figure 10.19, with their respective reduction of accelerance RMS-values, as well as volumetric rate of birch used in Table 10.10. The following bullet-points sum up the important points:

- The numerical results suggests that a scheme of applying birch along the perimeter of the CLT-plate, concentrated to the central layer, while keeping the internal portions of the CLT-plate birch-free, yields the greatest reductions of accelerance.
- Reduction of accelerance RMS-values is exceptional. Notably, ID22-1 reduced the RMS-value by roughly 50%, while being composed of slightly less than 20% birch.

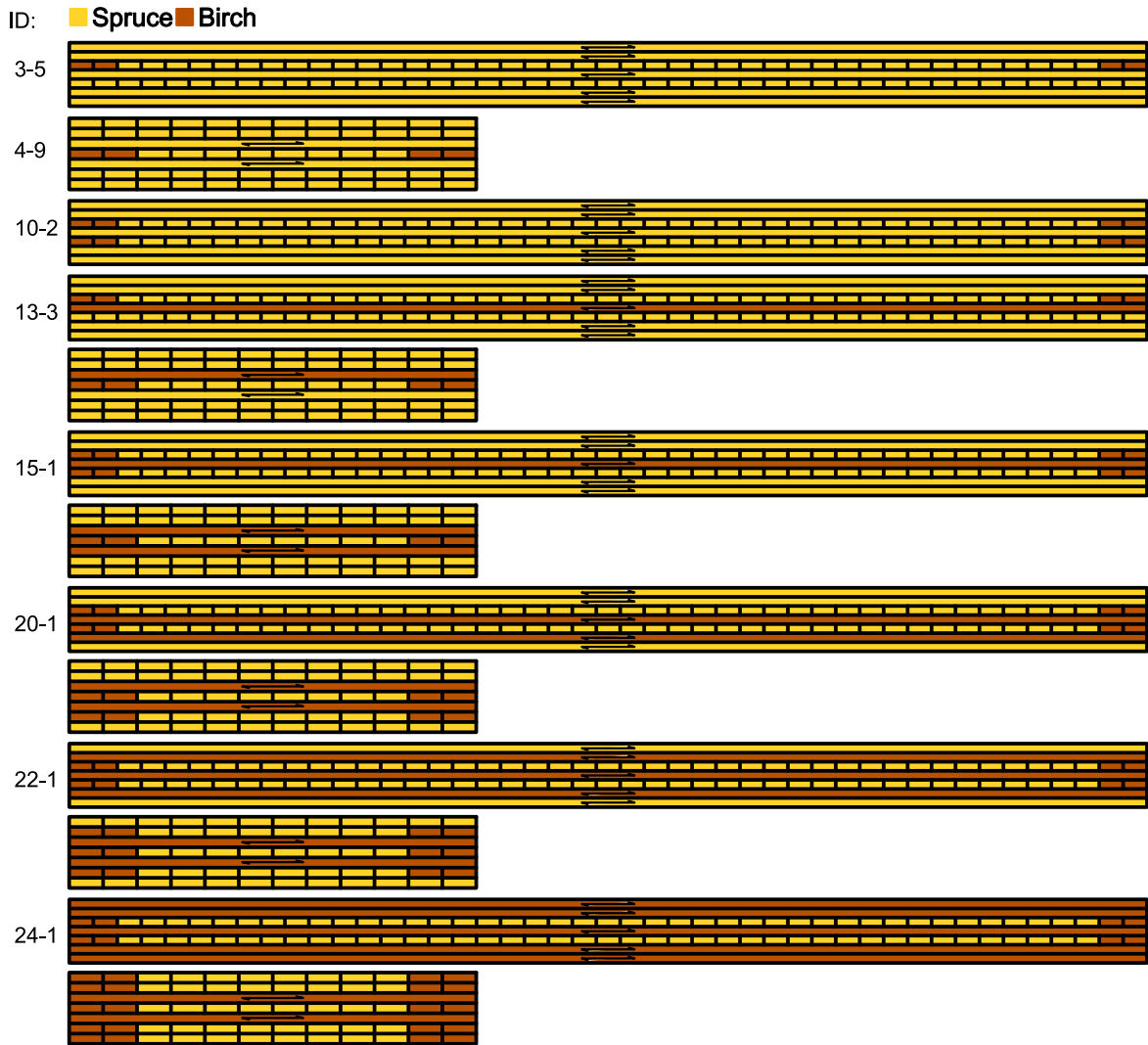


Figure 10.19: Notable birch sub-configurations.

Table 10.10: Notable birch sub-configurations, reduction of RMS-values and volumetric rates of birch.

ID	RMS diff. [%]	Vol. rate [%]
ID3-5	-13	1
ID4-9	-12	5
ID10-2	-22	3
ID13-3	-28	6
ID15-1	-38	7
ID20-1	-44	12
ID22-1	-49	17
ID24-1	-56	26

10.2 S-sized CLT-plate

This section presents the results concerning the S-sized CLT-plate. As mentioned in Section 9.4, the presentation is subdivided according to the three principal axes. Throughout this section, the reference case has been the homogeneous S-sized CLT-plate, made out of spruce with calibrated parameters.

10.2.1 Distribution of Lamellae – Thickness Direction

The layer configurations, pertaining to the thickness direction of the S-sized CLT-plate, are presented in Figure 10.20. Additionally, the relative difference of acceleration RMS-values, along with the volumetric rates of exchanged birch, are presented in Table 10.11. In contrast to the L-sized CLT-plate, the S-sized CLT-plate consists of five layers, which greatly limits the amount of symmetric layer configurations. The 3rd-octave band plots can be seen in Figure 10.21, for select configurations.

In Figure 10.21, improvement is found for a majority of the 3rd-octave bands for IDs 6S, 9S and 11S. Improvement across all a minority of the octave bands is found for ID2S and ID3S.

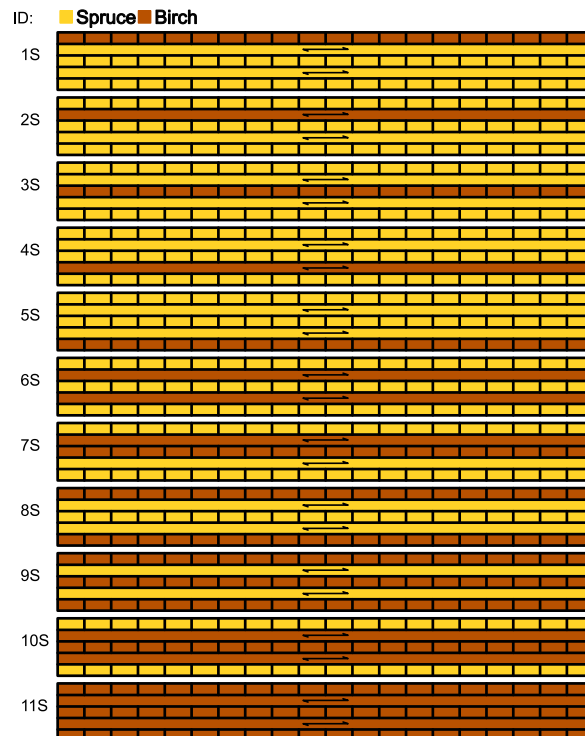


Figure 10.20: Layer configurations.

Table 10.11: Layer configurations, relative difference of RMS-values and volumetric rates of birch.

ID	RMS diff. [%]	Vol. rate [%]
ID1S	-2	20
ID2S	-3	20
ID3S	-2	20
ID4S	-4	20
ID5S	-4	20
ID6S	-15	40
ID7S	-12	40
ID8S	-15	40
ID9S	-20	60
ID10S	-14	60
ID11S	-30	100

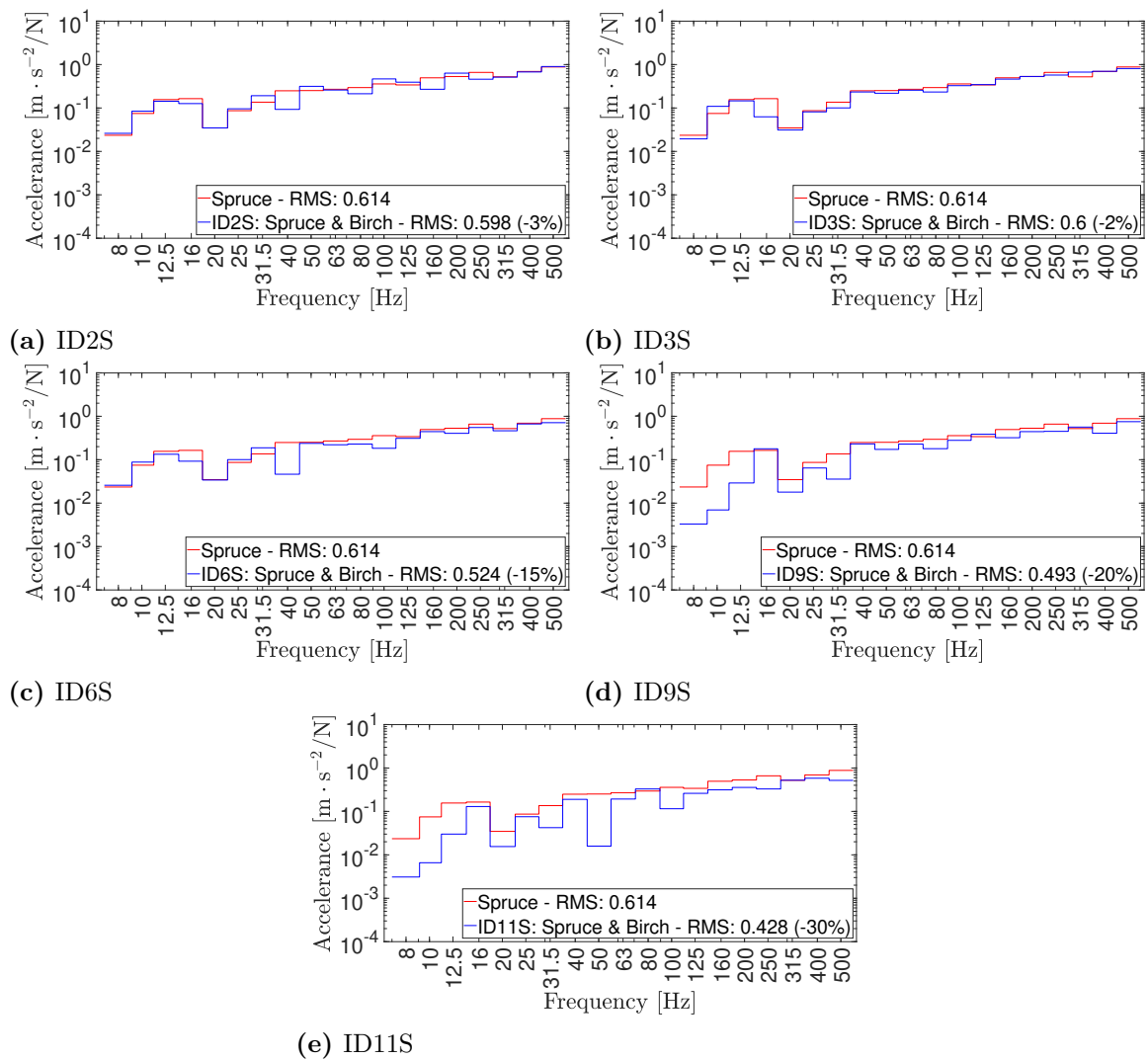


Figure 10.21: Accelerance plots, 3rd-octave band filters with RMS-values. Birch configurations ID2S, ID3S, ID6S, ID9S and ID11S.

Single-layer Configurations

The single-layer configurations, ID1S through ID5S, exhibited insignificant reduction of the accelerance RMS-values, on average 3%, and hence no pattern can be deduced regarding favourable layers.

Multilayer Configurations

With regards to the multilayer configurations, different implications are observed with respect to the number of layers involved. The number of layers involved varied between 2-3. Additionally, a homogeneous CLT-plate of birch was analysed for more lucid comparisons.

The 2-layer configurations, ID6S through IDS8, exhibited pronounced reduction of the accelerance RMS-values, averaging 21%. Notably, configuration ID7S involved the central birch layer, although performing equal to the configurations ID6S and ID8S that do not include the central birch layer. Furthermore, ID8S has the outer-most layers in birch, and still performs equal to the remaining configurations. Hence, no pattern can be deduced regarding the inclusion of the central layer.

The 3-layer configurations, IDS9 and IDS10, displayed moderate reduction of the accelerance RMS-values, namely, 20% and 15% respectively. IDS9 performs slightly better than the previous configurations, although no indication can towards a favourable birch position can be found.

Conclusion – Thickness Direction

By the conducted layer configurations, pertaining to the thickness direction of the CLT-plate, no specific pattern was observed favouring a specific placement of the birch. Although, it was observed that the CLT-plate performance increased drastically from single-layer to multilayer configurations. The highest recorded reduction of RMS-value was configuration ID10S at 20%, while composed of 20% birch. However, the remaining configurations could not compete with the homogeneous birch configuration ID11S, which reduced the RMS-value by 30%.

10.2.2 Distribution of Lamellae – Longitudinal Direction

The investigation of the lamellae distribution along the longitudinal direction was performed with a single layer. The only choices of suitable configurations to perform this study on are ID2S and ID4S, whereby the former was chosen to avoid redundancy. Furthermore, a 2-layer configuration have been further studied.

Figure 10.22 shows the tested sub-configurations of ID2S, namely, ID2S-1 through ID2S-9. The corresponding relative difference of accelerance RMS-values, as well as the volumetric rates of birch, are presented in Table 10.12. These sub-configurations

mimic the patterns of the same investigation done for the L-sized CLT-plate in Section 10.1.2, following the outline given in Section 9.4. The 3rd-octave band plots can be seen in Figure 10.23, for select configurations.

In Figure 10.23, improvement is found in around half of the 3rd-octave bands for ID2S-3 and ID2S-6.

Distribution Towards the Centre

Starting from ID2S, with a whole layer exchanged to birch, the birch lamellae are reduced from the edges, towards the centre. These sub-configurations, ID2S-1 through

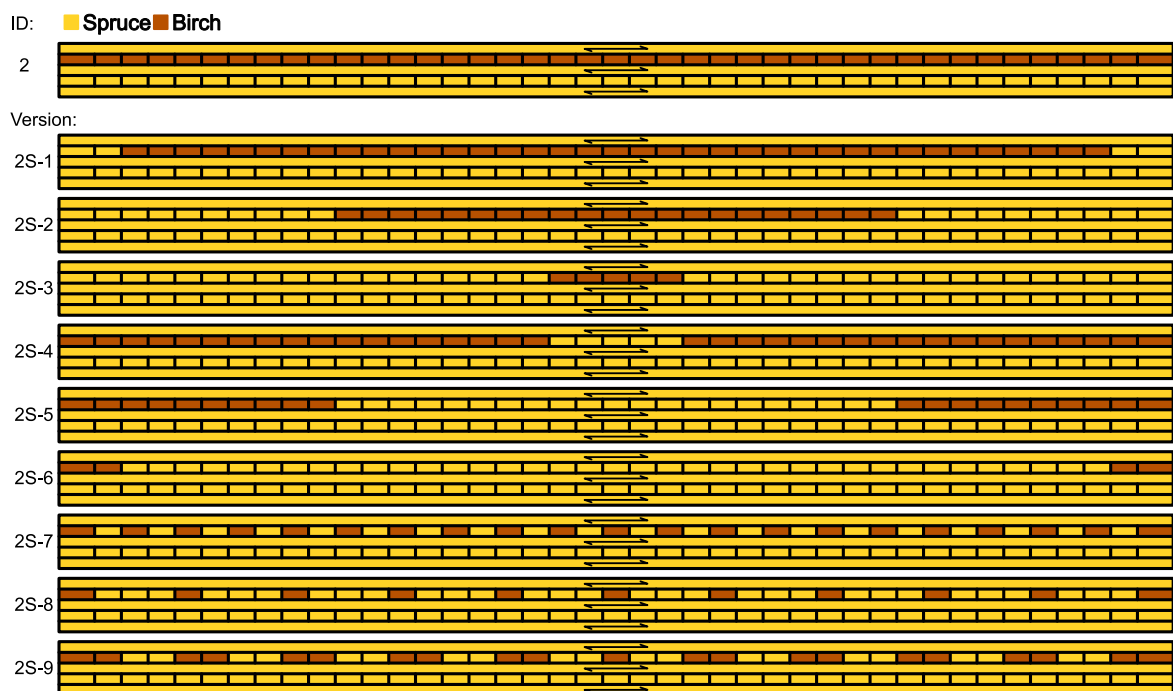


Figure 10.22: Birch sub-configurations of ID2S.

Table 10.12: Birch sub-configurations of ID2S, relative difference of RMS-values and volumetric rates of birch.

ID	RMS diff. [%]	Vol. rate [%]
ID2S	-3	20
ID2S-1	-1	18
ID2S-2	-0	21
ID2S-3	-7	2
ID2S-4	-2	18
ID2S-5	-2	10
ID2S-6	-9	2
ID2S-7	-4	10
ID2S-8	-9	6
ID2S-9	-2	10

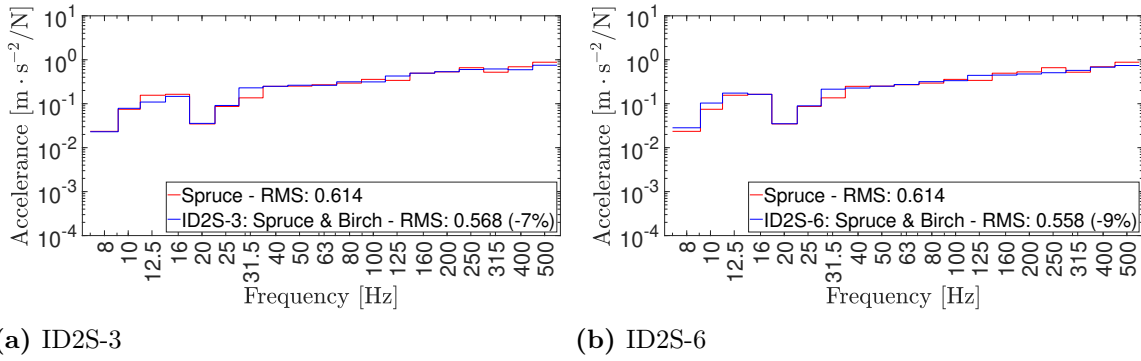


Figure 10.23: Accelerance plots, 3rd-octave band filters with RMS-values. Birch sub-configurations of ID2S.

ID2S-3, exhibited insignificant reduction overall. Namely, ID2S-1 and ID2S-2 had almost no influence on the RMS-value, while ID2S-3 reduced the RMS-value by 7%, which is deemed insignificant. Hence, this indicates that placing birch lamellae in the centre of the longitudinal direction is unfavourable.

Distribution Towards the Edges

Conversely to above, the birch lamellae are reduced incrementally from the centre of the longitudinal direction, towards the edges thereof. These sub-configurations, ID2S-4 through ID2S-6, exhibited marginal reduction of the accelerance RMS-values. However, ID2S-4 and ID2S-5 had almost no influence on the RMS-value, while ID2S-6 had 9% reduction which is considered marginal. Thus, the performance of the CLT-plate is not significantly improved by placing the lamellae towards the edges in the longitudinal direction, although only marginally improved.

Systematic Distribution

Some systematic distributions of the birch lamellae, in a periodic manner with different spacings of the birch lamellae, have been performed. These sub-configurations, ID2S-7 through ID2S-9, displayed marginal reduction of the accelerance RMS-values. It is noteworthy that ID2S-8 had the highest reduction of the RMS-value, at 9%, while having the least concentrated amount of birch lamellae to the centre of the longitudinal direction.

2-layer Configuration

A 2-layer sub-configuration of ID6S have been performed, namely ID6S-1, cf. Figure 10.24. The reduction of the RMS-value is given in Table 10.13. This sub-configuration maintains the reduction of the RMS-value, while using significantly less birch lamellae. The 3rd-octave band plots can be seen in Figure 10.25, for select configurations.

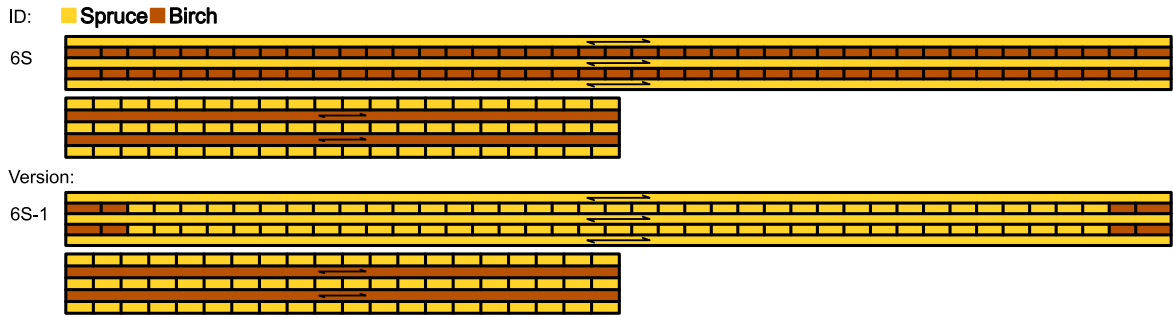


Figure 10.24: Birch sub-configuration of ID6S.

Table 10.13: Birch sub-configuration of ID6S, relative difference of RMS-values and volumetric rates of birch.

ID	RMS diff. [%]	Vol. rate [%]
ID6S	-15	40
ID6S-1	-12	3

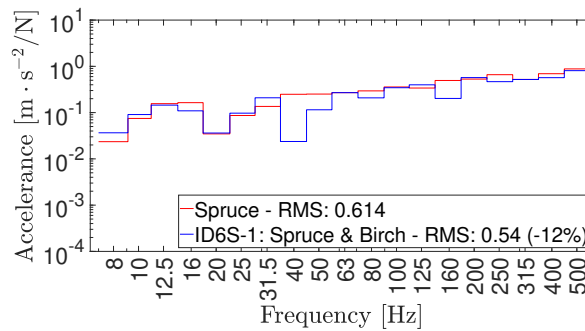


Figure 10.25: Accelerance plot, 3rd-octave band filters with RMS-values. Birch sub-configuration of ID6.

In Figure 10.25, improvement is found in a majority of the 3rd-octave bands.

Conclusion – Longitudinal Direction

By the conducted transversal lamellae configurations, pertaining to the longitudinal direction of the CLT-plate, it was observed that a favourable placement of the birch would be towards the edges. However, the reduction of the RMS-values was not significant. This may hint at the fact that the smaller sized CLT-plate is rigid and less susceptible to dynamical phenomena, as well as less sensitive to material variability, in terms of the longitudinal direction.

Additionally, increasing the number of layers involved, as in ID6S-1, contributed insignificantly to the reduction of the RMS-value, in comparison to ID2S-6. However, only one multilayer sub-configuration was performed, and thus, an unequivocal statement regarding the number of layers involved cannot be made, in terms of the longitudinal direction.

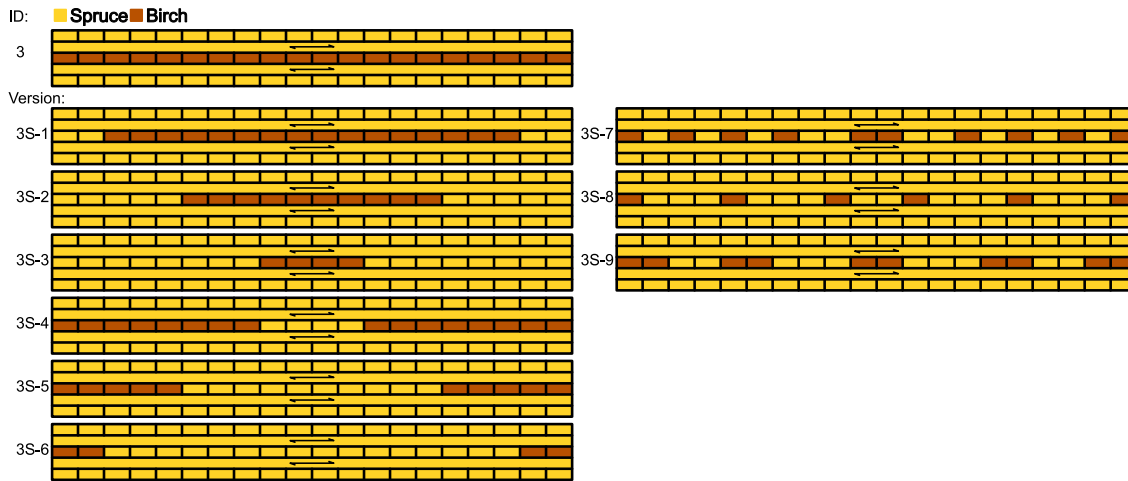


Figure 10.26: Birch sub-configuration of ID3S.

Table 10.14: Birch sub-configuration of ID3S, relative difference of RMS-values and volumetric rates of birch.

ID	RMS diff. [%]	Vol. rate [%]	ID	RMS diff. [%]	Vol. rate [%]
ID3S	-2	20			
ID3S-1	3	16	ID3S-7	-1	10
ID3S-2	3	10	ID3S-8	7	6
ID3S-3	0	4	ID3S-9	-1	10
ID3S-4	-4	16			
ID3S-5	-1	10			
ID3S-6	-10	4			

10.2.3 Distribution of Lamellae – Transversal Direction

The investigation of the lamellae distribution along the transversal direction have been performed with single-layer configurations as well as multilayer configurations. This was done based on the lack of prominent patterns, with significant reduction of RMS, in the previous study along the longitudinal direction.

Figure 10.26 shows the tested single-layer sub-configurations of ID3S, namely, ID3S-1 through ID3S-9. The respective relative difference of accelerance RMS-values is collected in Table 10.14, along with the volumetric rate of exchanged birch. The 3rd-octave band plots can be seen in Figure 10.27, for select configurations, where improvement is found in a majority of the 3rd-octave bands.

Distribution Towards the Centre

Starting from ID3S, with a whole layer exchanged with birch, the birch lamellae are reduced in the edges of the transversal direction, with greater reduction incrementing towards the centre. These sub-configurations, ID3S-1 through ID3S-3, displayed minimal change of the accelerance RMS-values. This hints at an unpreferable placement of birch lamellae towards the centre of the transversal direction.

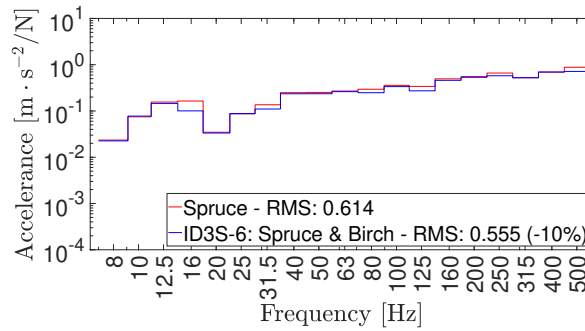


Figure 10.27: Accelerance plot, 3rd-octave band filters with RMS-values. Birch sub-configuration ID3S-6.

Distribution Towards the Edges

Conversely to above, birch lamellae are excluded incrementally from the centre, towards the edges. These sub-configurations, ID3S-4 through ID3S-6, displayed mixed reduction of the accelerance RMS-values. In particular, ID3S-4 and ID3S-5 exhibited insignificant change of the RMS, while ID3S-6 exhibited pronounced reduction thereof, at 10%. This indicates that less birch should be used in the centre, while maintaining birch lamellae to the edges.

Systematic Distributions

Some distributions, with systematic arrangement of the birch lamellae, have been performed. These sub-configurations, ID3S-7 through ID3S-9, displayed insubstantial reduction of the accelerance RMS-values. Notably, ID3S-8 showcased an unpreferable increase of the RMS. Thus, no indication is obtained regarding a favourable periodic birch placement.

2-layer Configuration

A 2-layer sub-configuration of ID8S have been performed, namely ID8S-1, cf. Figure 10.28. The accelerance RMS-value was unfavourably increased, to a significant extent, from the full layer configuration ID8S, cf. Table 10.15. The full layer configuration ID8S reduced the RMS with 15%, while sub-configuration increased the RMS with 10%, with respect to the reference case. This indicates that an increase of involved layers, in terms of the transversal direction, may not necessarily be preferred. The 3rd-octave band plots can be seen in Figure 10.29, for select configurations.

In Figure 10.29, improvement is found in a majority of the 3rd-octave bands.

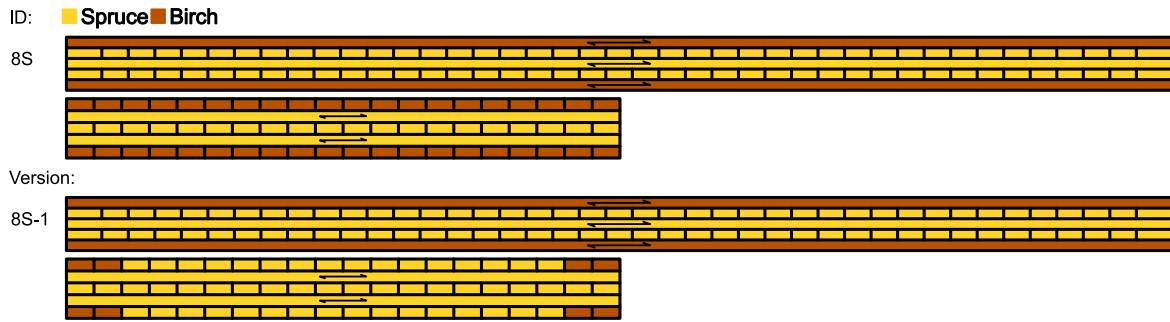


Figure 10.28: Birch sub-configuration of ID8S.

Table 10.15: Birch sub-configuration of ID3S, relative difference of RMS-values and volumetric rates of birch.

ID	RMS diff. [%]	Vol. rate [%]
ID8S	-15	40
ID8S-1	11	8

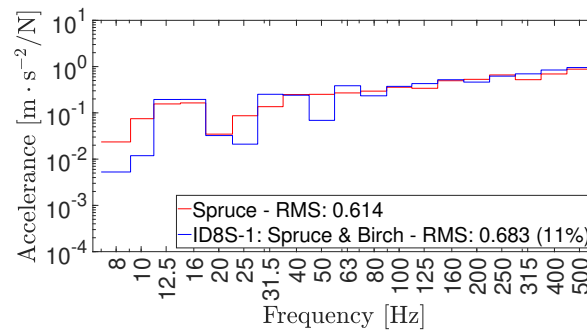


Figure 10.29: Accelerance plot, 3rd-octave band filters with RMS-values. Birch sub-configuration ID8S-1.

Table 10.16: Birch sub-configuration of ID9S, relative difference of RMS-values and volumetric rates of birch.

ID	RMS diff. [%]	Vol. rate [%]
ID9S	-20	60
ID9S-1	-1	12

3-layer Configuration

A 3-layer sub-configuration of ID9S have been performed, namely ID9S-1, cf. Figure 10.30. The accelerance RMS-value was insignificantly changed, cf. Table 10.16. Notably, the comparison of the full layer configuration ID9S and the sub-configuration ID9S-1, reveals unfavourably increased accelerance RMS-value, to a significant extent. This indicates that increasing the number of involved layers may not necessarily be preferable. The 3rd-octave band plots can be seen in Figure 10.31, for select configurations.

In Figure 10.31, improvement is found in a majority of the 3rd-octave bands.

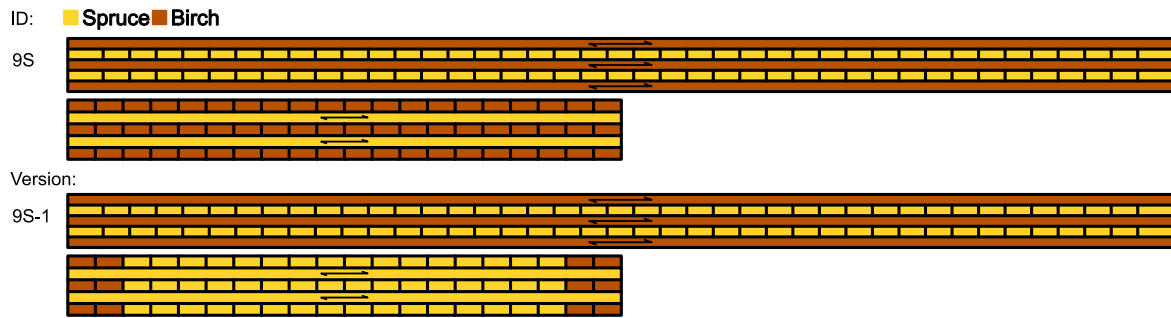


Figure 10.30: Birch sub-configuration of ID9S.

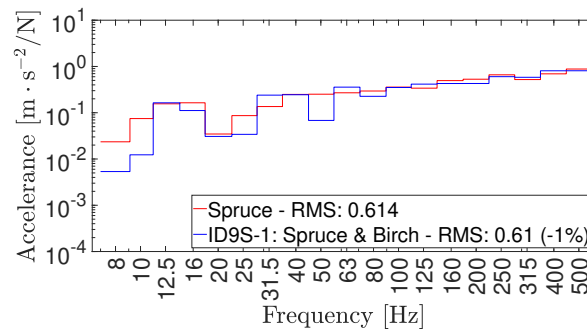


Figure 10.31: Accelerance plot, 3rd-octave band filters with RMS-values. Birch sub-configuration ID9S-1.

Conclusion – Transversal Direction

By the conducted longitudinal lamellae configurations, pertaining to the transversal direction of the CLT-plate, it was observed that a favourable placement of the birch would be towards the edges, while keeping the central parts unexchanged with birch. However, the extent of reduction of RMS-values by this approach is moderate. The periodic distributions did not reveal an optimal placement of the birch lamellae, although these included birch lamellae of the central portion, which was evidenced by ID3S-1 through ID3S-3 to be an unfavourable approach.

Furthermore, it was observed that increasing the number of involved layers unfavourably increased the RMS-values, to a significant extent. Hence, it would be preferable to only utilize a single layer, with respect to the sub-configurations.

10.2.4 Distribution of Lamellae – Combined Directions

Based on the previous distributions and conclusions thereof, a combination is made of these former observations. The theme of maintaining the birch lamellae towards the edges in the transversal and longitudinal direction, respectively, is followed. Multilayer configurations, cf. Figure 10.20, are altered in order to combine transversal and longitudinal lamellae. The choice of these sub-configurations was based on the feasibility to apply the previous recorded conclusions. These sub-configurations are categorized into the number of layers involved.

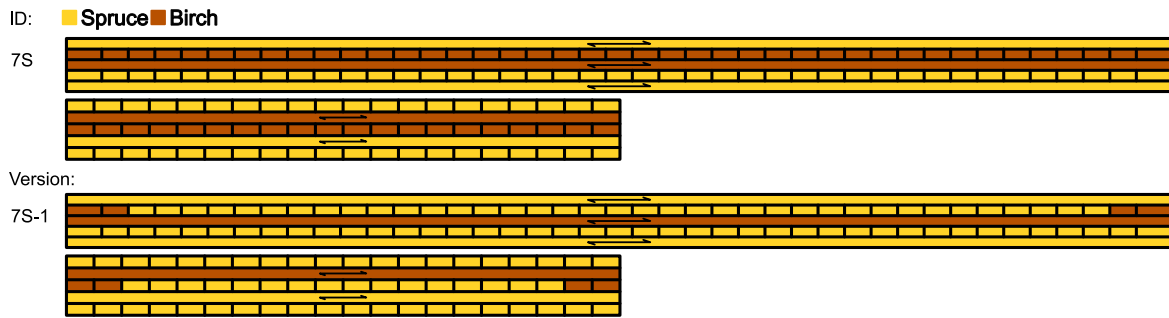


Figure 10.32: Birch sub-configuration of ID7S.

Table 10.17: Birch sub-configuration of ID7S.

ID	RMS diff. [%]	Vol. rate [%]
ID7S	-12	40
ID7S-1	-14	6

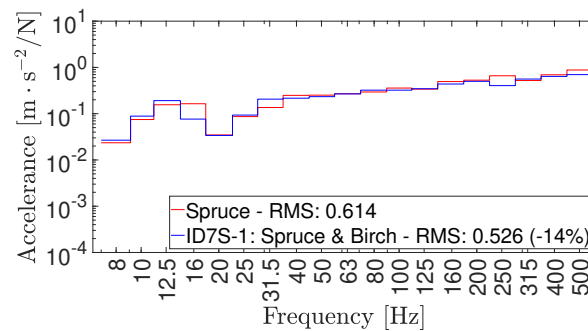


Figure 10.33: Accelerance plot, 3rd-octave band filters with RMS-values. Birch sub-configuration ID7S-1.

2-layer Sub-configuration

Configuration ID7S have been sub-configured into ID7S-1, cf. Figure 10.32, keeping the external birch lamellae in both the transversal and longitudinal directions. The accelerance RMS-value remained virtually unchanged in comparison to ID7S, cf. Table 10.17. The 3rd-octave band plots can be seen in Figure 10.33, for select configurations.

In Figure 10.33, improvement is found in a majority of the 3rd-octave bands.

3-layer Sub-configuration

Configuration ID10S have been sub-configured into ID10S-1, cf. Figure 10.34, keeping the external birch lamellae in both the transversal and longitudinal directions. These are concentrated about the central layer, whereby the accelerance RMS-value is reduced significantly, cf. Table 10.18, by 20%. The 3rd-octave band plots can be seen in Figure 10.35, for select configurations.

In Figure 10.35, improvement is found in a majority of the 3rd-octave bands.

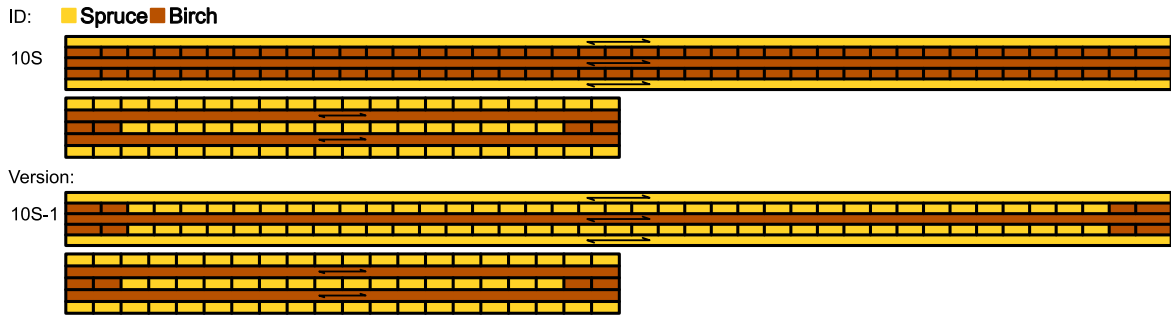


Figure 10.34: Birch sub-configuration of ID10S, relative difference of RMS-values and volumetric rates of birch.

Table 10.18: Birch sub-configuration of ID10S, relative difference of RMS-values and volumetric rates of birch.

ID	RMS diff. [%]	Vol. rate [%]
ID10S	-14	60
ID10S-1	-20	8

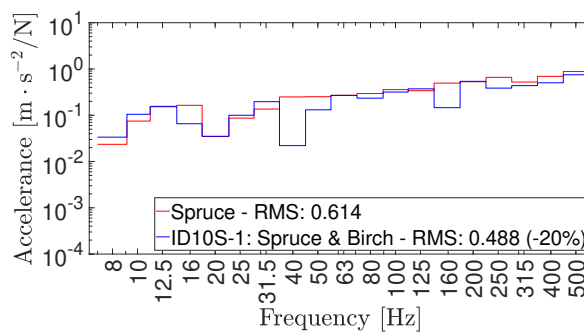


Figure 10.35: Accelerance plot, 3rd-octave band filters with RMS-values. Birch sub-configuration ID10S-1.

5-layer Sub-configuration

Configuration ID11S have been sub-configured into ID11S-1, cf. Figure 10.36, keeping the external birch lamellae in both the transversal and longitudinal directions. These are stacked as much as possible about the central layer, whereby the RMS-value is reduced substantially, cf. Table 10.19, by 32%. This reduction is similar to that of ID11S, and hence a similar performance is obtained with the homogeneous birch CLT-plate, while utilizing significantly less birch. The 3rd-octave band plots can be seen in Figure 10.37, for select configurations.

In Figure 10.37, improvement is found in a majority of the 3rd-octave bands.

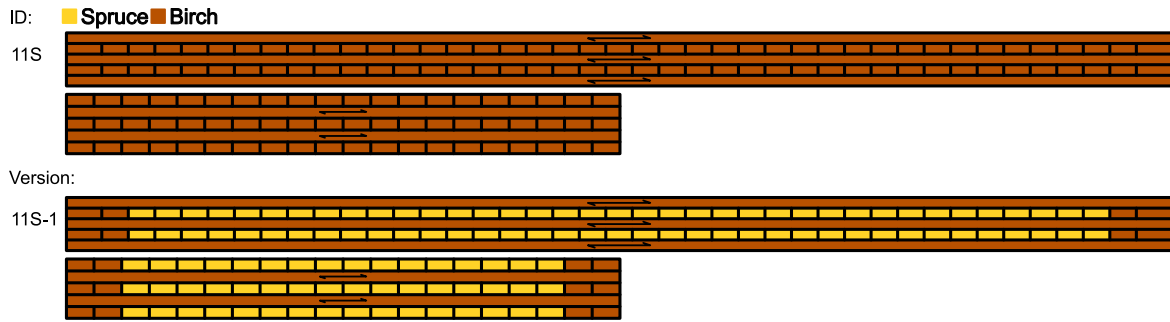


Figure 10.36: Birch sub-configuration of ID11S.

Table 10.19: Birch sub-configuration of ID11S, relative difference of RMS-values and volumetric rates of birch.

ID	RMS diff. [%]	Vol. rate [%]
ID11S	-30	100
ID11S-1	-32	16

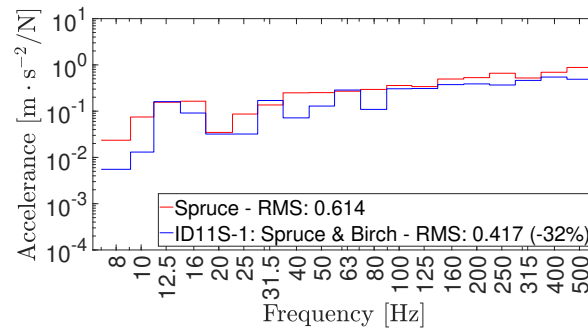


Figure 10.37: Accelerance plot, 3rd-octave band filters with RMS-values. Birch sub-configuration ID11S-1.

Conclusion – Combined Directions

The sub-configurations with combined transversal and longitudinal lamellae, respectively, have performed exceptionally, proving that the observed birch scheme is highly relevant. That is, placing birch lamellae in the perimeter of the CLT-plate, stacked about the central layer. Great reductions in RMS-values were obtained by applying this scheme, by upmost of roughly 30% as seen for ID11S-1. Although, the performance of the sub-configurations using the birch scheme is similar to the whole layer configurations, the usage of birch lamellae is heavily reduced by employing said birch scheme. This alludes perfectly to the concept of keeping the birch usage relatively limited, while maintaining heightened performance with regards to the acceleration response.

10.2.5 Conclusion – S-sized CLT-plate

This section ties together the previous observations, concluding them in a concise manner. Throughout the performed case study of the S-sized CLT-plate, the birch placement was predominantly favourable when collected along the perimeter of the CLT-plate, stacked about the central layer. This birch scheme proved to ameliorate the acceleration response, by heavily reducing said response. Even though periodic birch schemes have been studied, none hinted at a consistent behaviour and is hence deemed inconclusive, with respect to the limited amount of such periodic schemes.

Furthermore, it was possible to achieve a birch scheme that would greatly increase the reduction of accelerance RMS-values, while keeping the birch usage significantly low. This is advantageous from a material efficiency point of view, proving that there is a profit of investigating the lamellae distribution in CLT-plates, and not blindly incorporating stiffer and heavier material in abundance. Moreover, it was noticed that the reductions obtained from the various S-sized configurations were substantially lower than for the L-sized configurations. This indicates that there is a greater potential, and room for improvement, regarding the L-sized CLT-plate, than for the S-sized CLT-plate. This also showcases that the size of the CLT-plate also dictates how well the configurations perform. The following bullet-points sum up the important points:

- The numerical results suggests that a scheme of applying birch along the perimeter of the CLT-plate, concentrated to the central layer, while keeping the internal portions of the CLT-plate birch-free, yields the greatest reductions of accelerance.
- Reduction of accelerance RMS-values is substantial. Notably, sub-configuration ID11S-1 reduced the RMS-value by roughly 30%, on par with the homogeneous birch plate ID11S, while being composed of significantly less birch.
- The reduction of the RMS-values in the S-sized CLT-plate are substantially lower than in the L-sized CLT-plate.

11 Case Study – Densified Spruce

This chapter presents the results from the reduced modal-based steady-state analyses of different CLT-plate configurations with densified spruce.

The results of the analyses will be presented as 3rd-octave RMS plots, for select configurations. The data is presented in said plots with the RMS-value calculated for each 3rd-octave band. The amount of densified used in each configuration tested will be presented as a percentage of the total amount of timber in the CLT-plate.

11.1 L-sized CLT-plate

This section presents the results concerning the L-sized CLT-plate. The presentation is subdivided according to the three principal axes. Throughout this section, the reference case has been the homogeneous L-sized CLT-plate, made out of densified spruce with calibrated parameters.

11.1.1 Distribution of Lamellae – Thickness Direction

The layer configuration, pertaining to the thickness direction of the L-sized CLT-plate, are presented in figure 11.1. Additionally, the relative difference of acceleration RMS-values, along with the volumetric rates of exchanged material, are presented in Table 11.1. The 3rd-octave band plots can be seen in Figure 11.2, for select configurations.

Table 11.1: Densified spruce layer configurations, relative difference of RMS-values and volumetric rates of densified spruce

ID	RMS diff. [%]	Vol. rate [%]	ID	RMS diff. [%]	Vol. rate [%]
ID1	−8	14	ID13	−13	29
ID2	−6	14	ID14	−13	29
ID3	−8	14	ID15	−22	43
ID4	−10	14	ID16	−28	43
ID5	−8	14	ID17	−17	43
ID6	−10	14	ID18	−25	43
ID7	−11	14	ID19	−27	43
ID8	−19	29	ID20	−29	57
ID9	−13	29	ID21	−31	57
ID10	−19	29	ID22	−34	71
ID11	−17	29	ID23	−30	71
ID12	−20	29	ID24	−39	100

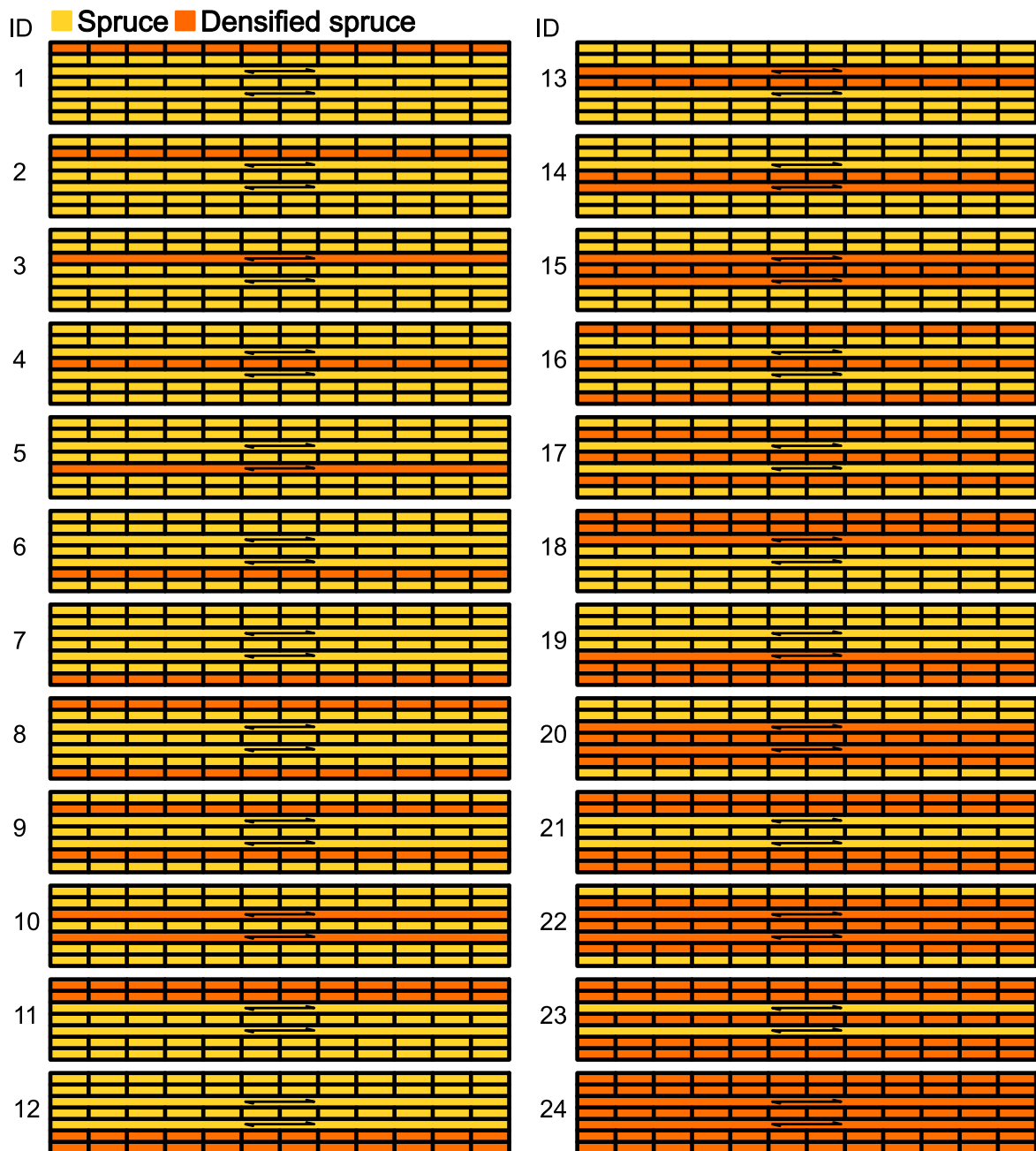


Figure 11.1: Densified spruce layer configurations.

In Figure 11.2, improvement is found for a majority of the 3rd-octave bands for IDs 3, 4, 7, 13 and 15. Improvement across all octave bands is found for ID20, ID22 and ID24.

Single-layer Configurations

The single-layer configurations, ID1 through ID7, exhibited pronounced reduction of the acceleration RMS-values, an average of roughly 9%, regardless of the densified spruce layer placement. Based on these configurations, that perform approximately on the same level, no indication can be found regarding the densified spruce placement.

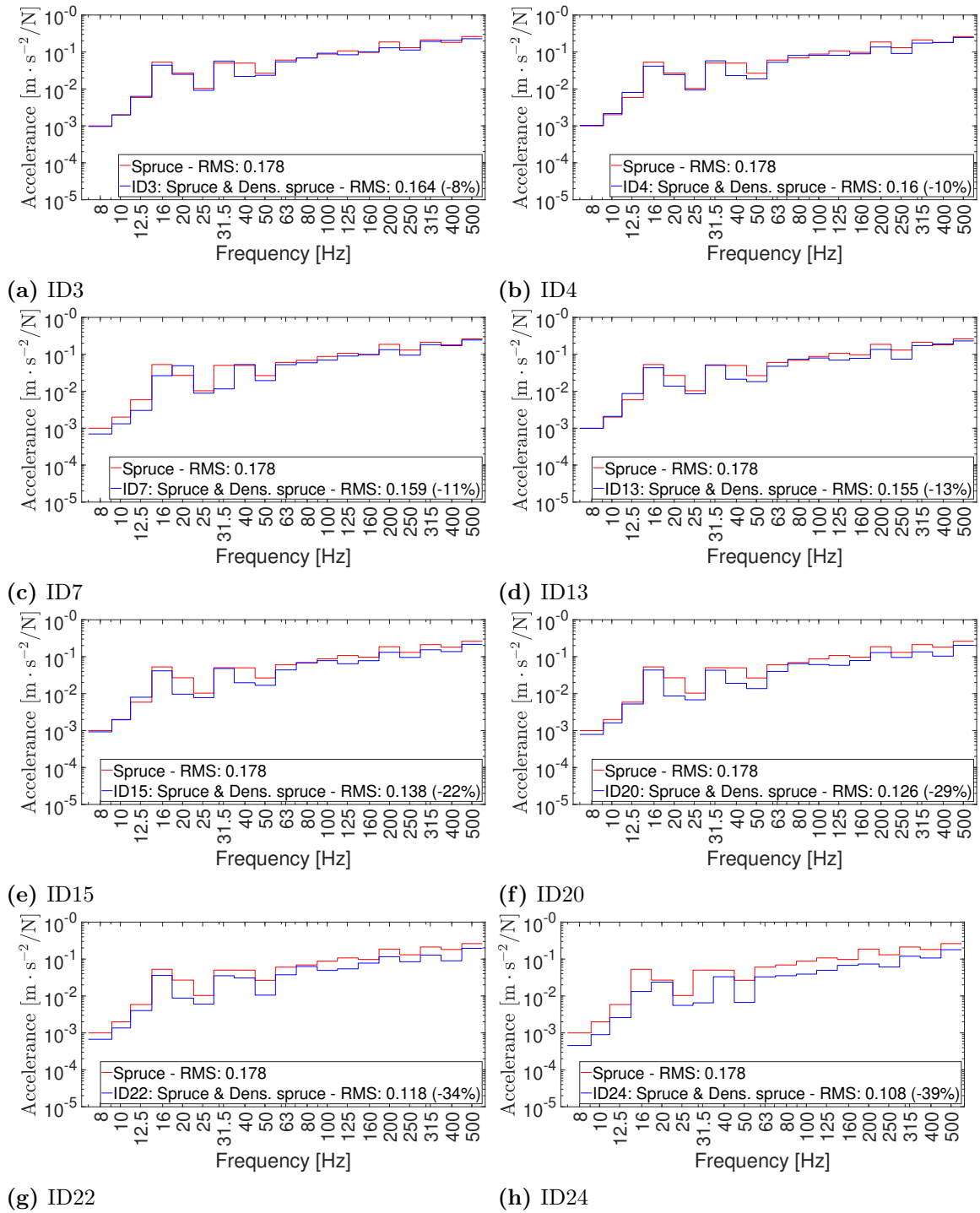


Figure 11.2: Accelerance plots, 3rd-octave band filters with RMS-values. Densified spruce configurations ID3, ID4, ID7, ID13, ID15, ID20, ID22 and ID24.

along the thickness direction. Due to the geometrical similarity of configuration ID3 and ID5, only the former is chosen to be further investigated with regards to the longitudinal direction. This choice is based on the fact that the same configuration was used in the case study of birch, as well as on avoiding redundancy. Moreover, ID4 and ID7 are chosen to be further investigated with regards to the transversal direction, since these configurations displayed the highest reduction of RMS-values.

Multilayer Configurations

With regards to the multilayer configurations, different implications are observed with respect to the number of layers involved. The number of layers involved varied between 2-5. Additionally, a homogeneous CLT-plate of densified spruce was analysed for more lucid comparisons.

The 2-layer configurations, ID8 through ID14, displayed significant reduction of the accelerance RMS-values, an average of roughly 16%. However, these configurations exhibited very similar reduction thereof, with no indication of favourable densified spruce placement. Although, the reduction of RMS-values is higher than with single layer configurations. For subsequent studies, configurations ID8 and ID10 are chosen with regards to the transversal and longitudinal direction, respectively.

The 3-layer configurations, ID15 through ID19, displayed substantial reduction the accelerance RMS-values, an average of roughly 24%. However, there is no substantial discrepancies between these configurations, and hence no hint is obtained regarding the placement of the densified spruce. Although, the increased reduction of RMS-values is attributed to the increased usage of densified spruce.

The 4-layer configurations, ID20 and ID21, exhibited substantial reduction of the accelerance RMS-values, an average of 30%. However, due to the limit number of configurations, as well as similar performance of these configurations, no indication can be observed regarding the densified spruce placement.

The 5-layer configurations, ID22, ID23 and ID24, exhibited substantial reduction of the accelerance RMS-values, an average of roughly 34%. Thus, these configurations are comparable with the homogeneous densified spruce configuration ID24, which had a reduction 39% of the RMS-value. Although, these configurations have similar performance whereby no indication is obtained regarding the densified spruce placement.

Conclusion – Thickness Direction

By the conducted layer configurations, pertaining to the thickness direction of the CLT-plate, no unique pattern or densified spruce scheme was observed. There was a lack of substantial discrepancies between the configurations, in accordance with the layer divisions. For example, no tangible decisions could be made regarding the inclusion or exclusion of central layer, nor concentrating the densified spruce along the edges of the thickness direction or stacking the layers about the central layer. However, the performance of the CLT-plates increased with increased volumetric rate of used densified spruce.

Moreover, some configurations were deemed of interest for further studies regarding the distribution of lamellae in the longitudinal, as well as transversal direction, respectively. The reason for multiple configurations to be further studied is based on the inconclusiveness of this conducted lamellae distribution study along the thickness direction of the CLT-plate. Hence, the abundance of further studied configurations may reveal some lamellae patterns otherwise not found. Furthermore, the refinement

of the configurations into sub-configurations aligns with the objective of maximizing the performance of the CLT-plate, while minimizing the material usage of densified spruce.

11.1.2 Distribution of Lamellae – Longitudinal Direction

The investigation of the lamellae distribution along the longitudinal direction have been performed both with a single-layer configuration ID3, as well as a 2-layer configuration ID10. The lack of tangible lamellae scheme from the previous study prompted a more detailed study than before. Additionally, the trend of increased performance with increased number of layers involved would also be put to the test. However, the amount of 2-layer sub-configurations are heavily limited to constrain the extent of the study.

Figure 11.3 shows the tested sub-configurations for ID3, namely, ID3-1 through ID3-16. Note that these sub-configurations coincide with those pertaining to the case study of birch in Section 10.1.2. The respective relative difference of RMS-values is collected in Table 11.2, along with the volumetric rate of exchanged densified spruce. Similarly, Figure 11.5 shows the tested sub-configurations for ID10, namely, ID10-1 through ID10-4, accompanied with their relative difference of RMS-values in Table 11.3. The 3rd-octave band plots can be seen in Figure 11.4, for select configurations if ID3 and Figure 11.6 for ID10.

In Figure 11.4, improvement is found for a majority of the 3rd-octave bands for ID3-1, ID3-2 and ID3-5. For ID3-9, improvement is found for a minority of the 3rd-octave bands

In Figure 11.6, improvement is found for a majority of the 3rd-octave bands for both sub-configurations.

Table 11.2: Densified spruce sub-configurations of ID3, relative difference of RMS-values and volumetric rates of densified spruce.

ID	RMS diff. [%]	Vol. rate [%]	ID	RMS diff. [%]	Vol. rate [%]
ID3	-8	14			
ID3-1	-11	11	ID3-9	1	5
ID3-2	-10	9	ID3-10	2	3
ID3-3	-8	6	ID3-11	0	1
ID3-4	-10	4	ID3-12	-8	7
ID3-5	-14	1	ID3-13	-6	5
ID3-6	6	13	ID3-14	-4	4
ID3-7	2	10	ID3-15	-5	3
ID3-8	-1	8	ID3-16	-15	4

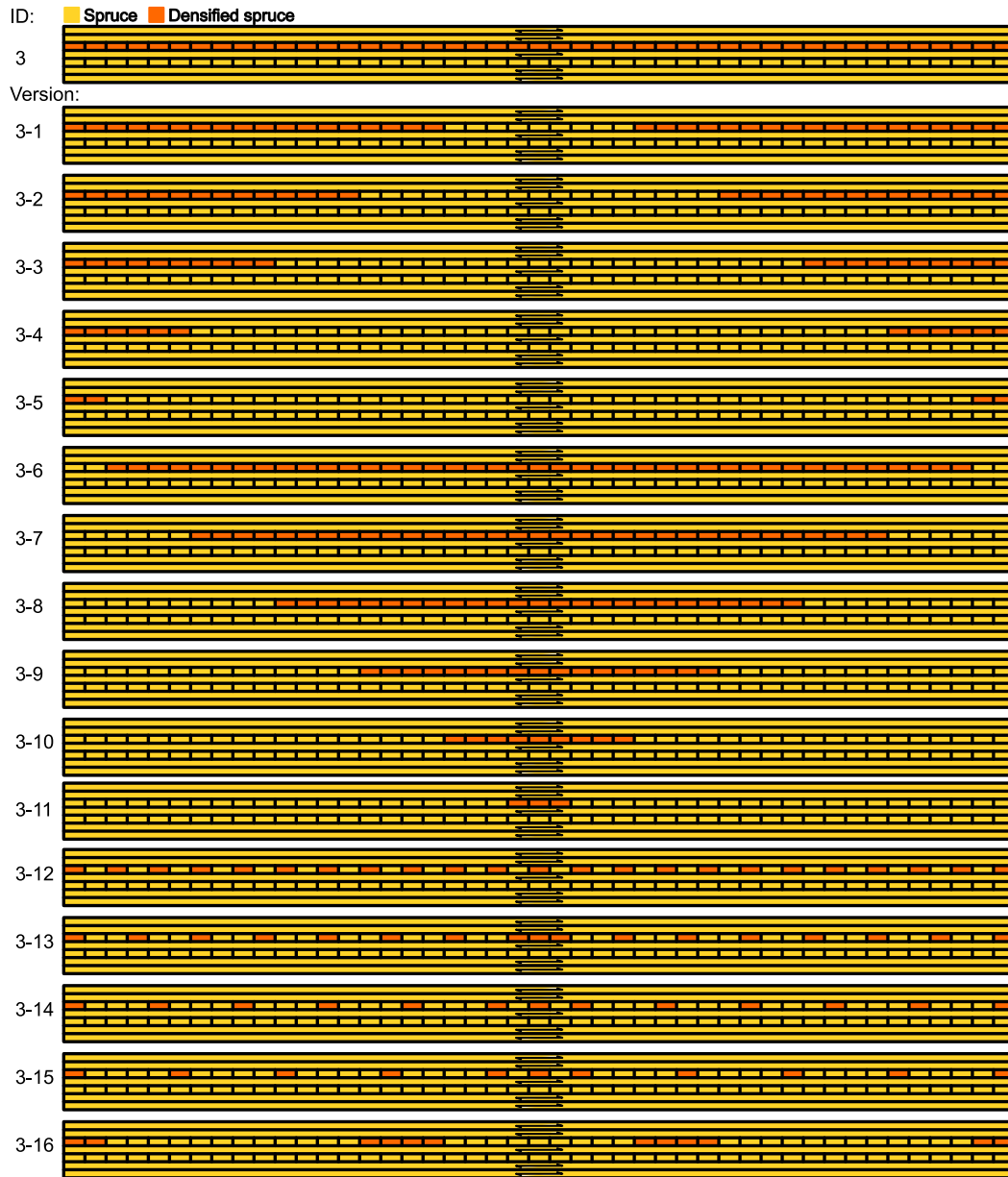


Figure 11.3: Densified spruce sub-configurations of ID3.

Table 11.3: Densified spruce sub-configurations of ID10, relative difference of RMS-values and volumetric rates of densified spruce.

ID	RMS diff. [%]	Vol. rate [%]
ID10	-19	29
ID10-1	-21	23
ID10-2	-25	3
ID10-3	-12	8
ID10-4	-26	8

Distribution Towards the Edges

Starting from ID3, with a whole layer exchanged to densified spruce, the densified spruce lamellae are reduced in the centre of the longitudinal direction, with greater re-

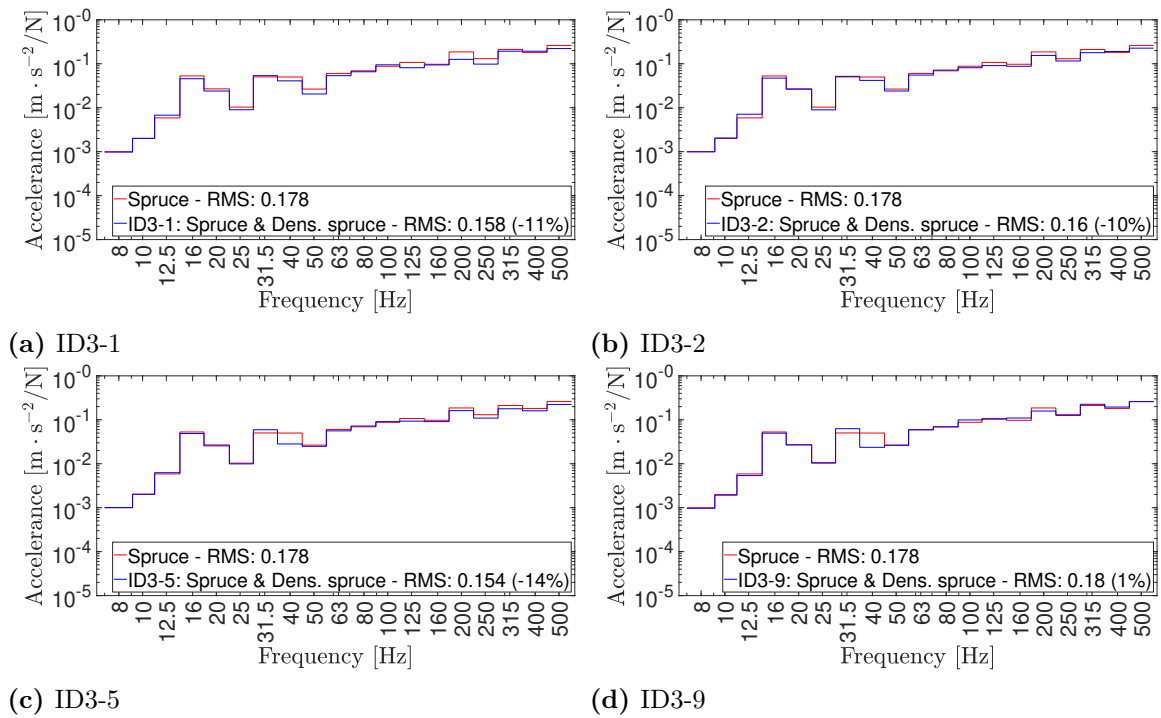


Figure 11.4: Accelerance plots, 3rd-octave band filters with RMS-values. Densified spruce sub-configurations of ID3

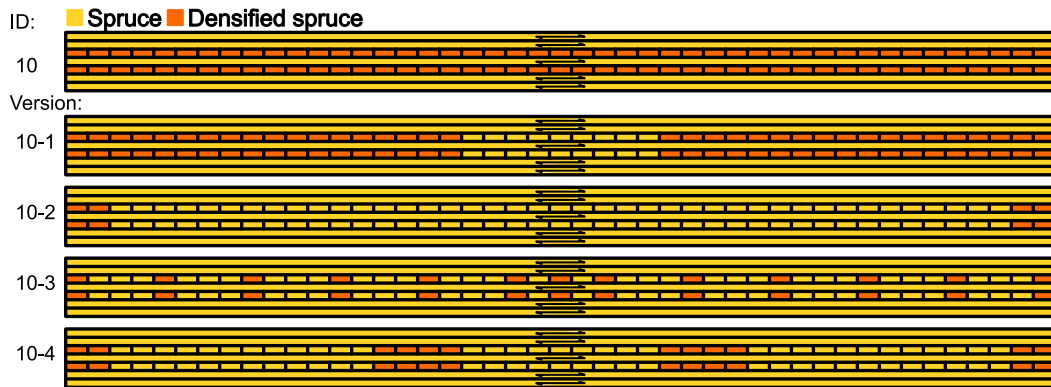


Figure 11.5: Densified spruce sub-configurations of ID10.

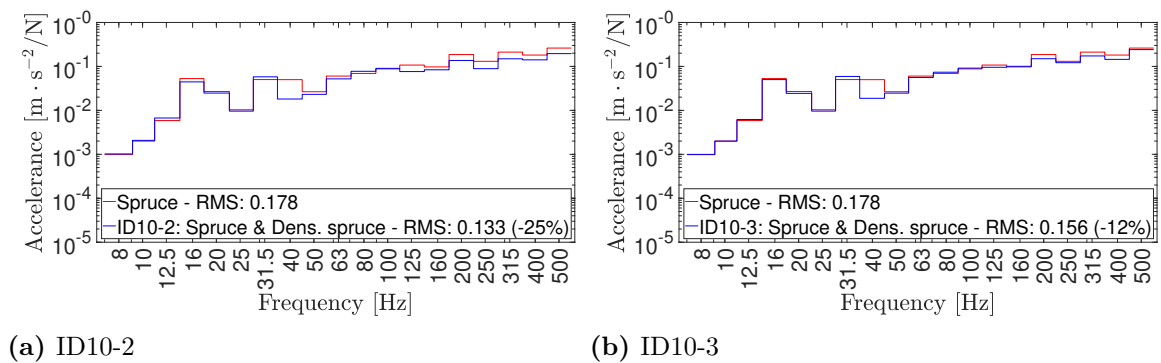


Figure 11.6: Accelerance plots, 3rd-octave band filters with RMS-values. Densified spruce sub-configurations of ID10.

duction incrementing towards the edges. These sub-configurations, ID3-1 through ID3-5, exhibited pronounced reduction of the accelerance RMS-values. More specifically, sub-configuration ID3-5 with densified spruce lamellae exclusively in the CLT-plate edges, performed slightly better than the rest, especially configuration ID3. Thus, sub-configuration ID3-5 can maintain the performance while drastically reducing the densified spruce usage. However, as the performance of these respective sub-configurations are similar, no insinuation regarding the lamellae distribution is obtained.

Distribution Towards the Centre

Conversely to above, densified spruce lamellae are excluded incrementally from the edges, towards the centre. These sub-configurations, ID3-6 through ID3-11, displayed unfavourable increases of the accelerance RMS-values, though marginally. This indicates that densified spruce lamellae should preferably be placed towards the edges, and less so towards the centre in the longitudinal direction.

Systematic Distribution

Some distributions, with systematic spacing between the densified spruce lamellae, have been performed. These sub-configurations, ID3-12 through ID3-16, displayed marginal reduction of the accelerance RMS-values, most notably sub-configuration ID3-16 at 15% reduction. This indicates that a uniform periodic distribution is obsolete, and that lumping the densified spruce lamellae may be the better approach, as in ID3-16. Although, the discrepancy in the RMS-value reduction may be attributed to the fact that ID3-16 does not contain include the middle portion of densified spruce. This exclusion was previously shown to be advantageous.

2-layer Configuration

The specific 2-layer sub-configurations, cf. Figure 11.5, have been chosen based on the substantial reduction of RMS-values of the single-layer case, given in Table 11.1. These 2-layer sub-configurations exhibited significant reduction of the accelerance RMS-values. Notably though, sub-configuration ID10-3 underperformed, hinting towards unfavourable uniform distributions of densified spruce lamellae. Additionally, ID10-4 outperformed the latter, hinting towards a more favourable lumped distribution of densified spruce lamellae. Moreover, ID10-2 had a slightly higher reduction of the RMS-value than ID10-1, while also using drastically less densified spruce. Even though these two sub-configurations are deemed to perform on the same level, the drastic material usage sets them apart. Finally, the fact that ID10 performed better than ID10-3 indicates that involving more layers in the sub-configurations does not necessarily equate to better performance thereof.

Conclusion – Longitudinal Direction

By the conducted transversal lamellae configurations, pertaining to the longitudinal direction of the CLT-plate, it was observed that a favourable placement of the densified spruce would be towards the edges, while an unfavourable placement would be towards the centre. The former statement is due to sub-configurations ID3-1 through ID3-5, while the latter is due to sub-configurations 3-6 through ID3-11. However, the extent of densified spruce towards the edges cannot be well defined since sub-configurations ID3-1 through ID3-5 performed roughly on the same level. Although, based on efficient material usage, sub-configuration ID3-5 would outperform the preceding sub-configurations. Hence, the desire to minimize material usage further dictates the placement of densified spruce lamellae concentrated to the edges of the CLT-plate.

Furthermore, the systematic sub-configurations, ID3-12 through ID3-16, with different periodic spacings of the densified spruce lamellae, displayed differing responses. It was observed that lumping the densified spruce lamellae while excluding the central portion, yielded significant reduction of the RMS-value. Meanwhile, the various uniformly distributed densified spruce lamellae, including the central portion, yielded insignificant reduction of the RMS-values. Nonetheless, due to the limited number of such sub-configurations, it is not possible to ascertain the behaviour of the CLT-plate if the densified spruce lamellae are lumped in conjunction with the inclusion of the central part.

Additionally, increasing the number of layers involved seem to increase the reduction of the RMS-values. However, this fact cannot be taken at face value since sub-configuration ID10-3 had a slightly less of an RMS-value reduction than ID10.

11.1.3 Distribution of Lamellae – Transversal Direction

The investigation of the lamellae distribution along the transversal direction have been performed with varying number of layers involved. This was done to compensate for the lack of evident densified spruce lamellae schemes during the study along the thickness direction of the CLT-plate. The outline given in Section 9.4 is followed for the single-layer configurations ID4 as well as ID7. The case of multilayer configurations ID8 and ID10, respectively, is separated from the case of single-layer configurations.

Figure 11.7 shows the tested sub-configurations of ID4. The relative difference of their accelerance RMS-values is collected in Table 11.4, along with the volumetric rate of exchanged densified spruce. Similarly, Figure 11.8 shows the tested sub-configurations of ID7 and Table 11.5 collects the relative difference of the accelerance RMS-values. The 3rd-octave band plots can be seen in Figure 11.9, for select configurations of ID4 and Figure 11.10 for ID7.

In Figure 11.9, improvement is found for a majority of the 3rd-octave bands for ID4-7, ID4-9 and ID4-15. For ID4-2, improvement is found in around half of the 3rd-octave bands. In Figure 11.10, improvement is found for a majority of the 3rd-octave bands for ID7-7, ID7-9 and ID7-15. For ID7-2, improvement is found in a minority of the 3rd-octave bands.

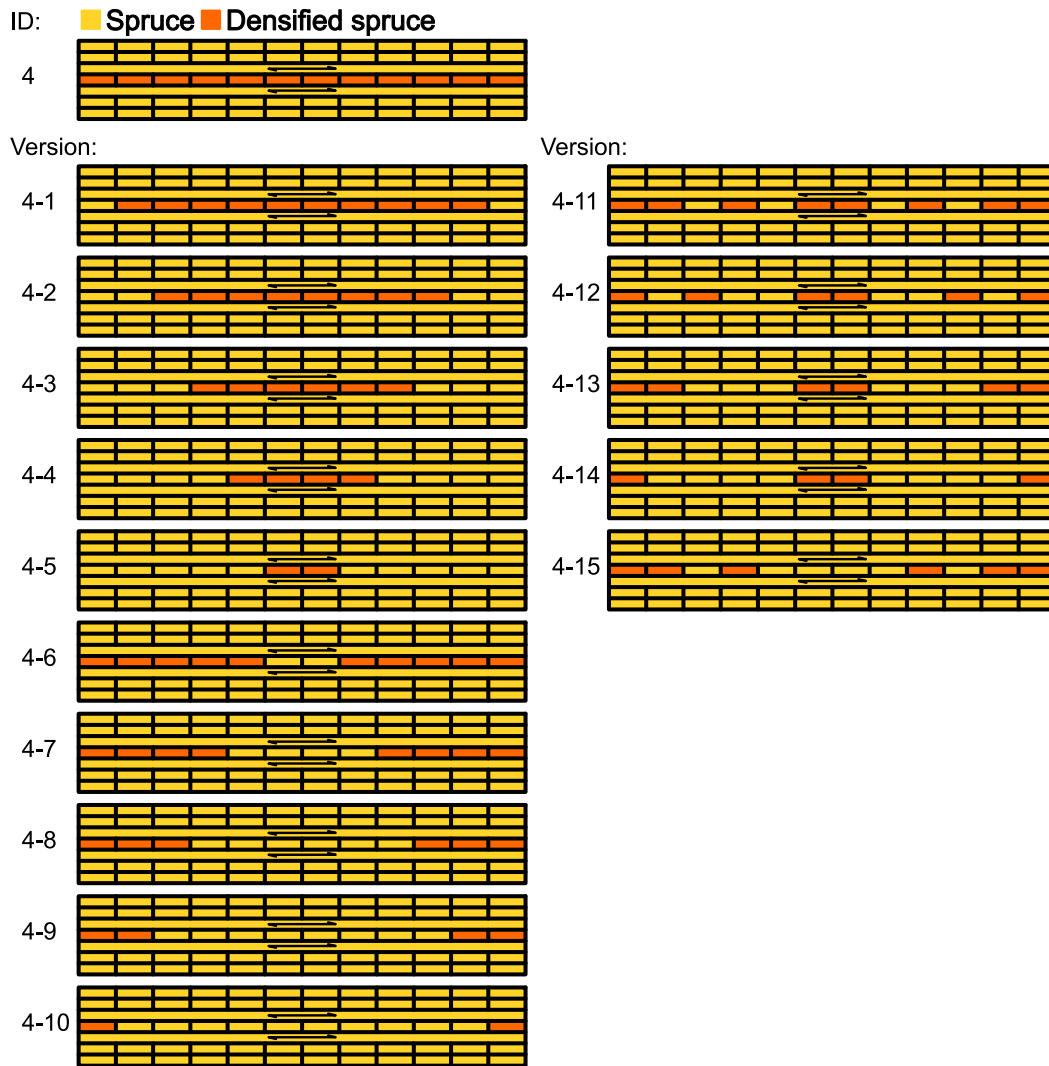


Figure 11.7: Densified spruce sub-configurations of ID4.

Table 11.4: Densified spruce sub-configurations of ID4, relative difference of RMS-values and volumetric rates of densified spruce.

ID	RMS diff. [%]	Vol. rate [%]	ID	RMS diff. [%]	Vol. rate [%]
ID4	-10	14	ID4-11	-11	10
ID4-1	11	12	ID4-12	-6	7
ID4-2	19	10	ID4-13	-14	7
ID4-3	10	7	ID4-14	-7	5
ID4-4	-5	5	ID4-15	-10	7
ID4-5	3	2			
ID4-6	-8	12			
ID4-7	-8	10			
ID4-8	-12	7			
ID4-9	-19	5			
ID4-10	-15	2			

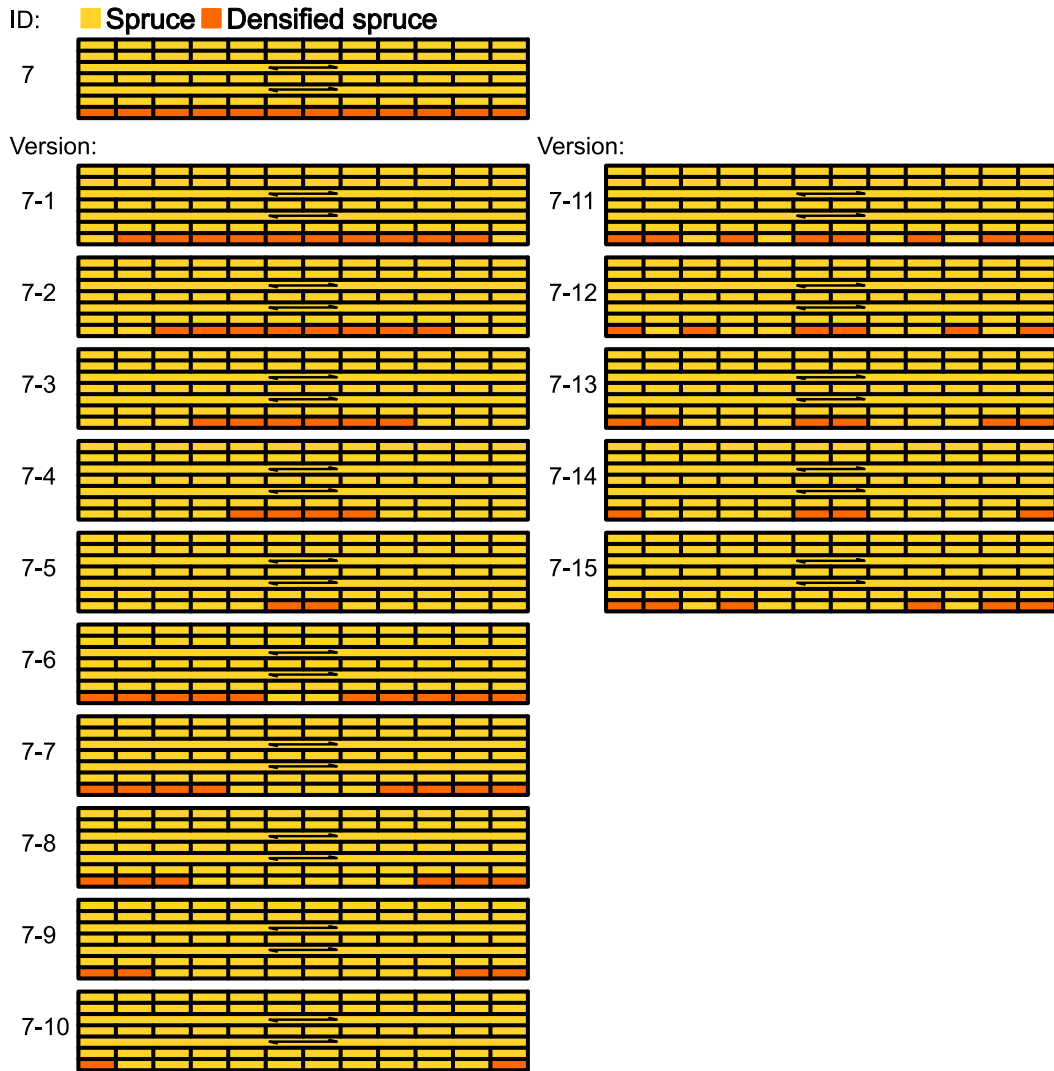
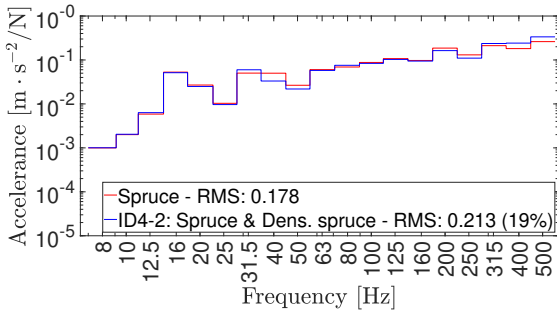


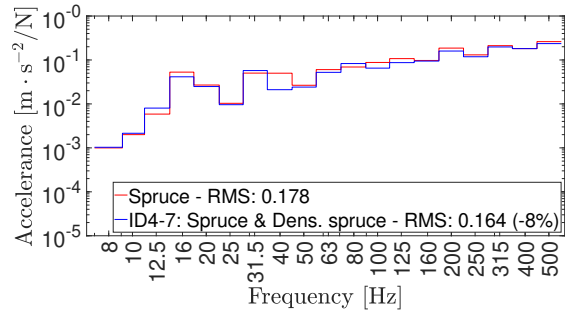
Figure 11.8: Densified spruce sub-configurations of ID7.

Table 11.5: Densified spruce sub-configurations of ID7, relative difference of RMS-values and volumetric rates of densified spruce.

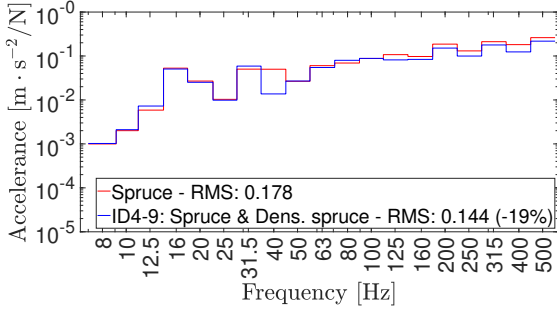
ID	RMS diff. [%]	Vol. rate [%]	ID	RMS diff. [%]	Vol. rate [%]
ID7	-11	14			
ID7-1	11	12	ID7-11	-16	10
ID7-2	10	10	ID7-12	-13	7
ID7-3	6	7	ID7-13	-17	7
ID7-4	-1	5	ID7-14	-13	5
ID7-5	2	2	ID7-15	-12	7
ID7-6	-10	12			
ID7-7	-10	10			
ID7-8	-12	7			
ID7-9	-18	5			
ID7-10	-15	2			



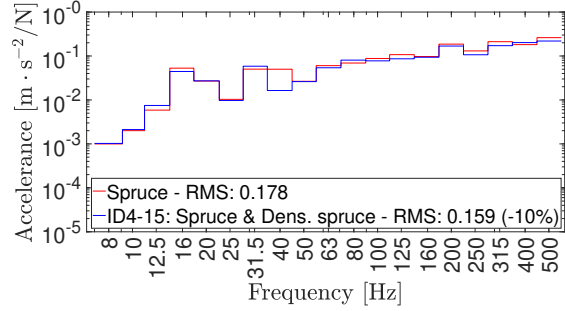
(a) ID4-2



(b) ID4-7

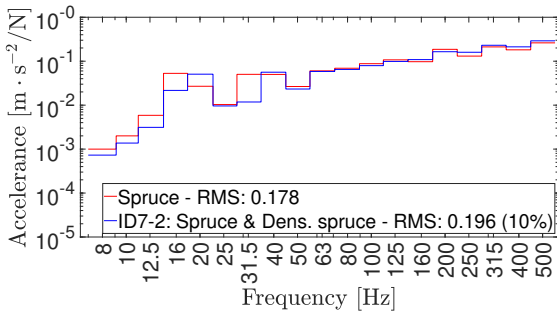


(c) ID4-9

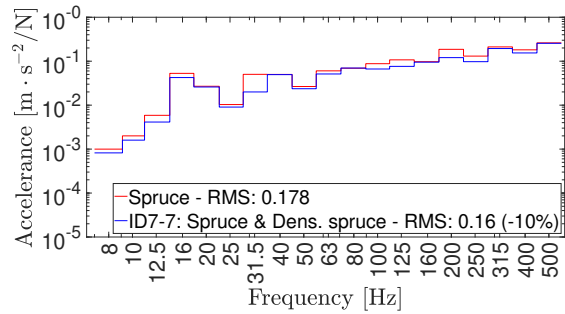


(d) ID4-15

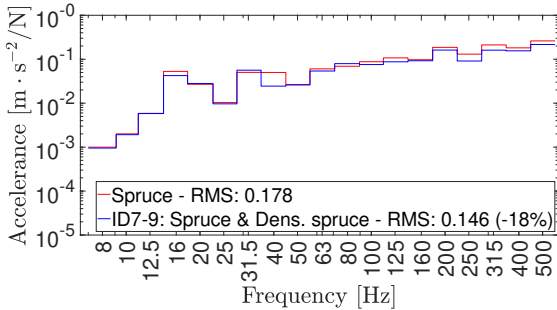
Figure 11.9: Accelerance plots, 3rd-octave band filters with RMS-values. Densified spruce sub-configurations of ID4.



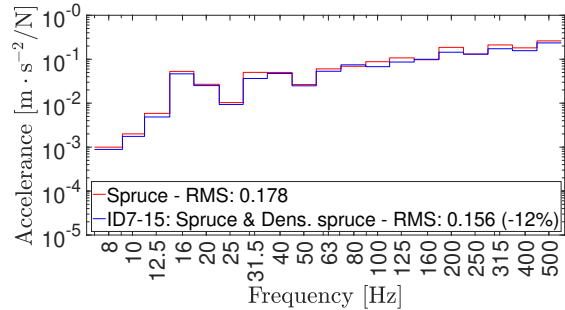
(a) ID7-2



(b) ID7-7



(c) ID7-9



(d) ID7-15

Figure 11.10: Accelerance plots, 3rd-octave band filters with RMS-values. Densified spruce sub-configurations of ID7.

Distribution Towards the Centre

Starting from ID4 and ID7, respectively, with a whole layer with densified spruce, the densified spruce lamellae are reduced in the edges of the transversal direction, with greater reduction incrementing towards the centre. These sub-configurations, ID4-1 through ID4-5, as well as ID7-1 through ID7-5, exhibited moderate increase in the accelerance RMS-values. This hints at a preferable placement of densified spruce lamellae towards the edges, as opposed to towards the centre of the transversal direction. Notably, these two sets of sub-configurations perform at a similar level.

Distribution Towards the Edges

Conversely to above, densified spruce lamellae are excluded incrementally from the centre, towards the edges. These sub-configurations, ID4-6 through ID4-10, as well as ID7-6 through ID7-10, displayed moderate reduction of the RMS-values. This indicates that less densified spruce should be used in centre, while maintaining densified spruce lamellae to the edges. Notably, these two sets of sub-configurations perform at a similar level, further indicating that the placement of densified spruce along the thickness direction is not of great importance.

Systematic Distributions

Some distributions, with systematic arrangement of the densified spruce lamellae, have been performed. These sub-configurations, ID4-11 through ID4-15, as well as ID7-11 through ID7-15, displayed moderate reduction of the accelerance RMS-values. Within the mentioned sets, the performance was at a similar level and no distinctive discrepancies could be discerned. Thus, no indication is obtained regarding a favourable exclusion of the central densified spruce lamellae, nor regarding the concentration of densified spruce lamellae close to the edges. Furthermore, these sets of sub-configurations performed at a similar level, further indicating that the placement of densified spruce along the thickness direction is not of great importance.

Multilayer Configurations

Some multilayer configurations have been performed in order to investigate the effect, of including more layers of densified spruce, on the lamellae distribution along the transversal direction.

A few 2-layer sub-configuration of ID8, namely, ID8-1 through ID8-4, are presented in Figure 11.37 and the relative difference of the accelerance RMS-values are presented in Table 11.6. Notably, ID8-1 which excludes the central part of densified spruce, performs significantly better than ID8-3 which includes some central densified spruce lamellae. Furthermore, ID8-1 also outperforms ID8-2, which has more densified spruce lamellas closer to the central part. Additionally, ID8-1 performs slightly better than

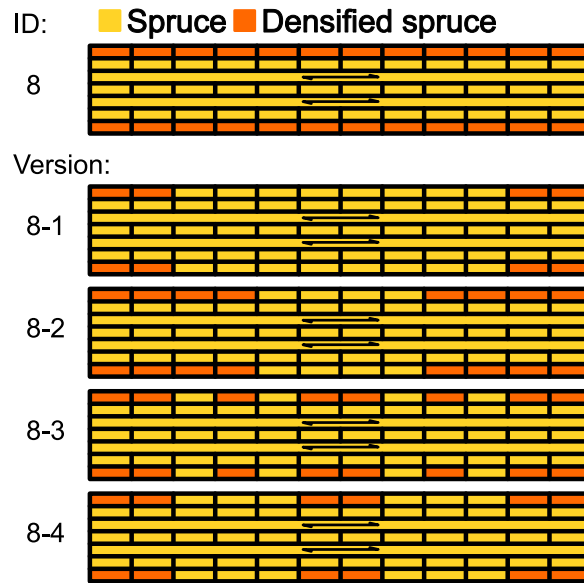


Figure 11.11: Densified spruce sub-configurations of ID8.

Table 11.6: Densified spruce sub-configurations of ID8, relative difference of RMS-values and volumetric rates of densified spruce.

ID	RMS diff. [%]	Vol. rate [%]
ID8	-19	29
ID8-1	-32	10
ID8-2	-13	19
ID8-3	-16	19
ID8-4	-26	14

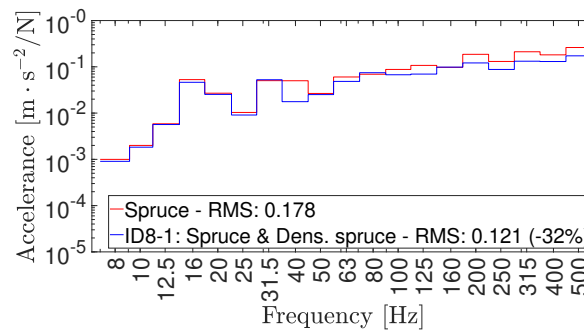


Figure 11.12: Accelerance plot, 3rd-octave band filters with RMS-values. Densified spruce sub-configuration ID8-1.

ID8-4, which differ only in including two middle densified spruce lamellae. Hence, these observations indicate a favourable placement along in the edges of the CLT-plate in the transversal direction. Moreover, a comparison between ID8-1 and the single-layer case, ID4-9 as well as ID7-9, showcases that the increased number of layers involved also increases the RMS-value reduction. A 3rd-octave band plot can be seen in Figure 11.12, whereby improvement is found for a majority of the 3rd-octave bands for ID8-1.

A 3-layer sub-configuration of ID16, namely, ID 16-1, is presented in Figure 11.13,

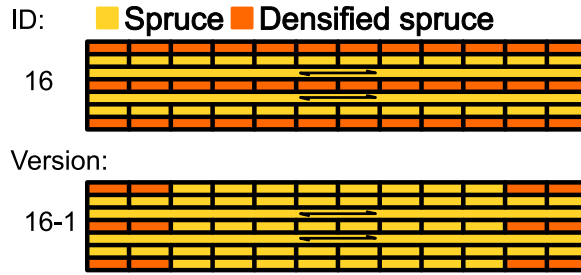


Figure 11.13: Densified spruce sub-configurations of ID16.

Table 11.7: Densified spruce sub-configuration of ID16, relative difference of RMS-values and volumetric rates of densified spruce.

ID	RMS diff. [%]	Vol. rate [%]
ID16	-28	43
ID16-1	-33	14

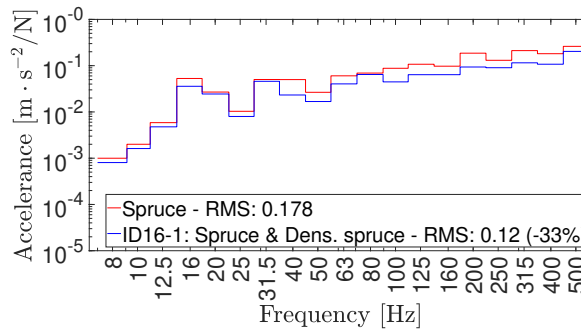


Figure 11.14: Accelerance plot, 3rd-octave band filters with RMS-values. Densified spruce sub-configuration ID16-1.

and the relative difference of the accelerance RMS-value is presented in Table 11.7. By excluding the central densified spruce lamellae, in the transversal direction, no significant change is obtained in the RMS-value. Furthermore, comparison of ID16-1 against ID8-1 reveals an almost identical reduction of the RMS-value. A 3rd-octave band plot can be seen in Figure 11.14, where improvement is found for a majority of the 3rd-octave bands for ID16-1.

A 4-layer sub-configuration of ID21, namely, ID21-1, is presented in Figure 11.15, and the relative difference of the accelerance RMS-value is presented in Table 11.8. By keeping the densified spruce lamellae stacked in the edges of the transversal direction, while excluding the central parts, a substantial reduction of RMS-value is obtained. A comparison of ID21-1 against ID8-1 reveals that the increased number of involved layers increased the reduction of RMS-value moderately. A comparison of ID21-1 against ID16-1 reveals a moderate reduction of the RMS-value for the former sub-configuration. A 3rd-octave band plot can be seen in Figure 11.16, where improvement is found for a majority of the 3rd-octave bands for ID21-1.

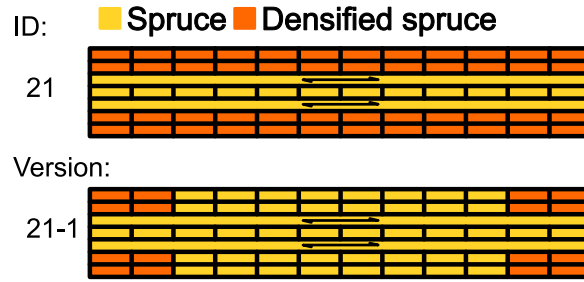


Figure 11.15: Densified spruce sub-configuration of ID21.

Table 11.8: Densified spruce sub-configuration of ID21, relative difference of RMS-values and volumetric rates of densified spruce.

ID	RMS diff. [%]	Vol. rate [%]
ID21	-31	57
ID21-1	-44	19

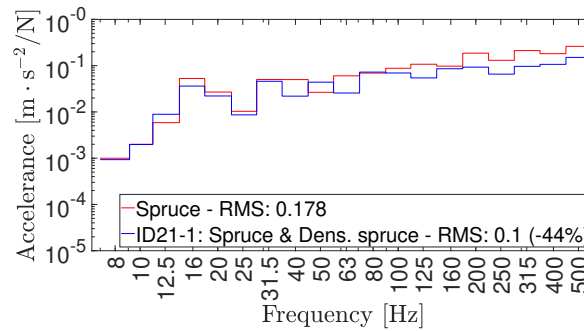


Figure 11.16: Accelerance plot, 3rd-octave band filters with RMS-values. Densified spruce sub-configuration ID21-1.

Conclusion – Transversal Direction

By the conducted longitudinal lamellae configurations, pertaining to the transversal direction of the CLT-plate, it was observed that a favourable placement of the densified spruce would be towards the edges, while keeping the central parts unexchanged with densified spruce. This is evidenced by the poor response of sub-configurations ID4-1 through ID4-5, as well as ID7-1 through ID7-5, while ID4-6 through ID4-10, as well as ID7-6 through ID7-10 performed significantly better. Furthermore, by comparing sub-configurations ID4-9 and ID4-10, against ID4-13 and ID4-14, respectively, it is seen that the exclusion of the central densified spruce lamellae slightly reduces the accelerance RMS-values. This plays into the previous observation of concentrating the densified spruce lamellae to the edges. Additionally, this approach minimizes the usage of densified spruce lamellae, while maintaining adequate performance. Although this trend was not observed with sub-configurations ID7-9 and ID7-10, the latter statement remains true.

From the multilayer configurations though, it was observed that ID8-1 and ID16-1 performed almost identically well, while ID8-1 did not include densified spruce lamellae of the central layer. This may indicate that even though the involved layers increased

in ID16-1, involving the central layer contributes insignificantly. Meanwhile, ID21-1 outperformed ID8-1, by stacking densified spruce lamellae in two layers, while not including the central layer. Thus, the increased number of layers involved is significant, as long as the central layer is not involved.

Overall, there is a theme of a favourable densified spruce lamellae placement along the edges in the transversal direction. Furthermore, adequate reduction of the acceleration RMS-values are maintained, even by reducing the amount of densified spruce lamellae in the central portions in the transversal direction. This is fitting with regard to maximizing the reduction of RMS-values, while minimizing the usage of densified spruce lamellae.

11.1.4 Distribution of Lamellae – Combined Directions

Based on the previous distributions and conclusions thereof, a combination is made of these former observations. Namely, a lamellae scheme of placing the densified spruce lamellae in the perimeter of the CLT-plate. However, as the study of the thickness direction was inconclusive, the mentioned perimeter will be stacked about the central layer for convenience. Multilayer configurations, cf. Figure 11.1, are altered in order to combine transversal and longitudinal lamellae. The choice of these sub-configurations was based on the feasibility to apply the previous recorded conclusions. These sub-configurations are categorised into the number of layers involved.

2-layer Sub-configuration

Configuration ID13 have been sub-configured into ID13-3, keeping only the external densified spruce lamellae in the transversal and longitudinal direction, respectively, while maintaining the distribution about the central layer in the thickness direction, cf. Figure 11.17. The relative difference of the acceleration RMS-value, cf. Table 11.9, was 32%. A 3rd-octave band plot can be seen in Figure 11.18.

In Figure 11.18, improvement is found for a majority of the 3rd-octave bands for ID13-3.

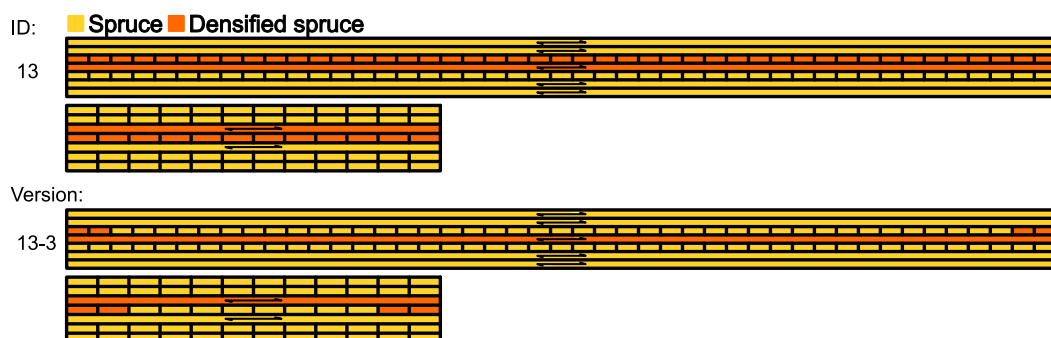


Figure 11.17: Densified spruce sub-configuration of ID13.

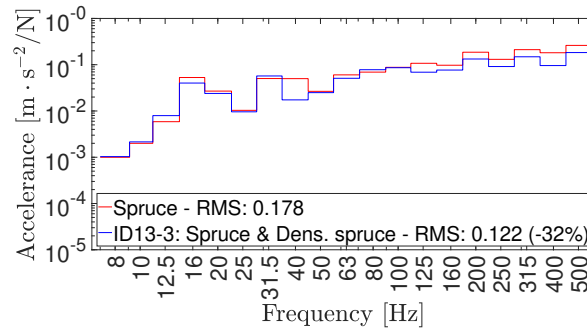


Figure 11.18: Accelerance plot, 3rd-octave band filters with RMS-values. Densified spruce sub-configuration ID13-3.

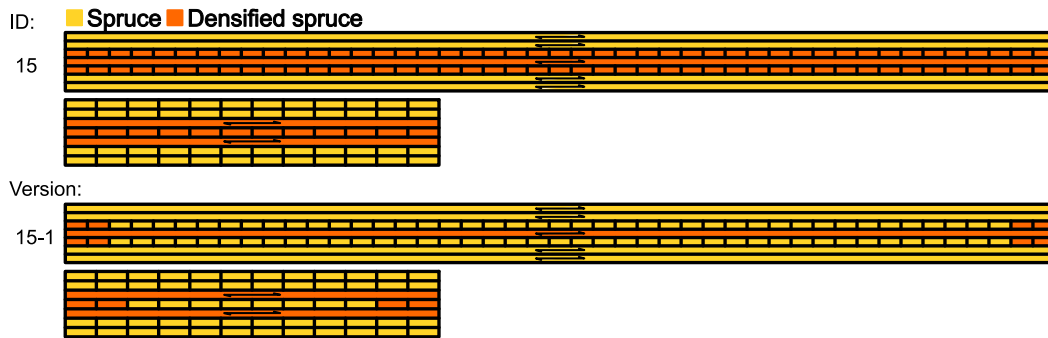


Figure 11.19: Densified spruce sub-configuration of ID15.

3-layer Sub-configuration

Configuration ID15 have been sub-configured into ID15-1, keeping only the external densified spruce lamellae in the transversal and longitudinal direction, respectively, while stacking the distribution about the central layer in the thickness direction, cf. Figure 11.19. The reduction of RMS-value, cf. Table 11.10, was 41%. A 3rd-octave band plot can be seen in Figure 11.20. In Figure 11.20, improvement is found for a majority of the 3rd-octave bands for ID15-1.

4-layer Sub-configuration

Configuration ID20 have been sub-configured into ID20-1, cf. Figure 11.21, keeping only the external densified spruce lamellae in the transversal and longitudinal direction, respectively, stacking the layers involved about the central layer. The reduction of RMS-value, cf. Table 11.11, was 47%.

Table 11.9: Densified spruce sub-configuration of ID21, relative difference of RMS-values and volumetric rates of densified spruce.

ID	RMS diff. [%]	Vol. rate [%]
ID13	-13	29
ID13-3	-32	6

Table 11.10: Densified spruce sub-configuration of ID15, relative difference of RMS-values and volumetric rates of densified spruce.

ID	RMS diff. [%]	Vol. rate [%]
ID15	-22	43
ID15-1	-41	7

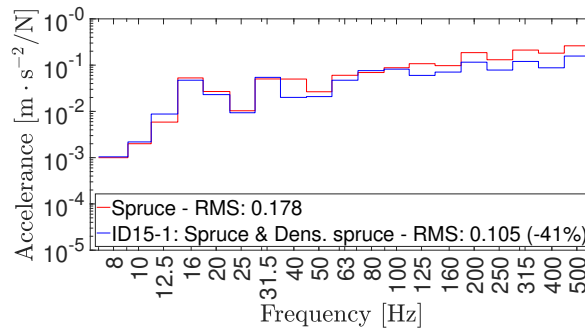


Figure 11.20: Accelerance plot, 3rd-octave band filters with RMS-values. Densified spruce sub-configuration ID15-1.

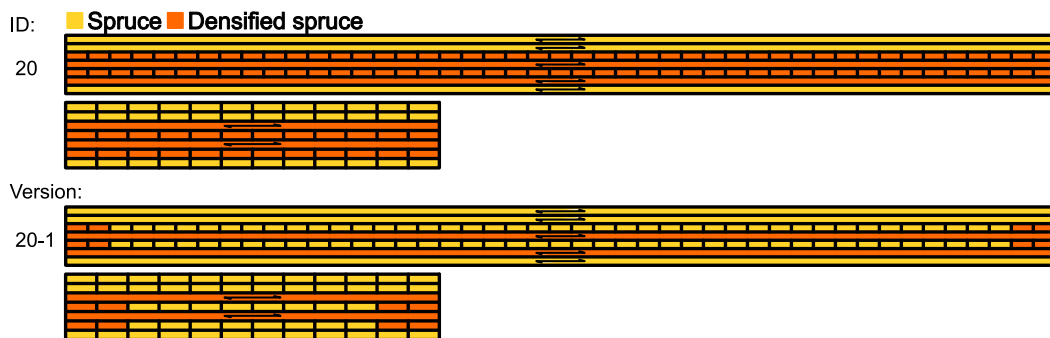


Figure 11.21: Densified spruce sub-configuration of ID20.

Table 11.11: Densified spruce sub-configuration of ID20, relative difference of RMS-values and volumetric rates of densified spruce.

ID	RMS diff. [%]	Vol. rate [%]
ID20	-29	57
ID20-1	-47	12

A 3rd-octave band plot can be seen in Figure 11.22, whereby improvement is found for a majority of the 3rd-octave bands for ID20-1.

5-layer Sub-configuration

Configuration ID22 have been sub-configured into ID22-1, keeping only the external densified spruce lamellae in the transversal and longitudinal direction, respectively, while stacking the layers involved about the central layer, cf. Figure 11.23. The reduction of RMS-value, cf. Table 11.12, was 55%.

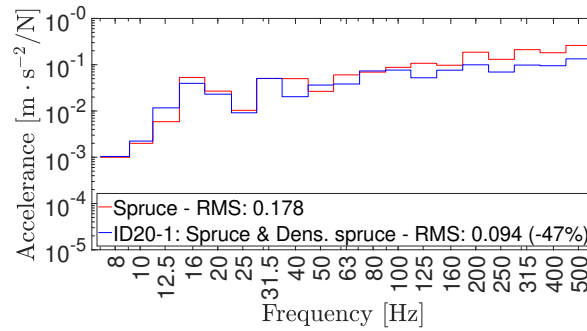


Figure 11.22: Accelerance plot, 3rd-octave band filters with RMS-values. Densified spruce sub-configuration ID20-1.

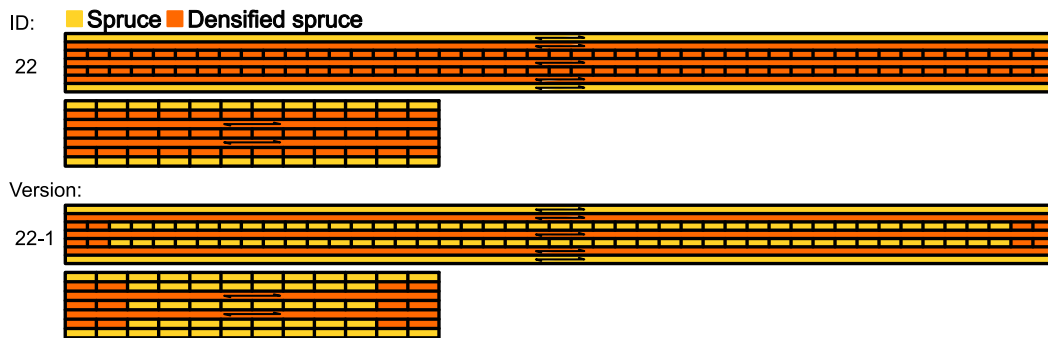


Figure 11.23: Densified spruce sub-configuration of ID22.

Table 11.12: Densified spruce sub-configuration of ID22, relative difference of RMS-values and volumetric rates of densified spruce.

ID	RMS diff. [%]	Vol. rate [%]
ID22	-34	71
ID22-1	-55	17

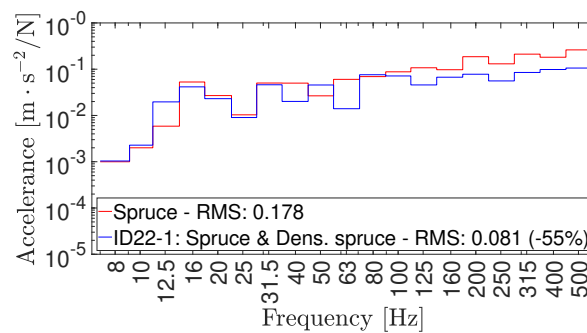


Figure 11.24: Accelerance plot, 3rd-octave band filters with RMS-values. Densified spruce sub-configuration ID22-1.

A 3rd-octave band plot can be seen in Figure 11.24, whereby improvement is found for a majority of the 3rd-octave bands for ID22-1.

7-layer Sub-configuration

Configuration ID24, which is the homogeneous CLT-plate of densified spruce, have been sub-configured into ID24-1. This sub-configuration keeps only the external densified spruce lamellae in the transversal and longitudinal direction, respectively, while maintaining the distribution about the central layer, cf. Figure 11.25. The reduction of RMS-value, cf. Table 11.13, was 62%. A 3rd-octave band plot can be seen in Figure 11.26.

In Figure 11.26, improvement is found for a majority of the 3rd-octave bands for ID24-1.

Conclusion – Combined Directions

The sub-configurations with combined transversal and longitudinal lamellae, respectively, have performed exceptionally, proving that the observed densified spruce scheme is highly relevant. That is, placing densified spruce lamellae in the perimeter of the

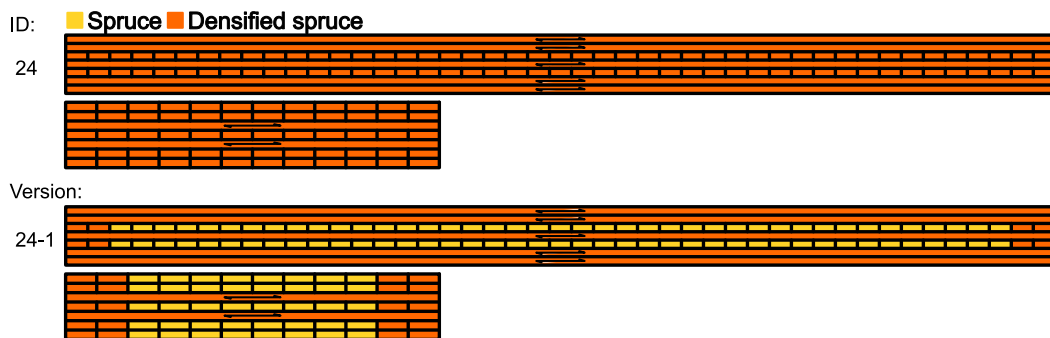


Figure 11.25: Densified spruce sub-configuration of ID24.

Table 11.13: Densified spruce sub-configuration of ID24, relative difference of RMS-values and volumetric rates of densified spruce.

ID	RMS diff. [%]	Vol. rate [%]
ID24	-39	100
ID24-1	-62	26

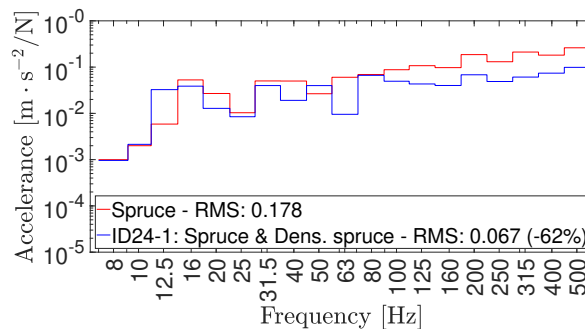


Figure 11.26: Accelerance plot, 3rd-octave band filters with RMS-values. Densified spruce sub-configuration ID24-1.

CLT-plate, stacked about the central layer. Great reductions in RMS-values were obtained by applying this scheme, by upmost of roughly 60% percent as seen for ID24-1. Furthermore, this scheme alludes perfectly to the concept of keeping the densified spruce usage relatively limited, while maintaining heightened performance with regards to the acceleration response.

11.1.5 Conclusion – L-sized CLT-plate

This section ties together the previous observations, concluding them in a concise manner. Throughout the performed case study of the L-sized CLT-plate, the reduction of the RMS-values was almost invariant with respect to the placement of densified spruce, upon replacing entire layers. However, the combination of transversal and longitudinal lamellae, respectively, showcased a predominantly favourable placement when collected along the perimeter of the CLT-plate, stacked about the central layer. This densified spruce scheme proved to ameliorate the acceleration response, by heavily reducing said response. Even though periodic densified spruce schemes have been studied, none hinted at a consistent behaviour and is hence deemed inconclusive, with respect to the limited amount of such periodic schemes performed.

Furthermore, it was possible to achieve a densified spruce scheme that would maximize the reduction of the acceleration RMS-values, while minimizing the densified spruce usage. This is advantageous from a material efficiency point of view, proving that there is a profit of investigating the lamellae distribution in CLT-plates, and not blindly incorporating stiffer and heavier material in abundance. The notable sub-configurations are collected in Figure 11.27 and Figure 11.28, with their respective reduction of the acceleration RMS-values, as well as volumetric rates of densified spruce used in Table 11.14 and Table 11.15, respectively. The following bullet-points sum up the important points:

- The numerical results suggests that a scheme of applying densified spruce along the perimeter of the CLT-plate, concentrated to the central layer, while keeping the internal portions of the CLT-plate birch-free, yields the greatest reductions of acceleration.
- Reduction of acceleration RMS-values is exceptional. Notably, ID22-1 reduced the RMS-value by roughly 50%, while being composed of slightly less than 20% densified spruce.

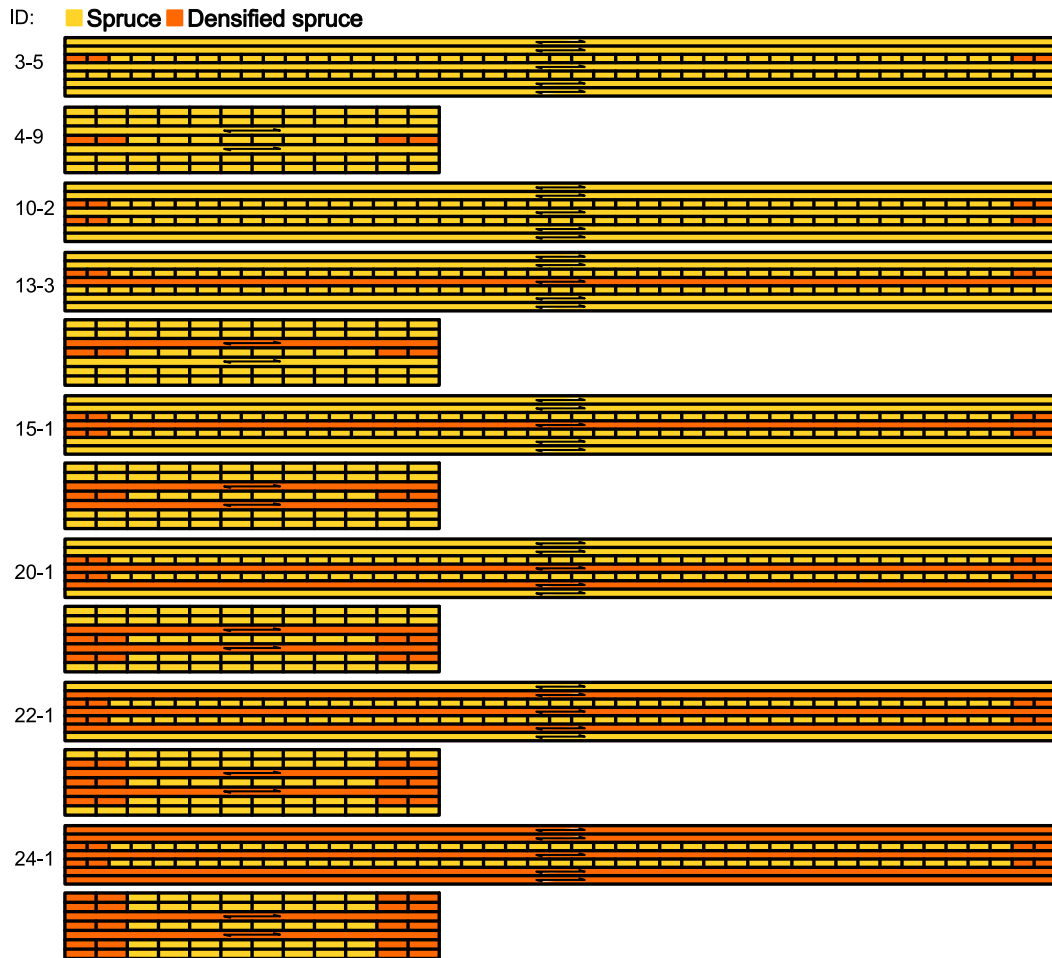


Figure 11.27: Notable densified spruce sub-configurations.

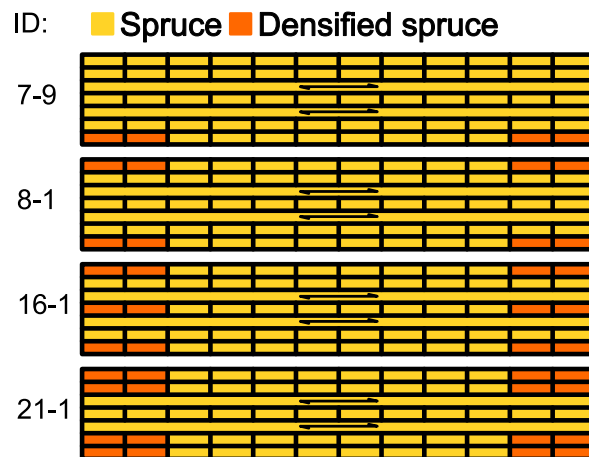


Figure 11.28: Notable densified spruce sub-configurations with longitudinal lamellae.

11.2 S-sized CLT-plate

This section presents the results concerning the S-sized CLT-plate. As mentioned in Section 9.4, the presentation is subdivided according to the three principal axes. Throughout this section, the reference case has been the homogeneous S-sized CLT-plate, made of spruce with calibrated parameters.

Table 11.14: Notable densified spruce sub-configurations, reduction of RMS-values and volumetric rates of densified spruce.

ID	RMS diff. [%]	Vol. rate [%]
ID3-5	-14	1
ID4-9	-19	5
ID10-2	-25	3
ID13-3	-32	6
ID15-1	-41	7
ID20-1	-47	12
ID22-1	-55	17
ID24-1	-62	26

Table 11.15: Notable densified spruce sub-configurations with longitudinal lamellae, reduction of RMS-values and volumetric rates of densified spruce.

ID	RMS diff. [%]	Vol. rate [%]
ID7-9	-18	5
ID8-1	-32	10
ID16-1	-33	14
ID21-1	-44	19

Table 11.16: Layer configurations, relative difference of RMS-values and volumetric rates of densified spruce.

ID	RMS diff. [%]	Vol. rate [%]
ID1S	-4	20
ID2S	-3	20
ID3S	-7	20
ID4S	-5	20
ID5S	-6	20
ID6S	-23	40
ID7S	-15	40
ID8S	-21	40
ID9S	-28	60
ID10S	-31	60
ID11S	-47	100

11.2.1 Distribution of Lamellae – Thickness Direction

The layer configurations, pertaining to the thickness direction of the S-sized CLT-plate, are presented in Figure 11.29. Additionally, the relative difference of the accelerance MS-values, along with the volumetric rates of exchanged densified spruce, are presented in Table 11.16. In contrast to the L-sized CLT-plate, the S-sized CLT-plate consists of five layers, which greatly limits the number of symmetric configurations. The 3rd-octave band plots can be seen in Figure 11.30, for select configurations.

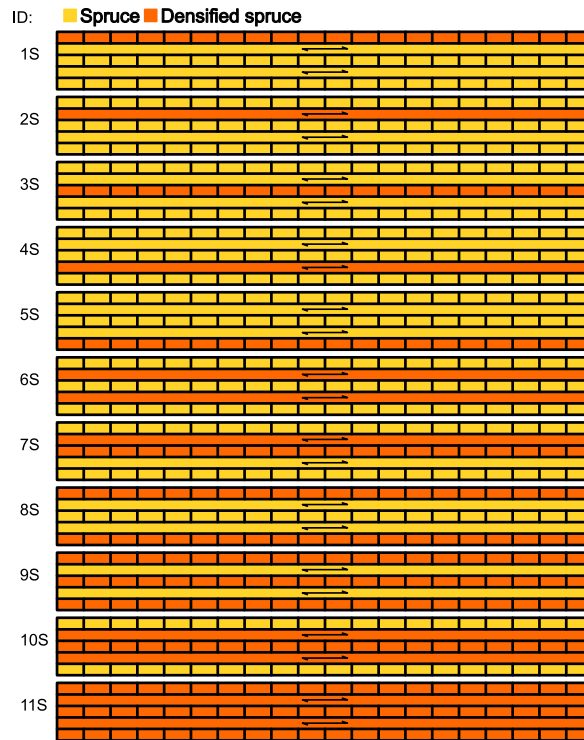


Figure 11.29: Layer configurations.

In Figure 11.30, improvement is found for a majority of the 3rd-octave bands for IDs 6S, 9S and 11S. Improvement across all a minority of the octave bands is found for ID2S and ID3S.

Single-layer Configurations

The single-layer configurations, ID1S through ID5S, exhibited insignificant reduction of the acceleration RMS-values and hence no pattern can be deduced regarding favourable placement along the thickness direction.

Multilayer Configurations

With regards to the multilayer configurations, different implications are observed with respect to the number of layers involved. The number of layers involved varied between 2-3. Additionally, a homogeneous CLT-plate of densified spruce was analysed for more lucid comparisons.

The 2-layer configurations, ID6S through ID8S, exhibited substantial reduction of the acceleration RMS-value. Notably, configuration ID7S involved the central densified spruce layer, although with a slightly less reduction of the RMS. However, this discrepancy is deemed negligible, and hence no indication is obtained regarding the favourableness of the central layer. However, the increase from a single layer to two layers moderately increased the reduction of the RMS.

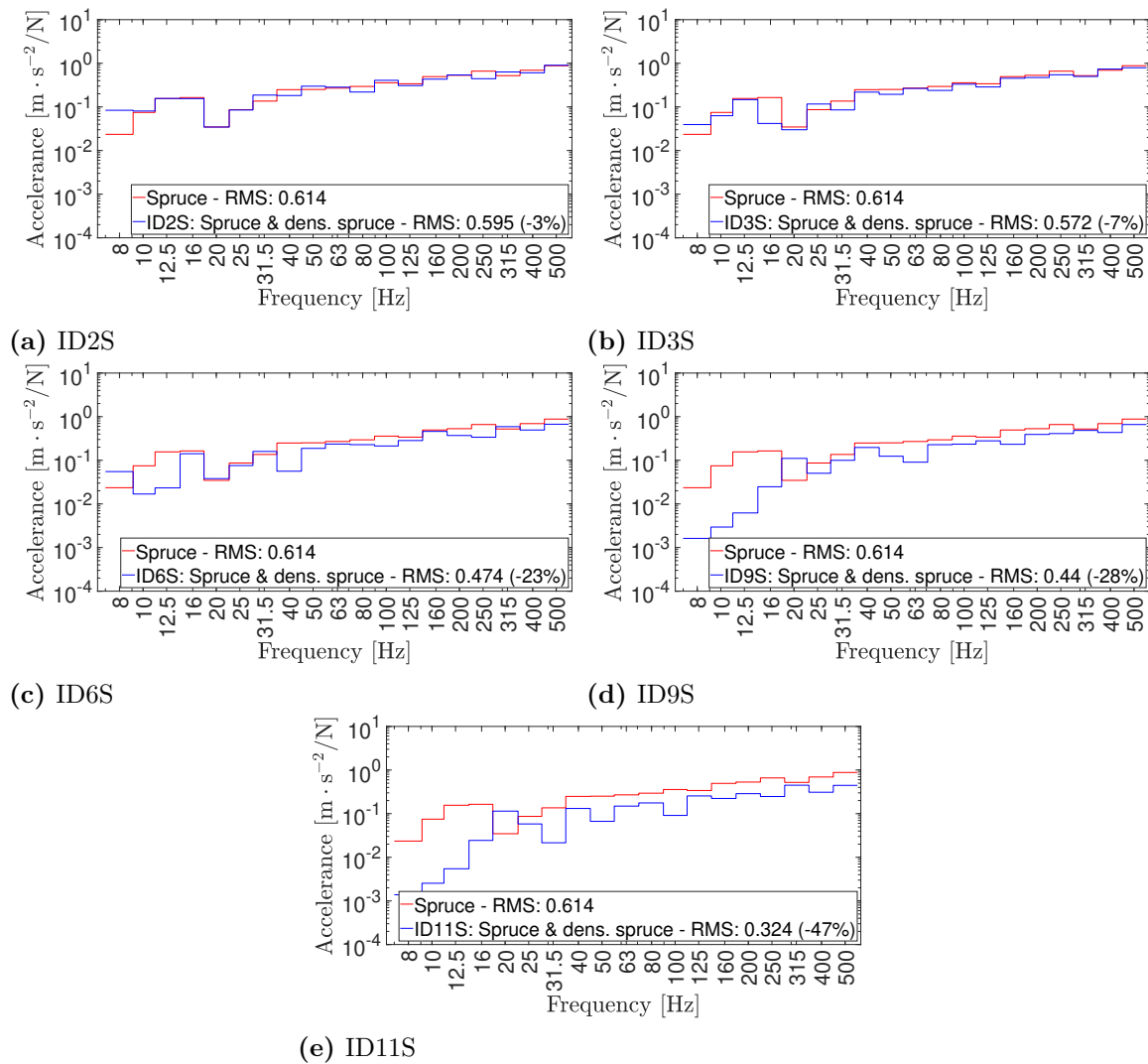


Figure 11.30: Accelerance plots, 3rd-octave band filters with RMS-values. Densified spruce configurations ID2S, ID3S, ID6S, ID9S and ID11S.

The 3-layer configuration, ID9S and ID10S, displayed significant reduction of the accelerance RMS-values, an average of roughly 30%. ID10S performs moderately better than the previous configurations, whereby the increase of involved layers seem to be favourable. However, the tested configurations are limited and therefore no indication is obtained regarding the importance of the central layer.

Conclusion – Thickness Direction

By the conducted layer configurations, pertaining to the thickness direction of the CLT-plate, no specific pattern was observed favouring a specific placement of the densified spruce. However, it was observed that the CLT-plate performance increase drastically from single-layer to multilayer configurations. The highest recorded reduction of the RMS-value was due to configuration ID10S at 31%. Although, this is moderately less than the reduction from the homogeneous densified spruce configuration ID11S, at 47%.

11.2.2 Distribution of Lamellae – Longitudinal Direction

The investigation of the lamellae distribution along the longitudinal direction was performed with a single layer. The only choices for suitable configurations to perform this study on are ID2S and ID4S, whereby the former was chosen to avoid redundancy. Furthermore, a 2-layer configuration have been further studied.

Figure 11.31 shows the tested sub-configurations of ID2S, namely ID2S-1 through ID2S-9. The corresponding relative difference of the accelerance RMS, as well as the volumetric rates of densified spruce, are presented in Table 11.17. These sub-configurations mimic the patterns of the same investigation done for the L-sized CLT-plate in Section 10.1.2, following the outline given in Section 9.4. The 3rd-octave band plots can be seen in Figure 11.32, for select configurations.

In Figure 11.32, improvement is found in around half of the 3rd-octave bands for ID2S-3 and ID2S-6.

Distribution Towards the Centre

Starting from ID2S, with a whole layer exchanged to densified spruce, the densified spruce lamellae are reduced from the edges, towards the centre. These sub-configurations, ID2S-1 through ID2S-3, exhibited negligible reduction of the RMS. Hence, this indicates that placing densified spruce lamellae in the centre of the longitudinal direction is unfavourable.

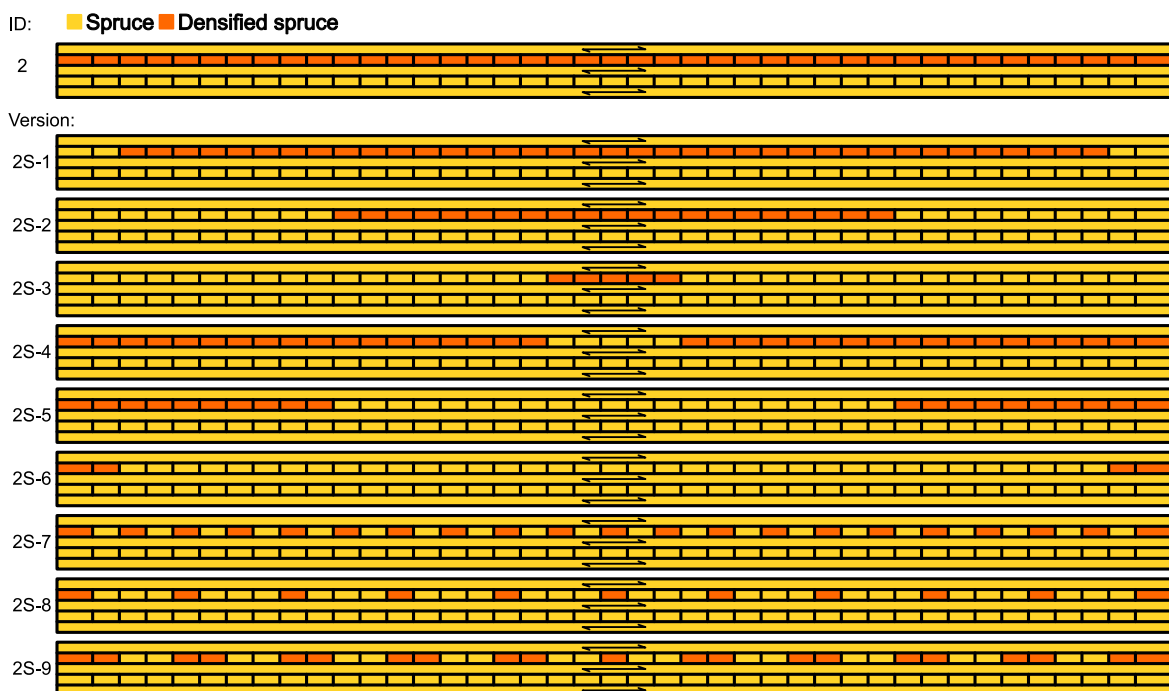


Figure 11.31: Densified spruce sub-configurations of ID2S.

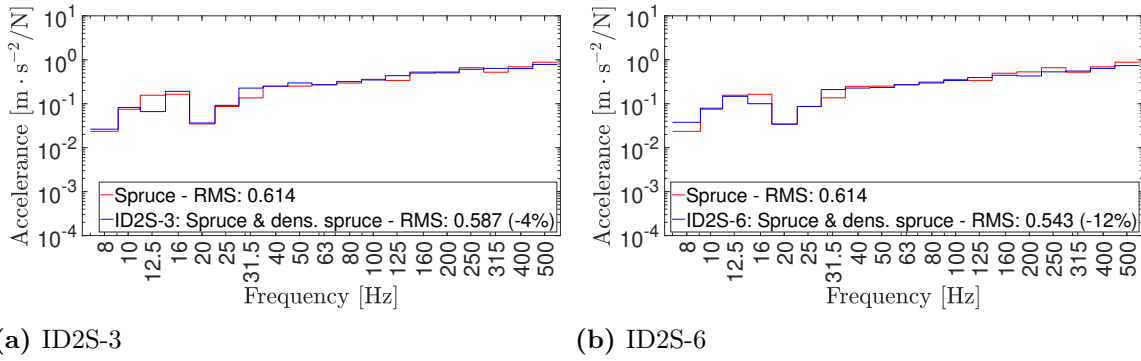


Figure 11.32: Accelerance plots, 3rd-octave band filters with RMS-values. Densified spruce sub-configurations of ID2S.

Distribution Towards the Edges

Conversely to above, the densified spruce lamellae are reduced incrementally from the centre of the longitudinal direction, towards the edges thereof. These sub-configurations, ID2S-4 through ID2S-6, exhibited marginal reduction of the accelerance RMS. Notably, sub-configuration ID2S-4 had no influence on the RMS, while ID2S-5 and ID2S-6 marginally reduced the RMS. Thus, the densified spruce lamellae should not be close to the centre of the longitudinal direction, and more concentrated to the edges of said direction.

Systematic Distribution

Some systematic distributions of the densified spruce lamellae, in a periodic manner with different spacings of the densified spruce lamellae, have been performed. These sub-configurations, ID2S-7 through ID2S-9, displayed marginal reduction of the accelerance RMS-value. No clear discrepancy can be observed between these sub-configurations and hence no indication towards an optimal distribution is obtained.

Table 11.17: Densified spruce sub-configurations of ID2S, relative difference of RMS-values and volumetric rates of densified spruce.

ID	RMS diff. [%]	Vol. rate [%]
ID2S	-3	20
ID2S-1	0	18
ID2S-2	-1	21
ID2S-3	-4	2
ID2S-4	0	18
ID2S-5	-9	10
ID2S-6	-12	2
ID2S-7	-7	10
ID2S-8	-11	6
ID2S-9	-6	10

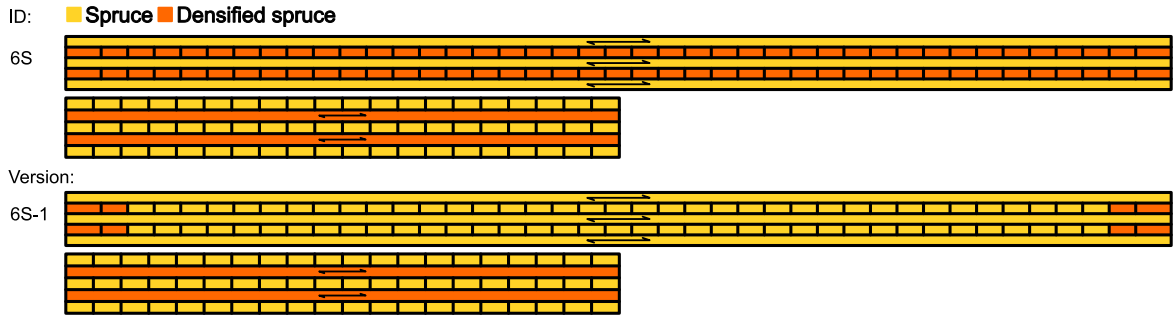


Figure 11.33: Densified spruce sub-configurations of ID6S.

Table 11.18: Densified spruce sub-configurations of ID6S, relative difference of RMS-values and volumetric rates of densified spruce.

ID	RMS diff. [%]	Vol. rate [%]
ID6S	-23	40
ID6S-1	-17	3

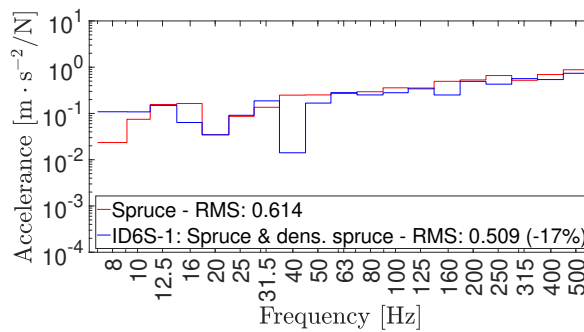


Figure 11.34: Accelerance plot, 3rd-octave band filters with RMS-values. Densified spruce sub-configuration ID6S-1.

2-layer Sub-configuration

A 2-layer sub-configuration of ID6S have been performed, namely, ID6S-1, cf. Figure 11.33. The reduction of the RMS-value is given in Table 11.18. This sub-configuration maintains the reduction of the RMS-value, while using significantly less densified spruce lamellae, than configuration ID6S. The 3rd-octave band plot can be seen in Figure 11.34, whereby improvement is found in a majority of the 3rd-octave bands.

Conclusion – Longitudinal Direction

By the conducted transversal lamellae configurations, pertaining to the longitudinal direction of the CLT-plate, it was observed that a favourable placement of the densified spruce would be towards the edges. However, the reduction of the RMS was not significant. This may hint at the fact that the smaller sized CLT-plate is sturdy and rigid and hence less susceptible to dynamical phenomena, as well as less sensitive to material variability, in terms of the longitudinal direction.

Additionally, increasing the number of layers involved, as in ID6S-1, contributed insignificantly to the reduction of the RMS-value, in comparison to ID2S-6. However, only one multilayer sub-configuration was performed, and thus, an unequivocal statement regarding the effect of increasing the number of involved layers cannot be made, in terms of the longitudinal direction.

11.2.3 Distribution of Lamellae – Transversal Direction

The investigation of the lamellae distribution along the transversal direction have been performed with single-layer configurations as well as multilayer configurations. This was done based on the lack of prominent patters, with significant reduction of RMS, in the previous study along the longitudinal direction.

Figure 11.35 shows the tested single-layer sub-configurations of ID3S, namely, ID3S-1 through ID3S-9. The respective relative difference of the accelerance RMS-value is collected in Table 11.19, along with the volumetric rate of exchanged densified spruce. The 3rd-octave band plots can be seen in Figure 11.36, for select configurations.

In Figure 11.36, improvement is found in a majority of the 3rd-octave bands.

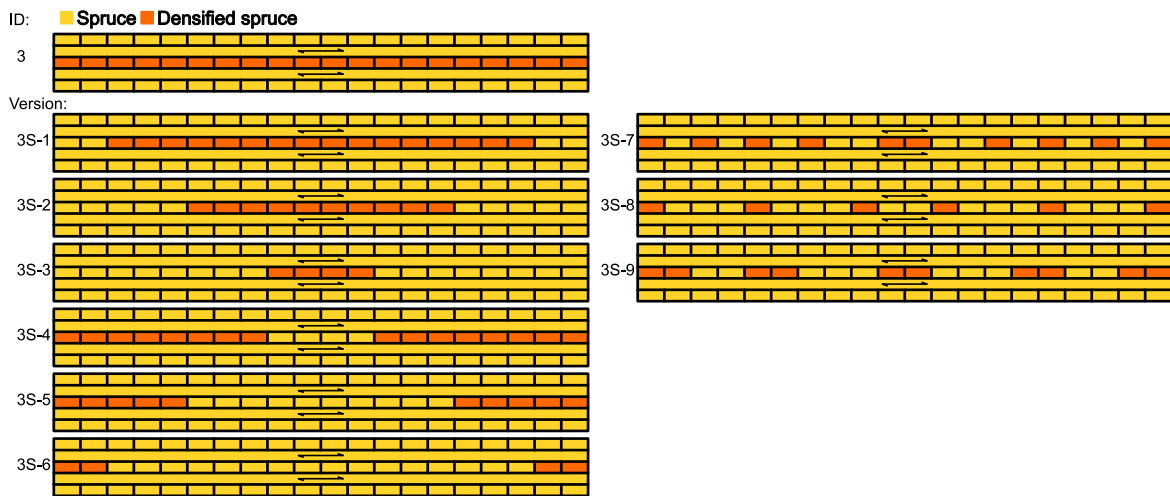


Figure 11.35: Densified spruce sub-configurations of ID3S.

Table 11.19: Densified spruce sub-configurations of ID3S, relative difference of RMS-values and volumetric rates of densified spruce.

ID	RMS diff. [%]	Vol. rate [%]	ID	RMS diff. [%]	Vol. rate [%]
ID3S	-7	20	ID3S-7	-10	10
ID3S-1	4	16	ID3S-8	2	6
ID3S-2	-1	10	ID3S-9	-8	10
ID3S-3	-1	4			
ID3S-4	-7	16			
ID3S-5	-6	10			
ID3S-6	-14	4			

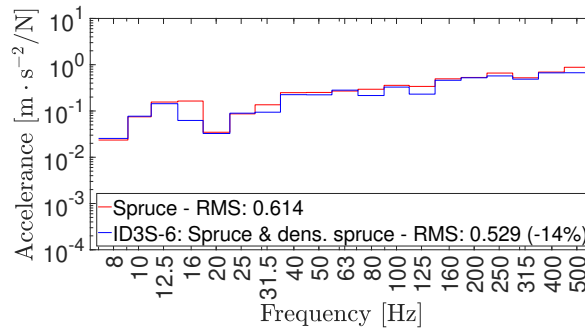


Figure 11.36: ID3S-6

Distribution Towards the Centre

Starting from configuration ID3S, with a whole layer exchanged to densified spruce, the densified spruce lamellae are reduced in the edges of the transversal direction, with greater reduction incrementing towards the centre. These sub-configurations, ID3S-1 through ID3S-3, displayed minimal change of the RMS. This hints at an unpreferable placement of densified spruce lamellae towards the centre of the transversal direction.

Distribution Towards the Edges

Conversely to above, densified spruce lamellae are excluded incrementally from the centre, towards the edges. These sub-configurations, ID3S-4 through ID3S-6, displayed marginal reduction of the acceleration RMS-value. Notably, though, ID3S-6 reduced the RMS with a moderate 14%. This indicates that less densified spruce should be used in the centre, while maintaining densified spruce lamellae to the edges.

Systematic Distribution

Some distributions, with systematic arrangement of the densified spruce lamellae, have been performed. These sub-configurations, ID3S-7 through ID3S-9, exhibited varied reduction of the acceleration RMS. While sub-configuration ID3S-8 had no significant impact on the RMS, ID3S-7 and ID3S-9 showcased a pronounced reduction of the RMS, averaging roughly 10%. However, as the latter sub-configurations performed similarly, and due to the limited number of periodic arrangements, no conclusion can be drawn towards a preferable distribution of densified spruce lamellae along the transversal direction.

2-layer Configuration

A 2-layer sub-configuration of ID8S have been performed, namely ID8S-1, cf. Figure 11.37. The acceleration RMS-value was marginally reduced, cf. Table 11.20. However, in comparison to the full layer configuration ID8S, the former sub-configuration

performed poorly. This indicates that an increase of involved layers in the sub-configurations, in terms of the transversal direction, may not necessarily be preferred. The 3rd-octave band plot can be seen in Figure 11.38.

In Figure 11.38, improvement is found in a majority of the 3rd-octave bands.

3-layer Configuration

A 3-layer sub-configuration of ID9S have been performed, namely ID9S-1, cf. Figure 11.39. The accelerance RMS-value was significantly reduced, cf. Table 11.21. Notably, the full layer configuration ID9S performed marginally better than the sub-configuration. The 3rd-octave band plot can be seen in Figure 11.40.

In Figure 11.40, improvement is found in a majority of the 3rd-octave bands.

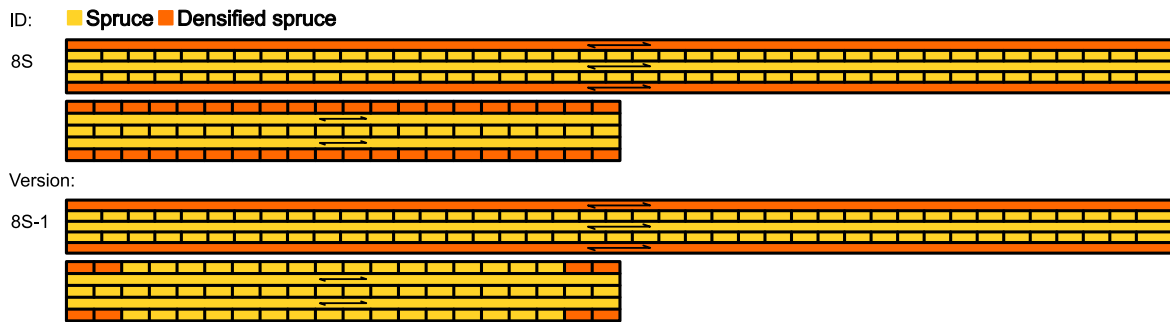


Figure 11.37: Densified spruce sub-configuration of ID8S.

Table 11.20: Densified spruce sub-configuration of ID8S, relative difference of RMS-values and volumetric rates of densified spruce.

ID	RMS diff. [%]	Vol. rate [%]
ID8S	-21	40
ID8S-1	-9	8

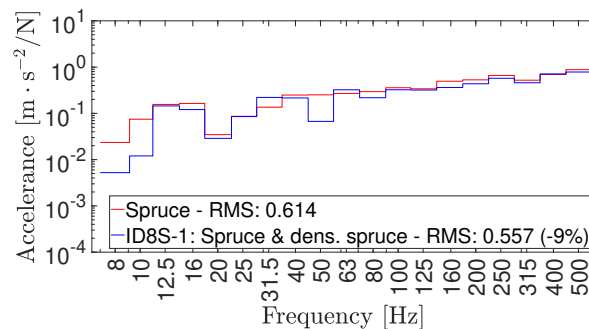


Figure 11.38: Accelerance plot, 3rd-octave band filters with RMS-values. Densified spruce sub-configuration ID8S-1.

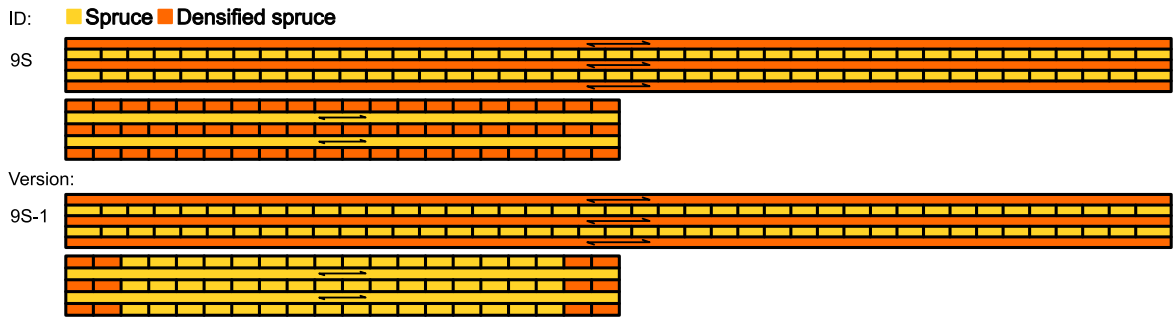


Figure 11.39: Densified spruce sub-configuration of ID9S.

Table 11.21: Densified spruce sub-configuration of ID9S, relative difference of RMS-values and volumetric rates of densified spruce.

ID	RMS diff. [%]	Vol. rate [%]
ID9S	-28	60
ID9S-1	-19	12

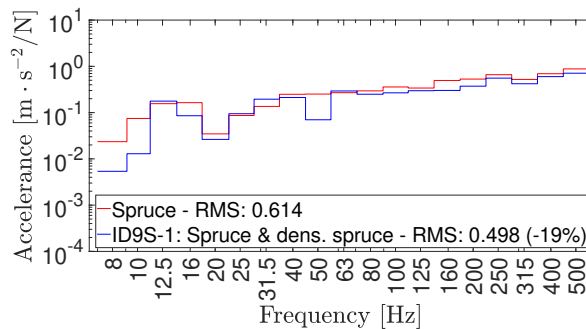


Figure 11.40: Accelerance plot, 3rd-octave band filters with RMS-values. Densified spruce sub-configuration ID9S-1.

Conclusion – Transversal Direction

By the conducted longitudinal lamellae configurations, pertaining to the transversal direction of the CLT-plate, it was observed that a favourable placement of the densified spruce would be towards the edges, while keeping the central parts unchanged with spruce. However, the extent of reduction of RMS-values by this approach is moderate. The periodic distributions did not reveal an optimal placement of the densified spruce lamellae.

Furthermore, it was observed that increasing the number of layers involved, in the sub-configurations, causes marginally reduced RMS in contrast to the corresponding full layer configurations. However, using more layers in the sub-configurations increases the reduction of RMS, as seen by comparing ID8S-1 against ID9S-1.

11.2.4 Distribution of Lamellae – Combined Direction

Based on the previous distributions and conclusions thereof, a combination is made of these former observations. The theme of maintaining the densified spruce lamellae to-

wards the edges in the transversal and longitudinal direction, respectively, is followed. Multilayer configurations, cf. Figure 11.29, are altered in order to combine transversal and longitudinal lamellae. The choice of these sub-configurations was based on feasibility to apply the previous recorder observations. These sub-configurations are categorized into the number of layers involved.

2-layer Sub-configuration

Configuration ID7S have been sub-configured into ID7S-1, cf. Figure 11.41, keeping the external densified spruce lamellae in both the transversal and longitudinal directions. The accelerance RMS-value remained virtually unchanged in comparison to ID7S, cf. Table 11.22. The 3rd-octave band plot can be seen in Figure 11.42.

In Figure 11.42, improvement is found in a majority of the 3rd-octave bands.

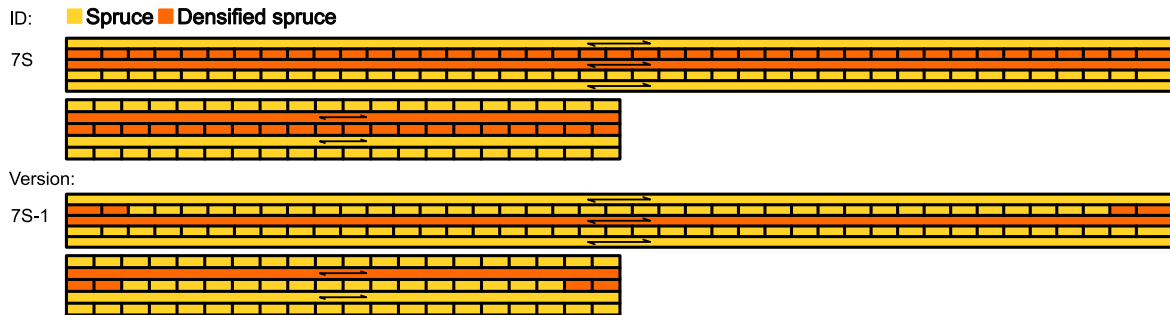


Figure 11.41: Densified spruce sub-configuration of ID7S, relative difference of RMS-values and volumetric rates of densified spruce.

Table 11.22: Densified spruce sub-configuration of ID7S, relative difference of RMS-values and volumetric rates of densified spruce.

ID	RMS diff. [%]	Vol. rate [%]
ID7S	-15	40
ID7S-1	-19	6

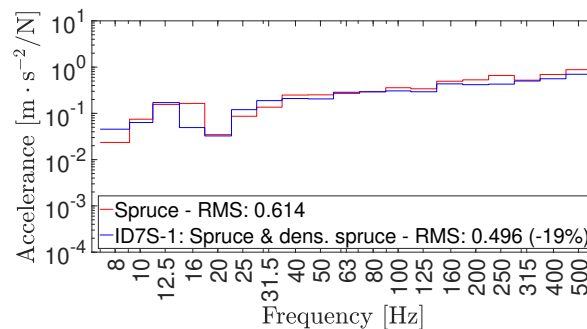


Figure 11.42: Accelerance plot, 3rd-octave band filters with RMS-values. Densified spruce sub-configuration ID7S-1.

3-layer Sub-configuration

Configuration ID10S have been sub-configured into ID10S-1, cf. Figure 11.43, keeping the external densified spruce lamellae in both the transversal and longitudinal directions. These are concentrated about the central layer, whereby the acceleration RMS-value is reduced significantly, cf. Table 11.23. Namely, ID10S had a reduction of 31% while ID10S-1 had a reduction of 27%. Thus, these two configurations perform similarly, while the latter is being composed only of 8% densified spruce. The 3rd-octave band plot can be seen in Figure 11.44.

In Figure 11.44, improvement is found in a majority of the 3rd-octave bands.

5-layer Sub-configuration

Configuration ID11S have been sub-configured into ID11S-1, cf. Figure 11.45, keeping the external densified spruce lamellae in both the transversal and longitudinal

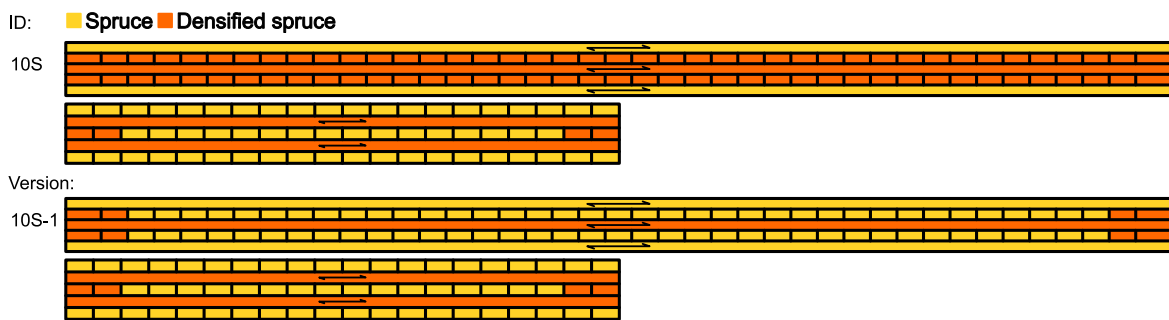


Figure 11.43: Densified spruce sub-configuration of ID10S, relative difference of RMS-values and volumetric rates of densified spruce.

Table 11.23: Densified spruce sub-configuration of ID10S, relative difference of RMS-values and volumetric rates of densified spruce.

ID	RMS diff. [%]	Vol. rate [%]
ID10S	-31	60
ID10S-1	-27	8

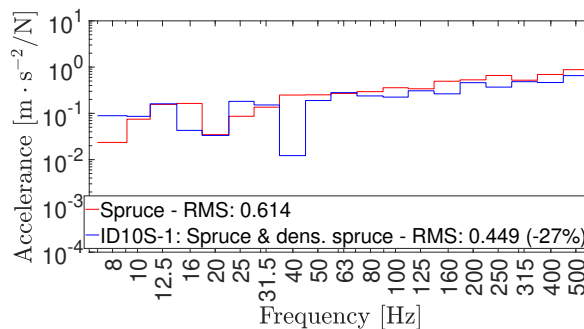


Figure 11.44: Accelerance plot, 3rd-octave band filters with RMS-values. Densified spruce sub-configuration ID10S-1.

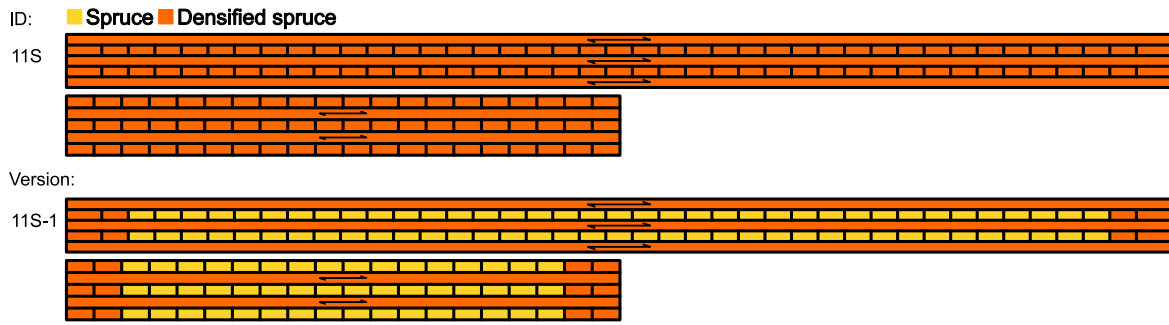


Figure 11.45: Densified spruce sub-configuration of ID11S.

Table 11.24: Densified spruce sub-configuration of ID11S, relative difference of RMS-values and volumetric rates of densified spruce.

ID	RMS diff. [%]	Vol. rate [%]
ID11S	-47	100
ID11S-1	-43	16

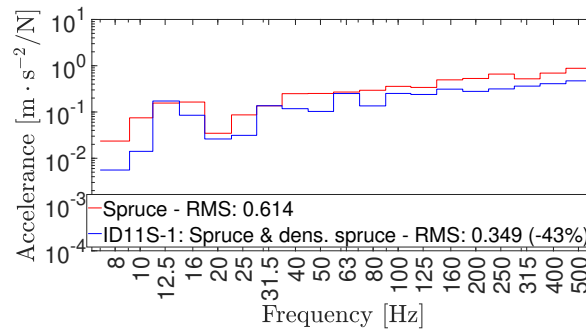


Figure 11.46: Accelerance plot, 3rd-octave band filters with RMS-values. Densified spruce sub-configuration ID11S-1.

directions. These are stacked as much as possible about the central layer, whereby the RMS-value is reduced substantially, cf. Table 11.24, by 43%. It is noteworthy that ID11S-1 performs at a similar level to the homogeneous densified spruce CLT-plate, configuration ID11S, while being composed of only 16% densified spruce. The 3rd-octave band plot can be seen in Figure 11.46.

In Figure 11.46, improvement is found in a majority of the 3rd-octave bands.

Conclusion – Combined Direction

The sub-configurations with combined transversal and longitudinal lamellae, respectively, have performed exceptionally, proving that the observed scheme is highly relevant. That is, placing densified spruce lamellae in the perimeter of the CLT-plate, stacked about the central layer. Great reductions in the accelerance RMS-values were obtained by applying this scheme, by upmost of roughly 40%, as seen for ID11S-1. Although, the performance of the sub-configurations using the densified spruce scheme is similar to the corresponding combined configuration, the usage of densified spruce

lamellae is heavily reduced by employing said densified spruce scheme. This alludes perfectly to the concept of keeping the densified spruce usage relatively limited, while maintaining heightened performance with regards to the acceleration response.

11.2.5 Conclusion – S-sized CLT-plate

This section ties together the previous observations, concluding them in a concise manner. Throughout the performed case study of the S-sized CLT-plate, the densified spruce placement was predominantly favourable when collected along the perimeter of the CLT-plate, stacked about the central layer. This densified spruce scheme proved to ameliorate the acceleration response, by heavily reducing said response. Even though periodic densified spruce schemes have been studied, none hinted at a consistent behaviour and is hence deemed inconclusive, with respect to the limited amount of such periodic schemes.

Furthermore, it was possible to achieve a densified spruce scheme that would maximize the reduction of the accelerance RMS-values, while minimizing the densified spruce usage. This is advantageous from a material efficiency point of view, proving that there is a profit of investigating the lamellae distribution in CLT-plates, and not blindly incorporating stiffer and heavier material in abundance. Moreover, it was noticed that the reduction obtained from the various S-sized configurations were substantially lower than for the L-sized configurations. This indicates that there is a greater potential, and room for improvement, regarding the L-sized CLT-plate, than for the S-sized CLT-plate. This also showcases that the size of the CLT-plate may dictate how well the configurations perform. The following bullet-points sum up the important points:

- Densified spruce scheme of applying densified spruce along the perimeter of the CLT-plate, concentrated to the central layer, while keeping the internal parts of the CLT-plate free from densified spruce.
- Reduction of accelerance RMS-values is substantial. Notably, sub-configuration ID11S-1 reduced the RMS-value by roughly 40%, on par with the homogeneous densified spruce CLT-plate ID11S, while being composed of significantly less densified spruce.
- The reduction of the RMS-values in the S-sized CLT-plate are substantially lower than in the L-sized CLT-plate.

12 Case Study – Spruce Strength Classes

This chapter presents the results from the reduced modal-based steady-state analyses of different CLT-plate configurations of spruce C24 combined with various strength classes of spruce.

The analyses conducted in this chapter will not follow the methodology as Chapters 10 and 11. Due to the limited time available during this dissertation, as well as the extent thereto, the configurations tested with varying strength grades of spruce were configurations which showed significant reduction of vibration levels in terms of birch and densified spruce. Thus, the goal of these analyses was to test if similar improvements are possible when implementing spruce of different strength classes. The configurations picked out for the analyses with varying strength grades of spruce, were configurations for which the lamellae in the perimeter were exchanged, concentrated about the central layers.

Since only one quality of spruce was included in the experiment in Chapter 8.1, appropriate mechanical properties of spruce of different strength classes were unknown. In order to be able to appropriately test various strength classes of spruce at the same time, reference values according to Eurocode SS-EN 338 were implemented, presented in Table 8.9.

The results of the analyses will be presented as 3rd-octave RMS plots, for select configurations. The data is presented in said plots with the relative change of the accelerance RMS-value calculated for each 3rd-octave band. The amount of spruce with different strength grade used in each configuration tested will be presented as a volumetric percentage of the CLT-plate.

12.1 L-sized CLT-plate

This section presents the results concerning the L-sized CLT-plate. The reference case used for determining improvement was a CLT-panel constructed of only C24 spruce.

During testing in Chapters 10 and 11, configuration ID10-2 showed a significant reduction in accelerance RMS with both birch and densified spruce. The configuration is presented in Figure 12.1, with the red highlighting where spruce of different strength classes was implemented.

In Table 12.1, the change in accelerance RMS is presented for all strength classes of spruce. All strength classes stronger than the reference value showed improvement and those of a weaker strength class showed an increase in accelerance RMS-values. Only

the reduction achieved by implementing C45 and C50 is noteworthy. The 3rd-octave band plots can be seen in Figure 12.2, for spruce qualities C14 and C50.

In Figure 12.2, improvement is found for a majority of the 3rd-octave bands for spruce quality C50. For C14, improvement is found for a small minority of the 3rd-octave bands.

Another configuration which showed notable improvement when combined with either birch or densified spruce was ID15-1. The configuration is presented in Figure 12.3.

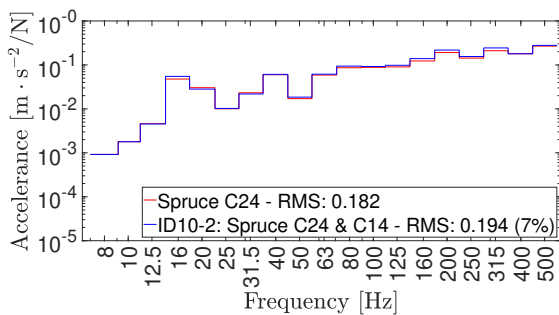
In Table 12.2, the change in accelerance RMS is presented for all strength classes of spruce. All strength classes stronger than the reference value showed improvement



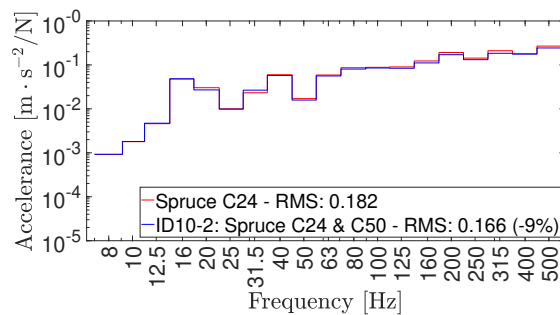
Figure 12.1: Spruce C24 combined with spruce of varying quality, ID10-2. Volumetric rate of exchanged material is 3%.

Table 12.1: Spruce strength classes sub-configuration ID10-2, relative difference of RMS-values and volumetric rates of densified spruce.

Parameter	C14	C16	C18	C20	C22	C24
Accelerance change [%]	7	5	4	2	1	0
	C27	C30	C35	C40	C45	C50
Accelerance change [%]	-1	-3	-4	-5	-7	-9



(a) C14



(b) C50

Figure 12.2: Accelerance plots, 3rd-octave band filters with RMS-values. Spruce strength grade C24 combined with C14 and C50 for ID10-2.

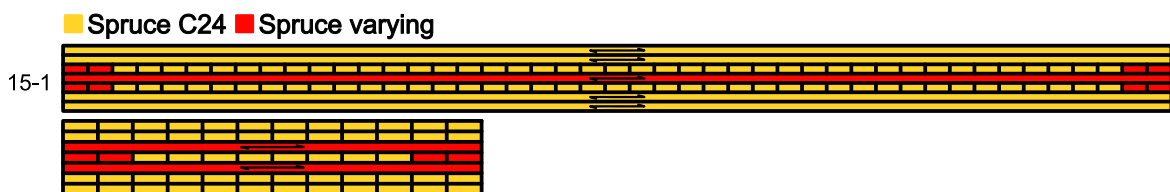


Figure 12.3: Spruce C24 combined with spruce of varying quality, ID15-1. Volumetric rate of exchanged material is 7%.

Table 12.2: Spruce strength classes sub-configuration ID15-1, relative difference of RMS-values and volumetric rates of densified spruce.

Parameter	C14	C16	C18	C20	C22	C24
Accelerance change [%]	21	15	10	6	3	0
	C27	C30	C35	C40	C45	C50
Accelerance change [%]	-2	-7	-9	-11	-13	-16

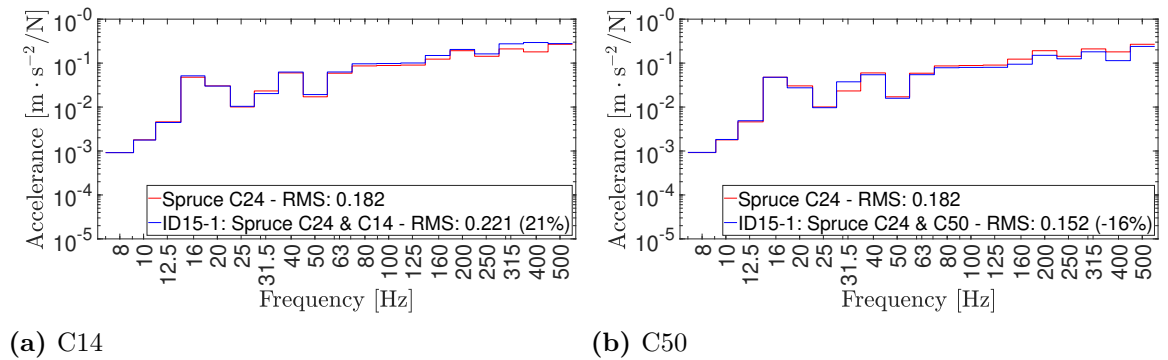


Figure 12.4: Accelerance plots, 3rd-octave band filters with RMS-values. Spruce strength grade C24 combined with C14 and C50 for ID15-1.

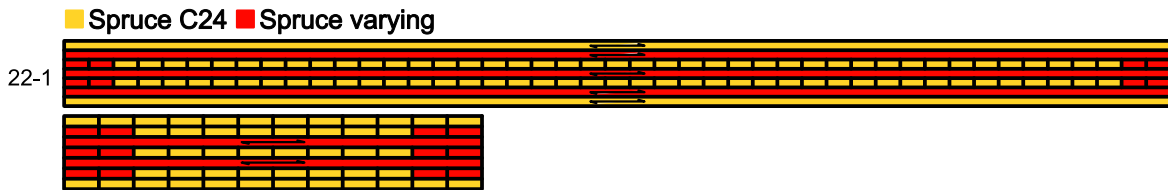


Figure 12.5: Spruce C24 combined with spruce of varying quality, ID22-1. Volumetric rate of exchanged material is 17%.

and those of a weaker strength class showed an increase in accelerance RMS-values. Improvement caused by implementing C30 and upward is noteworthy. The 3rd-octave band plots can be seen in Figure 12.4, for spruce qualities C14 and C50.

In Figure 12.4, improvement is found for a majority of the 3rd-octave bands for spruce quality C50. For C14, improvement is found for barely any of the 3rd-octave bands.

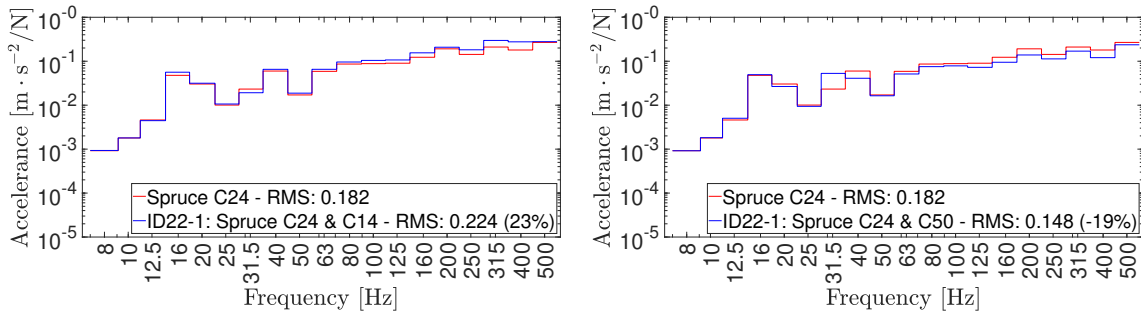
Configuration ID22-1 showed significant improvement for previous analyses. The configuration is presented in Figure 12.5.

Table 12.3 presents the change in accelerance RMS for all strength classes of spruce. All strength classes stronger than the reference value showed improvement, while those weaker exhibited an increase in accelerance RMS values. Notably, the implementation of C30 and higher strength classes resulted in significant improvement. The 3rd-octave band plots can be seen in Figure 12.6, for spruce qualities C14 and C50.

In Figure 12.6, improvement is found for a majority of the 3rd-octave bands for spruce quality C50. For C14, improvement is found for barely any of the 3rd-octave bands.

Table 12.3: Spruce strength classes sub-configuration ID22-1, relative difference of RMS-values and volumetric rates of densified spruce.

Parameter	C14	C16	C18	C20	C22	C24
Accelerance change [%]	23	16	11	5	2	0
Parameter	C27	C30	C35	C40	C45	C50
Accelerance change [%]	-2	-9	-10	-12	-14	-19



(a) C14

(b) C50

Figure 12.6: Accelerance plots, 3rd-octave band filters with RMS-values. Spruce strength grade C24 combined with C14 and C50 for ID22-1.

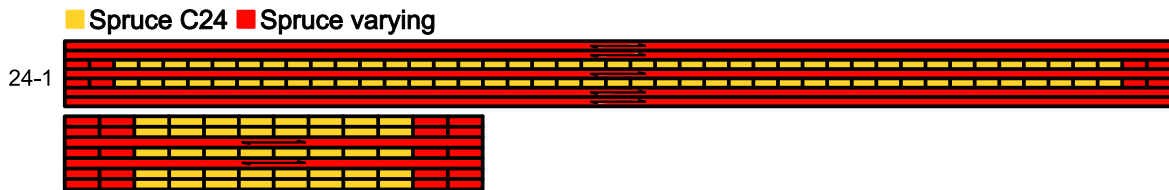


Figure 12.7: Spruce C24 combined with spruce of varying quality, ID24-1. Volumetric rate of exchanged material is 26%.

Table 12.4: ID24-1 Eurocode

Parameter	C14	C16	C18	C20	C22	C24
Accelerance change [%]	29	19	13	5	1	0
Parameter	C27	C30	C35	C40	C45	C50
Accelerance change [%]	-2	-10	-10	-11	-13	-18

Configuration ID24-1 also showed notable improvement when combined with either birch or densified spruce. This configuration is presented in Figure 12.7.

Table 12.4 displays the change in accelerance RMS for all strength classes of spruce. Classes stronger than the reference value demonstrated improvement, whereas weaker classes showed an increase in accelerance RMS values. The implementation of C30 and higher strength classes, in particular, resulted in significant improvement. The 3rd-octave band plots can be seen in Figure 12.8, for spruce qualities C14 and C50.

In Figure 12.8, improvement is found for all of the 3rd-octave bands, except for the

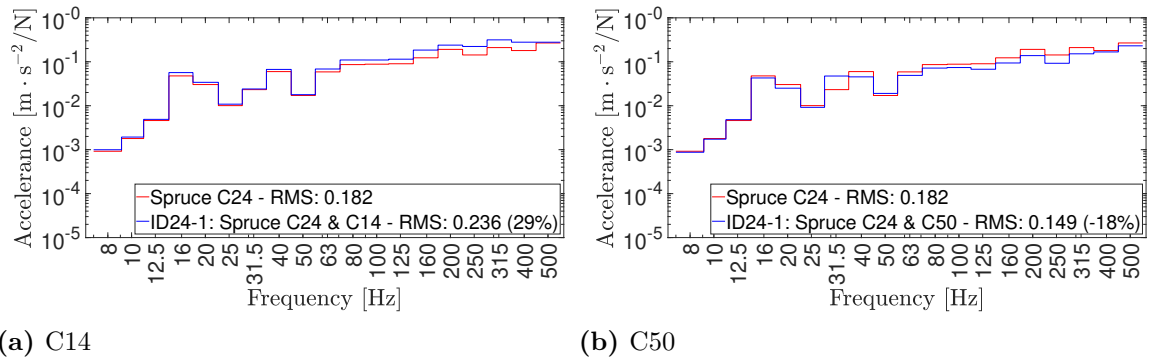


Figure 12.8: Accelerance plots, 3rd-octave band filters with RMS-values. Spruce strength grade C24 combined with C14 and C50 for ID24-1.

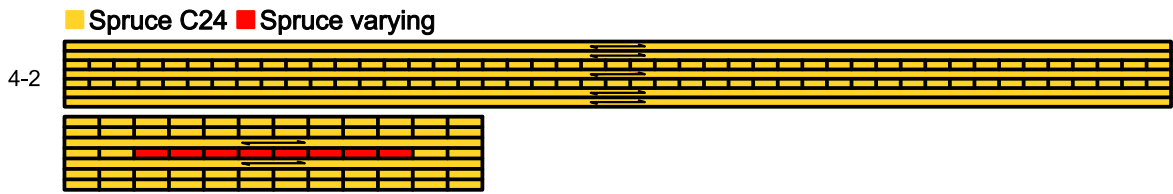


Figure 12.9: Spruce C24 combined with spruce of varying quality, ID4-2. Volumetric rate of exchanged material is 10%.

Table 12.5: Spruce strength classes sub-configuration ID4-2, relative difference of RMS-values and volumetric rates of densified spruce.

Strength class	C14	C16	C18	C20	C22	C24
Accelerance change [%]	2	6	6	5	2	0
	C27	C30	C35	C40	C45	C50
Accelerance change [%]	-1	0	2	7	11	14

bands of 12.5 Hz and 40 Hz, for spruce quality C50. For C14, improvement is found for none of the 3rd-octave bands.

Configuration ID4-2 worsened the dynamic response, when either birch or densified spruce was implemented into the configuration and can be seen in Figure 12.9. The aim of testing this configuration was to test if improvement was possible by implementing lower strength spruce.

Table 12.5 presents the change in accelerance RMS for all strength classes of spruce. No significant improvement in is available according to the table, it can be noted that the accelerance RMS only increased slightly for C14. The 3rd-octave band plots can be seen in Figure 12.10, for spruce qualities C14 and C50.

In Figure 12.10, improvement is found for barely any of the 3rd-octave bands for spruce quality C50. For C14, improvement is found for around half of the 3rd-octave bands.

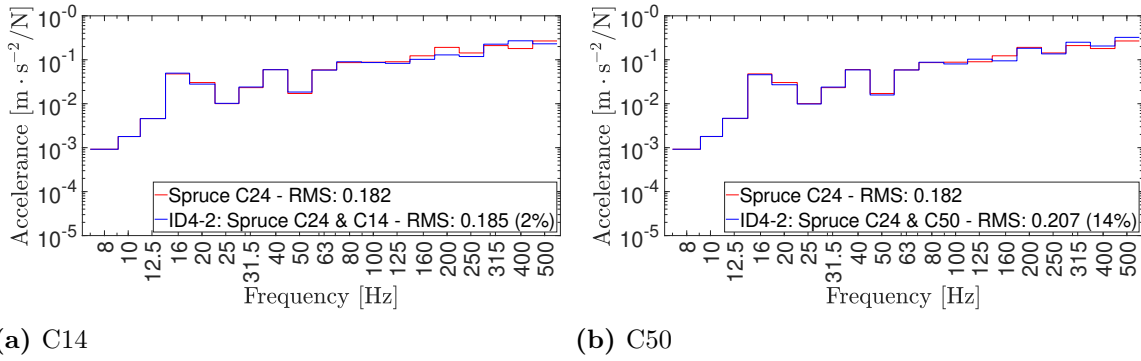


Figure 12.10: Accelerance plots, 3rd-octave band filters with RMS-values. Spruce strength grade C24 combined with C14 and C50 for ID4-2.

12.1.1 Conclusion – L-Sized CLT-plate

From the analyses on the L-sized CLT-plate, it is evident that the dynamic response can be improved by implementing higher strength spruce in favourable positions. In this case, favourable positions are those mitigating the vibration levels. ID22-1 and ID24-1 use significantly more higher strength spruce than ID15-1, 8 longitudinal and 16 longitudinal lamellae more, respectively. Despite the increase in use, no notable reduction of RMS is found for the former two. ID10-2 shows moderate reduction of RMS, despite minimal usage of higher quality spruce lamellae. A behaviour that is noted for all 4 configurations is that the increase or reduction in accelerance RMS varies almost linearly with each strength class.

ID4-2 was a test if it was possible to reduce the RMS value with lower quality spruce in configurations that have been unfavourable for birch and densified spruce. No improvement was noted by strength class C14 did not show any notable increase in RMS, which shows potential if a more favourable configuration is found.

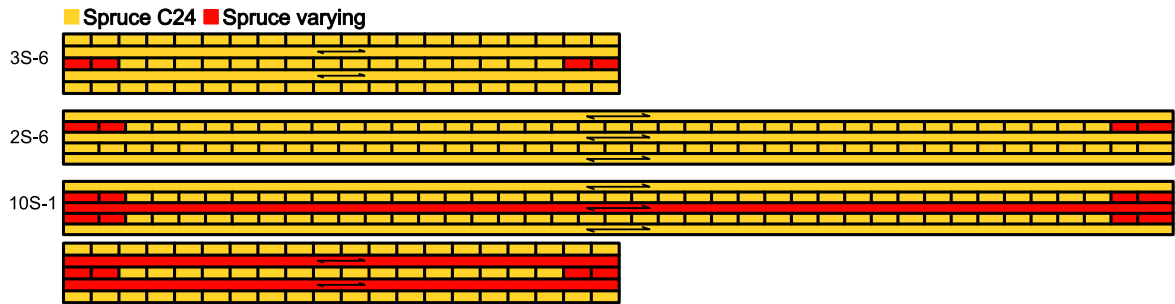


Figure 12.11: Spruce C24 combined with spruce of varying quality for the small CLT-panel.

Table 12.6: Spruce strength classes S-sized sub-configurations, relative difference of RMS-values and volumetric rates of densified spruce.

Configuration Strength class	ID2S-6		ID3S-6		ID10S-1	
	C14	C50	C14	C50	C14	C50
Accelerance change [%]	7	-6	21	-7	36	-20
Volumetric change [%]	4		2		8	

12.2 S-sized CLT-plate

This section presents the results concerning the S-sized CLT-plate. The reference case used for determining improvement was a CLT-panel constructed of only C24 spruce. For the L-sized CLT-plate, the most decrease or increase in accelerance RMS was noted by either strength class C14 or C50. For the following analyses, only strength classes C14 and C50 will be included.

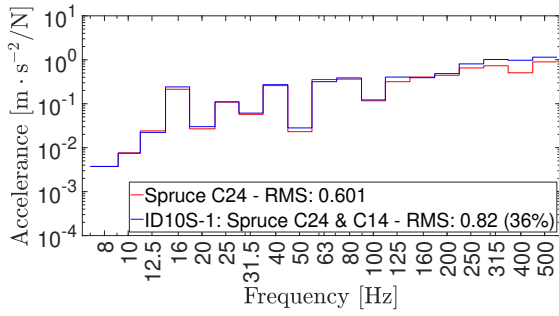
During testing in Chapters 10 and 11, configurations ID2S-6, ID3S-6 and ID10S-1 showed notable reduction in accelerance RMS when either birch or densified spruce was implemented. The configuration is presented in Figure 12.11, with the red highlighting where spruce of different strength classes was implemented.

In Table 12.6, the change in accelerance RMS is presented for all configurations, for the spruce strength classes C14 and C50. For all configurations, improvement is noted for all strength classes of C50 and those of a weaker strength class showed an increase in accelerance RMS-values. The 3rd-octave band plots for configuration ID10S-1 can be seen in Figure 12.12, for spruce qualities C14 and C50.

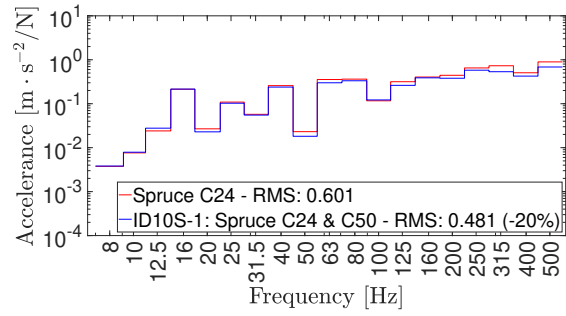
In Figure 12.12, improvement is found for a big majority of the 3rd-octave bands for spruce quality C50. For C14, improvement is found for barely any of the 3rd-octave bands.

12.2.1 Conclusion – S-sized CLT-plate

Improvement in accelerance RMS-response is found when implementing higher grade spruce in favourable positions, along the edges and in the central layers. When higher



(a) C14



(b) C50

Figure 12.12: Accelerance plots, 3rd-octave band filters with RMS-values. Spruce strength grade C24 combined with C14 and C50 for ID10S-1.

grade spruce is implemented in only a single layer, minimal improvement is found. When multiple layers are implemented with higher grade spruce, significant improvement in RMS-accelerance is found.

13 Discussion

This chapter consists of a discussion regarding the employed modeling procedure of the CLT-plate, as well as the results obtained from the case studies relating to the different wood materials.

13.1 Mechanical Properties of Wood

The mechanical properties of birch, as well as densified spruce, used in this dissertation were obtained from research articles. The mechanical properties are different for different birch species, as well as depending on the testing method used to obtain the properties. Furthermore, the research available on the mechanical properties of birch was not extensive, and as for densified spruce, even less so. Various sources, indicating several different values, were combined to the resulting mechanical properties of birch. This, in conjunction with the fact that the used birch was of an unknown species, imbues the adopted mechanical properties with a high level of uncertainty.

Therefore, some assumptions and approximations had to be made, especially for the lack of the rolling shear modulus G_{RT} . In one research article, the mechanical properties of birch were defined experimentally as rates of these properties [18]. In other articles, different rolling shear moduli were explicitly given [14][16]. Hence, a mean value was calculated of these different rolling shear moduli. Regarding the spruce analysis based upon Eurocode, the rolling shear moduli were based on a study of these parameters [22]. A ratio of the shear moduli, G_{LT}/G_{RT} was determined, whereby the rolling shear modulus G_{RT} could be calculated. This collective study with species of spruce not originating from Sweden and may not be reflective of the Swedish spruce species.

13.2 Reference Experiment

Following a literature review and determination of mechanical properties of the various wood species, a calibration of a selection of material parameters was performed based upon the results obtained from an experiment performed at Luleå Technical University, Sweden [8]. For spruce, 16 CLT-panels were tested, for birch four were tested and for densified spruce two were tested. Of the four birch panels tested, one deviated significantly and was excluded from the reference group in this dissertation.

Thus, having a reference group of three tests for birch and two tests for densified spruce may not be representative of the two types of wood since large deviations may exist for timber. Furthermore, this coupled with large uncertainties regarding the

mechanical properties of densified spruce necessitates further research to obtain more accurate and reliable results.

13.3 FE-model

The FE-model was based on several assumptions and approximations. Firstly, the CLT-plate was approximated as a completely homogeneous cuboid, to be partitioned into layers and lamellae. No extra modelling steps were taken to include the effects of the glue filled gaps between the lamellae. This was deemed reasonable, since the purpose of this glue is to ensure complete interaction between the lamellae. Moreover, it would be difficult to accurately model said timber-glue interaction. It should be highlighted that upon calibrating the material parameters, the mechanical properties of the wood species are reflective of how the species behaves in a CLT-panel and not as a timber plank. This means that the glue filled gaps are included in the model to some degree.

Furthermore, all lamellae were ascribed the same mechanical properties. This is an approximation since each individual lamella has its own set of mechanical properties. Additionally, each layer was ascribed a coordinate system that accounts for the orientation of the respective layers. This is also an approximation, since each individual lamella has its own set of principal axes, due to different lamellae being cut from different portions of the trees. However, these approximations are deemed reasonable, since the individual discrepancies would be smoothed out in the complete CLT-plate. Nonetheless, these approximations are necessary in order to facilitate an expeditious workflow, in order to avoid spending an unreasonable amount of time on the creation of the FE-models.

13.4 Loading Case and Measure Point

The load configuration used during the steady-state analyses was a unit load placed in one corner of the CLT-panel and a evaluation point in the opposite corner of the panel. Thus, the results of this dissertation are limited to the response of the setup used. Other placements of the measuring point may have resulted in exclusion of various eigenmodes if the point is located in a node of that mode. However, if multiple measuring points had been included, further examination of the results would have been possible, and more conclusions could have been obtained. Furthermore, the reliability of the conclusions would be further assessed, and not only apply for the single measure point defined in the corner of the CLT-plate.

13.5 Model Validity

The validity of the model boils down to ascertaining adequate accuracy thereof. Firstly, the material parameters were calibrated when using solid finite elements. Then, solid

shell elements were used with the obtained material parameters and identical results were obtained. Thus, solid shell elements were employed, reducing the computational effort of the FE-model. At this point, the accuracy of the model was mainly determined by the refinement of the finite element mesh, as well as the frequency step. The related convergence studies were limited due to the computational resources needed to adopt heavily refined meshes, requiring unreasonable amount of time. It would have been possible, with due time, to refine the mesh even further which could perhaps reveal that the adopted mesh has not entirely converged and would thus not be entirely accurate. However, with the level of accuracy deemed sufficient for the studies, the results obtained can be seen as credible.

13.6 Variation of Wood Material

Different species of wood can have very different ratios between the various moduli of elasticity. All three types of wood included in this dissertation had similar longitudinal modulus of elasticity, ranging from 12 to 15 GPa, although larger differences regarding the other material parameters. For densified spruce, G_{LT} and G_{RT} was thrice as large compared to spruce, and twice as large compared to birch. This increase in shear stiffness may imply why densified spruce configurations exhibited greater potential for decreasing the vibration levels in the CLT-plate, in contrast to the corresponding birch configurations.

The density of spruce was around 400 kg/m³, birch around 600 kg/m³ and densified spruce around 800 kg/m³. The angular natural frequency, for an SDOF-system, can be calculated as the ratio between stiffness, k , and mass, m , according to the following:

$$\omega_n^2 = k/m$$

This means that the stiffness and mass of the CLT-plate can be related to the eigenfrequencies of the plate. Independent of where the spruce lamellae are replaced with either birch or densified spruce, the mass will increase the same amount, but affect the distribution in the mass-matrix differently. Similarly, the distribution of stiffness in the stiffness-matrix will vary depending on the placement of the lamellae, as is evident by the results.

The replacement of the spruce lamellae around the perimeter in the central layers were found favourable for all materials tested. This may be explained by the stiffness distribution increasing in a favourable way. The distribution of stiffness and mass in a favourable way may also explain why more improvement was found when replacing a select number of lamellae according to the pattern explained above, compared to replacing the entire layer with the stiffer wood material. This can be observed Tables 10.9 and 11.13.

13.7 Results

The results obtained in the case studies for the respective wood materials, are consistent to a high degree. The case study performed on the L-sized CLT-plate of birch concluded that a favourable lamellae placement would be in the perimeter of the CLT-plate, about the central layer. Likewise, the same study regarding densified spruce also revealed the favourable placement in the perimeter of the CLT-plate. However, the level of the perimeter in the thickness direction of the CLT-plate was not necessarily constrained to the central layer. This is believed to be due to the specific ratios of the densified spruce mechanical properties. It may be that for certain ratios thereof, the response of the CLT-plate is invariant with the distribution of densified spruce along the thickness direction. Furthermore, the distribution along the longitudinal and transversal directions, respectively, were not as pronounced for densified spruce as it was for birch. This too could be ascribed to the specific material property ratios.

With regards to the S-sized CLT-plate, the results differed from the L-sized CLT-plates. Overall, though, the theme of placing the lamellae in the perimeter of the CLT-plate remained. However, some tested configurations that performed well in the L-sized case, performed poorly for the S-sized case. Thus, there is a geometric dependency that dictates, to some degree, the placement of the lamellae and the resulting response. This fact was observed in the case studies of the birch and densified spruce, respectively. Hence, a CLT-plate that is smaller than the L-sized plate while larger than the S-sized plate, would perhaps reveal a pattern with respect to the size of the CLT-plate. Likewise, a CLT-plate spanning longer than 9 m could perhaps showcase greater potential in reducing the acceleration response, than the L-sized CLT-plate. This would then induce an incentive to further analyse larger CLT-plates, both in terms of varying sizes, as well as in terms of plenty of new configurations that were not feasible in this dissertation.

With regards to the varying spruce strength classes, in accordance with the Eurocode timber strength classes, the reduction of the acceleration response was observed to be marginal, especially in comparison to the case studies on birch and densified spruce. This may be due to the fact that the ratios between the various elastic moduli are similar for most strength classes. Thus, the following acceleration responses did not vary as significantly as when comparing more dissimilar wood types. Additionally, the density of the highest strength grade of spruce did not surpass that of birch.

Nonetheless, the case studies performed were of a comparative nature, whereby the responses of the different configurations were always compared against a reference case, and hence only the improvement, or impairment, of the CLT-plates were studied. That is, no absolute values of the acceleration response were regarded in terms of comfortability in the built environment. This is mainly due to the fact that the free-free boundary condition, as well as the loading case of a single point load in a corner, and a single measure point was used. Therefore, the case studies showcase a great potential of improvement of the CLT-plates, rather than evaluating if a certain configuration performs well in the built environment.

Additionally, the fact that only a single measure point was used could perhaps imbue

the results with a certain degree of limitations, with regards to the conclusions that could be drawn. Certainly, the measure point in the corner shows the response in all eigenmodes. However, a measure point placed centrally in the CLT-plate could perhaps reveal that the perimeter scheme is not advantageous. Although, it is believed that exchanging the perimeter, to e.g. birch, provides a favourable mass and stiffness distribution with respect to the dominant eigenmodes. This further incentivises studies of multiple measure points, as well as tailoring the CLT-plate to the desired application, e.g. floor panel or wall panel.

14 Concluding Remarks

The aim of this dissertation was to mitigate the vibration level in CLT-plates, in order to increase the vibrational comfort, by investigating the acceleration response of different CLT-plate configurations, utilizing different types of wood materials. These configurations consisted of standard spruce in combination with birch, densified spruce as well as spruce with varying strength classes according to Eurocode. In this chapter, key results are highlighted, main conclusions summarized and suggestions for future work are presented.

14.1 Key Results

Key results for each material tested are summarized below. The numerical investigation suggests that:

- Exchanging 7% of the plate to either birch or densified spruce can achieve approximately 40% reduction of the vibration level. Exchanging 26% of the plate can achieve a reduction of up towards 60%, for a CLT-plate spanning 9 m.
- Exchanging 7% of the plate from spruce strength grade C24 to C50 can achieve approximately 15% reduction of the vibration level, for a CLT-plate spanning 9 m.
- Exchanging 3% of the plate to either birch or densified spruce can achieve approximately 10% or 20% reduction of the vibration level, respectively. Exchanging 16% of the plate can achieve a reduction of up towards 30% or 45%, respectively, for a CLT-plate spanning 5 m.
- Exchanging 8% of the plate from spruce strength grade C24 to C50 can achieve approximately 20% reduction of the vibration level, for a CLT-plate spanning 5 m.

14.2 Main Conclusions

In this section, the main conclusions of this dissertation are collected.

- Research on the six orthotropic elastic moduli of birch, as well as densified spruce, is scarcely available.

- The calibrated mechanical properties of densified spruce differed greatly from the mechanical properties given in the literature, utilizing different densification methods. Specifically, E_L increased marginally while G_{LT} increased substantially, compared to the mechanical properties of spruce.
- Utilizing birch in the CLT-plate reduces the vibration level substantially when the birch lamellae were concentrated to the middle of the plate, while utilizing densified spruce was invariant to the distribution along the thickness direction.
- Utilizing birch in the CLT-plate reduces the accelerance RMS substantially when the lamellae were concentrated to the edges of the plate, both in the longitudinal and transversal direction. Similarly, densified spruce lamellae should be concentrated in the edges of the CLT-plate.
- Stacking the involved layers about the centre of the CLT-plate, in conjunction with keeping the birch or densified spruce lamellae in the edges, further improves the acceleration response. This observation holds regardless of the size of the CLT-plate.
- Similar configurations of the replaced lamellae can give different results depending on the span of the CLT-plate. Different behaviour of similar configurations was observed for different sized CLT-plates.
- Utilizing higher strength class of spruce in the CLT-plate reduces the accelerance RMS when concentrated to the edges of the plate, both in the longitudinal and transversal direction. However, the reduction thereof is not as significant as to that of birch or densified spruce.
- Longer spans of CLT-plates provide greater potential of reducing the vibration level, than for smaller span plates.
- Greater reduction of the vibration level can be achieved by partly replacing the lamellae with birch or densified spruce, rather than by replacing the whole CLT-plate, if the panel has a span of 9 meters.

14.3 Future Work

Suggestions for future work are presented in this section. The suggestions entail ideas and objectives that we wanted to do, but were unable to due to time constraints, as well as aspects that are complementary to the work presented in the dissertation.

- Investigate different displacement boundary conditions, e.g., simply supported plate, to simulate realistic behaviour.
- Perform more lab experiments in order to better determine the mechanical properties of birch and densified spruce, both as timber and in a CLT-plate.
- Study velocity over the surface of the CLT-plate to determine how the sound radiation can be improved.

- Study acceleration in multiple measure points to compare how improvement may vary over the plate surface.
- Include more differently sized CLT-panels in the analysis, for example 7 meters and 11 meters long panel, as well as a 3 meters wide wall panel.
- Investigate if using lower strength timber in specific positions can mitigate or keep the same vibration level.
- Investigate the relationship between the ratio of the elastic moduli to the shear moduli, against the response of the CLT-plate. This is incentivised by the fact that the various spruce strength classes showcased insignificant variation in the results, except for C50 versus C14. This may be due to a relatively constant ratio, e.g. E_L/G_{RT} or even E_L/E_T , when incrementing the strength classes from C14 through C50.
- Study different load cases, by placing the point load in different locations on the CLT-plate. Furthermore, study different types of loads, e.g. distributed loads or footfall loads. Additionally, study loads with various frequency content.
- Study configurations that combine multiple different wood materials, e.g., birch lamellae as well as densified spruce lamellae in a single configuration of calibrated spruce.
- Study more configurations than presented in the dissertation, e.g., skew-symmetric or even non-symmetric placement of the different wood types, in the cross-section of the CLT-plate.

Bibliography

- [1] Swedish Wood and Marie Johansson. *Design of timber structures, Volume 1*. Swedish Forest Industries Federation, 2022. ISBN: 978-91-985212-5-2.
- [2] Johannes Jonasson and Olle Karlsson. “Utilisation of hardwood in cross-laminated timber - A numerical study on vibrations in floors”. Master’s thesis. Report TVSM-5258. LTH, Division of Structural Mechanics, 2022.
- [3] Per Gunnar Burström. *Byggnadsmaterial : tillverkning, egenskaper och användning*. Studentlitteratur AB, 2021. ISBN: 9789144151786.
- [4] *Standard - Eurocode: Träkonstruktioner – Konstruktionsvirke – Hållfasthetsklasser SS-EN 338:2016*. URL: <https://www.sis.se/produkter/trateknik-15e6ae2b/tra-sagtimmer-och-sagat-virke/ssen3382016/>.
- [5] Swedish Wood. *Design of timber structures*. Vol. 2. 2022. ISBN: 9789198521269.
- [6] Benedikt Neyses. *Surface densification of solid wood: Paving the way towards industrial implementation*. Luleå University of Technology, Department of Engineering Sciences, Mathematics, Division of Wood Science and Engineering, 2019.
- [7] Alexander Scharf, Benedikt Neyses and Dick Sandberg. *Continuous densification of wood with a belt press: The process and properties of the surface-densified wood*. Vol. 18. 4. Wood Material Science & Engineering. 2023, p. 1573–1586. DOI: 10.1080/17480272.2023.2216660.
- [8] Fredrik Ljunggren. *Innovative solutions to improved sound insulation of CLT floors*. Vol. 13. Developments in the Built Environment. 2023. DOI: 10.1016/j.dibe.2022.100117.
- [9] Swedish Wood. *The CLT Handbook*. 2019. ISBN: 978-91-983214-4-3.
- [10] Erol Karacabeyli and Sylvain Gagnon. *Canadian CLT handbook*. FPInnovations, 2019.
- [11] Swedish Wood. *KL-trähandbok*. Swedish Forest Industries Federation, 2017. ISBN: 978-91-981922-5-4.
- [12] Peter Persson, Ola Flodén, Henrik Danielsson, Andrew Peplow and Lars Vabbersgaard Andersen. *Improved low-frequency performance of cross-laminated timber floor panels by informed material selection*. Vol. 179. Applied Acoustics. 2021. DOI: 10.1016/j.apacoust.2021.108017.
- [13] Beatrice Bartolucci, Andrea De Rosa, Chiara Bertolin, Filippo Berto, Francesco Penta and Anna Maria Siani. *Mechanical properties of the most common European woods: A literature review*. Vol. 14. 54. Frattura ed Integrità Strutturale. Aug. 2020, p. 249–274. DOI: 10.3221/igf-esis.54.18.
- [14] T. Ehrhart and R. Brandner. *Rolling shear: Test configurations and properties of some European soft- and hardwood species*. Vol. 172. Engineering Structures. 2018, p. 554–572. DOI: 10.1016/j.engstruct.2018.05.118.

- [15] *Timber structures - Structural timber and glued laminated timber - Determination of some physical and mechanical properties*. URL: <https://www.sis.se/en/produkter/wood-technology/wood-sawlogs-and-sawn-timber/ssen4082010a12012/>.
- [16] J. Eberhardsteiner, W. Winter, A. Fadai and M. Pöll. In: *WCTE 2016 e-book : containing all full papers submitted to the World Conference on Timber Engineering (WCTE 2016), August 22-25, 2016, Vienna, Austria*. TU Verlag Wien, 2016, p. 612. URL: <https://resolver.obvsg.at/urn:nbn:at:at-ubtuw:3-2204>.
- [17] H. Holmberg and D. Sandberg. *Structure and Properties of Scandinavian Timber*. 1997.
- [18] Robert J. Ross. *Wood handbook: Wood as an engineering material*. Forest Products Laboratory, Department of Agriculture of Forest Service, 2021. ISBN: 979-8846323247.
- [19] Benedikt Neyses. *Surface-Densified Wood: From Laboratory-Scale Research Towards a Competitive Product*. Luleå University of Technology, Department of Engineering Sciences, Mathematics, Division of Wood Science and Engineering, 2016.
- [20] Benedikt Neyses and Alexander Scharf. “Using machine learning to predict the density profiles of surface-densified wood based on cross-sectional images”. In: *European Journal of Wood and Wood Products* (2022), p. 1121–1133.
- [21] John Paul Cabral, Bidur Kafle, Mahbube Subhani, Johannes Reiner and Mahmud Ashraf. “Densification of timber: A review on the process, material properties, and application”. In: *Journal of Wood Science* 68.1 (2022). DOI: 10.1186/s10086-022-02028-3.
- [22] K. B. Dahl. “Mechanical properties of clear wood from Norway spruce”. PhD thesis. 2009.
- [23] Anil K. Chopra. *Dynamics of Structure eBook, Global Edition*. en. Pearson Higher Ed, 2015. ISBN: 9780273774266.
- [24] George Lindfield and John Penny. *Numerical Methods*. Academic Press, 2019.
- [25] HP Wallin, U. Carlsson, M. Abom, H. Bodén and R. Glav. *Sound and vibration*. Institutionen for farkostteknik, Kungliga Tekniska hogskolan, 2017. ISBN: 9789174155532.
- [26] Thomas Lee Paez. *Introduction to model validation*. 2008. URL: <https://www.osti.gov/biblio/1142730>.
- [27] Niels Saabye Ottosen and Hans Petersson. *Introduction to the Finite Element Method*. en. Pearson, 1992.
- [28] Johannes Jonasson, Peter Persson and Henrik Danielsson. “Mitigating footfall-induced vibrations in cross-laminated timber floor-panels by using beech or birch”. In: *Journal of Building Engineering* 86 (2024), p. 108751. ISSN: 2352-7102. DOI: <https://doi.org/10.1016/j.jobe.2024.108751>. URL: <https://www.sciencedirect.com/science/article/pii/S235271022400319X>.